Bioactive Surfaces for Improved Coronary Stent Performance

By

Sarah Morgan

University of Strathclyde

Department of Biomedical Engineering

Thesis for the award of EngD Medical Devices

2017

Declaration of Authenticity and Author's Rights

This thesis is the result of the author’s original research. It has been composed by the author and has not been previously submitted for examination which has led to the award of a degree.

The copyright of this thesis belongs to the author under the terms of the United Kingdom Copyright Acts as qualified by University of Strathclyde Regulation 3.50. Due acknowledgement must always be made of the use of any material contained in, or derived from, this thesis.

Signed:

Date:

Abstract

Drug eluting stents (DES) are widely used to treat coronary heart disease. Although current DES generally perform well, restenosis and delayed endothelium healing still remains an issue following stent implantations. Research efforts are now focused on the development of stent coatings that address these limitations.

Amongst many different materials currently being investigated as stent coatings, conducting polymers, such as polypyrrole (PPy) have particular promise. Drug-containing polypyrrole coatings can be deposited onto metal surfaces through electropolymerisation, a process that may be superior to the spray coating techniques commonly used by stent manufacturers. However, the full potential of this approach for use in stent coatings remains to be determined. An anti-inflammatory agent, Salicylate (Sa) was incorporated into PPy coatings by electropolymerisation in the present study and four key aspects of the coatings were characterised.

Firstly, the surface morphology and topography of the polypyrrole/salicylate (PPy/Sa) coatings were examined using Scanning Electron Microscopy (SEM) and Atomic Force Microscopy (AFM). These methods were optimised through an initial investigation into surface topography of a limited number of existing bare metal stents (BMS) and DES. The surface roughness (RMS) ranged from 14 ± 11 nm (Gazelle™, scan size 5µm) to 182 ± 37 nm (Yukon®, scan size 5µm) with similarities noted between the DES. The surfaces roughness values of the PPy/Sa coatings were found to be within this range of roughness values.

Secondly, the release of Sa from the PPy/Sa coatings was examined. Coatings produced by either galvanostatic or potentiostatic electropolymerisation were immersed in phosphate buffered saline and the release of salicylate monitored over time using UV-spectroscopy. Both polymerisation methods released a similar total mass of drug (~12 µg), with the release period ranging from 1 day for potentiostatic coatings to 3 days for galvanostatic coatings. Thirdly, the biocompatibility of the coatings was analysed by live/dead staining and LDH assay, showing porcine endothelial cells to successfully grow on both PPy/Sa coating types.

Finally, the antioxidative activity of the coatings was investigated using a DPPH assay. The coatings were found to possess antioxidative activity for a period of 24 hours, an effect which was independent of salicylate release. This represents a potentially beneficial action that has not previously been demonstrated within a stent coating. By virtue of their controllable drug

release properties and a novel anti-oxidant mechanism, polypyrrole surfaces warrant further development as a potential stent coating.

Research Outputs

Attended Conferences - Poster Presentations

Morgan, S., Black, R., McCormick. C., Development and Characterisation of Novel Polypyrrole Coatings for Coronary Stents. TransMed Student Conference, Edinburgh, Scotland, 2016.

Morgan, S., Black, R., McCormick. C., Investigation into the Surface Characteristics of Coronary Stents. European Society of Biomaterials, Krakow, Poland, 2015.

Morgan, S., Black, R., McCormick. C., Conducting Polymer Coatings for Improved Coronary Stent Performance. PGBiomed International Student Conference, Liverpool, England, 2015.

Morgan, S., Black, R., McCormick. C., Investigation into the Surface Topography of Coronary Stents. Scottish Cardiovascular Forum Annual Meeting, Edinburgh, Scotland, 2015.

Journal Publications

T Vo, T., Morgan, S., McCormick, C., McGinty, S., McKee, S., Meere, M. 2017. An Experimental and Theoretical Investigation of Drug Release from Polymer-Free Coronary Stents with Microporous Surfaces. Int. J. Pharmaceutics (Accepted for publication on 8th December 2017)

List of Abbreviations

AFM	Atomic Force Microscope
BMS	Bare Metal Stent
CABG	Coronary Artery Bypass Graft
CHD	Coronary Heart Disease
CVD	Cardiovascular Disease
DES	Drug Eluting Stent
EC	Endothelial Cell
HUVEC	Human Umbilical Vein Endothelial Cell
HPLC	High Performance Liquid Chromatography
PCI	Percutaneous Coronary Intervention
PTCA	Percutaneous Transluminal Coronary Angioplasty
PI	Phase Imaging
PPy	Polypyrrole
Py	Pyrrole
ROS	Reactive Oxygen Species
R_{RMS}	Root Mean Squared Roughness
Ry	Peak-to-Valley distance
SA	Surface Area
Sa	Salicylate
SEM	Scanning Electron Microscope
SMC	Smooth Muscle Cell
NaSa	Sodium Salicylate
SD	Standard Deviation
UV	Ultra Violet

Acknowledgements

Firstly, I would like to thank my supervisors, Dr Christopher McCormick and Dr Richard Black for their knowledge and support throughout the completion of my doctorate degree. I would especially like to thank Dr Christopher McCormick for his constant enthusiasm and guidance which has been key to this thesis. The funding for this study was provided by the EPSRC and I am grateful for the opportunity this has given me.

I would like to thank Catherine Henderson and Brian Cartlidge for their knowledge and expertise in the lab. Thanks to Prof Keith Oldroyd for supplying the majority of the stents used for this study. Thanks also to Dr Robertson at the School of Chemistry for distilling Pyrrole, often at very short notice.

I want to thank my family and friends for their constant distractions over the years, it has definitely kept me going! I would like to thank my parents for always giving me the best opportunities and supporting me along the way. Thanks also for supplying a coffee shop, restaurant, garage, bank, and hotel, I'll pay you back one day…

Last but not least I would like to thank Matthew for supporting me in all of my endeavours. Thanks for always being there and listening to every presentation, reading every piece of work, and still looking interested. It's your turn now!

Table of Contents

"A scientist in his laboratory is not a mere technician: he is also a child confronting natural phenomena that impress him as though they were fairy tales."

- *Marie Curie*

Chapter 1

1. Introduction and Background

Chapter 1 provides an introduction to the subject of coronary heart disease, the need for improved coronary stents and the impact of surface features on vascular cell behaviour. It will describe some of the main coronary stents currently used, outlining some of their most important limitations. A consideration of how the surface features of a stent may be tuned to improve healing post stent implant will then be presented. The potential use of a novel conducting polymer coating for drug eluting stents will also be introduced in this section. The chapter will conclude with a summary of the key aims and objectives of the study.

1.1. Cardiovascular Disease (CVD)

Cardiovascular disease (CVD) is the number one cause of death worldwide, amounting to 31 % of all deaths in 2012 (WHO, 2015). Healthcare relating to CVD is estimated to cost the UK £11 billion each year with around 7 million people living with CVD in the UK (BritishHeartFoundation, 2015). With a growing and ageing population, it is predicted that these numbers will rise, with increasing need for improved methods of prevention and treatment.

1.1.1. Coronary Heart Disease (CHD)

Coronary Heart Disease (CHD) is the blockage of blood supply to the heart, caused by the presence of atherosclerotic plaques in the walls of coronary vessels. Atherosclerosis is the build-up of these atherosclerotic plaques in the walls of arteries, causing the artery to narrow and harden. As a result of this, the flow of oxygen-rich blood to the heart can become partially or completely blocked causing further complications such as angina pectoris or myocardial infarction. Contributing risk factors include high cholesterol, high blood pressure, diabetes and smoking (BritishHeartFoundation, 2015).

1.2. Treatment of Coronary Heart Disease

The treatment of CHD involves coronary artery bypass grafting (CABG) or percutaneous coronary intervention (PCI). These will be detailed in the following sections, including details of the benefits and risks associated with each procedure.

1.2.1. Coronary Artery Bypass Graft (CABG)

One type of procedure to treat a blocked or narrowed coronary artery is a coronary artery bypass graft (CABG). Around 20,000 CABG procedures are performed in England each year (NHS, 2014b). It involves moving a blood vessel from one part of the body, most commonly the internal mammary arteries or the greater saphenous veins and connecting one end to the aorta or subclavian artery and the other end to the affected coronary artery beyond the blockage. This graft diverts the blood flow around the diseased vessel, restoring blood flow and oxygen supply to the cardiac muscle (NHS, 2014b).

There are many risks associated with a CABG procedure, including death, myocardial infarction, stroke, kidney failure, infection, and lengthy recovery time. A myocardial infarction is the most common cause of death in those who have undergone a CABG procedure and it is estimated that one in every 15-50 people have a heart attack during surgery or shortly after (NHS, 2014c).

1.2.2. Percutaneous Coronary Intervention (PCI)

The most common non-invasive technique for the treatment of CHD is PCl, amounting to more than 92,000 procedures performed in the UK in 2013 (BritishHeartFoundation, 2015).

1.2.2.1. Percutaneous Transluminal Coronary Angioplasty (PTCA)

Percutaneous Transluminal Coronary Angioplasty (PTCA) involves a balloon catheter being threaded up the radial or femoral artery to the site of blockage in the coronary artery. The balloon is inflated, then deflated and removed. This causes the plaque to be compressed against

the artery wall, restoring blood flow to the cardiac muscle. The balloon catheter is guided by continuous X-ray fluoroscopy, allowing for accurate positioning and sizing of the balloon.

The need for only a small incision to be made in the groin or arm eliminates the need for open heart surgery thus making the procedure less invasive and greatly reduces the risk associated with it. Compared to the CABG procedure, the risk of heart attack is also greatly reduced, occurring in less than one in every one hundred patients who have undergone PTCA (NHS, 2014a).

1.2.2.2. Complications Following PTCA

Restenosis

Although PTCA is an invaluable technique in terms of invasiveness and recovery for the patient, restenosis is a common complication. Restenosis is the re-narrowing of the artery due to elastic re-coil, neointimal growth and arterial re-modelling (see Figure 1-1 for visual representation of restenosis). Elastic recoil occurs when the artery wall that had previously been stretched, begins to contract, thus reducing the lumen diameter (see Figure 1-1, label A). Negative arterial remodelling is the shrinkage of the external elastic membrane over a period of time, again resulting in a reduction in the lumen diameter (see Figure 1-1, label B). It is also common for neointimal hyperplasia to occur which is the rapid growth of smooth muscle cells on the tunica intima, increasing its thickness and decreasing the diameter of the lumen (see Figure 1-1, label C).

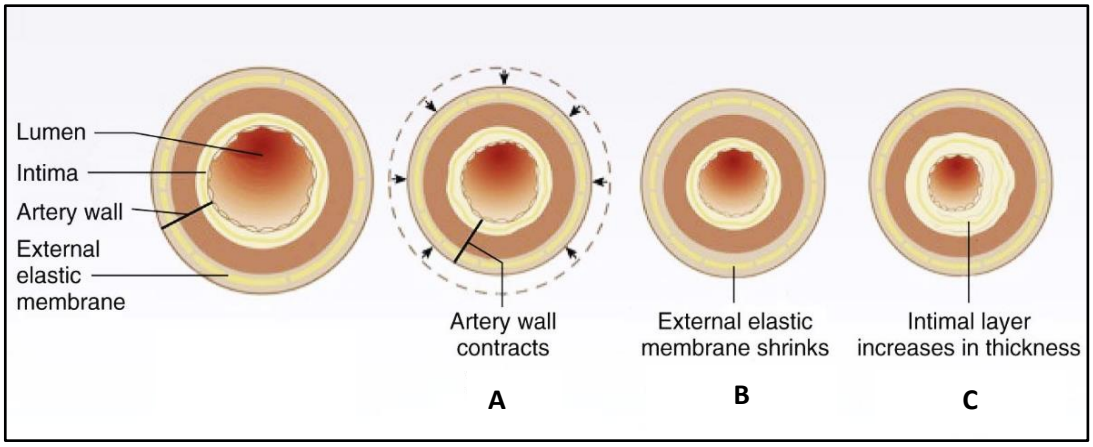

Figure 1-1: Artistic representation of the causes of restenosis following PTCA: A-elastic recoil, B-negative arterial remodelling and C-neointimal hyperplasia. Image adapted from (Price, 2013).

1.2.2.3. Stent Implantation

To prevent elastic re-coil and negative arterial remodelling, giving the lumen an improved chance of staying open, a stent is usually delivered percutaneously immediately following balloon angioplasty and expanded into the artery to provide permanent mechanical support to the vessel wall.

1.2.3. Bare Metal Stent (BMS)

A Bare Metal Stent (BMS) is a thin tube-like structure composed of a very thin wire mesh which acts as a biomedical scaffold to keep a vessel wall open following a blockage. The structure is initially crimped onto a balloon catheter where it is threaded up the radial or femoral artery and positioned in the blocked or narrowed vessel (see Figure 1-2 for artistic representation of procedure). The balloon with mounted stent is inflated, expanding the stent and pushing the plaques against the artery walls. The balloon is then deflated, and removed, leaving the stent in place.

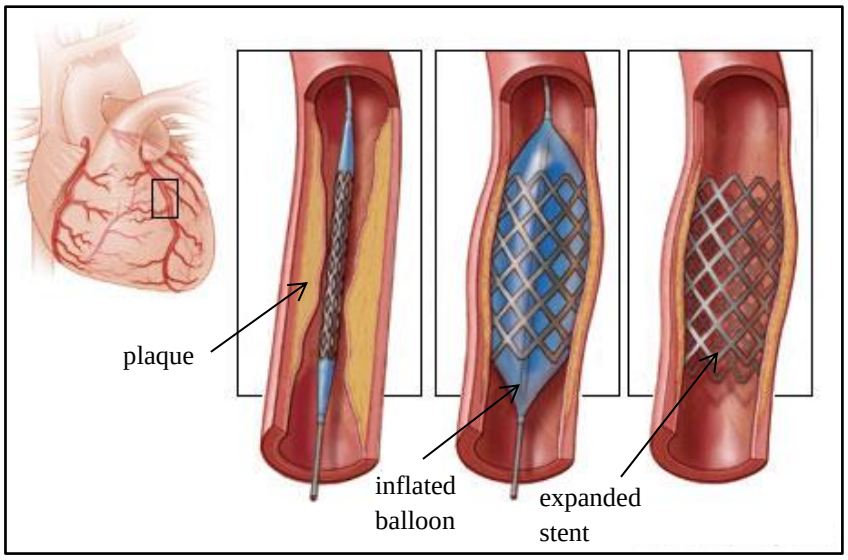

Figure 1-2: Artistic representation of stent implantation into a coronary artery as in Percutaneous Coronary Intervention (PCI). Image adapted from (Thomas, 2011).

Despite the reduced occurrence of elastic re-coil and negative arterial modelling, neointimal hyperplasia often remains an issue following stent implantation.

1.3. Cellular Events Following Stent Implantation

1.3.1. In-Stent Restenosis (ISR)

When a stent is implanted into an artery, mechanical injury of that artery occurs and local inflammation takes place which can lead to In-Stent Restenosis (ISR). The occurrence of ISR is defined when the diameter of the lumen is reduced by more than 50 % within the stent. It is estimated that 15 – 20 % of patients who have received a BMS due to a coronary lesion will suffer from ISR but this figure is estimated to increase to 30 – 60 % when considering those treated with a complex lesion (Puranik et al., 2013). The extent of the restenosis is thought to be correlated with the severity of the injury induced by the balloon and stent expansion (Schwartz et al., 1992)(Morton et al., 2007). It is therefore one of the main issues associated with PCI and continuous research is being undertaken in an attempt to reduce its occurrence.

1.3.2. In-Stent Restenosis Timeline

Once a stent is implanted into a vessel, there are a number of cellular responses that take place. These can be separated into four main events (thrombosis, inflammation, proliferation and extracellular matrix production) typically over a 6-month period and the cellular responses in each event will be discussed in this section. The timeline of these events has been estimated from animal and human data and this is reviewed in the study by (Weintraub, 2007).

Thrombosis 0-1 day

Mechanical injury of the artery wall results in the removal of the endothelium and damage to the elastic lamina and tunica media. This damage triggers a repair mechanism, involving platelets, neutrophils and monocytes (see Figure 1-3 for visual representation of cellular events following stent implantation); this local inflammatory response is instrumental in restenosis. The exposed sub-endothelial matrix makes contact with flowing blood whereby platelets and fibrin begin to adhere to the stent surface. This is deemed thrombosis, which is a key event in the first day post stent implantation (Inoue et al., 2011).

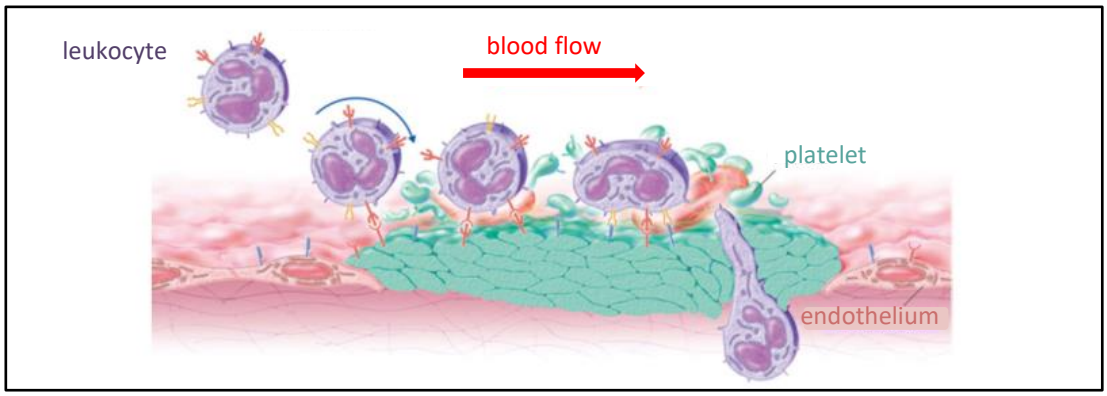

Figure 1-3: Image representing cellular events following stent implantation. Image adapted from (Inoue et al., 2011).

Inflammation 0-7 days

Leukocytes are recruited at the site of injury which then begin to adhere to the already adhered platelets, a process which is directed by platelet and leukocyte adhesion molecules (P-selectin,

platelet glycoprotein (GP) Ibα) (Inoue et al., 2011). This inflammation event occurs in the initial 7 days post stent implantation.

Proliferation 0-30 days

Cytokines (monocyte chemo attractant protein – 1, IL-6, IL-8) enable leukocytes to cross-link with fibrinogen to the GP IIb – IIIa receptor. The migration and proliferation of smooth muscles cells (SMCs) at the site of injury is stimulated by chemotactic factors (PDGF, Thrombin GF-β, Epidermal GF, serotonin, thromboxane A) released by activated platelets (Inoue et al., 2011). This event occurs over the initial 30-day period post stent implantation.

Extracellular Matrix Production 1-6 months

As previously mentioned, neointimal hyperplasia is a persisting problem following stent implantation. Growth factors stimulate the proliferation of SMCs in the tunica intima where they begin to migrate into the lumen, attempting to repair the damage. This begins to form neointimal tissue which is composed of SMCs (~11 %), extracellular matrix, proteoglycans and collagen. This tissue continues to grow, gradually narrowing the artery and further reducing blood flow to the cardiac muscle (Haridas et al., 2008). This extracellular matrix production is active in the first 6 months post stent implantation.

1.3.3. Re-endothelialisation

The endothelium is a layer of endothelial cells that lines the blood vessel and is essential for proper function of the cardiovascular system. It provides a non-thrombogenic surface for blood flow and controls the movement of important molecules and cells in and out of the bloodstream. It is also responsible for controlling the vasoconstriction and vasodilation of the blood vessel, functions that are essential for the control of blood flow and pressure. Re-endothelialisation is the growth of a new layer of endothelial cells once they have been removed or damaged by stent implantation. The issue concerning stent implantation is that the endothelial layer does not often form properly following the implantation. This leaves the artery wall vulnerable to further cellular responses and complications, including thrombosis.

1.3.4. Stent Thrombosis

Stent thrombosis occurs when a blood clot forms on the surface of a stent implanted in a vessel wall. There are several stages of stent thrombosis that may occur and can be separated into two main categories; early and late.

1.3.4.1. Early Stent Thrombosis

Early stent thrombosis occurs in the first 30 days following stent implantation. The initial stage of stent thrombosis, referred to as 'acute stent thrombosis' occurs within the first 24 hours of implantation. Sub-acute stent thrombosis occurs after the initial 24 hours following stent implantation and up to a period of 30 days. According to the literature (Inoue et al., 2011), these early stages of in stent thrombosis are likely to be caused by several issues including mechanical complications with the stent, insufficient platelet inhibition or pro-thrombotic patient risk factors. Treatment with dual anti-platelet therapy (DAPT) is associated with reduced incidences of stent thrombosis and clinical recommendations are for treatment with DAPT for a period of 6-12 months post stent implantation (Helft, 2016).

1.3.4.2. Late and Very Late Stent Thrombosis

Advanced stages of stent-thrombosis are known as either 'late stent thrombosis' which occurs up to one year following implantation or 'very late thrombosis' which occurs after one year. The main causes of these later stages of thrombosis are thought to be as a result of delayed re-endothelialisation or the inhibition of vascular repair (Inoue et al., 2011). This will be discussed in relation to the use of drug eluting stents in the following sections.

1.4. Drug Eluting Stent (DES)

The introduction of the Drug Eluting Stent (DES) came about in an attempt to reduce the negative issues associated with BMS, specifically the occurrence of ISR. The first-generation DES were BMS that have been coated with a polymer containing a drug which was slowly released from the polymer into the surrounding artery wall to prevent excessive cellular proliferation within the artery.

There are many distinct types of DES, incorporating different types of drugs, coating technologies, stent platforms, with emerging technologies including bioresorbable stents. Despite all of their differences in mode of function, the number one aim for all DES is to treat the diseased artery, while inducing minimal damage and keep it open to restore and maintain blood flow to the cardiac muscle. The following section will summarise the most widely used coronary stents since the first DES was made commercially available over 15 years ago.

1.4.1. First Generation DES

The first-generation DES were mostly medical grade stainless steel (316L) stent platforms coated with well-known polymer and drug components.

1.4.1.1. Cypher™ SES

The first DES made commercially available was the Cypher™ Sirolimus-Eluting Stent (SES) (Johnson and Johnson) in 2002. The Cypher™ SES consists of a BMS (Bx Velocity, 316L SS), coated with three different layers. The initial layer, directly adhered to the BMS is a coating of Parylene, providing adherence for the other polymer layers. The second layer is a mixture of two polymers (Poly(ethylene-co-vinyl-acetate) PEVAC and Poly (butyl methacrylate) (PBMA)) and sirolimus. The final layer that is designed to be in direct contact to the vessel wall is a mixture of two polymers (PEVAC and PBMA) but no drug is present (see Figure 1-4 for a visual representation of the Cypher™ polymer/drug layers).

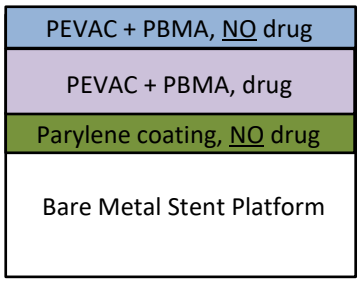

Figure 1-4: Schematic representation of drug eluting coating on Cypher™ SES Stent. Image adapted from (Venkatraman and Boey, 2007).

The choice of an additional drug-free layer ensures the steady release of sirolimus (140 µg/cm^2) over a 30 day period (80 % released by day 30 post implantation) (Martin and Boyle, 2011). The significance of this slow release is in relation to the stent inflammation timeline as proliferation of SMCs, targeted by the release of sirolimus is most prominent in the first 30 days post implantation (Haridas et al., 2008). Despite the fact that 80% of the drug is released over this period, it takes a total of 168 days for the drug to be completely eluted from the stent. This may be an attempt by the manufacturer to tackle the extracellular matrix production which is thought to occur from 1-6 months post stent implantation.

Clinical Trials

A number of clinical trials have been undertaken to assess the safety and efficacy of the Cypher™ SES. Results from the RAVEL randomised trial (Morice et al., 2002) showed superiority of the sirolimus coated stent compared to the BMS (Bx-Velocity) in terms of late luminal loss and overall rate of major cardiac events at the 1-year follow up. The superiority of the Cypher™ SES over the BMS (Bx-Velocity) was also demonstrated in the SIRIUS trials (SIRIUS, C-SIRIUS, E-SIRIUS) where lower rates of target-lesion revascularisation and adverse clinical events were observed (Schofer et al., 2003, Schampaert et al., 2004, Moses et al., 2003).

The Cypher™ SES once accounted for 75% of stents utilised in 2005 (Nebeker et al., 2006), but it was not without its problems. It is reported in the Summary of Safety and Effectiveness Data Sheet (SSEDCypher, 2003) that one failure of the Cypher™ stent was the presence of stress cracks along the edges of the stent struts. These cracks in the coating (visualised by SEM analysis) appeared following stent expansion, exposing the underlying layers. This may alter

the rate of drug delivery from the stent, affecting the healing process following stent implantation and the biocompatibility of the stent.

1.4.1.2. Taxus® Express^{2} ™ PES

The Taxus® Express^{2} ™ Paclitaxel Eluting Stent (PES) (Boston Scientific) is a BMS (Express, 316L SS) coated with SIBS (styrene-b-isobutylene-b-styrene), and an antiproliferative drug (paclitaxel). The release of paclitaxel (100 µg/cm^{2}) from the coating occurs in two stages; an initial 48 hour burst where the drug is rapidly released, after which it is released slowly over a period of 10 days (Martin and Boyle, 2011).

The highly lipophilic nature of the drug means that despite this initial release, the drug remains in the artery wall for prolonged periods so it can inhibit the smooth muscle cell response in the longer term. The continued release over the following 10 days is to slow the initial stages of Smooth Muscle Cell (SMC) proliferation and may also aid the inflammatory response. The total release period of the paclitaxel from the stent coating is unknown.

Clinical Trials

This 'bi-phasic' release system of paclitaxel has been investigated in many clinical trials (TAXUS I, II, III,IV,V,VI) showing superiority compared to a BMS in many areas (Stone et al., 2004). For example, the TAXUS IV clinical trial showed significantly fewer incidence of myocardial infarction, target-vessel revascularisation and major adverse cardiac events for patients with the paclitaxel eluting stent than the bare metal control (Stone et al., 2004). The commercial product, Taxus® Express^{2} ™ PES has been directly compared to a BMS control (Express^{2} or Liberte) in the 'PASSION' clinical trial (Laarman et al., 2006). Results from this trial showed general trends in data supporting the Taxus® Express^{2} ™ PES but no significant differences between the performances of the two stent types was observed.

1.4.1.3. Taxus™ Liberte PES

The approval of the Taxus™ Express^{2} PES was shortly followed by the introduction of the Taxus™ Liberte PES, also manufactured by Boston Scientific. The Taxus™ Liberte PES coating is composed of the same polymer-drug matrix as the Taxus® Express^{2} ™ PES but on an alternative BMS platform that differs in its geometry. The Taxus™ Liberte stent also has thinner stent struts (97 µm) compared to the Taxus® Express^{2} ™ PES (132 µm) (Martin and Boyle, 2011).

Clinical Trials

Results from the TAXUS ATLAS clinical trial showed similar outcomes of the Taxus™ Liberte PES and the Taxus® Express² ™ PES, suggesting that the drug-eluting coating is imperative in its performance and not just the geometry of the stent struts (Turco et al., 2007).

1.4.2. Second Generation DES

The second generation DES introduced the use of cobalt-chromium (CoCr) stent platforms, providing stents with thinner struts whilst maintaining the desired strength to keep an artery wall open. A select few of these stents are described in more detail in the following sections.

1.4.2.1. Endeavour™ ZES

The first of these second generation DES to come about was the Endeavour™ ZES (Medtronic), consisting of a MP35N CoCr BMS ('Driver', Medtronic) coated with phosphorylcholine (PC) polymer and zotarolimus. The zotarolimus (100 µg/cm stent length) is gradually released following implantation, with 95 % of the zotarolimus released by day 14 (Iqbal et al., 2013). Total drug release is reported to be complete after 20-22 days. Zotarolimus is a similar drug to sirolimus, that was used in the Cypher™ SES, in terms of mode of function, and therefore has similar targets that include reducing the proliferation of SMCs.

The strut thickness of the Endeavour™ stent is just 91 µm, much less than that of the first generation DES (Cypher™ SES 140 µm, Taxus™ Express² PES 132 µm) (Price, 2013). Reduced strut thickness is thought to allow for improved healing abilities following stent implantation, due to less injury to the artery wall and therefore less restenosis

Clinical Trials

The ENDEAVOUR IV clinical trial compared the performance of the Endeavour™ ZES to the Taxus™ PES. In the early stages of the trial there was little difference observed between the performance of the two stent types (Leon et al., 2009). The findings from later stages of the trials showed some differences, with significantly less incidences of very late stent thrombosis in the patients with Endeavour ™ ZES stents compared to those with the Taxus™ PES (Leon et al., 2010). This may be a result of reduced strut thickness or drug type.

1.4.2.2. Xience™ V EES (Xience Pro)

The Xience™ V/Pro EES consists of a cobalt chromium alloy platform (CoCr) coated with a primer layer (PBMA (Poly (butyl methacrylate)) and a top layer of poly (vinylidene fluoride-co-hexafluoropropene) (PVDF-HFP) and everolimus (Ding et al., 2009). Similar to the Cypher™ SES, the Xience™ V/Pro EES releases 80% of its everolimus (100 μg/ cm^2) within a 30-day period. The total mass of drug is released by approximately 120 days post stent implantation (Ding et al., 2009). Similar to sirolimus and zotarolimus, used in first and second-generation stents, everolimus targets the proliferation of SMCs. In addition to the inhibition of SMCs, everolimus is recognised for having high potency and high lipophilicity, making it an attractive drug for DESs and has been used in many other DESs.

Clinical Trials

The SPIRIT FIRST clinical trial compared the performance of the Xience™ V/Pro EES to the BMS platform (Multi-Link BMS). It was found that the Xience™ V/Pro EES performed better in terms of in-stent late loss and binary in-stent restenosis at 6-months post stent implantation (Stone et al., 2011).

During two other clinical trials (SPIRIT II, III), the performance of the Xience™ V/Pro EES was found to be superior to the Taxus® Express^2 ™ PES in a number of areas at 6, 9 and 12 month time points (Serruys et al., 2006, Stone et al., 2008). At the 12 month time point, the Xience™ V/Pro EES was shown to be superior to the Taxus® Express^2 ™ PES in terms of target-lesion failure and target-lesion revascularisation (SPIRIT IV) (Stone et al., 2010).

1.4.3. Third Generation DES

One of the focuses of third generation stents was to improve the radiopacity of the stent by altering the composition of the stent platform. Improved visibility of the stent during deployment would ensure accurate placement of the stent into the affected vessel with minimal damage to the surrounding vessels. Thicker stent struts have improved radiopacity than thinner stent struts, so the aim for manufacturers was to create a stent with improved radiopacity, without increasing the bulk of the stent platform.

1.4.3.1. Promus Element™ EES

The Promus Element™ EES is a third generation DES manufactured by Boston Scientific which consists of a platinum chromium (PtCr) alloy stent platform which has been designed to achieve higher radiopacity and radial strength (Tandjung et al., 2012). The coating is composed of a fluoropolymer and elutes everolimus. The strut thickness of this type of stent is notably less than previous generations with a value of 81 μm and the fluoropolymer/ everolimus coating has a thickness of 7 μm.

Clinical Trials

In the PLATINUM clinical trial, the performance of the Promus Element™ EES was compared to the Xience™ V EES (Stone et al., 2011). These two stents both elute everolimus but differ in their stent platforms (Xience™ V – CoCr, Promus Element™ – PtCr). The results from the trial showed no significant difference in the safety and performance of the two stents at the 1 year follow up. This was a favourable outcome for the Promus Element™ EES, with the added advantage of increased radiopacity when compared to the Xience™ V stent, making it potentially a more desirable stent.

1.4.4. Biodegradable (Bioresorbable) DES Coating

Biodegradable stent coatings have been developed in an attempt to reduce the incidence of in-stent restenosis, late stent-thrombosis, and hypersensitivity reactions associated with the long term presence of a polymer in the stented artery (Strohbach and Busch, 2015). A selection of commercially available stents with biodegradable coatings will be outlined in the following sections.

1.4.4.1. Yukon® Choice PC

The Yukon® Choice PC manufactured by Translumina is composed of a microporous stainless steel (316L) platform, a biodegradable coating and sirolimus. The biodegradable components of the coating are polylactide (PLA) and a shellac topcoat. As the polymer mix degrades and the sirolimus is released, the underlying microporous structure is exposed. This microporous structure has been purposefully manufactured with the intention of improving endothelial cell healing. This will be further discussed in section 3.4.7.

Clinical Trials

The ISAR-TEST 4 clinical trial compared the performance of the Yukon® Choice PC SES to the Cypher™ SES which has a permanent polymer coating. The study showed similar incidences of cardiac death, myocardial infarction, and revascularisation for both stent types at the 1 and 3 year time points (Byrne et al., 2009). Despite this initial lack of difference in performance between the two stent types, a reduction in very late stent thrombosis was observed at the 4 year follow up for patients with the Yukon® Choice PC SES compared to the Cypher™ SES (Stefanini et al., 2012). This is thought to be due to the use of the biodegradable polymer, eliminating the negative effects associated with the long-term presence of a polymer in the affected artery.

1.4.4.2. Orsiro

The Orsiro stent is manufactured by Biotronik and consists of a CoCr platform and the same biodegradable component as the Yukon® Choice PC stent (poly-L-lactide acid (PLLA)). This stent also elutes sirolimus, and has a very small strut thickness of 60 µm.

Clinical Trials

The BIOFLOW II clinical trial compared the biodegradable coated stent (Orsiro) to a permanent polymer stent (Xience Prime ™). At the 9 month follow up, the Orsiro stent was found to be non-inferior to the Xience Prime™ stent in terms of late-lumen loss (Schildwächter, 2013).

1.4.4.3. Synergy

The Synergy EES stent by Boston Scientific is composed of a PtCr platform with a biodegradable polymer/drug coating (4 µm thick). The polymer component is fully absorbed 3-4 months post stent implantation, shortly after completion of drug release.

Clinical Trials

In the EVOLVE II randomised clinical trial, patients received an everolimus eluting stent with either a biodegradable coating (Synergy) or a permanent coating (Promus Element Plus) (Kereiakes et al., 2015). Results showed that the Synergy stent with the biodegradable coating was non-inferior to the Promus Element Plus stent with the permanent coating at the 1 year-

follow up comparing the incidence of target lesion revascularisation, myocardial infarction and cardiac death.

A recent review from Transcatheter Cardiovascular Therapeutics 2016 has suggested no superiority in the performance of DES with biodegradable coatings compared to those with permanent coatings. This review of recent clinical trials (BIO-RESORT, TRANSFORM-OCT, PRISON IV) suggests the performance of the two stent types to be equivocal (Fornell, 2017). However, the long-term effects of biodegradable coatings are still to be confirmed and may show the benefit of the long-term absence of the polymer coating. This includes ongoing trials into reducing the need for long-term dual anti platelet therapy (DAPT). DAPT is required in certain patients who have an adverse reaction to the presence of the permanent polymer. Long-term DAPT can cause further complications in patients, including increased bleeding risks and is therefore avoided where possible.

1.4.5. Polymer Free DES

Research has been ongoing into the development of DES that eliminate the use of a polymer to act as a drug carrier. This involves using the bare metal platform as the drug carrier with the aim to eliminate the negative issues associated with the presence of a polymer, as was mentioned in the previous sections.

1.4.5.1. Yukon® Choice 4

Similar to the Yukon® stent discussed above, the Yukon® Choice 4 DES has a microporous stent platform where the drug sits. The drug component is directly applied to the stent surface using a dedicated stent coating machine housed within the catheterisation lab, therefore the dose of drug can be adjusted accordingly for each patient. Pure sirolimus can be applied to the Yukon® Choice 4 stent with outcomes from clinical trials discussed below. Other combinations of drugs such as sirolimus and probucol have also been applied to the Yukon® microporous platform with promising results (Abizaid and J. Ribamar Costa, 2010).

Clinical Trials

The ISAR-TEST clinical trial compared the performance of the Yukon® Choice 4 SES (2% sirolimus) to the Taxus™ PES at the 6 month time point (Mehilli et al., 2006). There was no significant difference noted for angiographic restenosis rates and target lesion revascularization rates due to restenosis between the two stent types.

1.4.5.2. Bio-Freedom

Another surface modified stent is the Bio-Freedom Biolimus A9™ (BA9) eluting stent by Biosensors International™. This stent has a selectively micro-structured (SMS) abluminal surface in which the BA9 is contained. The BA9 is released within 28 days, leaving the underlying BMS exposed. Biosensors International™ claim that this stent promotes rapid re-endothelialisation and allows for a shorter DAPT duration of 1 month.

Clinical Trials

The LEADERS FREE clinical trial compared the Biolimus A9TM eluting stent to the Gazelle™ (Biosensors InternationalTM) BMS in patients specifically with increased bleeding risk. All patients received 1 moth DAPT. Early results from the trial suggest that the Bio-Freedom stent was superior to the Gazelle™ stent in terms of the primary efficacy end point at the 390 day end point (clinically driven target-lesion revascularization) (Urban et al., 2015). The two-year outcome further demonstrated the superiority of the Bio-Freedom stent to the BMS it was compared to. The primary efficacy end point at the two-year time point was 6.8% for the Bio-Freedom stent compared to 12 % for the Gazelle™ stent (Garot et al., 2017).

1.4.6. Fully Bioresorbable DES

Current research is now focussed on fully bioresorbable stents that slowly degrade at the site of implantation after a period of time. This type of stent is designed to provide a physical scaffold to hold the diseased vessel open, but once healed completely degrades and is absorbed into the body. A stent that is fully resorbable could allow for restoration of vasomotion once the scaffold has disappeared and also allows for repeat procedures to be performed without the problems associated with multiple layers of metallic stents.

1.4.6.1. Absorb

The first fully bioresorbable vascular scaffold (BVS) is the Absorb (Abbott Vascular). Instead of a bare metal platform, the stent is composed of Polylactic Acid (PLA) plastic which is completely resorbable, omitting the use of a permanent foreign object in the body. The scaffold is fully dissolved within 2-3 years, which manufacturers believe to be ample time for healing of the diseased artery.

Clinical Trials

Clinical trials for this product have shown varied results. The earliest results from the ABSORB II clinical trial states that the Absorb stent is comparable to the Xience^{TM} stent in terms of performance at the 1 year follow-up (Serruys et al., 2015). However, a more recent summary of Absorb stent clinical trials presented by (Sorrentino et al., 2017) showed recurring issues with the Absorb stent. Findings from the ABSORB III clinical trials showed significantly higher rates of target lesion failure and a greater risk of stent thrombosis when compared to the Xience^{TM} stent. The Food and Drug Administration (FDA) released a safety alert regarding the use of the Absorb stent based on the results from the ABSORB III clinical trial. It was advised that DAPT was provided to patients to prevent incidences of major adverse cardiac events. A combination of these studies resulted in the Absorb stent being removed from the market for safety reasons.

1.4.7. Limitations of Drug Eluting Stent Coatings

The previous section discussed some clinically relevant DES and how they have evolved over the years. Although superior to BMS is most cases, DES are not problem free and have been linked to such complications as late-stent thrombosis as briefly outlined in section 1.3.4.2. The possible causes of late-stent thrombosis linked to the use of DES are discussed in the following section.

1.4.7.1. Late-Stent Thrombosis Due to Type of Drug

Drugs such as paclitaxel and sirolimus are commonly used in DES as they have a positive antiproliferative effect on SMCs and inflammatory cells. However, it has been reported (Curfman et al., 2007) that these antiproliferative drugs may also cause delayed re-endothelialisation at the area of stent implantation, leading to the adherence of platelets, red blood cells (RBCs), fibrin and white blood cells (WBCs) to the exposed stent struts. A consequence of this is the occurrence of late-stent thrombosis, resulting in acute reocclusion of the artery. A visual comparison of the ISR experienced in BMSs and the late stent thrombosis experienced in DES is illustrated in Figure 1-5 and Figure 1-6.

Research efforts surrounding choice of drug in DES coatings are ongoing with new polymer-drug coatings constantly evolving. The type of drugs used in a number of popular clinically relevant DES will be discussed in the following section.

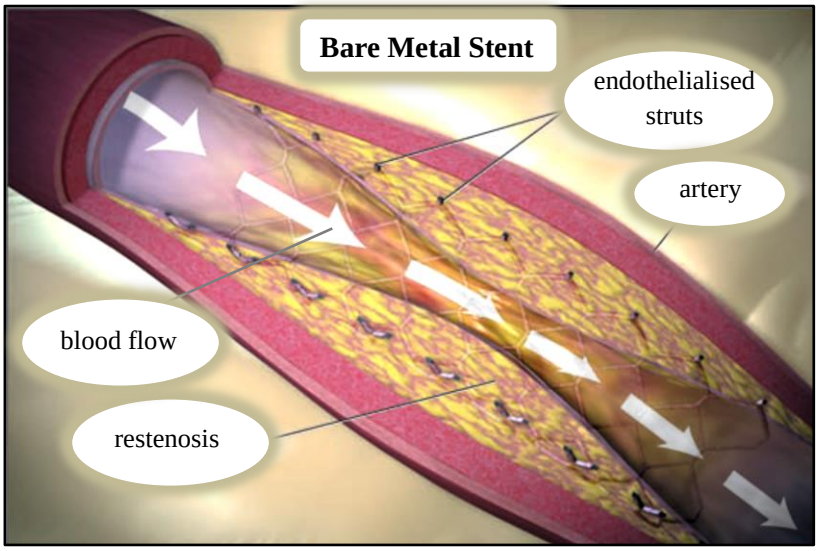

Figure 1-5: Artistic representation of ISR following implantation of BMS into artery. Image adapted from (Curfman et al., 2007).

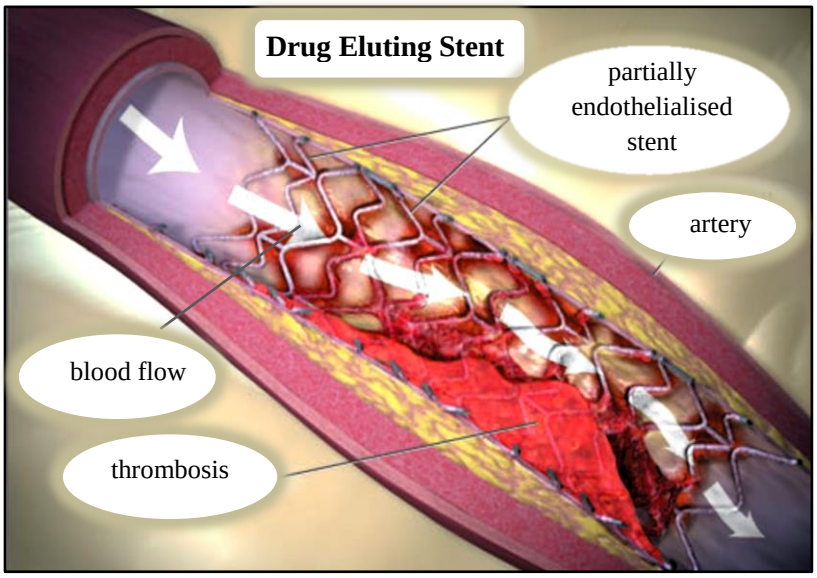

Figure 1-6: Artistic representation of stent thrombosis following implantation of DES into artery. Image adapted from (Curfman et al., 2007).

1.4.7.2. The Role of Polymer Coatings in Late-Stent Thrombosis

Due to the fact that late stent thrombosis can occur a long period after the completion of drug elution from a DES, it has been suggested that the occurrence of delayed vascular repair is therefore not solely due to drug type. Although the drug has been eluted, the polymer still remains on the surface of the stent, pressed against the artery wall. Studies have shown that the nature of the polymeric compound can lead to biocompatibility, immunogenicity and thrombogenicity issues emphasized by remaining in the body for the duration of its use (Inoue et al., 2011).

There are a number of studies that have investigated the role of polymer hypersensitivity in early generation DES and history shows issues with clinically used stents, for example, the US Food and Drug Administration issued a warning regarding the Cypher™ stent because of subacute thrombosis and hypersensitivity reactions. A study by Virmani et al (Virmani et al., 2004) investigated a patient who died of late-stent thrombosis 18 months after being implanted with two Cypher™ stents to treat unstable angina. At 8 months post stent implantation, angiographic and intravascular ultrasound results showed that there was no neointimal formation but there was vessel enlargement. Following an autopsy, aneurysmal dilation of the stented arterial segments was uncovered. There was severe localized hypersensitivity reaction surrounding polymer fragments, suggesting that a reaction to the polymer may have caused late-stent thrombosis.

A study by van der Giessen et al (van der Giessen et al., 1996) investigated the biocompatibility of a variety of biostable and biodegradable polymer loaded stents by implanting them into porcine coronary arteries. One-month post stent implantation, the coronary arteries were examined by angiography and also investigated by microscope. It was concluded that both biostable polymers (polyurethane (PUR), silicone (SIL)) and biodegradable polymers (polycaprolactone (PCL), polyorthoester (POE), polyhydroxybutyrate valerate (PHBV) caused extensive inflammatory responses and subsequent neointimal thickening. The author suggests the reaction is likely to be due to a combination of the reaction to the polymer and biodegradation products from the polymer. Implant geometry was also suggested as a possible contributing factor.

This leads onto research into biodegradable stent coatings, polymer free stents and even bioresorbable stents, attempting to eliminate the problems associated with the long-term presence of a polymer or indeed a stent platform in the body. Some of these available stents have been discussed in sections 1.4.4, 1.4.5 and 1.4.6. The following section will discuss the challenges associated with the design of DES and the emerging technology in terms of their application in clinically relevant stents.

1.4.8. Challenges Relating to the Design of DES

There are many challenges facing the design of DES, some of which differ from those experienced with the use of BMS. These include stent platform, type of polymer, uniformity of drug elution and type of drug which will all be discussed in the following section. These are constantly evolving with new approaches being researched and developed.

1.4.8.1. Stent Platform

As reported in the literature (Okner et al., 2007, Peng et al., 1996), a metal stent surface is recognised as a thrombogenic foreign body. It is suggested that the net electrical charge or potential of the metal surface is somewhat responsible for the biological response when in contact with the blood (Peng et al., 1996). As the surfaces of most BMS are electropositively charged and conversely, blood (and proteins) is negatively charged, the interaction between these two materials can cause a thrombogenic response. In addition to this, the majority of metals also possess a high critical surface tension which can also lead to increased thrombogenicity.

1.4.8.2. New Approaches to Stent Platform Design

Causes of ISR following BMS implantation include hypersensitivity reactions to the components of the commonly used medical grade stainless steel (316L), including nickel and molybdenum alloys (Köster et al., 2000). In an attempt to avoid this hypersensitivity reaction, the second generation of DES introduced the use of cobalt chromium (CoCr) as their stent platform. This also provided a stent that had thinner stent struts whilst maintaining the desired strength. As discussed in section 1.4.3.1, there has more recently been the development of platinum chromium (PtCr) stent platforms, which, in addition to the benefits of the CoCr platforms, have increased radiopacity for improved visualisation during implantation.

Despite the progress made with the development of stent platforms, the additional polymer and drug components of a DES mean that hypersensitivity still remains an unresolved issue with further problems to consider. New approaches to stent design are now seeing an increased number of DES without permanent polymer coatings by developing biodegradable and even polymer free stents, which will be discussed in the following sections. These new designs make the stent platform even more significant as it is this surface that will be in contact with the vessel wall.

1.4.8.3. Type of Polymer

The desired polymer stent surface should be uniform, have good adhesion with the metal substrate and possess good deformation ability (Shanshan et al., 2013). It is also essential that the surface is capable of withstanding the tensile and compressive strains that are required when positioned and deployed *in vivo* (Pan et al, 2006). If the polymer coating becomes damaged or deformed in some way, small parts of the polymer coating could become detached, causing further complications including inflammatory response and neointimal thickness as has been discussed in section 1.4.7.2.

As with all stents, the coating and platform must be able to withstand further processing such as sterilisation which should not have an adverse effect on the structure or composition of the stent (Ranade et al., 2004).

1.4.8.4. New Polymer Technologies

As briefly mentioned in sections 1.4.4 and 1.4.6, new polymer technologies including biodegradable coatings and bioresorbable stents are currently being developed. These coatings allow for the polymer coating to be present for only a temporary period as it is gradually absorbed into the body. An example of the biodegradable coating is the Polymer Resomer R202S used on the Yukon® CHOICE PC DES (Translumina). This stent type provides a 50% reduction in definite stent thrombosis and a 78% reduction in very late stent thrombosis compared to first generation DES (Stefanini et al., 2012).

This is a key finding, suggesting that the biodegradable coating, omitting the long-term presence of polymer in the body, could reduce the occurrence of one of the main problems associated with the use of DES. However, the surface of the Yukon® stent is also purposefully

manufactured to aid re-endothelialisation so it is unclear as to which feature of this stent provides the beneficial outcome.

1.4.8.5. Pharmacological Approaches

Anti-restenosis Drugs

A number of antiproliferative and immunosuppressive drugs have been researched for their ability to act as a suitable agent in DES. Such immunosuppressive drugs, including sirolimus, zotarolimus and everolimus are known to inhibit the proliferation of SMCs. Their mode of function (see Figure 1-7) involves binding to the cytosolic FK-bind protein 12 (FKBP12). As a result of this, the activation of the mammalian target of rapamycin (mTOR) is prohibited and the cell cycle is interrupted at the G1-S phase and SMC proliferation is inhibited (Martin and Boyle, 2011).

Another class of drugs used in DES are antiproliferative drugs, such as paclitaxel which binds to and stabilises microtubules to subsequently reduce neointimal growth. The added stability of these microtubules makes them too difficult to disassemble and so they become non-functional. As a result of this, the cell-cycle is stopped in the G0-G1 and the G2-M phases, inhibiting the proliferation of SMCs (see Figure 1-7). Further evidence has shown that paclitaxel delivered locally from a stent surface is indeed cytostatic but not cytotoxic (Jordan et al., 1993).

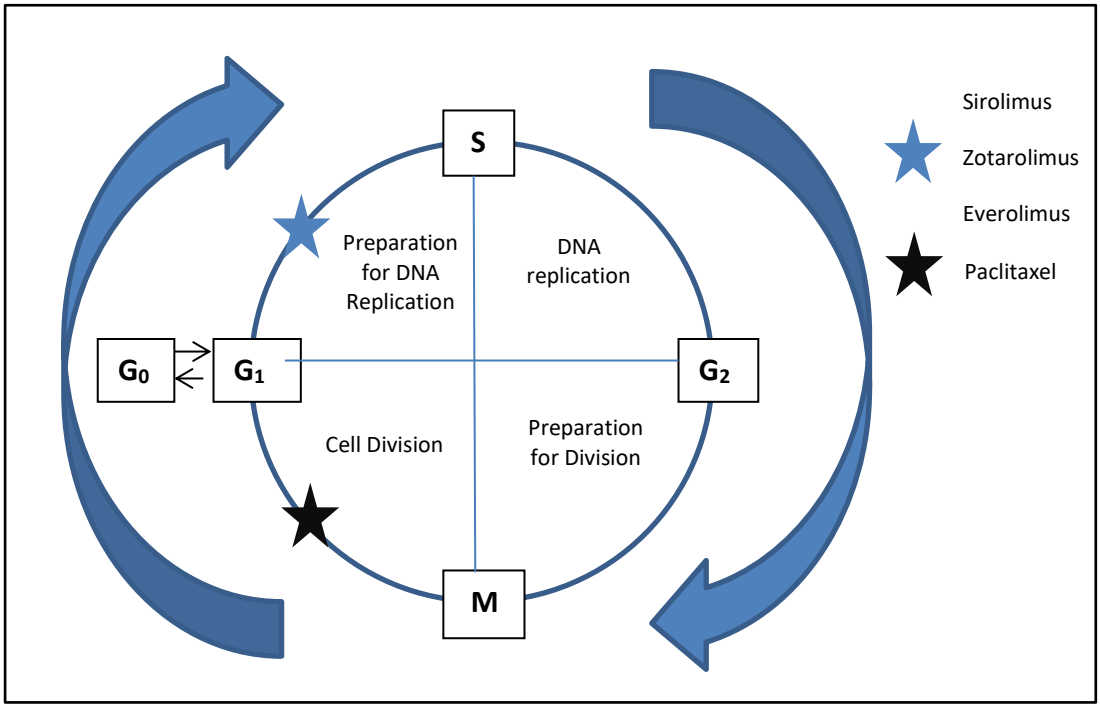

Figure 1-7: Image representing action of anti-restenosis drugs on cell cycle. Blue star indicates where cell cycle stops for sirolimus, zotarolimus and everolimus (G1-S phase). Black star indicates where cell cycle stops for paclitaxel (G1 – M phase). Image adapted from (Martin and Boyle, 2011).

1.4.8.6. New Pharmacological Approaches

Most DES currently on the market use antiproliferative and immunosuppressive drugs (everolimus, zotarolimus, paclitaxel) as the active component in their product. The emerging generations of DES also make use of these drugs with most alterations focused on the polymer and stent platform designs.

Antioxidative Agents

There have been reported links between oxidative stress and altered endothelial and smooth muscle cell function following stent implantation. These changes have the potential to cause restenosis, thrombosis and impaired endothelial function in the stented artery (Juni et al., 2013). The presence of an 'antioxidative agent' that has the potential to scavenge free radicals generated following stent implantation may be advantageous, reducing the negative effects following stent implantation (Watt et al., 2013).

More recently, a polymer free DES utilising the antioxidative agent probucol has been investigated (Massberg et al., 2011). This coating consisted of both sirolimus and probucol and was applied to the Yukon® BMS (Translumina). Clinical results showed that it was non-inferior to the Resolute ZES (Medtronic) in terms of incidence of stent thrombosis and in-stent late lumen loss at the 12 month time point (Massberg et al., 2011). Despite this initial trial, there does not appear to be any DES commercially available that contains an antioxidative agent and this area does not appear to be widely researched. Use of antioxidative agents in coronary stents is more extensively discussed in chapter 6.

1.4.8.7. Uniformity of Drug Elution

The surface of a DES has additional requirements to a BMS as it has to allow for a consistent dose of drug to be released at a controlled rate (Ranade et al., 2004). The ability of a drug to be delivered locally into the surrounding tissue has many advantages. As the drug eluting device will be in closer proximity to the target area, greater control of the administered dose is achievable. The increased contact with the surrounding tissue allows for a lower dose of the drug to be given, omitting the need for it to be delivered systemically. Consequently, there is decreased risk of toxicity to the patient (Lyndon et al., 2014).

The distribution of a drug from a DES is required to be uniform, allowing for transmural and circumferential distribution throughout the vessel (Dangas et al., 2010). Previous studies have used computational modelling to identify a number of variables that interfere with the uniformity of drug elution from a stent (Balakrishnan et al., 2005, Hwang et al., 2005). These variables included strut overlap, alterations in local blood flow and polymer damage.

The vessel wall coverage which is determined by the metal-to-artery ratio of the metal stent platform is also of great importance when considering the uniformity of drug distribution (Dangas et al., 2010). The under expansion of a stent would lead to a smaller stent surface area in contact with the vessel wall and consequently an impact on the drug release profile.

As previously mentioned, during the deployment of the DES, the polymer coating may become damaged. This has been reported for the Cypher™ stent (Johnson and Johnson), where SEM imaging indicated cracks in the coating along the edges of the stent struts. This damage has the potential to alter the drug release properties of the stent, subsequently changing its performance.

The responsibility of uniformity of drug elution partially lies with the application process of the drug and therefore the coating technologies associated with this. The newest coating technologies will be discussed in the following section.

1.4.8.8. Coating Technologies

Through the years, coating technologies have emerged from dip coating to spray coating. Most manufacturers produce the finished stent product on site in a variety of diameters and lengths and a specified dose of drug. Now the more advanced technologies allow the user to apply the specific drug coating to the stent themselves by portable machines provided with the stent product.

The Stent Coating Machine (SCM) was designed by Translumina to be used with their Yukon® microporous BMS platform. This coating technology allows different pharmaceutical agents to be applied to the stent surface with variable doses achievable and without the requirement of a polymer carrier. The drug is mixed with Ethanol and is applied to the stent by the spray nozzle in the sterile encased environment. The overall process of coating and drying the stent takes a maximum of 10 minutes depending on the size of the stent and can be implanted immediately into the patient. A big advantage of this process is the possibility of patient specific dosing, allowing the surgeon to decide upon drug type and dose for each individual patient depending on lesion type and condition.

1.4.9. Optimising Drug Release Profiles

In section 1.4 a variety of clinically relevant stents were discussed and an insight into their targeted mode of function and drug release properties were obtained. One important factor to note was the wide range of drug release profiles reported for each product. For example, the Endeavour™ ZES is reported to elute drug over a maximum of 21-22 days whereas the Cypher™ SES is over a period of 168 days. The drugs eluted from both of these stents are immunosuppressive drugs (zotarolimus and sirolimus), targeting proliferation of SMCs. Therefore, if they have the same target but are released over vastly different time frames, it can be suggested that the time course of restenosis is not fully understood.

Another example of the need for optimised drug release is the study by (Contractor et al., 2008). In this study, four Endeavour™ ZES were implanted into a patient's severely diseased left anterior descending artery (LAD). Restenosis was not noted in the patient until week eight

post implantation. As the Endeavour™ ZES has a total drug release time of 21-22 days, it is thought that the initial release of drug prevented restenosis during the early weeks but failed to prevent restenosis at the later time point.

It is therefore apparent that research still needs to be undertaken to further understand and improve upon the drug release period of DES. Hence, significant research is currently focused on optimisation of this aspect of stent design.

1.5. Effect of Surface Properties on Cell Behaviour

As has been discussed in previous sections, many clinically relevant stents have been designed to reduce neointimal formation and achieve rapid endothelial cell re-growth post stent implantation. The modes of function of these stents differ by many factors; stent platform, strut thickness, drug type, drug release profile and polymer type.

Until recently, there has been no commercially available stent that uses the surface topography or morphology to address the issue of neointimal healing. Translumina introduced the first coronary stent widely used in patients using surface topography to target improved endothelial healing (Yukon®). This product claims that its increased surface roughness and microporous structure is key to the product's success in improving re-endothelialisation (Dibra et al., 2005).

However, studies that investigate the growth of ECs on this specific microporous surface are lacking. Numerous clinical trials have been undertaken to assess the safety and effectiveness of this stent type, but it is also important to look into the indirect evidence using *in vitro* studies. This type of analysis allows the healing abilities of these medical products to be investigated at the cellular level and the influence surface properties may have.

There are other microstructured stents available, including the Bio-Freedom BA9 eluting stent by Biosensors International™ (see section 1.4.5.2 for details). It appears that the purpose of the Bio-Freedom stent microstructure is more so to encase the drug, with less emphasis by the manufacturer on the possible effect the microstructure has on re-endothelialisation. The stent has the microstructured surface on the abluminal side only which suggests its lack of influence on the effect the microstructures surface has on healing.

1.5.1. Surface Roughness

It has been suggested in the literature that the naturally occurring nano roughness of a vessel wall should be mimicked in order for an implantable material to integrate better with the surrounding tissue (Samaroo et al., 2008).

The study by Xu et al analysed the behaviour of human coronary artery endothelial cells (HCAECs) on Poly L- Lactic Acid (PLLA) surfaces of varied roughness (Xu et al., 2004). Results showed improved proliferation/adhesion of this cell type on 'smooth' solvent cast surfaces (R_{RMS} 137 ± 17 nm, scan size 50 μm x 50 μm) compared to the 'rough' electrospun surfaces (R_{RMS} 1557 ± 211 nm, scan size 50 μm x 50 μm). These surfaces had the same PLLA

concentration and only differed in production method (electrospun/solvent cast), making this study a good comparison for the behaviour of HCAECs on rough and smooth surfaces.

In another study which compared the effect of surface roughness on cell behaviour, HUVECs were grown on titanium surfaces of varied roughness (An et al., 2010). The numerical roughness was not specified in this study but improved proliferation and migration (MTT assay, time lapse microscopy) of the cells were noted on the 'smoother' surfaces (An et al., 2010).

The preferred growth of HUVECs on a smooth surface was reiterated by further findings in the literature (Stewart et al., 2012). In the study by Stewart et al, the smoother heparin doped polypyrrole surface proved favourable for the adhesion and proliferation of HUVECs in comparison to a rougher surface doped with alternative drugs. This further suggests that a smooth stent surface is desirable for the growth of HUVECs but also emphasises the influence of drug type.

In contrast to these reports, there are a number of studies in the literature that suggest increased surface roughness is preferential for improved EC growth and proliferation. A study by (Chung et al., 2003) suggested that an increase in surface roughness of $10^1 – 10^2$ nm does have an effect on the growth and proliferation of HUVECs. This cell type had a more pronounced adhesion/proliferation on surfaces with larger roughness (39.79 ± 10.48 nm/34.58 ± 9.89 nm) when compared to surfaces of lower roughness (20.10 ± 7.87 nm/ 18.63 ± 5.30 nm). The difference in surface roughness is at the nanometre scale which is relevant to this study and suggests that endothelial cells will have improved adhesion and proliferation on surfaces of larger surface roughness.

Another study looked into the effect of increased nano roughness on the behaviour of RASMCs (Rat aortic smooth muscle cells) and RAECs (Rat aortic endothelial cells) (Miller et al., 2004). In this study, it was found that both EC and SMC densities were seen to increase on surfaces of increased nano roughness.

These two studies (Chung et al., 2003, Miller et al., 2004) are in agreement with the clinically relevant stent by Translumina (Yukon®) that has a purposefully manufactured microporous structure with a large surface roughness to improve endothelial healing post stent implantation (Dibra et al., 2005).

Although studies have begun to look into the preferred topography to encourage rapid endothelial cell regrowth and discourage the proliferation of SMCs, most of the studies focus

on simply a ‘rough’ or a ‘smooth’ surface. The numerical roughness values of these surfaces are less commonly reported, leaving speculation as to what is classed as ‘rough’ or ‘smooth’.

These studies also emphasise the importance of the varying cell type. For example, the study by Miller et al reports increased density of RAECs on surfaces of larger roughness whereas the study by Xu et al reports improved HUVEC adhesion/proliferation on surfaces of smaller roughness. Additionally, not all of the studies report the numerical roughness, simply labelling them as ‘smooth’ or ‘rough’ so it is difficult to compare findings from different studies.

By identifying the roughness of surfaces that encourage the desired behaviour of ECs and SMCs, these findings could be used to contribute towards identifying the desired stent surface.

Although the surface roughness is a good measure of the overall topography of a surface, it does not provide information about the specific features on a surface, for example particle size. The study by (Samaroo et al., 2008) investigated the growth of RAECs on NiTi and it was found that the cells adhered best to the surface with the fine grain size (< 60 μm) and tended to migrate to the outer edges of the grains (fluorescent microscopy). Subsequently, the surface with the smaller grain size had a higher abundance of grains and therefore a larger number of cells on the surface. This suggests the possible influence of surface features on cell behaviour.

1.6. Summary of Clinical Challenges

More than 92,000 PCI procedures were carried out in the UK in 2013 which is more than two times greater than a decade ago (BritishHeartFoundation, 2015). This demonstrates the increasing demand for coronary stents that are capable of restoring blood flow to the cardiac muscle.

By obtaining information regarding cellular events following stent implantation and researching the most up-to-date technologies available to tackle negative impacts following stent implantation, the clinical challenges relating to stent design has become apparent. Rapid healing following stent implantation is necessary, enabling full coverage of the foreign body within the body and a smooth lining for blood flow. Therefore, a stent that promotes rapid re-endothelialisation is desirable. Stents must also to be suitable for all patients, including those with multi-vessel diseases and co-morbidities that may influence stent performance.

Current stent manufacturers are focussed on drug type, platform type and coating method. Surface roughness has been identified as a potential promoter of rapid re-endothelialisation (Dibra et al., 2005) but evidence at the cellular level is lacking. The surface topography of clinically relevant stents is also not well reported and therefore the true effect of stent surface topography on healing is not well understood.

1.7. Conducting Polymers

1.7.1. What is a Conducting Polymer?

Conducting polymers are electrically conductive polymers that are known for their uses in biosensors, gas sensors, rechargeable batteries (Ebrahimiasl et al., 2014) and have more recently sparked an interest with their potential use in drug eluting coatings. The main advantage of conducting polymers and the reason they are becoming increasingly popular in a variety of applications is that their electrical, chemical and physical properties can be specifically tailored to the requirements of a given application (Balint et al., 2014).

1.7.1.1. Use of Conducting Polymers in Medical Devices

In terms of their use in biomedical engineering, conducting polymers have been investigated for many applications, including tissue scaffolds, biosensors and neural probes. Such conducting polymers include Polyacetylene (PA), Polyaniline (PANI), Polythiopene (PTh), Polypyrrole (PPy) and Poly(3,4-ethylenedioxythiophene) (PEDOT) (Guimard N K et al, 2007). Their use in biomedical applications varies, with studies reporting PANI to cause chronic inflammation *in vivo*, deeming it unsuitable for many biomedical applications (Balint et al., 2014). Other conducting polymers such as Polythiopene derivatives (PTh, PEDOT) have proved more successful with their potential use in neural electrodes and heart muscle patches reported (Balint et al., 2014).

1.7.2. Polypyrrole

The conducting polymer, Polypyrrole (PPy), has been recognised for its good biocompatibility, chemical stability in air and water and stimulus-responsive properties. Its ease of synthesis and ability to entrap biological molecules which can be subsequently released into the body makes polypyrrole an attractive polymer for DES (Guimard et al., 2007).

1.7.2.1. Polypyrrole as a DES Coating

Over the years, interest in polypyrrole (PPy) as a coating for DES has developed, including an important study by (Arbizzani et al., 2007) which investigated polypyrrole coatings on platinum electrodes (Pt foils, Pt discs and Pt/quartz). This study investigated the use of salicylate and naproxene as anionic drugs to be incorporated into a PPy coating on Pt electrodes for DES applications. The study by (Okner et al., 2007) investigated polypyrrole coatings on stainless steel electrodes, for use in DES. The drug component of the coating was paclitaxel which is incorporated into the coating after the polypyrrole coating has been applied to the stainless steel by simple dip coating. Another study suggests the use of a PPy/salicylate coating deposited onto iron electrodes for use in coronary stents (Cysewska et al., 2015). From these studies, it is evident that PPy is flexible in terms of the metal it can be deposited on. Okner et al shows the suitability of PPy to form on stainless steel, a common stent platform which is relatively inexpensive compared to the Pt electrode reported by Arbizzani et al.

Another main advantage of using PPy as a DES coating is that the drug can be simultaneously incorporated into the coating during production. Arbizzani et al incorporates salicylate (Sa), an anti-inflammatory agent into the PPy coating. It is also possible to incorporate common DES drugs into the already formed polypyrrole coating as in the study by (Okner et al., 2007).

Despite these studies (Arbizzani et al., 2007, Okner et al., 2007), there are currently no commercially available DES that make use of this conducting polymer. Instead, polymers already widely recognised for their mechanical strength and biocompatibility are still the most commonly used. The studies mentioned in this section will be described in more detail in chapters 4 and 5.

1.7.3. Limitations of Polypyrrole as a DES Coating

As mentioned in previous sections, PPy has not yet been incorporated into a DES for clinical use. This is likely due to the limitations of this polymer, including sub-optimal drug release.

1.7.3.1. Sub-optimal Drug Release

Due to the ease of incorporation of biological molecules into polypyrrole, the uptake and release of a number of biological molecules has been investigated. Salicylates are recognised for use in cardiovascular disease, in the form of aspirin. They are also known to inhibit the

proliferation of SMCs (Marra et al., 2000) and would therefore be beneficial as a component of a DES coating. Salicylates can be easily incorporated into PPy coatings makes them an ideal choice for use in the present study The study by Arbizzani et al investigated the incorporation and subsequent release of anti-inflammatory agents naproxen and salicylate with polypyrrole coatings (Arbizzani et al., 2007). Despite the findings of this study that state the release of salicylate occurred over a 7-day period, it is apparent that more than 90% of the salicylate was released within 2 days. Although the effect of this release over a short period of time is unknown for restenosis, it is likely to be suboptimal for use in a DES. The release of a drug from a DES varies but most DES have release periods of at least one month (Arbizzani et al., 2007).

1.7.3.2. Lack of Topographical Information

As has been discussed, the surface topography of DES has been shown to be a potentially important driver of stent performance *in vivo* and in particular on the processes involved in endothelium recovery. It is for this reason that the surface topography and morphology of polypyrrole surfaces as a potential DES coating is of interest. There are few studies that provide information regarding the topography and morphology of polypyrrole surfaces in the literature (Paramo-Garcia et al., 2013, Mîndroiu et al., 2013). Additionally, the studies that are available, fail to combine their topographical findings with both drug release and cell culture studies and therefore lack a complete data set. It is of interest in this study to investigate the surface topography, drug release and biocompatibility of novel polypyrrole coatings as a potential DES coating.

1.8. Aims and Objectives

Coronary DES designs are constantly evolving, with current manufacturers focused on the development of stents that can inhibit restenosis without adversely affecting recovery of the endothelium. The stent coating, including drug type, platform type and coating method play a key part in the performance of a DES. It is essential that the correct material is selected and that this material can form a uniform coating that can provide adequate drug delivery but is also capable of withstanding the stresses of expansion within an artery without experiencing delamination or polymer fragmentation; events that could lead to inflammatory responses within the stented vessel and subsequent neointimal thickening (Virmani et al., 2004).

Amongst many different materials currently being investigated as stent coatings, conducting polymers, such as PPy, have particular promise. When incorporated through electropolymerisation, a drug can be simultaneously incorporated into the PPy coating during the coating process, potentially providing fine control over drug dose and elution kinetics. This process may also help overcome some of the other challenges associated with conventional stent coating methods, including variability in the production process, webbing during polymer deposition, as well as delamination and cracking of the coating during stent deployment.

Studies which have already investigated the potential of PPy as a DES coating report short drug release periods and biocompatibility relevant to cardiovascular applications is lacking (Arbizzani et al., 2007, Okner et al., 2008). The study by Arbizzani et al successfully coated Pt platforms with polypyrrole coatings containing various drugs, including the anti-inflammatory agent salicylate (Sa). From the study by Arbizzani et al, it was apparent that more that 90 % of the Sa was released from the coatings within 2 days, a short time when compared to drug release profiles from clinically relevant stents. The substrate type on which the coating was formed also differed from common DES platforms, and as such, the behaviour of the coating on a more relevant material was not determined. Okner et al investigated polypyrrole coatings on stainless steel electrodes whereby paclitaxel was subsequently incorporated by simple dip coating method. Although the use of stainless steel and paclitaxel enhances the clinical relevance of this study, the additional drug loading step compromises the fine control of dose and delivery kinetics that the method proposed by Arbizzani et al offers. Although the study by Okner et al did investigate the biocompatibility of the coatings by implanting the coated platforms subcutaneously into mice, neither study investigated the

compatibility of the coatings produced with endothelial cells. As a result, the potential of electropolymerised pyrrole to act as an effective stent coating remains unclear

The overall aim of the present study was therefore to develop and characterise a novel PPy coating containing the anti-inflammatory agent, salicylate (Sa) on stainless steel wire and to assess its potential for use as a novel DES coating. Informed by findings from a review of the literature, this study was focused on characterising four key aspects of the PPy/Sa coatings produced and these are detailed below.

Surface Topography

A number of studies have suggested that there is a link between surface roughness and endothelial cell behaviour (Chung et al., 2003, Liliensiek et al., 2010, Xu et al., 2004). Surface topography has previously been considered for use in coronary stent design (Palmaz et al., 2002) and is becoming of increasing interest (ter Meer et al., 2017) but it is only recently that surface topography has been integrated into stent design for widespread clinical application (Dibra et al., 2005). In this context, surface roughness has been identified as a potential promoter of rapid re-endothelialisation. Given this, it was important that the surface topography of the novel polypyrrole coatings produced in the present study were characterised and could be compared to the topography used in existing stent platforms. However, from a review of the literature, it become apparent that information on the surface topography of clinically relevant stents is rarely published, with studies focusing more on their performance *in vivo* and drug elution characteristics. Where information has been published, methodological differences makes comparisons of the data between studies difficult.

The first objective of this study, as is addressed in chapter 3, was therefore to characterise the surface topography and morphology of a range of clinically relevant stents. By analysing the surfaces of stents which have demonstrated clinical safety and efficacy, a benchmark could be set, against which the polypyrrole coatings produced later on in the study could be compared. This also allowed a period of method development to take place, in order to ensure that the surface analysis techniques were optimised, before their use in subsequent parts of the study. For selected DES investigated in this chapter, it was also decided to investigate if drug elution from these surfaces leads to changes in surface characteristics, as any change could potentially influence cell behaviour. The final objective of chapter 3 was to investigate the adhesion and proliferation of porcine endothelial cells onto BMS of distinct surface roughness. This was with the view that insight into the potential healing properties of clinically used stents may be gained, with the influence of surface roughness on the behaviour of endothelial cells further

investigated. Furthermore, this could prove useful in the evaluation of the PPy coatings subsequently produced.

The surface morphology and topography of PPy coatings is not widely reported in the literature and with the link between surface topography and cell behaviour, one of the objectives of chapter 4 was to investigate the surface topography and morphology of a novel Polypyrrole/Salicylate (PPy/Sa) coating through AFM and SEM.

Drug Release

In contrast to information on surface topography, there is a wealth of information within the literature on drug release kinetics from DES ((Venkatraman and Boey, 2007, Acharya and Park, 2006, Papafaklis et al., 2012). It is clear from this that the optimal release profile and duration are dependent on the mechanism of action of the drug that is being released. For this reason, it was important that this study investigated if electropolymerisation could be used to provide different release profiles and durations of drug. The work detailed in chapter 4 therefore sought to characterise the release of salicylate from the range of PPy stent coatings produced. Electropolymerisation was performed either potentiostatically or galvanostatically and the impact of these two different methods on the release kinetics and the surface topography was explored.

Vascular Biocompatibility

As a potential DES coating, it is important to assess the biocompatibility of the novel PPy/Sa coating. There are studies that show the biocompatibility of PPy in many forms (Garner et al., 1999, Stewart et al., 2012), but few have been relevant to cardiovascular applications (Jakubiec et al., 1998). Furthermore, the biocompatibility of the novel PPy/Sa coating from the present study has not been analysed. This will be investigated in chapter 5 through cell culture studies with porcine endothelial cells and analysed by live/dead staining and cell viability assay.

Antioxidant Activity

Amongst many different approaches to improve healing post stent implantation, studies have reported links between oxidative stress and altered endothelial and smooth muscle cell function following stent implantation (Kochiadakis et al., 2010, Pendyala et al., 2009). These changes have the potential to cause restenosis, thrombosis and impaired endothelial function in the stented artery. As such, the presence of an ‘antioxidative agent’ that has the potential to

scavenge free radicals generated following stent implantation, subsequently reducing oxidative stress may be advantageous (Watt et al., 2013).

Polypyrrole has been recognised for its antioxidative properties in many forms (Ebrahimiasl et al., 2014, Hsu et al., 2008) but it was found that this has not been investigated for use in coronary stents to specifically target the negative implications associated with the occurrence of oxidative stress following stent implantation. It was therefore the final aim of this study, as will be addressed in chapter 6, to investigate the antioxidative activity of a novel PPy/Sa coating for potential use as a coronary stent coating, by method of DPPH assay. This could further enhance the PPy/Sa coating for use in DES.

The aims of this study can be broken down into four broad objectives that will be presented in each chapter as indicated below.

1. Investigate the surface topography of commercially available stents and the impact surface topography could have on the growth of endothelial cells. (Chapter 3)
2. Develop and characterise polypyrrole coatings for potential use as a DES coating. (Chapter 4)
3. Investigate the biocompatibility of polypyrrole/salicylate coatings by analysing the growth of ECs onto the coatings. (Chapter 5)
4. Analyse the antioxidative properties of polypyrrole/salicylate coatings. (Chapter 6)

Chapter 2

2. Materials and Methods

Chapter 2 will outline the theory behind the experimental methods used in this study. Initially, the theoretical workings of the Atomic Force Microscope and Scanning Electron Microscope used to analyse the surface topography and morphology of materials in this study will be discussed. This will be followed by the electropolymerisation method used to produce a novel polypyrrole coating. Finally, this chapter will conclude with cell culture techniques and cell viability assays used to analyse cell behaviour on various surfaces in this study.

2.1. Atomic Force Microscopy (AFM)

Atomic Force Microscopy (AFM) is an imaging technique, capable of achieving surface images at the nanometre scale. The main feature of the AFM is the sensitive cantilever that is scanned over the sample, building up a map of the sample's surface topography. There are three main features that make up the AFM; piezoelectric transducer, force transducer and feedback control. The piezoelectric transducer is responsible for the movement of the cantilever tip over the sample and the force transducer senses the force between the cantilever tip and the sample surface (Eaton and West, 2011). It is the feedback control that maintains a constant force between the cantilever tip and the sample surface, by feeding the signal received from the force transducer back to the piezoelectric. This controls the expansion of the z piezoelectric transducer and the variation in the value provides a measure of the sample topography. The raster-like pattern produced during scanning is controlled by the x-y piezoelectric elements.

The AFM used in this study was the MP3D AFM (Asylum Research, Santa Barbara) (see Figure 2-1 for schematic representation). This particular AFM relies upon a superluminescent diode (SLD) to supply columnized light to the back of the cantilever. This light is reflected back from the cantilever and detected by the position sensitive diode (PSD). The PSD sends a voltage value to a feedback loop that has been programmed to maintain a set-point value.

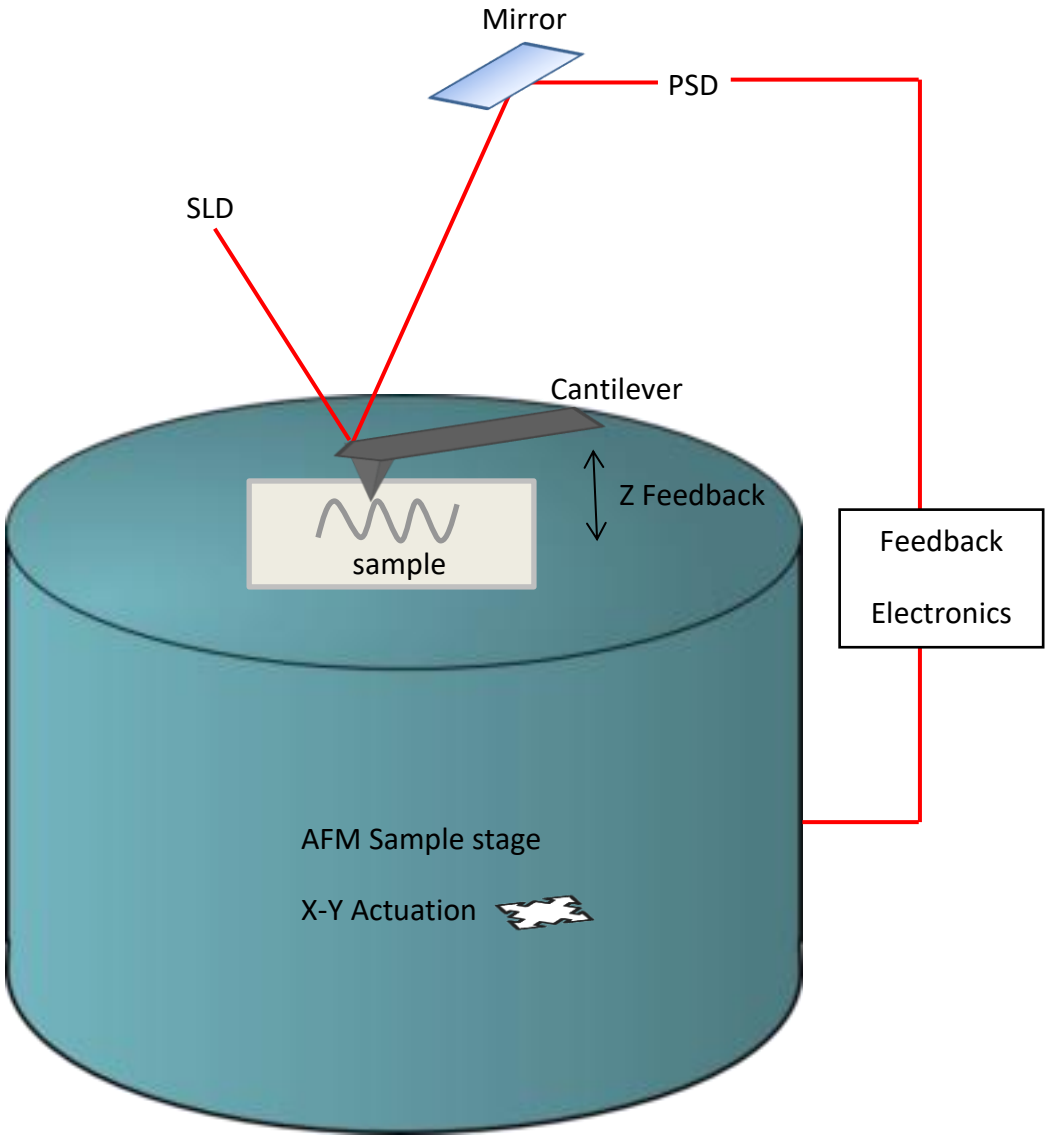

Figure 2-1: Schematic representation of the AFM used in this study. Image adapted from (MP3D AFM manual, Asylum Research). SLD: superluminescent diode, PSD: position sensitive diode.

2.1.1. Topographical Characterisation Modes

There are various modes in which an AFM can operate to obtain information on the surface topography of a sample, including contact mode and intermittent contact mode (tapping mode).

2.1.1.1. Contact Mode

In contact mode, the cantilever tip lightly touches the sample surface and is raster scanned over the sample. As the cantilever tip approachaes the surface, a brief 'attractive force' is experienced as the tip jumps into contact with the surface. The cantilever is lowered further towards the surface whereby the tip is now applying a force to the sample and the sample is applying an oppostie force to the tip (repulsive force) (Eaton and West, 2011). The vertial deflection of the cantilever is measured by the PSD, providing an indication of the local height of the sample (Fuierer, 2009). In this mode, the tip is constantly in contact with the sample surface.

2.1.1.2. Intermittent Contact Mode (IC-AFM)

In intermittent contact mode (tapping/AC mode), the cantilever oscillates over the sample and the amplitude of the oscillation is used as the feedback signal. The cantilever tip intermittently makes contact with the sample and is not dragged over the samples surface as in contact mode. The cantilever tip passes from the zero force regime to attractive regime and into the repulsive regime. The repulsive forces between the sample and the cantilever are measured by the PSD and, as in contact mode AFM, provide the local height of the sample (Fuierer, 2009).

Contact Mode Vs Intermittent Contact Mode

Contact and intermittent contact mode are common AFM modes with advantages and disadvantages existing for both. One of the advantages of intermittent contact mode is that the tip is moved perpendicular to the surface during scanning, resulting in the almost complete elimination of lateral forces (Eaton and West, 2011).This is in comparison to contact mode whereby the lateral forces are experienced as a result of constant interaction between the tip and sample, causing the cantilever to move horizontally which can lead to sample drag and damage to the sample surface.

Another advantage of intermittent contact mode is that the tip is able to pass through the so called 'contamination layer' on the sample (Eaton and West, 2011). The forces experienced between the tip and the surface are governed by the capillary forces between the tip and the 'contamination layer'. In intermittent contact mode, the tip is removed from the surface after each cycle and re-engaged, allowing it to make contact with and scan the true surface (see Figure 2-2 for visual example).

Despite contact mode being the fastest topographical mode due to the deflection of the cantilever leading directly to the surface topography, the advantages of intermittent contact mode discussed above make it the preferred mode for this study.

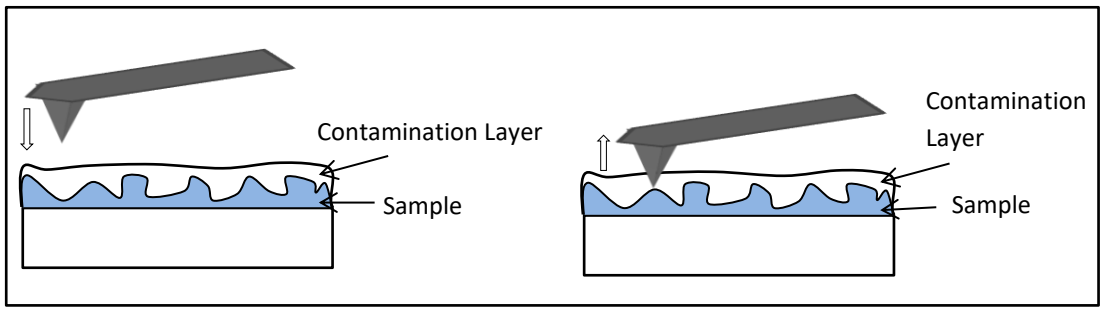

Figure 2-2: Schematic image shows probe passing through 'contamination layer' to sample surface in intermittent-contact-mode. Image adapted from (Eaton and West, 2011).

2.1.1.3. Phase Imaging (PI-AFM)

Phase imaging is performed by AFM in intermittent contact mode and can be used to analyse the homogeneity of a surface. When performing a topography height retrace scan on a sample, the cantilever is operated at or near its resonant frequency, corresponding to 300 kHz for the cantilevers used in the present study. In phase imaging, the movement of the probe can be characterised by monitoring the phase shift between the driven oscillation of the cantilever and its response. A shift in the phase signal arises from a difference in the energy dissipation between the tip and the sample (James et al., 2001).

A shift in phase angle of the oscillating probe is sensitive to the material properties of the sample surface and has been linked to changes in surface adhesion, mechanical properties and surface charge (Scott and Bhushan, 2003, Magonov et al., 1997, Eaton and West, 2011). Tip to sample contact area, which is influenced by topographical features, can indirectly influence a shift in phase angle (Eaton and West, 2011). This can subsequently lead to a shift in phase angle on the resultant image when no difference in the material's properties is necessarily

apparent. By overlaying a phase image onto a height retrace image, a better representation of the sample surfaces can be identified.

Furthermore, a shift in phase angle on its own cannot be used to qualitatively measure changes in material properties. Therefore, in the present study, the shift in phase angle is used to indicate areas of different mechanical properties of the surface. This may distinguish between areas of drug and polymer and can allow for the difference between polymer phases to be identified. This technique is of particular interest for drug eluting stents as it can be used to provide insights into the mechanisms governing drug release from polymer coated stent surfaces. It has previously been used to analyse the polymer coating on a Taxus^{TM} DES, in order to distinguish between a polymer and a drug and how this may change over the drug elution period (Ranade et al., 2004).

2.1.2. Cantilevers and Probes

A typical AFM cantilever has a probe at its end which makes contact with the sample surface. The geometry of this probe is vital to obtain an accurate AFM image and if the probe becomes blunt when in use, a poor image will be obtained. For example, if the probe is not able to reach the bottom of a 'surface pit' or does not have the ability to accurately scan the sides of a particle, an incorrect sample geometry of the sample will be obtained.

2.1.2.1. Silicon Nitride (Si_3Ni_4)

The most commonly used AFM cantilevers are composed of silicon or silicon nitride (Eaton and West, 2011). Silicon nitride generates probes of a low force constant, typically 1 Nm^{-1} and can be used in both contact and non-contact mode.

However, these cantilevers are recognised for having residual stress, leading to curvature along their primary axis. Silicon nitride cantilevers are also known for their poor reflectivity and are consequently coated with gold on the rear side. This improves the reflection of the laser beam which is responsible for the detection of the cantilever deflection (Friedrichs et al., 2013). A disadvantage of the gold coating is that the cantilever becomes more responsive to slight temperature changes, leading to increased thermal drift and increased difficulty for thermal equilibration.

2.1.2.2. Silicon (Si)

Silicon probes tend to have less residual stress than those composed of silicon nitride and consequently do not suffer from bending. An important limitation of silicon probes is that they are easily damaged on contact with the surface, which once damaged can lead to an inaccurate image.

The probes used in this study were Silicon with an Aluminium coating (AC160TS, AC160TS-R3, Olympus). These probes were rectangular in shape with a sharpened tetrahedral tip (radius 7 nm, length 14 µm).

2.1.3. Atomic Force Microscopy Parameters

2.1.3.1. Scan Size

Scan size, can points and scan lines are all important features when achieving an accurate AFM image. To identify the most suitable scan size for the sample, the equation for calculating pixel size should be considered (see Equation 2-1).

$$Pixel\ Size\ =\ Scan\ Size\ /\ Number\ of\ Pixels$$

Equation 2-1: Equation relating pixel size, scan size and number of pixels for AFM imaging (Grobelny et al., 2009).

The number of pixels is associated with the resolution of the final image, with most studies using at least 256 pixels. For higher resolution images and for visualisation in 3D, the number of pixels is often increased to 512.

Sample features that are below the calculated pixel size will not be visible at the specified scan size. From previous studies in the department concerning SEM imaging of stainless steel plates, the image features ranged from 3 µm – 10 µm in width (Reay, 2012). As a result of this, when imaging these samples, the pixel size cannot be any less than 3 µm. A similar study in the literature (Abbott et al., 2006) successfully analysed stainless steel alloys by AFM imaging, using a scan size of 50 µm and 256 pixels.

For imaging other materials, such as DES in this study, their surface features are likely to be smaller and the scan size should be adjusted accordingly for each sample. For example, the study by (Ranade et al., 2004) used a scan size of 1 µm in order to visualise the pores created on the surface of a paclitaxel eluting stent, following drug release. In the present study, number

of pixels was maintained at 256 and scan size varied (1 µm – 20 µm) depending on surface features.

2.1.3.2. Scan Rate

In AFM, the scan rate is the frequency of the raster-scan movement of the cantilever across the sample. A larger scan rate can be used when imaging soft samples in comparison to harder samples. This is because the cantilever deflection experienced tends to be less for soft samples than for harder samples, meaning an accurate scan can be obtained in a shorter period of time (Gopalakrishnan et al., 2011). It is true that working at a slower scan rate can allow the feedback to keep up with the image features but too slow a scan rate can produce image artefacts as a result of drift. For the different materials investigated during this study, scan rates in the range 0.25 – 1 Hz were used.

2.1.4. Data Analysis

AFM analysis allows for a variety of information on the surface characteristics to be collected. The key measurements made in this study are described briefly below.

2.1.4.1. Surface Roughness

Average roughness (R_a) and Root Mean Squared roughness (R_{RMS} or R_q) are commonly used to report the roughness of a given surface. The values are often quite similar, however, R_{RMS} is more sensitive to outlying points such as large peaks, resulting in a larger value where these occur. See Figure 2-3 for visual representation of the two values.

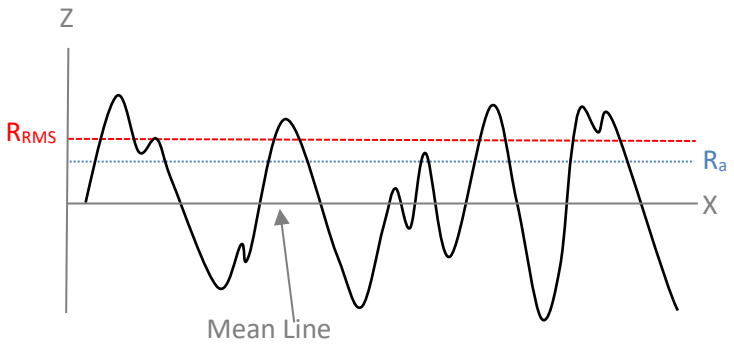

Figure 2-3: Schematic representation of the difference between R_a and R_{RMS}. Red dashed line shows the inclusion of larger peaks in data collection. Blue dotted line represents data included in calculation of R_a values, excluding large peaks. Grey line indicates mean line. Image adapted from (Rubert&CoLtd).

Root Mean Squared Roughness (R_{RMS})

R_{RMS} is a term used to express quantitatively the root mean square average of the roughness profile ordinates and can be obtained from the AFM software (see Equation 2-2). Larger values of R_{RMS} are indicative of a higher surface roughness.

$$R_{RMS} = \sqrt{\frac{1}{N}\sum_{i=1}^{N} Z_i^2}$$

Equation 2-2: Equation used by AFM software to calculate the Root Mean Squared (RMS) roughness where N is the number of 'sampling points' (i.e image pixels, therefore in this case $N= 256^2$), Z_i is the height at a given pixel i.

2.1.4.2. Peak-to-Valley (R_y) Distance

The R_y value is a measure of the distance between the highest and the lowest point in the sample area (Cech et al., 2013). The value of peak-to-valley distance (R_y) is greatly dependent on each individual sample point and can be indicative of a defect present on the surface, such as a deep scratch. This is important when analysing stent surfaces as a coating defect could have a major implication on performance of the stent following implantation. In addition to this, when imaging a microporous surface, the value of peak-to-valley distance can give an insight into pore depth.

2.1.4.3. Surface Area (SA)

The surface area (SA) is the area of the surface (X µm x Y µm), taking into account the Z position per XY (Fuierer, 2009). This was calculated by the Asylum Research software and presented in μm^2 in the present study.

The values of $R_{RMS,}$ R_y and SA have all been used to provide quantitative measures of the surface properties of stents and polypyrrole coatings investigated in this study.

2.1.4.4. Kurtosis

Kurtosis (Ku) is a measure of the peaks on a surface and can be obtained from the AFM software (see Equation 2-3). A large kurtosis value (>3) indicates few high peaks or very low valleys whereas a low (<3) or negative kurtosis value indicates more moderate surface features with few peaks present (Eaton and West, 2011). In the present study, this parameter may indicate the presence of large peaks of drug on a surface.

$$R_{ku} = \frac{1}{N}\sum_{i=1}^{N}\left(\frac{Z_i - \bar{Z}}{\sigma}\right)^4 - 3$$

Equation 2-3: Equation used by AFM software to calculate Kurtosis (Ku) where Z_i is the height at a given pixel i, N is the number of 'sampling points' (i.e image pixels, therefore in this case N= 256^2), $\bar{Z}$ is the average height of the entire image, σ is standard deviation.

2.1.4.5. Skewness

Skewness (Sk) is a measure of the asymmetry of the distribution of heights within the surface, obtained by the AFM software (see Equation 2-4). A value of zero indicates a random variation. A positive value indicates a flat surface with height values considerably above average whereas a negative value indicates the presence of pits and depressions with height values considerable below average (Eaton and West, 2011).

The values of kurtosis and skewness will be used to identify the presence of peaks and pores due to the release of drug from DES coatings.

$$R_{sk} = \frac{1}{N}\sum_{i=1}^{N}\left(\frac{Z_i - \bar{Z}}{\sigma}\right)^3$$

Equation 2-4: Equation used by AFM software to calculate Skewness (Sk) where Z_i is the height at a given pixel i, N is the number of 'sampling points' (i.e image pixels, therefore in this case N= 256^2), $\bar{Z}$ is the average height of the entire image, σ is standard deviation.

2.2. Scanning Electron Microscope (SEM)

2.2.1. Principles of Operation

Scanning Electron Microscopy (SEM) is an imaging technique that produces magnified images of a surface by scanning it with a focused beam of electrons under vacuum (10^{-5} – 10^{-11} Torr) (see Figure 2-4 for schematic representation). A vacuum is required as electrons will rapidly disperse or scatter when in contact with molecules. A narrow beam of electrons, accelerated from the cathode, is passed through several electron lenses and is then brought to a focus on the surface of the sample. The electron lenses are positioned in such a way so as to ensure the diameter of the focused beam is very small (~ 5 nm). The scanning coils create a magnetic field using fluctuating voltage, allowing the movement of the focused beam of electrons back and forth over the sample (Oatley, 1972).

When the electron beam hits the sample, secondary electrons are dislodged from the sample surface. These secondary electrons are slow moving and negatively charged, making them easily detected by the positively charged secondary electron detector. The data from the secondary electron detector is taken to the amplifier and the output from this amplifier controls the brightness of the spot on the cathode-ray tube. The great attractive force between the secondary electrons and the detector allow electrons to be pulled towards the detector from a wide area and from around corners. This gives the resultant image a 3D-type appearance (I.S.U.ofScience/Technology, 2013).

Electrons that emerge through the surface by which it entered the sample are referred to as back scattered electrons and also contribute to the final image. In order to increase the magnification of the image, the electron beam simply scans a smaller surface area. As the sample is scanned, the variation in surface morphology is represented in the electron current collected by the plate and subsequently, the brightness of the cathode-ray tube spot (Oatley, 1972).

To operate the SEM, a sample is secured to the sample holder by adhesive tape (carbon) that ensures complete conductance from the surface of the sample to the sample holder. As the tape is adhesive, it also secures the sample in place when the vacuum is applied.

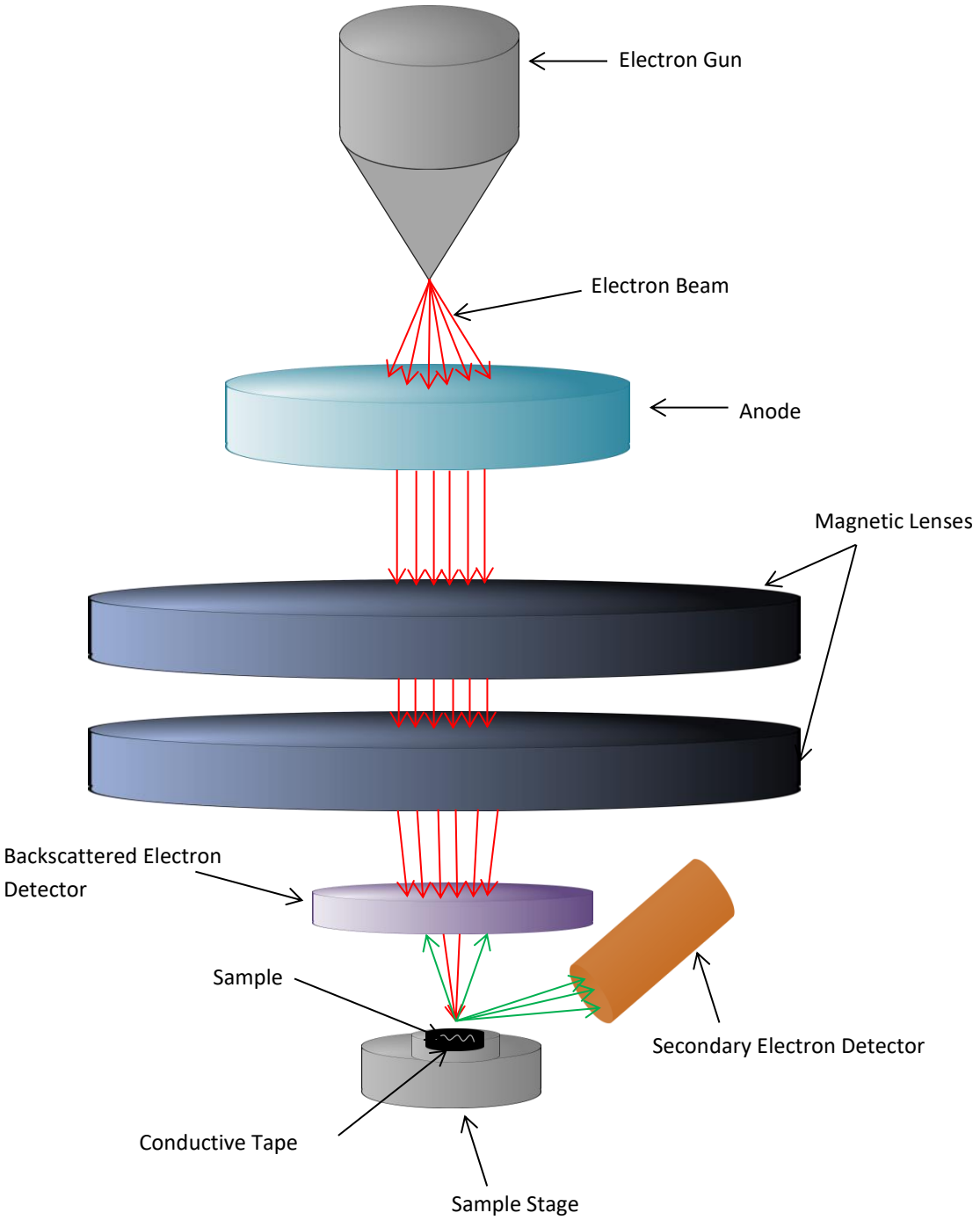

Figure 2-4: Schematic representation of SEM microscope. A narrow beam of electrons, accelerated from the cathode, is passed through several electron lenses and then brought to a focus on the surface of the sample.

2.2.2. Sample Preparation

2.2.2.1. Sputter Coating

Scanning electron microscopy is ideal for imaging electrically conductive materials that can withstand interaction with the high energy beam of electrons. Polymers are long chains of repeating units, mostly comprising of elements of low atomic number, including carbon, hydrogen, nitrogen, and oxygen. They are generally non-conductive materials and during SEM imaging their repeating chains have fewer interactions with the electron beam, yielding an image of poor resolution.

To counteract this problem and to obtain accurate images of non-conductive materials, the samples are often sputter coated with a metal, such as gold by a technique involving Physical Vapour Deposition (PVD). The vacuum chamber is filled with Argon and a high voltage is applied, creating a glow discharge. This causes the bombardment of Argon ions to the gold surface, resulting in the ejection of sputtering gold (see Figure 2-5 for visual representation). The sputtered material will form a layer on the sample of nanometre thickness.

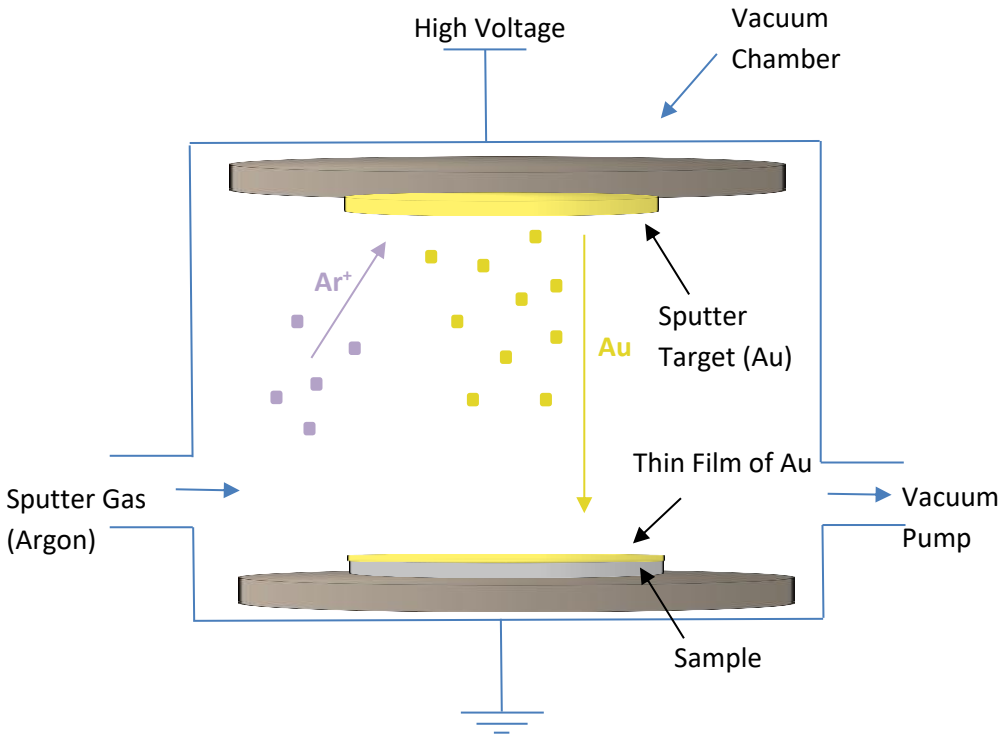

Figure 2-5: Schematic representation of the Particle Vapour Deposition (PVD) equipment. Au indicates gold atoms and Ar^+ indicates positive Argon ions.

2.3. Electropolymerisation of Polypyrrole

2.3.1. Principles of Operation

There are several known methods for the polymerisation of conducting polymers, including layer-by-layer assembly, emulsion, chemical polymerisation and electrochemical polymerisation (Shi and Zhitomirsky, 2010). Electrochemical polymerisation of conducting polymers is the chosen method in this study. With the use of electrochemical polymerisation, a film of thin composition is easily deposited on the surface which is a main advantage over chemical polymerisation. A thin layer is desirable for a stent coating as it minimises the bulk of the stent and consequently the negative impact on the vessel wall (Okner et al., 2007). This is another reason why electrochemical polymerisation would be preferential over chemical polymerisation for DES manufacture.

With the use of electrochemical polymerisation, doping is also simultaneous, allowing for the incorporation of molecules into the coating at the time of synthesis. This allows for less processing steps; an advantage when considering the potential future commercialisation and clinical application of the technique.

2.3.1.1. Electrode System

The electrochemical polymerisation (electropolymerisation) of conducting polymers can occur by three separate methods; potentiostatic, galvanostatic or cyclic voltammetry. Potentiostatic electropolymerisation is whereby a fixed voltage is applied to a three electrode setup whereas for galvanostatic polymerisation, a fixed current is applied to a two electrode setup. In cyclic voltammetry, the potential of the working electrode is cycled and the resultant current measured. Electropolymerisation is only suitable for conducting polymers whose monomer can readily undergo oxidation when an electrical potential is applied. The reason for this is that the electrical current supplied in the reaction allows for the monomer to deposit and oxidise on the working electrode (WE), resulting in the formation of insoluble polymer chains.

In an electropolymerisation reaction, the working electrode (WE) is the material to be coated. The purpose of the counter electrode (CE) is to close the electrical circuit and it is usually composed of an inert material such as graphite or in this case Platinum (Pt). The current flows between the CE and the WE. To eliminate any limiting factors regarding the kinetics of the reaction, the surface area (SA) of the CE should be larger than the SA of the WE. Lastly, as

its name suggests the reference electrode is a source of reference in the reaction and has a defined and stable electrode potential (Metrohm, 2011).

Potentiostatic Electropolymerisation

For the potentiostatic electropolymerisation method used in this study, the experimental set up consisted of three electrodes (WE, CE, RE) and was controlled by a potentiostat/galvanostat (PGSTAT, SI 1287, Solartron Analytical, Hampshire, England). The three electrodes were immersed into the electrolyte solution containing the monomer/dopant and the applied potential was controlled by a PGSTAT. Over a period of time, the polymer/dopant coating formed on the surface of the working electrode.

See Figure 2-6 for a visual representation of the potentiostatic electropolymerisation experimental setup used in this study.

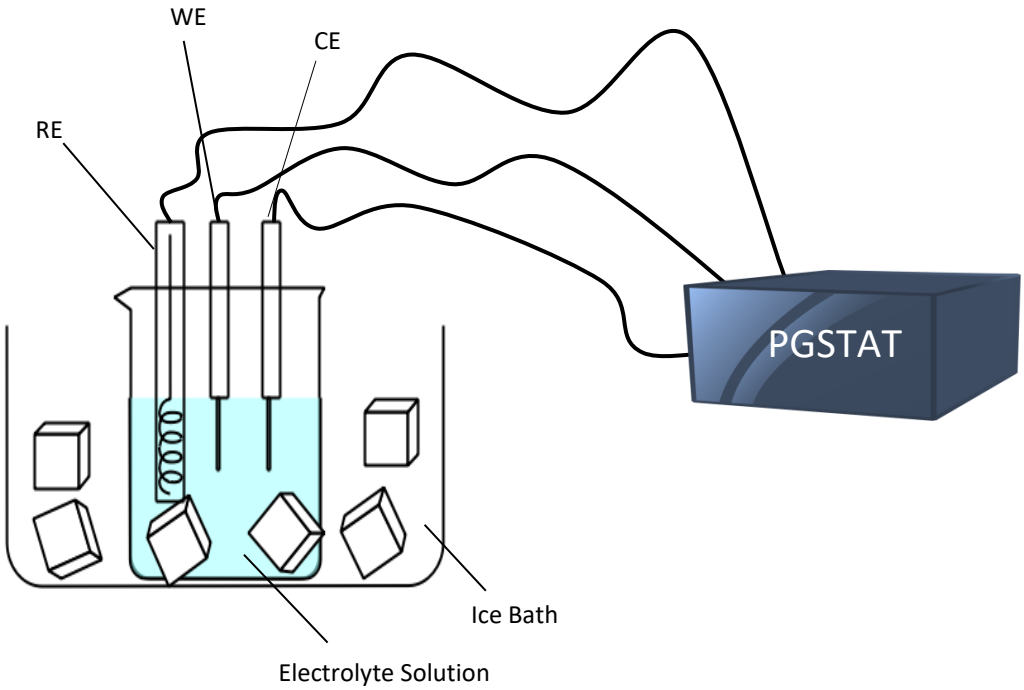

Figure 2-6: Visual representation of the experimental set-up of the electropolymerisation procedure. RE – reference electrode (KR5), CE – counter electrode (Pt), working electrode – SS wire. Electrolyte solution – Pyrrole/H_20/Sodium Salicylate.

Galvanostatic Electropolymerisation

In the galvanostatic electropolymerisation method used in this study, there were only two electrodes present (WE and CE), eliminating the RE. The current flow between the WE and the CE was controlled by the PGSTAT and the potential difference between the RE and WE was continuously monitored.

See Figure 2-7 for a visual representation of the galvanostatic electropolymerisation experimental setup used in this study.

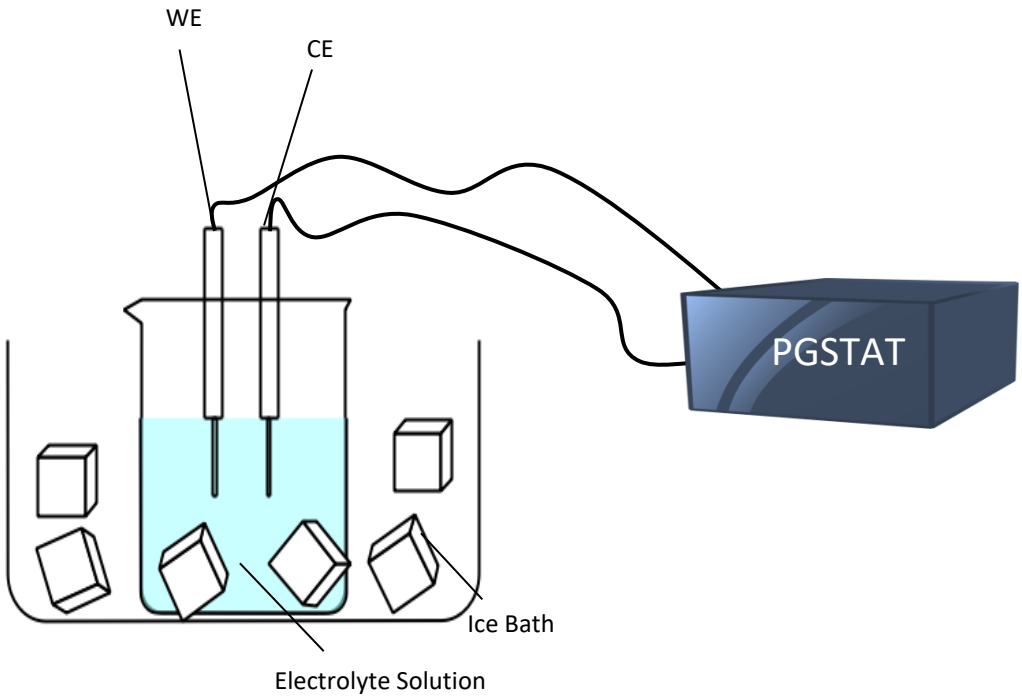

Figure 2-7: Visual representation of the experimental set-up of the electropolymerisation procedure. CE – counter electrode (Pt), WE-working electrode (SS wire). Electrolyte solution – Pyrrole/H_20/Sodium Salicylate.

2.3.1.2. Electropolymerisation Conditions

As reported in the literature (Guimard et al., 2007), there are a number of variables that are responsible for the film morphology, mechanics and conductivity of the deposited layer on the WE . These include electropolymerisation duration, temperature, electrolyte, electrode system and deposition charge.

Electrolyte Solution

The electrolyte solution is made up of a monomer, dopant ion and solvent. The concentration of the monomer in the electrolyte solution is an important factor to consider and has implications on the resultant coating. The effect of monomer concentration on the morphology of a PPy coated Mg alloy was reported by (Srinivasan et al., 2013). The findings showed that a uniform coating was obtained with a monomer (Pyrrole) concentration of above 0.2 M. For concentrations below this, the coatings achieved were uneven, suggesting that a higher monomer concentration leads to a more uniform coating.

However, the monomer concentration is not the only component in an electrolyte solution to influence the resultant coating and is often varied when coupled with different dopant ions. The study by (Arbizzani et al., 2007) used a range of Py concentrations (0.1 M– 0.07 M) with various dopant ions (sodium salicylate (NaSa), sodium toluenesulphonate (NaTS), naproxen(Np)). Doped PPy coatings were produced on Pt electrodes by potentiostatic electropolymerisation at 0.8 and 0.9 V.

In the present study, a solution of Pyrrole (0.1 M, monomer), Sodium Salicylate (0.1 M, dopant ion) and distilled water (solvent) was used. This was based on the study by Arbizanni et al and has previously been used in the department (Reay, 2012) to produce PPy coatings of good characteristics on to stainless steel.

pH of Electrolyte Solutions

The pH of the electrolyte solution is known to have an impact on the rate of deposition of PPy onto a working electrode during the electropolymerisation process. In acidic conditions, the rate of polymerisation is faster, slows at a neutral pH, and no polymerisation occurs at an alkali pH (Svirskis et al., 2010). The pH of the electrolyte solution in this study was maintained at acidic conditions (pH 6.30).

Purification of Monomer

Pyrrole is air and light sensitive and the accumulation of reaction products such as polypyrrole and amine oxides over time leads to a change in colour from transparent to yellow/brown. The presence of these impurites may have an influence on the resultant coating, including its composition. The literature often reports the use of single, double or even triple distilled pyrrole, eliminating the presence of impurities, creating a more accurate study (Arbizzani et al., 2007). The pyrrole used in this study was single distilled and stored under an inert atmosphere (N_2) prior to use.

Temperature

The temperature of the electrolyte solution is thought to have an effect on the regularity of the PPy coating. Initial experiments were attempted at room temperature (~22 °C) and surrounded by an ice bath (4 °C). SEM analysis found the coatings produced at the lower temperature (4 °C) to have more uniform coatings, therefore, the lower temperature was used for this study.

Mixing

Electrolyte solutions are often agitated during electropolymerisation to aid the dispersion of its components and ultimately create a more uniform coating. This can be obtained by using a rotating working electrode but this method is expensive and often only suitable for a specific electrode, making it impractical for this study. Alternatively, the use of a magnetic stirrer and a stirrer plate to aid solution agitation is a convenient and inexpensive method that allows the electrolyte solution to be agitated at a constant rate. This method has been previously used in the literature (Zhou and Greenbaum, 2010, Nam et al., 2013).

Dopant

During electropolymerisation, the size and nature of a dopant ion influences the way in which it is entrapped and subsequently released from the polymer. Dopant ions of larger size are thought to be physically trapped in the conducting polymer, making them more stable within the structure. A consequence of the increased stability of the compound is that the large molecules are not readily leached out under the desired conditions. On the other hand, small dopant molecules leach out more readily and are more likely to interact with ions in the surrounding environment. This is an important factor to consider in terms of use in DES, as the rate at which the drug is released from the polymer coated stent surface into the surrounding tissue can significantly impact upon device efficacy and performance (Venkatraman and Boey, 2007).

It is thought that dopant size can also have an effect on the morphology of the resultant PPy surface (Zhang et al., 2006). For example, the study by Shi et al found that PPy films prepared with sodium salicylate (NaSa) had a larger surface roughness than those prepared with tiron, a smaller molecule (Shi and Zhitomirsky, 2010).

2.3.1.3. Pre-treatment of Stainless Steel Working Electrode

Pre-treatment of the working electrode for electropolymerisation is widely reported in the literature, with various methods noted. Consistent with the literature is the use of carborundum powder (silicon carbide, SiC) to pre-treat stainless steel stents as working electrodes (Okner et al., 2009, Domb, 2008). The study by Okner et al pre-treated the working electrode (stent), increasing the surface roughness from 1.18 nm (scan size 2 μm, before treatment) to 28.6 nm (scan size 2 μm, after treatment). It was observed that the increase in surface roughness led to better adhesion of the N-pyrrole derivatives during electropolymerisation.

Another study by (Leprince et al., 2010), explored the use of Pt nanopillars to increase the surface area of the working electrode. The working electrode was then coated by electropolymerisation with findings suggesting the improved mechanical stability and adherence of the PPy coating to the metal substrate.

A small part of the present study investigated the effect of the pre-treatment of the working electrode on coating characteristics. Pre-treatment of the working electrode (SS wire) in this study was performed in line with the literature by immersing a vial containing the working electrode, SiC and EtOH into a heated ultrasonic bath for 1 hour (Okner et al., 2009).

Ultrasonic Bath

An ultrasonic bath consists of a stainless steel tank with ceramic piezoelectric transducers attached to its bottom or side. When excited, these transducers are capable of converting electrical energy to mechanical energy in the ultrasonic frequency range. It is this change that causes the bottom or side of the tank to move, generating a pressure wave within the liquid in the tank. These high frequency ultrasonic waves create small cavities within the liquid, where it interacts with the SiC. These cavities expand as a result of the vibration induced by the wave oscillation until they become unstable and violently collapse. This collapse creates hammering

pressures concentrated on a very limited area. The collapse of the cavity is violent enough to tear material away from the boundary of the surface, causing the SiC to be removed from the wire and leaving a pitted surface. To aid the process, the liquid is heated, helping to eliminate trapped air (Lacoma, 2015, TMAssociates).

2.4. Drug Release Measurement

2.4.1. *In Vitro* Drug Elution

2.4.1.1. Drug Release Experimental Conditions

In order to perform drug elution *in vitro*, conditions of the human body must be mimicked. The pH of arterial blood plasma is in the range of 7.37 to 7.43, therefore using Phosphate Buffered Saline (PBS) solution with a pH of 7.4 is ideal (Seidlitz et al., 2013). Another reason PBS is used *in vitro* is that its ionic components and concentrations are similar to that of the human body. The temperature of the environment should also be maintained at 37 ˚C, again mimicking body temperature.

Other substances may also be added to the drug release media to aid the release of a particular compound. An example of this is the study by (Ranade et al., 2004) which added Tween20 to the drug release media to enable the release of paclitaxel from a stent coating.

Drug release from a stent into the surrounding vessel does not occur in a static environment. The flow of blood through the stented vessel is an important factor and may impact upon the rate at which the drug is released. To accurately mimic blood flow through a stent *in vitro*, there are numerous experimental setups that can be used and these will be described below.

Flow Through Model

To assess the drug elution from a DES specifically, only one method has been approved by the FDA, named the 'flow-through cell'. This closed system set-up is designed to mimic the blood flow through a vessel using media as the blood component. The flow rate of blood through coronary arteries has been approximated to be 35 ml/min (Seidlitz et al., 2013). The flow rate is important as it affects the drug elution rate from a DES.

Non-Compendial Incubation Setup

Although not approved by the FDA, the non-compendial incubation setup has been reported as the simplest setup available for the dissolution of a drug from a DES. This method involves placing the DES in a vial with a small volume of media and incubating it under agitation (Seidlitz et al., 2013). The sample media is removed and refreshed at regular time points. One issue that has been associated with this method is the lack of 'sink conditions' which refers to

the volume of dissolution medium that is required to provide complete dissolution of the estimated mass of drug in the sample.

The non-compendial incubation setup has been used in the literature to perform drug dissolution from a Cypher™ SES (Biggs et al., 2012). The sample was removed at certain time points to analyse its change in coating morphology. The experimental setup in the present study will be based upon the study by Biggs et al and the specific conditions detailed in section 3.2.4.

2.5. UV-spectroscopy

2.5.1. Principles of Operation

UV spectroscopy relies upon a beam of UV light that is passed through a diffraction grating where it is separated into its constituent wavelengths. Each monochromatic beam is split into two beams of equal intensity, with one beam passing thorough the sample and the other through the reference solution. Electronic detectors measure the intensities of these light beams (I = intensity of sample beam, I_o = intensity of reference beam) and take the difference between the values.

The scan range for UV spectroscopy is typically 200-400 nm and if the sample solution does not absorb light at the given wavelength then $I = I_o$. However, if the sample does absorb the light at the given wavelength then $I < I_o$, giving a difference in absorbance value. The difference in absorbance can be plotted against wavelength, providing a curve and the maximum absorbance (λ_{max}) can be identified. See Figure 2-8 for schematic representation of UV-spectroscopy apparatus.

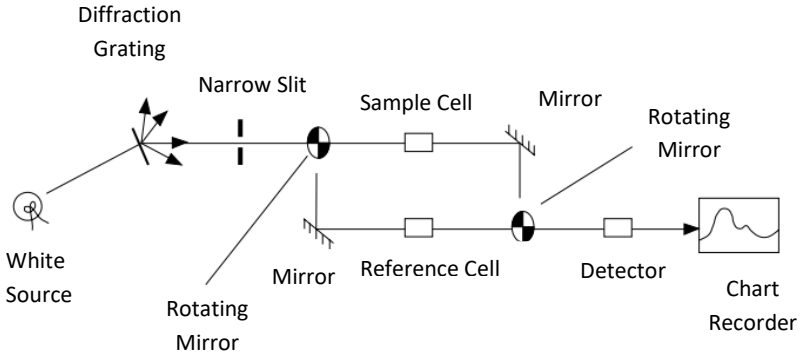

Figure 2-8: Visual representation of the workings of a spectrophotometer. Image adapted from (Clarke, 2016).

A calibration curve can be produced by measuring the absorbance of standard solutions of known concentrations at a specific wavelength. From the calibration curve, a trend line is applied and an equation obtained that is used to calculate the concentration of the drug present in subsequent samples.

From the drug concentration, the mass of drug present in the sample solution can be calculated using Equation 2-3.

$$M = CVMw$$

Equation 2-5: Equation used to calculate mass of drug. M is the mass of the drug, C is concentration of the drug, V is the sample volume, Mw is the molecular weight of the drug.

At specific time points, the drug release media is removed and replaced with fresh media. The cumulative drug release at a specific time point can be identified by Equation 2-6 (England et al., 2015).

$$Cumulative\ Drug\ Release\ (\%) = \frac{Mt}{Mtotal}\ x\ 100$$

Equation 2-6: Equation used to calculate percentage cumulative drug release. Mt is the mass of drug released at time t and M_{total} is the overall mass of drug released.

2.6. Cell Culture Studies

2.6.1. Cell Type

The effect of surface topography and morphology on cell behaviour has been reported in the literature for a variety of cells and surfaces. It is important to note that cells from different size vessels behave differently to topographical features (Liliensiek et al., 2010). Therefore, when researching this field, one must be vigilant in making a comparison between the behaviour of different cell types.

The ideal cell type to research for growth on coronary stents would be human coronary artery endothelial/smooth muscle cells (HCAEC/SMCs) as these are the cell types present at the site of stent implantation and are therefore a good representation of the target environment (Busch et al., 2014, Li et al., 2013). However, human vascular cells are not always used due to feasibility issues and other cell types (HUVECs, RAECs, PCAECs) are often used as an alternative.

The use of animal cells in the field of cardiovascular applications is commonly reported (Wong et al., 1994, Fang et al., 2005). Porcine vascular ECs/SMCs have previously been used within the department in a similar study (Reay, 2012) and continue to be used due to their effectiveness. The advantage of using porcine vascular cells over human non-vascular cells (for example HUVECs) is that they have similar physiology to specifically vascular cells that we are interested in for this study.

In the present study, primary porcine vascular endothelial cells were isolated from the pulmonary artery of pig hearts. The specific cell culture methods are described in chapter 3.

2.6.2. Cell Viability Assays

2.6.2.1. LDH Assay

Cytotoxicity testing is an important feature in this study as it gives an indication as to the biocompatibility of a material. Cell cytotoxicity can be measured by means of an LDH assay, a technique which is widely reported in the literature (Busch et al., 2014, Li et al., 2013) and has been used to analyse HUVECs on laser engineered stent surfaces (Li et al., 2013). This

technique has previously been analysed in the department to analyse the viability of porcine EC/SMC on similar PPy surfaces (Reay, 2012).

When a cell is damaged, LDH enzyme is leached out and this converts NADH to NAD within the assay. The absorbance of NADH is measured at 340 nm and a decrease in absorbance at 340 nm is indicative of the NADH being converted to NAD due to the presence of the LDH enzyme. See Figure 2-9 for schematic representation of the LDH assay mechanism.

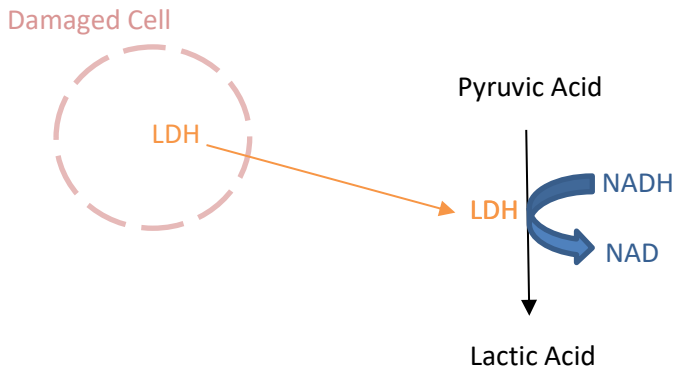

Figure 2-9: Schematic representation of LDH assay. Image shows LDH being excreted from damaged cell, subsequently converting NADH to NAD.

The absorbance at 340 nm can be plotted against time and a linear curve obtained. The enzyme activity can be calculated using Equation 2-7.

$$Enzyme\ Acitivity = \frac{change\ in\ abs}{extinction\ coefficient(E)}$$

Equation 2-7: Equation of enzyme activity, using change in absorbance at 340 nm. The extinction coefficient (E) of NADH at 340 nm is 6.22 mM-1.

2.6.2.2. Live/Dead Staining

A method of measuring, qualitatively, the viability of cells is live/dead staining. This gives visual data regarding the state of cells (live or dead). Propidium Iodide (PI) is a nuclei staining dye that cannot enter through a viable cell membrane. Instead, it enters through damaged areas of dead cell membranes and once it reaches the nucleus, intercalates with the DNA double helix of the cell. This dye stains the nuclei of dead cells red. Fluorescein diacetate (FDA) is used to stain live cells green. FDA (non-fluorescent) is converted to fluorescein (green fluorescent) in live cells.

This assay enabled the visualisation of cells on a specific surface using fluorescence microscopy. From this the proportion of live/dead cells on the sample surface was analysed.

Chapter 3

3. An Investigation into the Potential Impact of Surface Topography on Coronary Stent Performance

Chapter 3 will provide the specific background and aims of the study surrounding the subject of the characterisation of the surface topography of clinically relevant coronary stents in section 3.1. It will then lead on to outline the main results from this section of the study in section 3.3 and will finally provide an in depth discussion of these findings in section 3.4.

3.1. Background and Aims

Coronary stent designs have evolved over time, with some of the most notable advances resulting from changes in the stent platform, strut thickness and the introduction of drug and polymer coatings (see section 1.4 for a detailed description).

It is only recently that surface topography has been integrated into stent design for widespread clinical application (Dibra et al., 2005). However, it is not the first time surface topography has been considered for use in coronary stent design (Palmaz et al., 2002) and is becoming of increasing interest (ter Meer et al., 2017). When taken together with the results from recent studies that reveal a potential link between surface roughness and endothelial cell behaviour (Chung et al., 2003, Liliensiek et al., 2010, Xu et al., 2004), the surface topography of coronary stents is becoming of increasing interest. However, the surface topography of clinically relevant stents has not been well documented and compared, with studies focusing more on their performance *in vivo* and drug elution characteristics.

The main aim of the work presented in this chapter is therefore to characterise the surface topography and morphology of a range of clinically relevant stents. It was also decided to investigate if the process of drug elution leads to changes in surface characteristics. As it is known that surface topography can affect cell behaviour, a final aim of this work is to investigate the adhesion and proliferation of endothelial cells on surfaces of distinct roughness, thereby providing insight into the potential healing properties of currently used stents. The aims can be broken down to the four main objectives below.

1. Analyse surface morphology of clinically relevant stents using SEM
2. Analyse surface topography of clinically relevant stents using AFM
3. Analyse effect of drug release on surface morphology and topography

4. Analyse effect of surface topography on growth of porcine endothelial cells

3.2. Materials and Methods

3.2.1. Data Analysis and Statistical Methods

Except where indicated otherwise, data represent the mean ± one standard deviation, obtained from n samples. Details on the statistical tests performed on the various datasets collected are provided within each separate results chapter.

3.2.2. SEM Analysis

The principles of operation of the Scanning Electron Microscope is available in chapter 2, section 2.2.

3.2.2.1. Materials and Equipment

Adhesive carbon tape was used to mount samples onto the SEM sample holder. A Scanning Electron Microscope (Hitachi, TM-1000 Tabletop Microscope, 20 x – 10,000 x magnification) was used to perform surface analysis at the micrometre scale. A sputter coater similar to the design shown in section 2.2.2.1 was used to coat all DESs in this study prior to SEM analysis.

3.2.2.2. Experimental Procedure

Control Materials

Four different types of stainless steel (SS 316L) materials were analysed in this study (unpolished SS plate, polished SS plate, untreated SS wire and pre-treated SS wire). Three of each types of SS wire were analysed. One of each type of the SS plate was analysed due to lack of availability. Each sample was secured to a SEM stub with adhesive carbon tape.

Coronary Stents

Five different types of stents were analysed in this study; Cypher™ SES (Cordis Corporation), Taxus® Express² ™ PES (Boston Scientific), Xience Pro EES (Abbot Vascular), Gazelle™ BMS (Biosensors International ™) and Yukon® RES (Translumina) (pre-drug application and

post drug-elution). See Table 3-1 for list of stents analysed in the present study and their associated materials.

Table 3-1: Table of stents analysed in the present study, including their stent platform, polymer and drug type.

Stent Name	Stent Type	Platform	Polymer	Drug
Gazelle™	BMS	316 L SS	N/A	N/A
Yukon®	BMS	316 L SS	N/A	N/A
Cypher™	DES	316 L SS	Parylene/PEVAC/PBMA	Sirolimus
Taxus® Express^{2} ™	DES	316 L SS	SIBS	Paclitaxel
Xience Pro	DES	CoCr	PBMA/PVDF-HFP	Everolimus

Three of each type of stent, differing in length and diameter (n=2 Yukon® stent *post drug release due to lack of availability) were expanded for 30 seconds in air to the nominal pressure indicated in the manufacturers guidelines. A small section, consisting of several stent struts was cut from each stent with scissors. The section was adhered to a SEM sample stub with conductive tape for SEM imaging (see Figure 3-1 for visual representation).

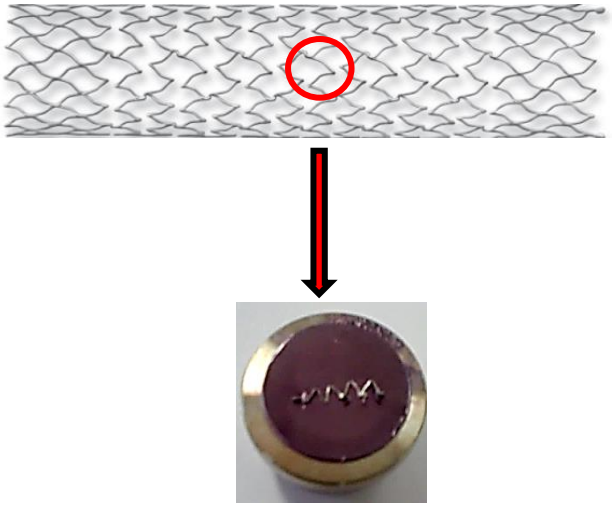

Figure 3-1: Image showing SEM sample preparation. Several stent struts were adhered to the SEM sample stub by conductive tape prior to imaging.

The DES were sputter coated with gold prior to analysis. Each sample was sputter coated for three 15 second periods to produce a gold coating of nanometre thickness. No sample

preparation was performed on the Gazelle™ BMS (Biosensors International™) or Yukon® RES (Translumina,*pre-drug application and post-drug elution) due to their already conductive surface.

All analysis was performed at a magnification varying from x 100 to x 5000.

3.2.3. AFM Analysis

The principles of operation of the Atomic Force Microscope is described in detail in chapter 2, section 2.1.

3.2.3.1. Materials and Equipment

An Atomic Force Microscope (MFP 3D, Asylum Research, USA) was used to perform surface analysis at the nanometre scale.

A rectangular silicon probe with an aluminium coating was used to analyse all samples in this study (160 TS, Olympus). The spring constant of this cantilever type was 26 Nm^{-1}. Standard microscope slides and nail polish were used to mount samples.

3.2.3.2. Experimental Procedure

The AFM analysis was performed in intermittent contact mode in air (unless otherwise specified), imaging four random points per sample.

Control Materials

Four different types of stainless steel (SS 316L) materials were analysed in this study as described in section 3.2.2.2. Each sample was secured to a standard glass microscope glass slide with transparent nail polish.

Coronary Stents

Five different types of stents were analysed in this study as described in section 3.2.2.2. Three of each type of stent, differing in length and diameter were studied (n=2 Yukon® stent *post-drug release due to lack of availability). A small section, consisting of several stent struts was cut from each stent with scissors. The section was adhered to a standard glass microscope slide with transparent nail polish for AFM imaging (see Figure 3-2)

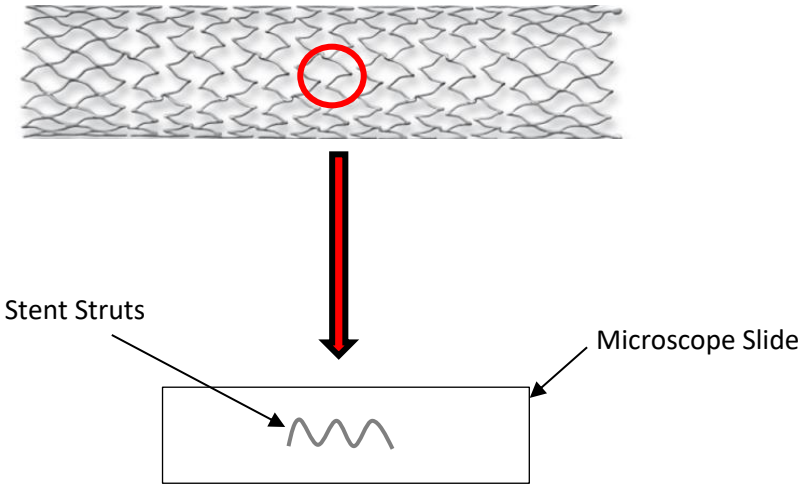

Figure 3-2: Image showing AFM sample preparation. Several stent struts are adhered to standard microscope slide with nail polish.

AFM scans were performed at a frequency of 1 Hz with scan size ranging from 1 µm – 20 µm (as specified on in each figure legend) to obtain images of important surface features, such as pores and grain boundaries. The number of pixels in each image was 256. All quantitative measures of surface topography ($R_{RMS,}$ $R_{y,}$ SA, Sk and Ku) were obtained at a scan size of 5 µm to allow comparison between samples. Unless otherwise stated, data are presented as the mean ± standard deviation (SD) from three independent samples and four points per sample.

Statistical Analysis

In order to compare the AFM data between two individual sample groups and assess its significance, Two-tailed T test ($p<0.05$) was used. To identify the significance between more than two independent groups, one-way ANOVA ($p<0.05$) and Tukey Post Hoc test was used. To identify the significance between more than two non-independent groups, one-way ANOVA ($p<0.05$) and Multiple Paired Two-tailed T test with Bonferroni correction was used. The Bonferroni correction and p value is specified in the legend associated with the data.

3.2.4. Drug Release

3.2.4.1. Materials and Equipment

Phosphate Buffered Saline (PBS) and Tween20 were both purchased from Sigma Aldrich, UK.

Standard culture dishes (35 mm) were used to contain DES (Taxus® Express$^{2\ TM}$) during drug release and samples were secured to the surface with transparent nail polish. An incubator with agitation was used to contain the samples for the duration of the drug elution. Samples were imaged by AFM imaging at specified time points to identify any changes in surface topography.

3.2.4.2. Experimental Procedure

A section of seven stent struts was cut from a stent and adhered to the base of a culture dish (35 mm) with transparent nail polish to allow the abluminal surface of the stent to be imaged, remaining in the culture dish at each time point. Release media ((0.05 wt% Tween20/ 0.01 M PBS), 1.5 ml) was added to the dish and the dish was clamped together and sealed with parafilm. The samples were agitated at 10 rpm at a temperature of 37 ˚C. The release media was removed and replaced with fresh media at regular time points (15 min, 2 hr, 1 d, 2 d, 7 d, 14 d, 28 d) over a period of 28 days.

3.2.5. Cell Culture

3.2.5.1. Materials and Equipment

TrypLE™ Express dissociation medium, large vessel endothelial cell medium (Medium 200), Low Serum Growth Supplement (LSGS), Penicillin and Streptomycin (PenStrep) and Foetal Bovine Serum (FBS) were all purchased from Thermo Fisher Scientific (Glasgow, UK). Fresh pig hearts were obtained from John Robertson and Sons (Ham Curers) Ltd. (Ayrshire, UK).

Light microscopy was carried out using a Nikon Diaphot inverted microscope. Samples were centrifuged using a MSE mistral 2000 benchtop centrifuge. All sterile work was carried out in a laminar flow fume hood acquired from Bassaire Ltd (UK). Cells were grown in T25 flasks and experiments were performed in standard well-plates and culture dishes of various sizes.

3.2.5.2. Experimental Procedure

Cell Isolation

Primary porcine vascular endothelial cells were isolated from the pulmonary artery of pig hearts and cultured in large vessel endothelial cell medium (Medium 200 with 2 % LSGS, 1 % PenStrep). Fresh pig hearts were acquired from the abattoir, with the pulmonary artery still partially in-tact. The pulmonary artery was carefully trimmed from the heart, placed in a large culture dish and moistened with cell medium. The pulmonary artery was then cut to expose the inner side of the artery. A scalpel was gently scraped over the inner surface several times before being rinsed in cell medium. The medium containing the cells was decanted into a T25 flask and topped up with fresh medium. Cells were cultured in a humidified environment at 37 °C (5 % CO_2) for the duration of the present study. Media was changed every 3 days and cells were passaged when approaching confluence.

Cell Passaging

To passage cells, media was removed and cells were incubated (37 ºC) with TrypLE™ (2 ml) for 5 minutes or until cells were identified as being detached from the surface (using light microscopy). The TrypLE™ was neutralised with media (Medium 200 with 2 % LSGS, 1 % PenStrep, 4 ml). The cell suspension was centrifuged at 300 G for 10 minutes (in line with previous method used in the department). Excess media was decanted off and the cells re-suspended in fresh media (1 ml). The cells were split into new flasks (T25) and fresh media (5 ml) added.

Experimental Setup

The experimental setup was initially attempted in culture dishes (35 mm). The samples were either (A) placed onto a confluent monolayer of cells or (B) the cell suspension pipetted directly on top of the sample. The setup in culture dishes was found to be unsuitable for the stent samples as the large surface area (9 cm^2) of the culture dishes caused the sample to move around, resulting in cell detachment from the sample's surface.

To counteract this problem, the experiment was attempted in 96 well plates with a smaller surface area (0.143 cm^2). This setup proved more successful and was the chosen setup for this study.

Seeding Density

Various seeding densities were attempted ($1 \times 10^5 – 2 \times 10^5$ cells/cm^2), based on the literature (Prasad et al., 2005) and previous methods in the department (Holland, 2016). Following initial experiments, it was confirmed that a seeding density of 2×10^5 cells/cm^2 was best for this study.

Samples

A small section, consisting of 9 stent struts was cut from each stent (Gazelle™/Yukon®, n=3) with scissors. Each piece of stent was immersed in Ethanol and left to dry in a sterile environment.

The samples were either used immediately after sterilisation or were incubated with Foetal Bovine Serum (FBS) for one hour prior to use. The section of stent was placed in a 96 well plate well with media and the cell suspension pipetted directly on top (see Figure 3-3 for schematic representation of experimental setup). The total volume within the well was 200 µl.

For the control experiments, cell suspension was pipetted directly into wells containing media (n=3 for each time point). For some experiments, media was removed every 3-4 days for LDH analysis (see section 3.2.6 for experimental protocol). Samples were stained (live/dead) and imaged at the experimental end point, in line with the procedure that is shown in section 3.2.7.

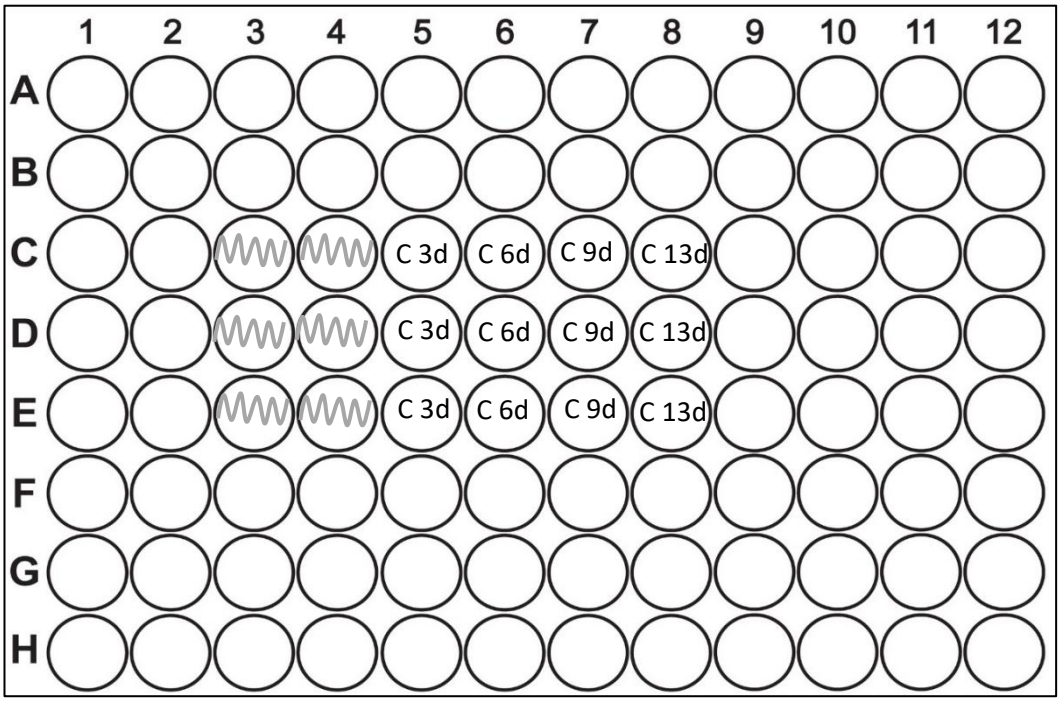

Figure 3-3: Schematic representation of experimental setup. Image represents 96-well plate. Zigzag line indicates stents struts. C indicates control well (cells only) for various time point. N=3 for all samples. 3d – 3 days, 6d- 6days, 9d- 9 days, 13d – 13 days.

3.2.6. LDH Assay

3.2.6.1. Materials and Equipment

NaPi buffer, NADH (β-Nicotinamide adenine dinucleotide) and Pyruvic Acid were all obtained from Sigma-Aldrich, UK. A UV spectrophotometer (UV 2401 PC, Shimadzu Coorporation) was used to analyse the absorbance of NADH in this study.

3.2.6.2. Experimental Procedure

The solutions and samples used in this assay were prepared fresh for each set of experiments.

At certain times points (3 days, 6 days, 9 days, 13 days) media was removed from each well (containing cells and/or samples) and decanted into Eppendorf tubes. Removed media was replaced with fresh media and returned to the incubator. For a positive control, media was removed from the control wells (analysed by LDH assay as negative control) and replaced with Triton X-100 (1 wt %). Following incubation, the Triton X-100 solution was removed and analysed by LDH analysis as positive control.

The spectrophotometer was setup in time course mode at a wavelength of 340 nm and time period of 60 s. NADH in buffer solution (3 mg in 500 µl NaPi buffer) was added to Pyruvic acid in buffer solution (3 mg in 500 µl NaPi buffer) in an Eppendorf tube and briefly vortexed. In each cuvette, NaPi buffer solution (860 µl), NADH/Pyruvic acid solution (40 µl) and sample media (100 µl) were combined, the cuvette inverted 3 times and analysed immediately. NaPi buffer solution (1 ml) was used as the baseline recording.

An absorbance vs time curve was obtained and absorbance values were taken at t = 0s and 60s. If the curve was not linear, absorbance values were taken at the most linear points. This gave an enzyme activity level in 100 µl of media. To get the enzyme activity in each well (200 µl) which are the values referred to throughout this study, the LDH enzyme activity was multiplied by two.

3.2.7. Live/Dead Staining

3.2.7.1. Materials and Equipment

Propidium Iodide (PI) and Fluorescein diacetate (FDA) were purchased from Sigma Aldrich (UK). Fluorescence microscopy was carried out using a fluorescence microscope (Carl Zeiss, Germany).

3.2.7.2. Experimental Procedure

A stock solution of PI in PBS (pH 7.4) was prepared at a concentration of 2 µg/ml (PI/PBS). A stock solution of CFDA in DMSO was diluted in PBS (pH 6.75)

The sample (7 stent struts) was removed from the culture media (using tweezers) and the very end of the sample inserted into a blue tac mount in a culture dish (35 mm). PI (500 µl) was gently pipetted onto the sample and left in darkness for 1 min. The PI was pipetted off and CFDA (500 µl) was added to the sample and left in darkness for 5 min. The CFDA was pipetted off and PBS (pH 6.75) was added to the culture dish. The sample was immediately analysed by fluorescence microscopy.

Washing steps with PBS (pH 7.4 and pH 6.75) were performed in the initial experiments but cells appeared to be washed away and so after the stain was removed no additional washing steps were performed.

Statistical Analysis

In order to compare the cell count between sample groups and assess its significance, Two-tailed T test ($p<0.05$) was used.

3.3. Results

3.3.1. Surface Topography of Control Materials

Initial experiments were carried out to determine the suitability of the AFM and SEM for use in this study and to establish the robust procedures that could then be taken forward to investigate the surface of coronary stents. The surfaces of four different stainless steel (316L) materials (polished SS plate, unpolished SS plate, untreated SS wire, pre-treated SS wire) were imaged by AFM and SEM analysis in line with the method discussed in sections 3.2.2 and 3.2.3. The findings on their surface topography and morphology will be discussed in the following sections.

3.3.1.1. Polished and Unpolished Stainless Steel Plates

SEM analysis of polished and unpolished stainless steel (SS 316L) plates showed a noticeable difference between the two surfaces. The surface of the unpolished SS (316L) had a prominent cobblestone structure throughout with some scratches visible at low magnification (2.5k) (see Figure 3-4). The surface of the polished SS (316L) was noticeably smoother with the cobblestone structure no longer visible (see Figure 3-5). Fine lines were also visible on the polished SS (316L), although not as prominent as the features present on the unpolished SS (316L).

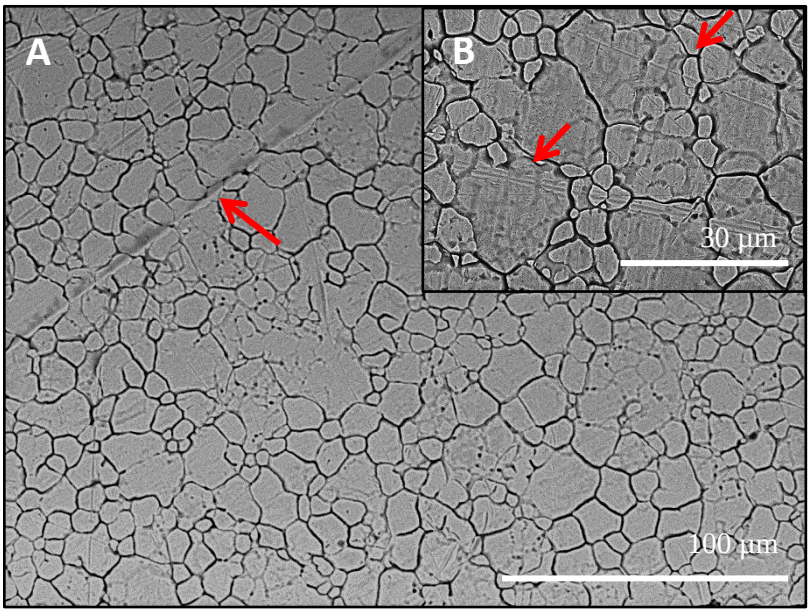

Figure 3-4: SEM images of surface of unpolished SS (316L) plate. Grain boundaries and scratches visible. Scratches indicated by red arrows. Images representative of 1 sample.

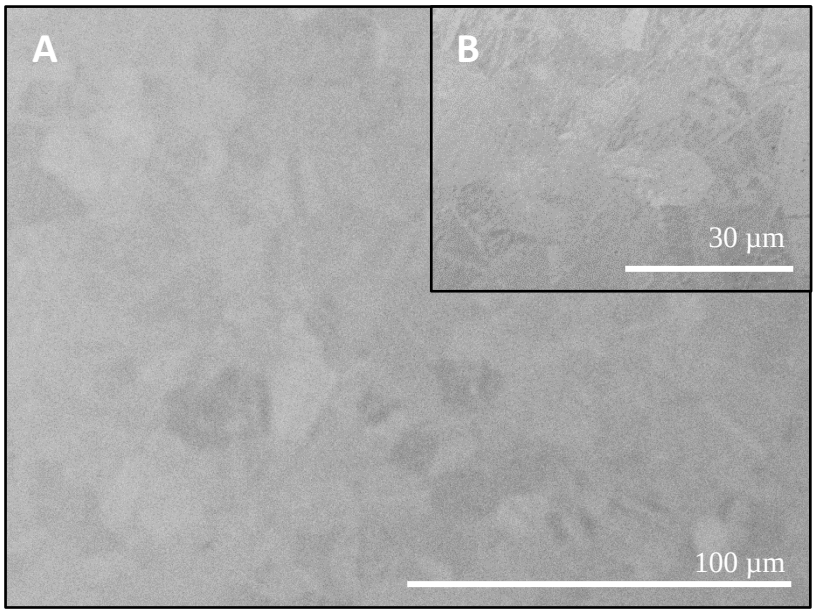

Figure 3-5: SEM images of surface of polished SS (316L) plate. Grain boundaries no longer visible. Images representative of 1 sample.

AFM analysis of the polished/unpolished surfaces emphasised the initial findings from the SEM analysis that the surfaces were quite different. Height retrace images of the unpolished SS (316L) plate showed the prominence of the grain boundaries with the blue colour representing the deep valley of the grain boundary (see Figure 3-6). This is in comparison to the height retrace images of the polished SS (316L) plate (see Figure 3-7), showing the absence of grain boundaries.

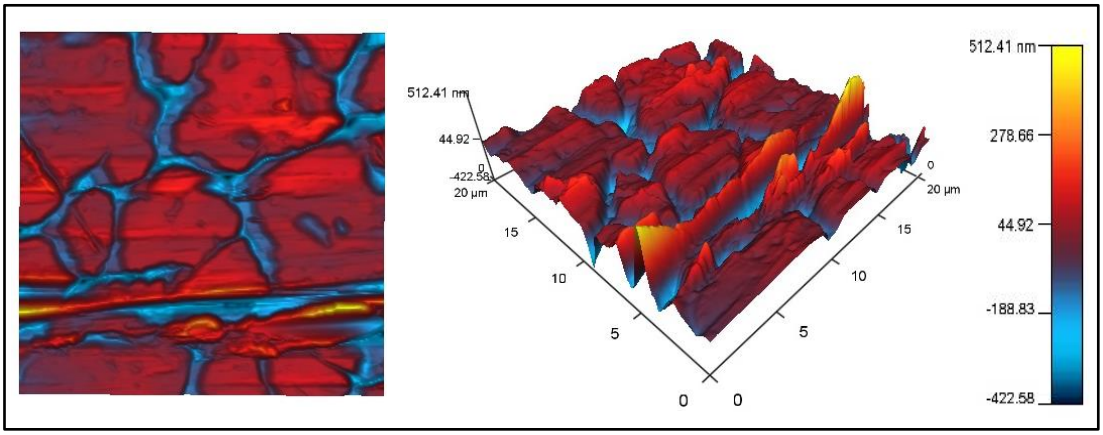

Figure 3-6:Sample: Unpolished SS (316L) plate. AFM height retrace image (ortho projection LHS, standard 3D RHS), Scan size 20 µm. Image shown is representative of four random points on one sample.

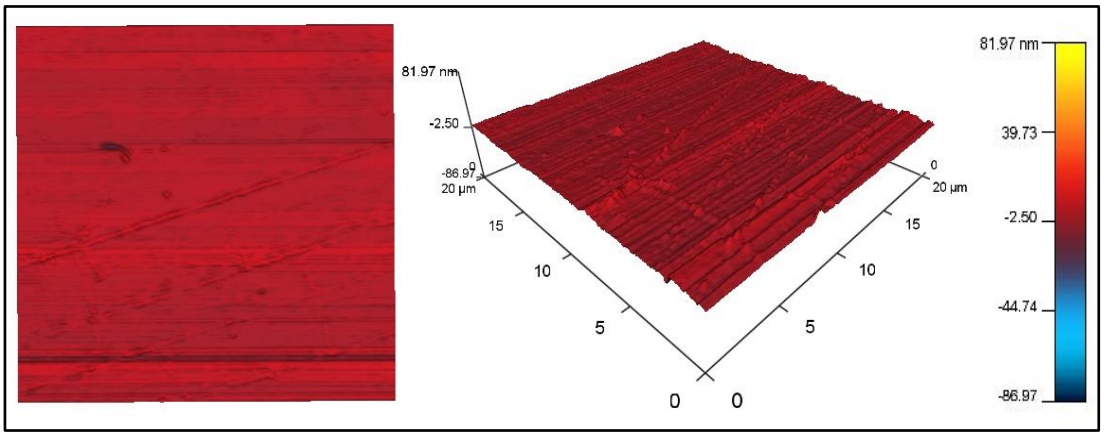

Figure 3-7 Sample: Polished SS (316L) plate. AFM height retrace image (ortho projection LHS, standard 3D RHS), Scan size 20 µm. Image shown is representative of four random points on one sample.

A summary of the data obtained from AFM analysis is shown in Table 3-1. It indicates that the unpolished SS (316L) plate had an average R_{RMS} value (44.64 nm ± 8.67 nm) more than 10 x larger than that of the polished SS (316L) plate (4.07 ± 2.71 nm). The average peak-to-valley distance value (R_y = 428.56 ± 46.81 nm) was also more than 10 x larger than that of the polished surface (R_y = 34.50 ± 14.12 nm). The skewness value was negative for the unpolished

surface and positive for the polished surface. The average kurtosis value was lower for the polished surface than the unpolished surface.

*Table 3-2: Table of mean values of RMS roughness (R_{RMS}), surface area (SA), peak-to-valley distance (Ry), kurtosis (R_{KU}) and skewness (R_{SK}) calculated by AFM software at a scan size of 5µm. Samples are polished and unpolished SS (316L) plates. Mean values and standard deviation (SD) values calculated from four points per sample. (n=1). Two-tailed T test (*p<0.05).*

Sample	**Mean R_{RMS} ± SD (nm)**	**Mean SA ± SD (µm^2)**	**Mean Ry ± SD (nm)**	**Mean (R_{KU}) ± SD**	**Mean (R_{SK}) ± SD**
Unpolished SS (316L) plate	44.64 ± 8.67	25.68 ± 0.24	428.56 ± 46.81	5.08 ± 2.98	-1.30 ± 0.69
Polished SS (316L) plate	*4.07 ± 2.71	*25 ± 0.00	*34.50 ± 14.12	3.78 ± 2.20	*1.00 ± 0.76

3.3.1.2. Pre-treated and Untreated Stainless Steel Wire

SEM and AFM analysis revealed differences between the surface of the untreated stainless steel wire when compared to that of the pre-treated SS (316L) wire. SEM images of the untreated SS (316L) wire (see Figure 3-8) showed visible grain boundaries on the surface with some defects also visible. The SEM images of the pre-treated SS (316L) wire surface (see Figure 3-9) showed consistent elongated pits throughout the surface of the wire, similar to a porous structure. Grain boundaries were not easily visible on either the pre-treated or untreated surfaces.

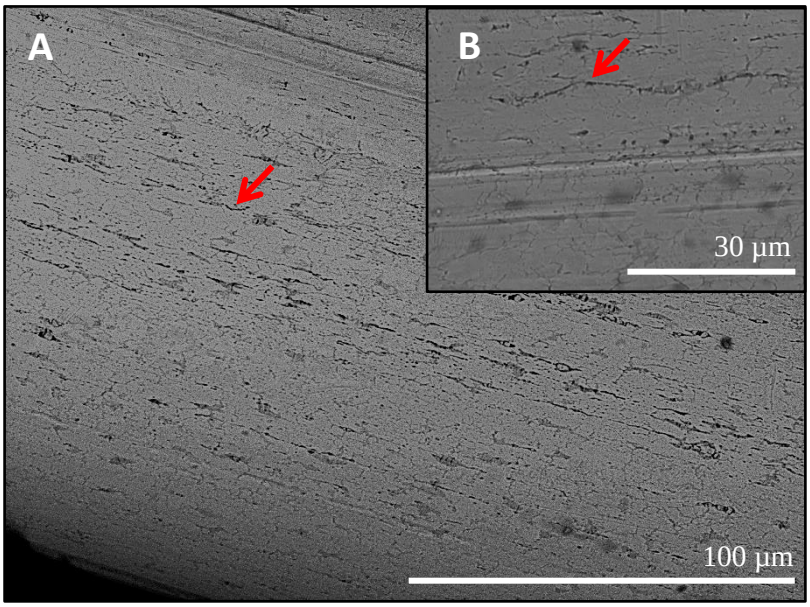

Figure 3-8: SEM images of surface of untreated SS wire. Surface defects indicated by red arrows. Images representative of 3 samples.

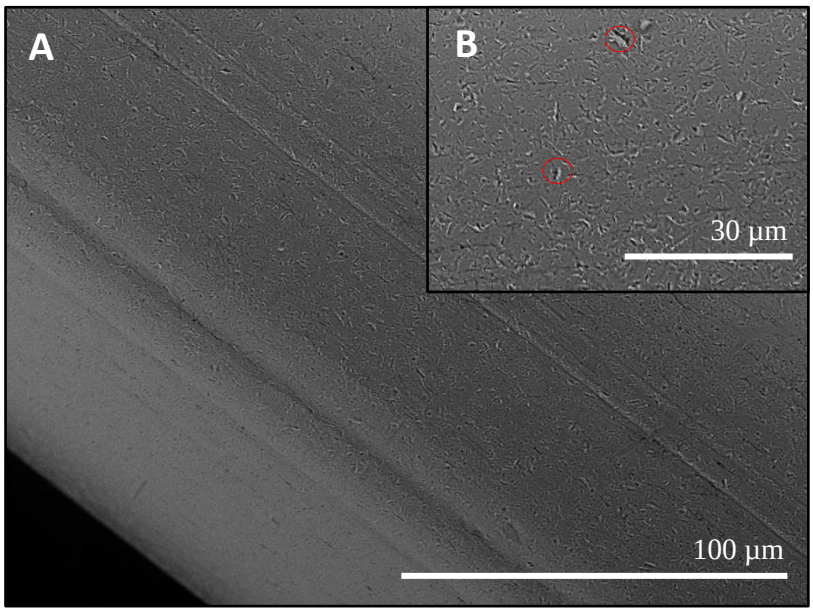

Figure 3-9: SEM images of surface of pre-treated SS wire. Elongated pits easily visible, indicted by red circles. Images representative of three samples.

AFM analysis of the pre-treated/untreated SS (316L) wire exhibited similar surface features. Height retrace images of the pre-treated SS (316L) wire showed elongated pits throughout the surface, indicated by the blue coloured areas (see Figure 3-10). The surface of the untreated stainless steel wire showed surface deformations throughout which appeared as pits, not dissimilar to those present on the pre-treated surface (see Figure 3-11).

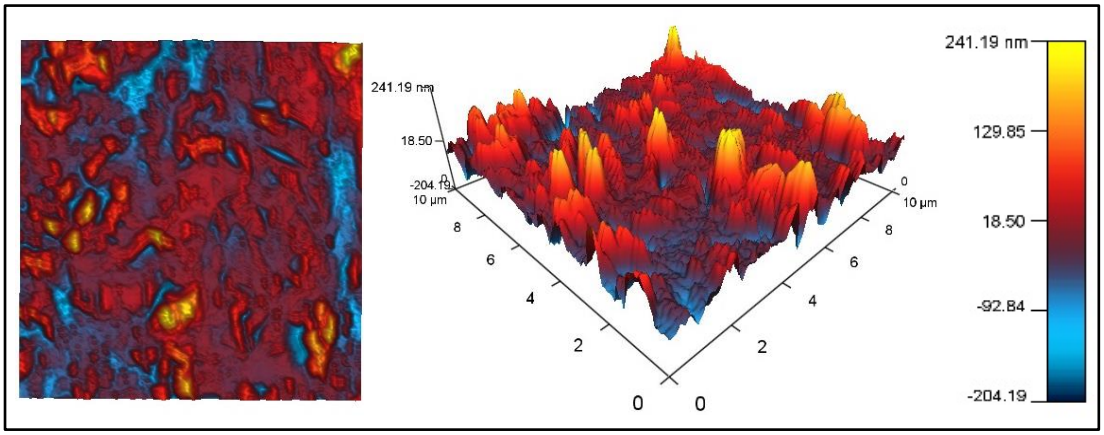

Figure 3-10:Sample:Pre-treated SS (316L) wire. AFM height retrace image (ortho projection LHS, standard 3D RHS), Scan size 10 µm. Blue colour representative of low height, indicating elongated pits. Image shown is representative of three samples.

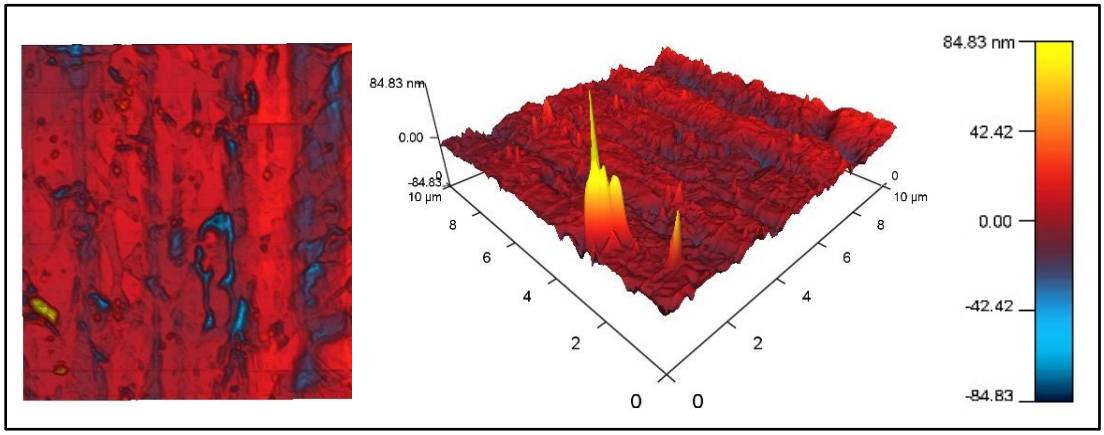

Figure 3-11: Sample: Untreated SS(316L) wire. AFM height retrace image (ortho projection LHS, standard 3D RHS), Scan size 10 µm. Deformations shown by blue areas (low height) and yellow peaks (large height). Image shown is representative of three samples.

A summary of the data obtained from AFM analysis is shown in Table 3-2. It indicates that the pre-treated SS (316L) wire had an average RMS roughness value (43.57 ± 14.10 nm) larger than that of the untreated SS wire (23.53 ± 8.13 nm). The average peak-to-valley distance value of the pre-treated surface (379.58 ± 97.18 nm) was also larger thatn the untreated surface (171.6 ± 37.47 nm). The average kurtosis values were similar for both the pre-treated and untreated surfaces, with values less than 3 obtained in each case. The average skewness value was negative for the untreated wire and positive for the pre-treated wire.

*Table 3-3: Table of mean values of RMS roughness (R_{RMS}), surface area (SA), peak-to-valley distance (Ry), kurtosis (R_{KU}) and skewness (R_{SK}) calculated by AFM software at a scan size of 5µm. Samples are treated and untreated SS (316L) wire. Mean values and standard deviation (SD) values calculated from four points per sample. (n=3). Two-tailed T test (*p<0.05).*

Sample	**Mean R_{RMS} ± SD (nm)**	**Mean SA ± SD (µm^2)**	**Mean Ry ± SD (nm)**	**Mean (R_{KU}) ± SD**	**Mean (R_{SK}) ± SD**
Untreated SS (316L) wire	23.53 ± 8.13	25.42 ± 0.15	171.6 ± 37.47	1.39 ± 2.76	-0.08 ± 0.80
Pre-treated SS (316L) wire	*43.57 ± 14.10	*26.52 ± 0.61	*379.58 ± 97.18	1.84 ± 1.54	0.43 ± 0.27

The difference in average RMS roughness for the four control materials is graphically displayed in Figure 3-12. This shows how the AFM can be used successfully to differentiate between surfaces of varied topographical features and surface roughness.

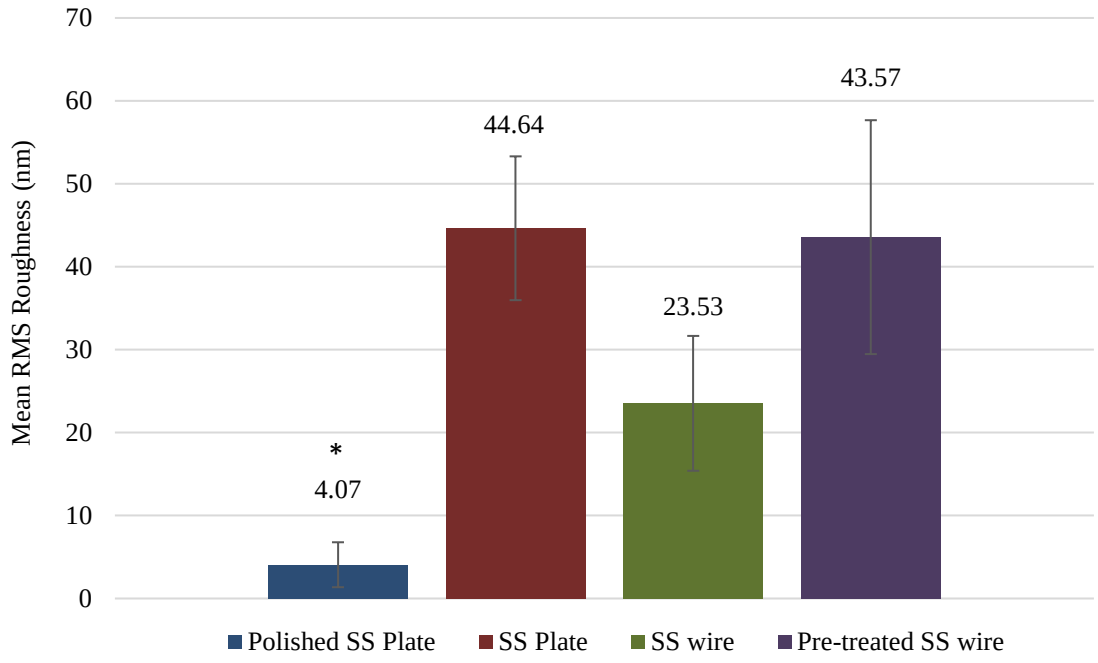

Figure 3-12: Bar chart showing difference in average RMS roughness of control materials. Numerical values are mean RMS roughness values. N=1 polished SS (316L) plate/ unpolished SS (316L) plate. N=3 untreated and pre-treated SS (316L) wire. Four points analysed per sample. Error bars are indicative of standard deviation values. indicates significant difference compared to all other sample types.*

3.3.2. Surface Topography of Clinically Relevant Coronary Stents

The surfaces of five clinically relevant BMS and DES (Gazelle™, Yukon®, Cypher™, Taxus™ Express² ™ and Xience Pro) were imaged by AFM and SEM analysis in line with the method described in sections 3.2.2 and 3.2.3. The findings on their surface topography and morphology will be presented in this section.

3.3.2.1. Surface Topography of Bare Metal Stents

3.3.2.1.1. Gazelle™

When comparing the three Gazelle™ stents that differed only in length and diameter, no qualitative difference in their surface characteristics was observed. A representative SEM

image of this type of stent surface is shown in Figure 3-13. The presence of grain boundaries was easily identified at low-medium magnification (x600 – 2.5k), ranging in width from ~ 6 µm to 30 µm (see Figure 3-13, insert A). Fine lines or 'brush marks' were observed within the grain boundaries and appeared to be in all directions (see Figure 3-13, insert B).

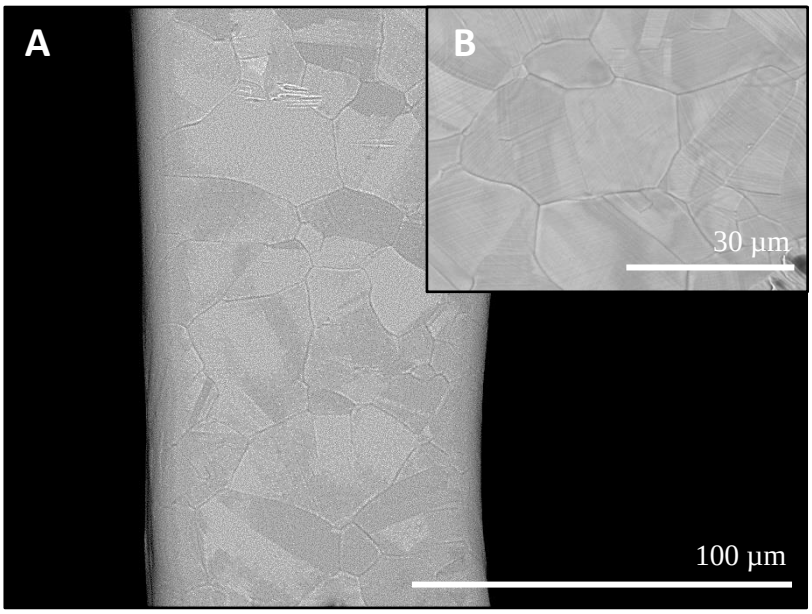

Figure 3-13: SEM images of surface of Gazelle™ BMS. Grain boundaries visible, width 6-30 µm. Images representative of three samples.

A representative height-retrace image of the Gazelle™ BMS surface is shown in Figure 3-14. Increasing the scan size from 5 µm to 20 µm allowed visualisation of the grain boundaries, represented by the blue area in the ortho projection (see Figure 3-14, LHS image). The rest of the surface shown in the image remained relatively flat in comparison to these grain boundaries. AFM analysis provided an average R_{RMS} value of 14.39 ± 11.24 nm. A full list of the AFM numerical data (R_{RMS}, SA, Ry, Sk, Ku) is displayed in Table 3-3.

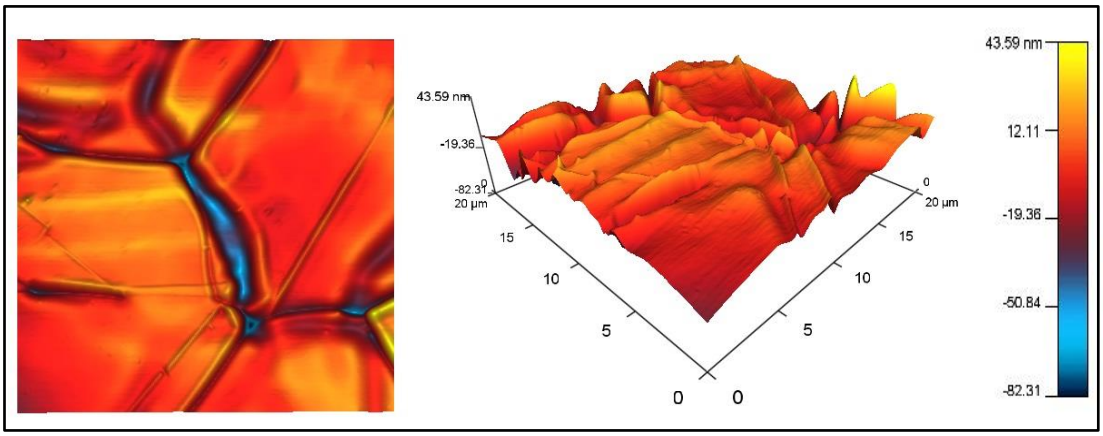

Figure 3-14: Sample: Gazelle™ BMS. AFM height retrace image (ortho projection LHS, standard 3D RHS), Scan size 20 µm, contact mode. Grain boundaries are clearly identified as shown by the blue colouring in the ortho projection, indicating areas of low height. Image is representative of three separate stents.

3.3.2.1.2. Yukon®

Post Drug Release

The Yukon® CHOICE 4 DES is a rapamycin eluting stent with an underlying microporous surface. In this study, the rapamycin elution had already taken place and the stent had been immersed in methanol to remove residual rapamycin. As a result of this, the Yukon® stent is treated as a bare metal stent platform and the following section describes the results from the AFM and SEM analysis of its surface.

SEM images show the microporous surface of the Yukon® stent, known as the 'PEARL surface' (see Figure 3-15, insert A and B). Although these pores are visible by SEM imaging, it proved difficult to assess their size accurately using this method as precise images could not be obtained at higher magnifications. To obtain dimensions of pores, including pore depth, AFM analysis is better suited for this purpose. Also visible from the SEM images are small flat areas (see Figure 3-15, insert B).

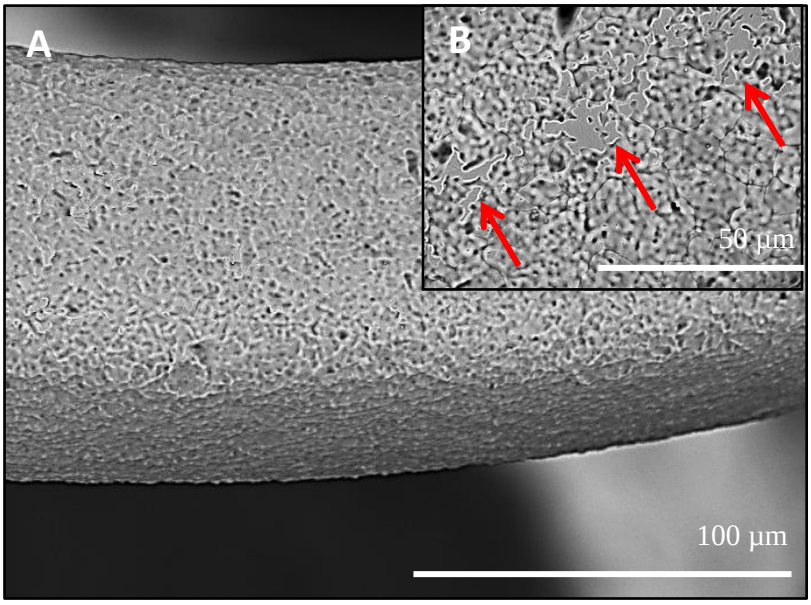

Figure 3-15: SEM images of Yukon® stent post-drug elution. Microporous structure visible throughout. Red arrows are indicative of flat areas in insert B. Images representative of two samples.

AFM analysis was performed at a scan size of 20 µm to better visualise pore depth. The height-retrace images demonstrate the microporous structure well, showing the irregularity of the surface structure (see Figure 3-16). A clear difference in height between the peaks and valleys is observed and amounts to an average peak-to-valley distance of around 2 µm (1782.9 nm ± 214.93).

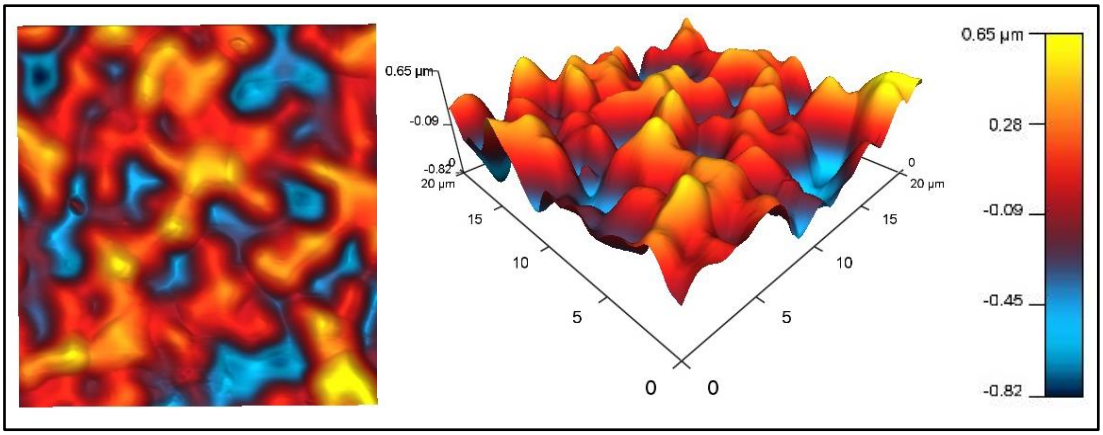

*Figure 3-16: Sample: Yukon® stent *post-drug release. AFM height retrace image (ortho projection LHS, standard 3D RHS), Scan size 20 µm, contact mode. Pores are clearly identified and shown by the blue sections in ortho projection. Image shown is representative of two separate stents.*

As was observed from the SEM imaging of the Yukon® stents (see Figure 3-15), a number of flat areas are present on the surface. These areas are better visualised by the 3D height retrace images, corresponding to the areas that appear flat and of increased height (areas of yellow, see Figure 3-17).

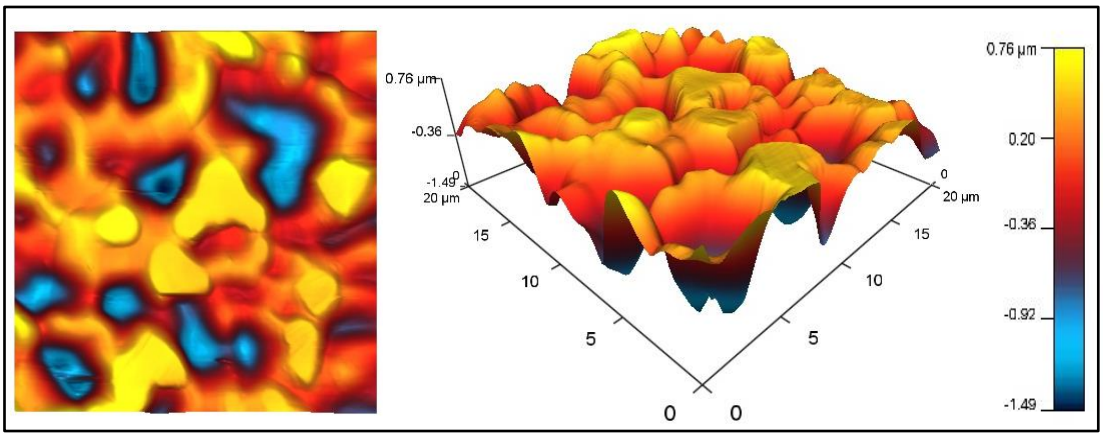

*Figure 3-17: Sample: Yukon® stent *post-drug release. AFM height retrace image (ortho projection LHS, standard 3D RHS), scan size 20 µm, contact mode. Pores are clearly identified and shown by blue sections in ortho projection. Flat areas from SEM images thought to correspond to flat yellow areas shown in ortho projection. Image shown is representative of two separate stents.*

Overlaying the phase retrace image with the height retrace image at a scan size of 1 µm show most areas of the stent to be one phase, however, random areas of the surface express a phase difference (see Figure 3-18).

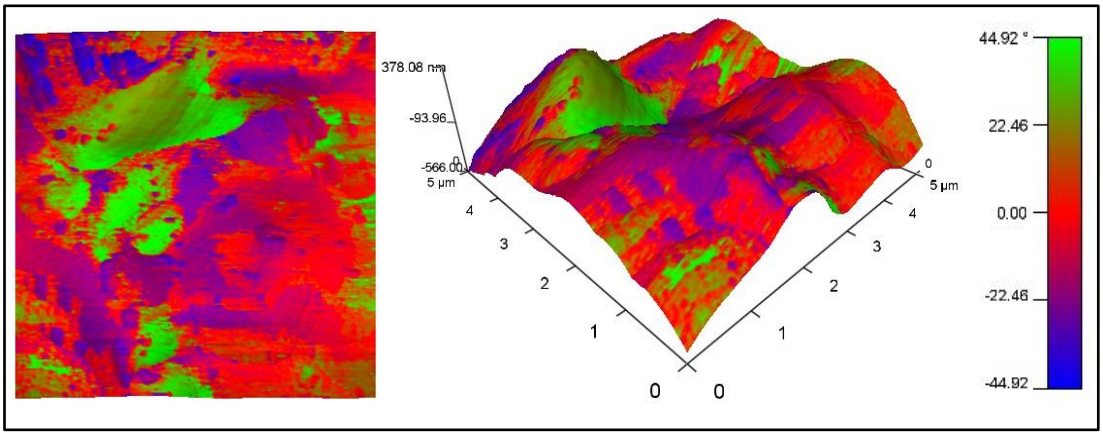

*Figure 3-18: Sample: Yukon® stent *post-drug release. AFM height retrace image with phase overlay (ortho projection LHS, standard 3D RHS) Scan size 5 µm. Areas of increased and decreased shift in phase angle identified by different colours. Green indicates increased shift in phase angle, blue indicates decreased shift in phase angle. Image shown is representative of two separate stents.*

The average R_{RMS} roughness value of the Yukon® stent post drug release (182.02 ± 37.04 nm) is significantly greater than that of the Gazelle™ BMS (14.39 ± 11.24 nm). The average skew value was found to be negative (-0.42 ± 0.18), suggesting the surface has deep valleys and no peaks, consistent with the appearance of the surface topography. The average kurtosis value was <3 (0.25 ± 0.86), which also supported the microporous morphology.

Pre-Drug Application

Analysis was performed on three Yukon® CHOICE 4 DES, freshly opened and prior to the application of a drug layer. SEM images again successfully show the microporous surface of the Yukon® stent (see Figure 3-19, insert A and B), although they appear less well defined than the surfaces of the Yukon® stents post drug release (see Figure 3-15, insert A and B).

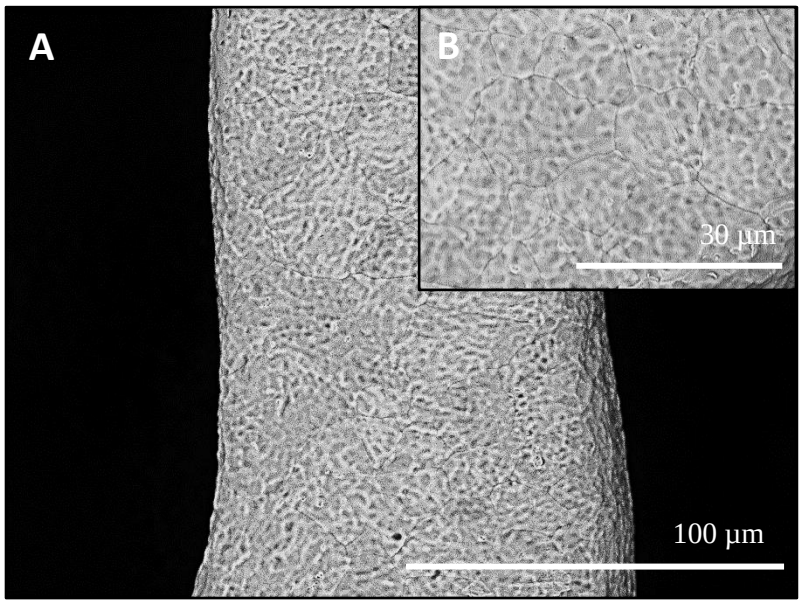

*Figure 3-19: SEM images of Yukon® stent *pre-drug application. microporous structure visible. Images representative of three samples.*

AFM analysis of the Yukon® stents (pre-drug application) show the porous structure to be shallower than those analysed post-drug release. This is shown qualitatively by the height retrace images (see Figure 3-20). The differences between these two surfaces is further demonstrated by the smaller average peak-to-valley distance at a scan size of 20 µm (1167 ± 271.13 nm) compared to that of the surface post-drug release (1782.9 ± 214.93 nm). The average R_{RMS} value (85.52 nm ± 26.07 nm) is also smaller compared to the surface post-drug

release (182.02 nm ± 37.04 nm). Values of R_{RMS}, Ry and SA are statistically different between these two Yukon® stent types (pre-drug application and post-drug release).

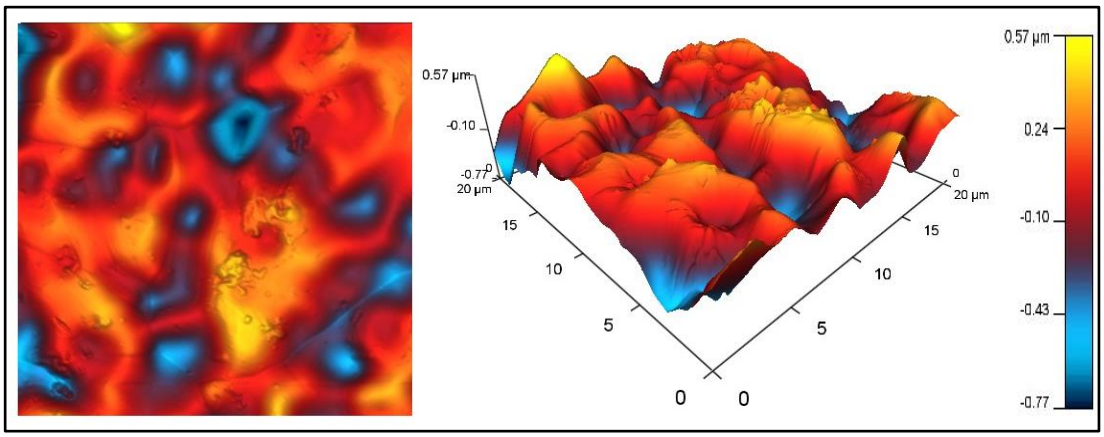

*Figure 3-20: Sample: Yukon® stent *pre-drug application. AFM height retrace image (ortho projection LHS, standard 3D RHS) Scan size 20 µm. Pores are clearly identified and shown by the blue sections in ortho projection. Image shown is representative of three separate stents.*

3.3.2.2. Surface Topography of Drug Eluting Stents

3.3.2.2.1. Cypher™

SEM analysis shows the Cypher™ stents to have a smooth, relatively featureless polymer surface in most places (see Figure 3-21, insert B). However, other features including possible areas of crystalline drug, stress cracks and ripple marks are also visible (see Figure 3-21, insert A).

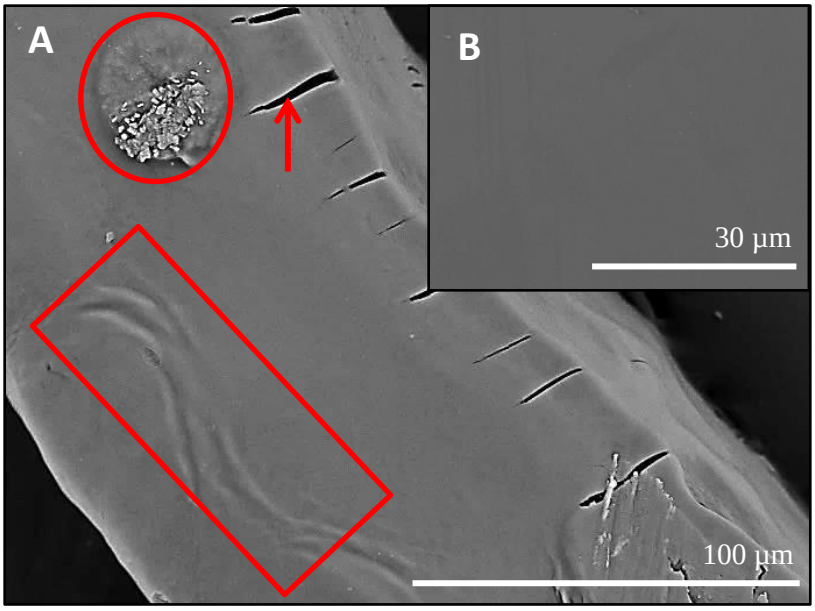

Figure 3-21: SEM images of Cypher™ stent. Possible crystalline drug labelled by red circle, ripple marks labelled by red rectangle, stress crack indicated by red arrow. Images representative of three samples.

Some of the smaller cracks were visualised by AFM analysis, with the height retrace image showing the depth of these cracks (see Figure 3-22).

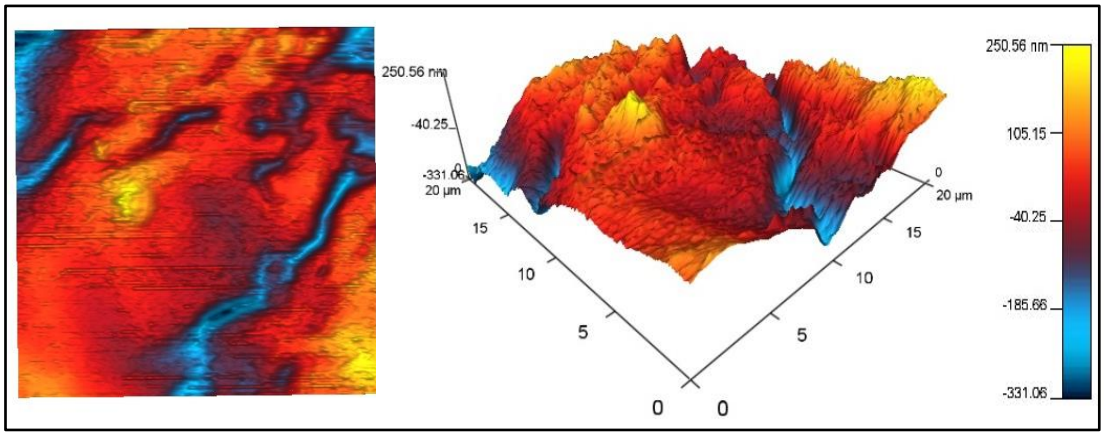

Figure 3-22: Sample: Cypher™ stent. AFM height retrace image (ortho projection LHS, standard 3D RHS), Scan size 20 µm. Stress cracks are clearly identified by the blue colouring in the ortho projection, indicating area of low height. Image shown is representative of three separate stents.

In contrast to the relatively flat morphology observed by SEM analysis, AFM analysis reveals that the Cypher™ stent has a mountainous surface with crater like topography visible in places (see Figure 3-23).

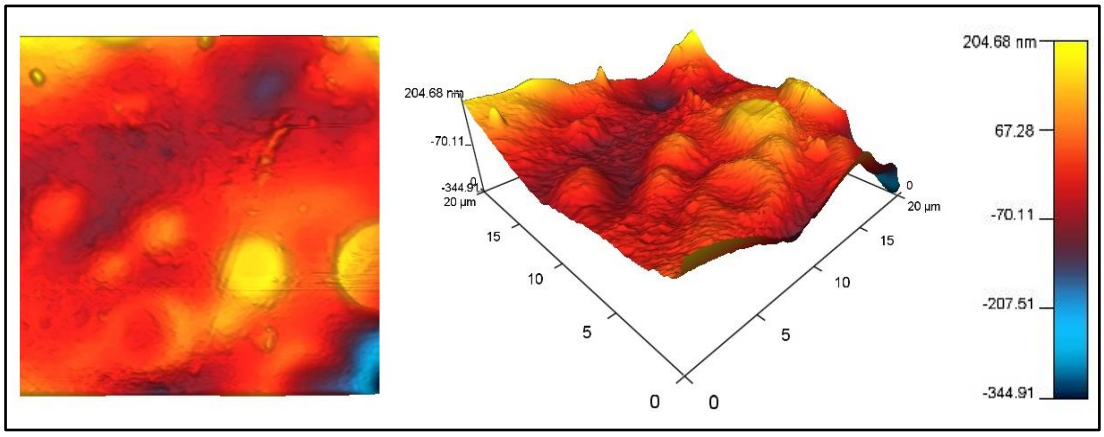

Figure 3-23: Sample: Cypher™ stent. AFM height retrace image (ortho projection LHS, standard 3D RHS), Scan size 20 µm, contact mode. 'Crater like' topography identified by yellow areas. Image shown is representative of three separate stents.

Overlaying the phase retrace image with the height retrace image at a scan size of 5 µm does not show any significant link between height and shift in phase angle (see Figure 3-24). The shift in phase angle that is noted on the surface may be representative of the difference in the two polymers (PEVA and PBMA) in the outermost layer of the coating and will be further discussed in section 3.4.3.

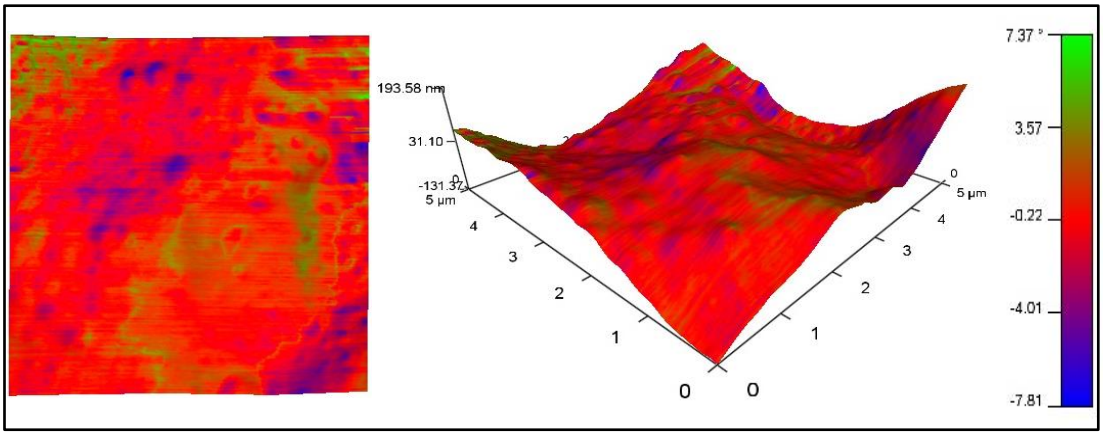

Figure 3-24: Sample: Cypher™ stent. AFM height retrace image with phase overlay (ortho projection LHS, standard 3D RHS) Scan size 5 µm. Slight shift in phase angle shown in ortho projection. Green indicates increased shift in phase angle, blue indicates decreased shift in phase angle.

The average R_{RMS} roughness value of the surface of the Cypher™ stent was calculated to be 34.67 nm ± 34.77 nm, which is closer to that of the Gazelle™ stent than the Yukon® stents. The average values of RMS roughness, peak-to-valley distance, surface area, skew and kurtosis are displayed in Table 3-3. From this, the similarity of these numerical values to the other DES analysed in this study can be noted.

3.3.2.2.2. Taxus® Express^{2} ™

SEM analysis of the surface of the Taxus® Express^{2} ™ stents at low magnification show a fairly featureless surface (see Figure 3-25, insert A). However, analysis at a higher magnification (x2.5k) show ripple marks throughout the surface, highlighting an uneven coating that is likely to have formed during the coating process (see Figure 3-25, insert B).

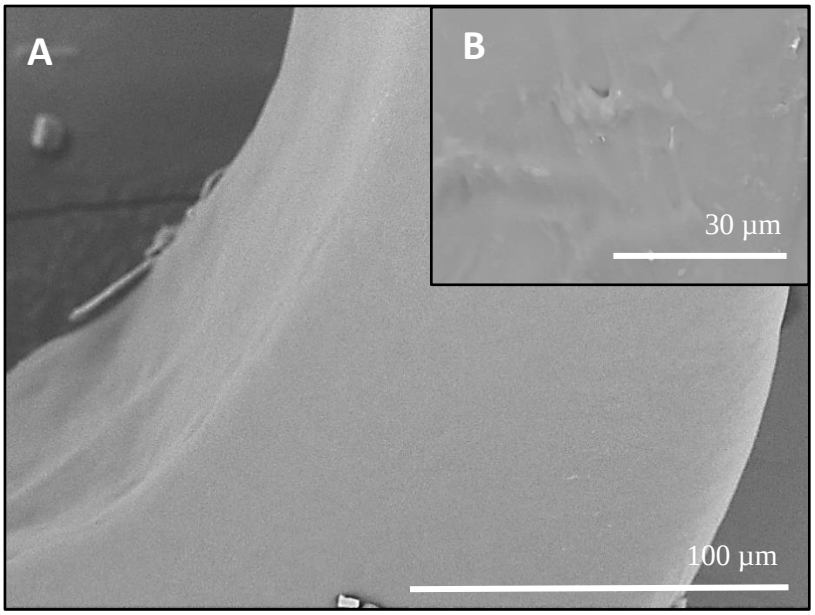

Figure 3-25: SEM images of Taxus® Express^{2} ™ stent strut surfaces. Fairly featureless surface with some ripple marks visible. Images representative of three samples.

SEM analyses also gives an indication of two different 'types' of surfaces on the Taxus® Express^{2} ™ stent. SEM images show some sections of the stent to be smooth and featureless (see Figure 3-26, insert A), and others to have particles present on the surface (see Figure 3-26, insert B).

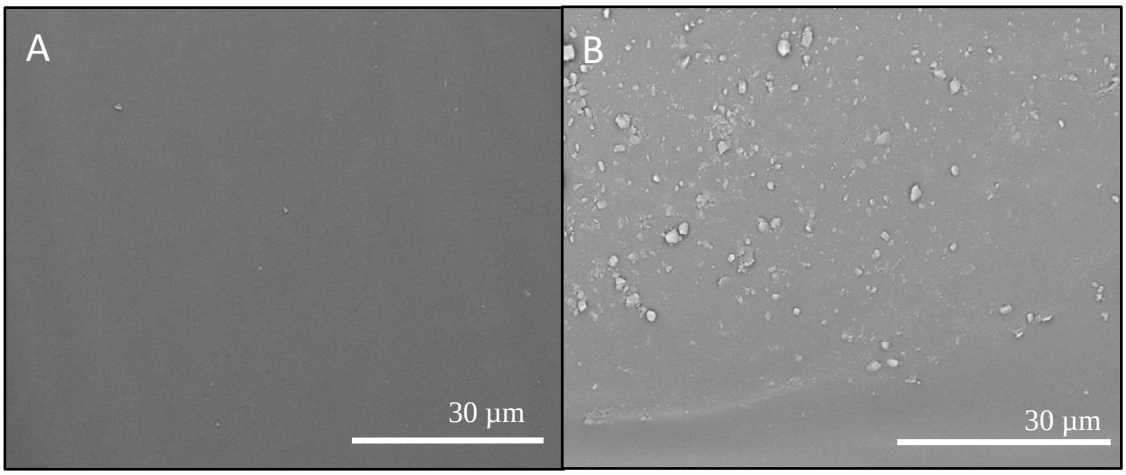

Figure 3-26: SEM images of two different types of surfaces on Taxus® Express^{2TM} stent. A: featureless surface. B: particles visible on surface. Images representative of three samples.

AFM analysis provided height retrace images, showing a wave-like morphology with peaks present throughout the surface (see Figure 3-27).

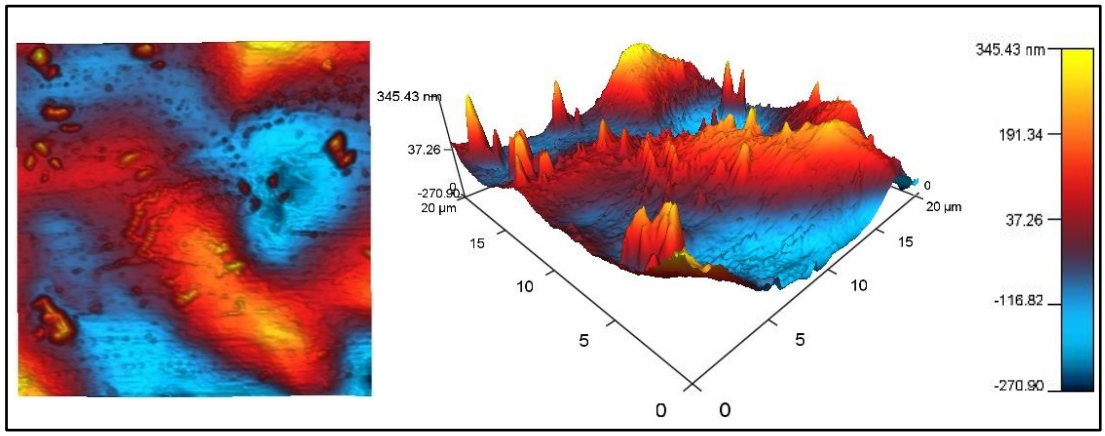

Figure 3-27: Sample: Taxus® Express^{2TM} stent. AFM height retrace image (ortho projection LHS, standard 3D RHS), Scan size 20 µm. Image shown is representative of three separate stents.

The AFM phase image was overlaid with the height retrace image (see Figure 3-28 and Figure 3-29), showing a decrease in phase angle to correspond to the large height values. It is expected that these areas of large height are areas of high paclitaxel concentration and these will become pores during drug elution. The change in surface topography of the Taxus® Express$^{2\ TM}$ surface throughout the drug elution period is presented in section 3.4.4.

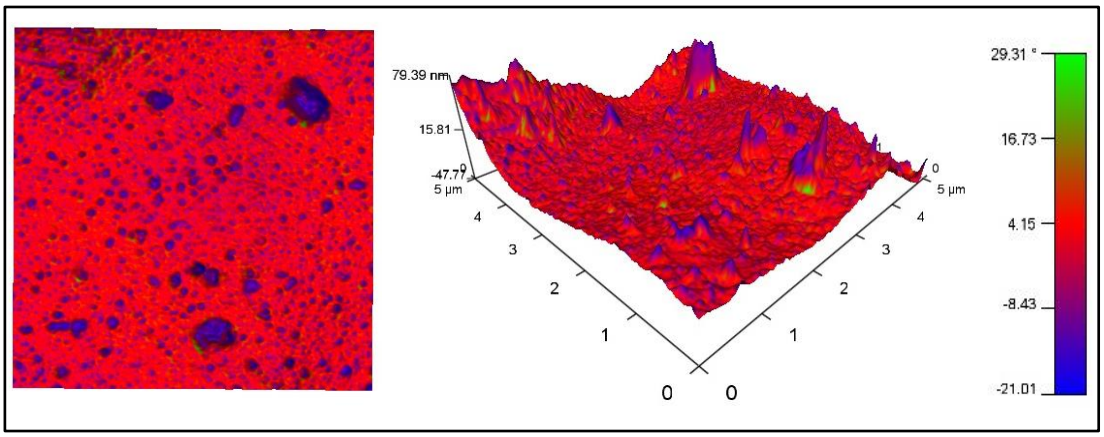

Figure 3-28: Sample: Taxus® Express$^{2\ TM}$ stent. AFM height retrace image with phase overlay (ortho projection LHS, standard 3D RHS), scan size 5 µm. Blue areas are indicative of decreased shift in phase angle and correspond to larger height values. These areas are sharp peaks as identified in the standard 3D image (RHS). Image shown is representative of three separate stents.

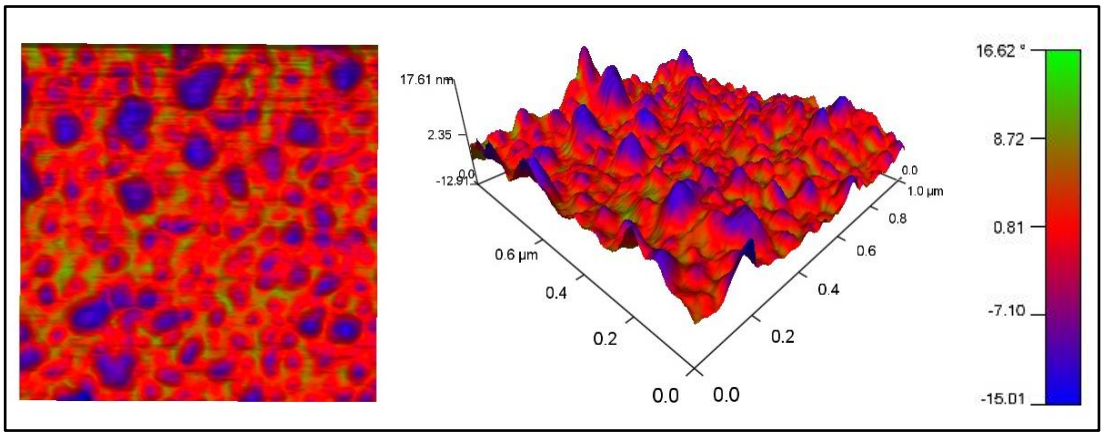

Figure 3-29: Sample: Taxus® Express^{2TM} stent. AFM height retrace image with phase overlay (ortho projection LHS, standard 3D RHS). Scan size 1 µm. Blue areas are indicative of decreased shift in phase angle and correspond to larger height values. These areas are rounded peaks. Green areas are indicative of increased shift in phase angle. Image shown is representative of three separate stents (image is 1 µm section of image in Figure 3-27)

The average R_{RMS} value of the Taxus® Express$^{2\ TM}$ surface has been calculated to be 33.36 ± 30.02 nm with the large standard deviation value thought to be due to the surface variations described above. The average values of RMS roughness, peak-to-valley distance, surface area, skew and kurtosis are displayed in Table 3-3. From this, the similarity of these numerical values to the other DES can be examined.

3.3.2.2.3. Xience Pro

The SEM images reveal the surface of the Xience Pro stent to be uneven (see Figure 3-30, insert A), with stress cracks evident throughout the surfaces that were examined (see Figure 3-30, insert B). The cracks are well defined and present in almost every curve of the stent strut.

Uneven sections of the coatings, including wrinkles, webbing and exposure of the bare metal platform are highlighted by the SEM images and are indicative of the coating being thicker in certain areas than others (see Figure 3-31, irregularities highlighted in red). There is also evidence of fragments of the coating becoming dislodged from the stent (see Figure 3-31, irregularities highlighted in red).

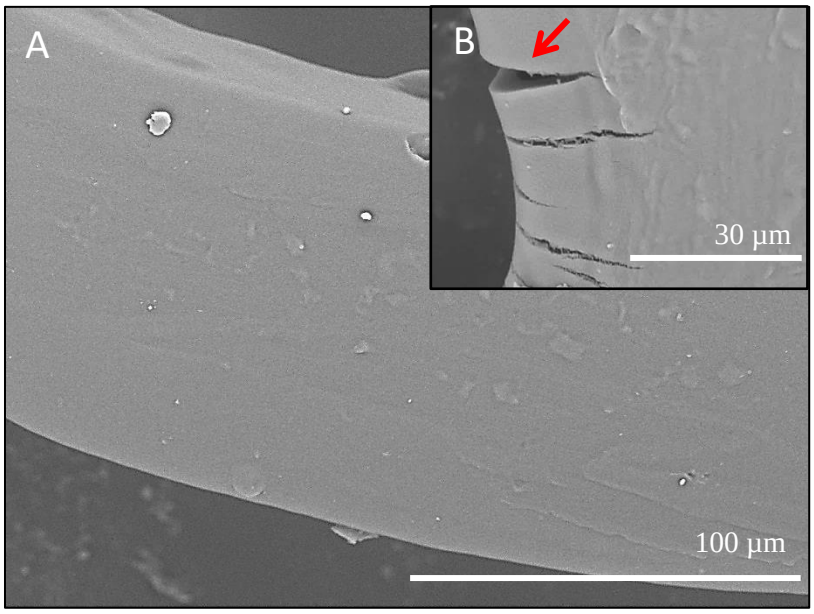

Figure 3-30: SEM images of Xience Pro stent strut surfaces. Example of stress crack labelled by red arrow. Images representative of three samples.

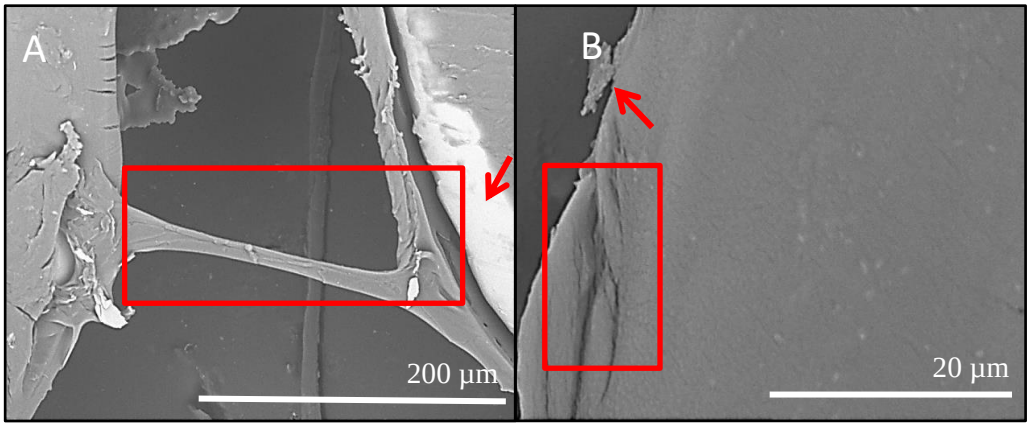

Figure 3-31: SEM images of Xience Pro stent strut surfaces showing coating irregularities A: Webbing indicated by red rectangle, exposed BMS platform indicated by red arrow. B: Wrinkles labelled by red rectangle, dislodged fragment of coating labelled by red arrow. Images representative of three separate samples

AFM analysis shows the surface of the Xience Pro stent to have a wave-like morphology with small pits often visible (see Figure 3-32).

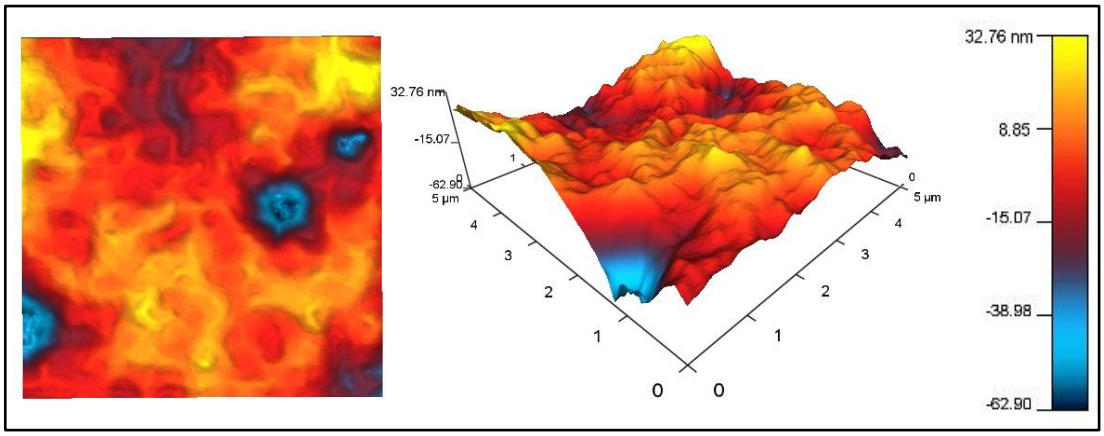

Figure 3-32: Sample: Xience Pro stent. AFM height retrace image (ortho projection LHS, standard 3D RHS), Scan size 5 µm. Blue areas are indicative of lower height and random pits. Image shown is representative of three separate stents.

One sample point at a scan size of 10 µm appears to capture the topography of a stress crack (see Figure 3-33). By reducing the scan size to 1 µm and overlaying the phase retrace image with the height retrace image (see Figure 3-34), a significant shift in the phase angle is observed. This will be further discussed in section 3.4.3.

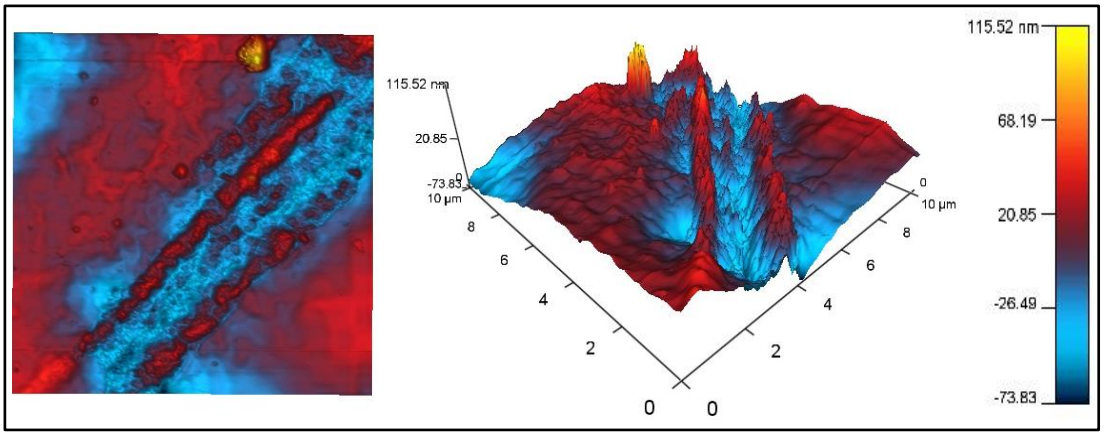

Figure 3-33: Sample: Xience Pro stent. AFM height retrace image (ortho projection LHS, standard 3D RHS), Scan size 10µm. Blue areas are indicative of lower height and possible stress crack. Image shown is representative of one sample point.

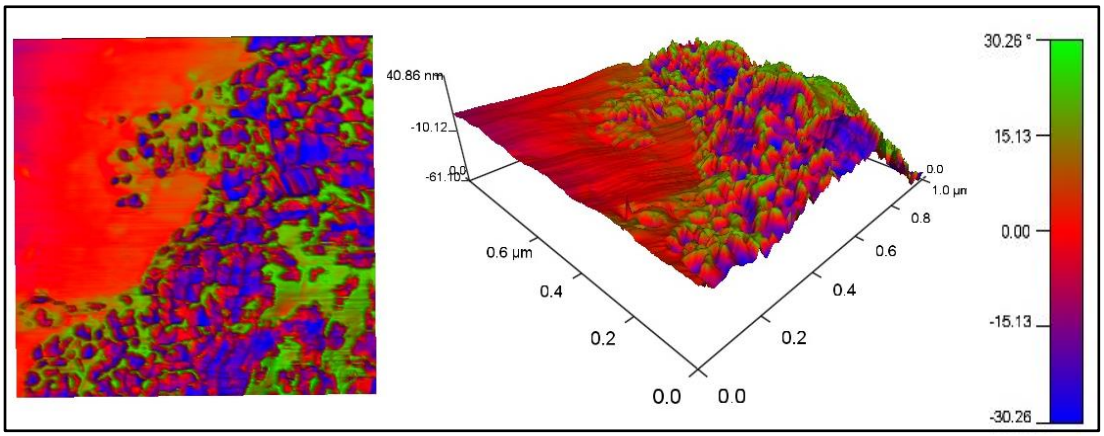

Figure 3-34: Sample: Xience Pro stent. AFM height retrace image with phase overlay (ortho projection LHS, standard 3D RHS), Scan size 1µm. Blue areas are indicative of decreased shift in phase angle and green areas are indicative of increased shift in phase angle. Area is small portion of the 'stress crack' displayed in Figure 3-33. Image shown is representative of one sample point.

The average R_{RMS} value has been calculated to be 32.59 nm ± 20.55 nm, similar to the other DES. The key quantitative measures of surface topography are gathered together in Table 3-3. It is clear that all of the DES examined display similar characteristics. However, the Yukon® stent displays quite distinct topographical differences, characterised by significantly greater roughness compared to all other stent types examined. The similarity between the R_{RMS} roughness values of the DES and BMS are graphically shown in Figure 3-34.

Table 3-4: Table of mean values of RMS roughness (R_{RMS}), surface area (SA), peak-to-valley distance (Ry), kurtosis (R_{KU}) and skewness (R_{SK}) calculated by AFM software at a scan size of 5µm. Mean values and standard deviation (SD) values calculated from four points per sample. (n=3). One-way ANOVA was significant ($p<0.05$).$p<0.05$ versus all other stent types (Tukey post hoc test) *$p<0.05$ significant difference between Yukon® (pre-drug release) and Xience Pro (Tukey post hoc test).*

Sample	Mean R_{RMS} ± SD (nm)	Mean SA ± SD (μm^2)	Mean Ry ± SD (nm)	Mean (R_{KU}) ± SD	Mean (R_{SK}) ± SD
Gazelle™	14.39 ± 11.24	25.15 ± 0.14	108.33 ± 71.40	0.25 ± 0.72	2.05 ± 3.63
Yukon® (post-drug release)	*182.02 ± 37.04	28.02 ± 0.98	*1167 ± 271.13	0.25 ± 0.86	-0.42 ± 0.18
Yukon® (pre-drug application)	*85.52 ± 26.07	25.73 ± 0.37	*523.05 ± 153.89	0.39 ± 0.65	-0.33 ± 0.22
Cypher™	34.67 ± 34.77	25.27 ± 0.34	273.41 ± 259.36	2.43 ± 3.56	0.44 ± 0.81
Taxus® Express 2™	33.36 ± 30.02	25.66 ± 0.69	251.64 ± 205.04	2.66 ± 3.66	0.71 ± 0.88
Xience Pro	32.59 ± 20.55	25.23 ± 0.23	244.92 ± 169.66	1.37 ± 2.95	0.34 ± 1.68

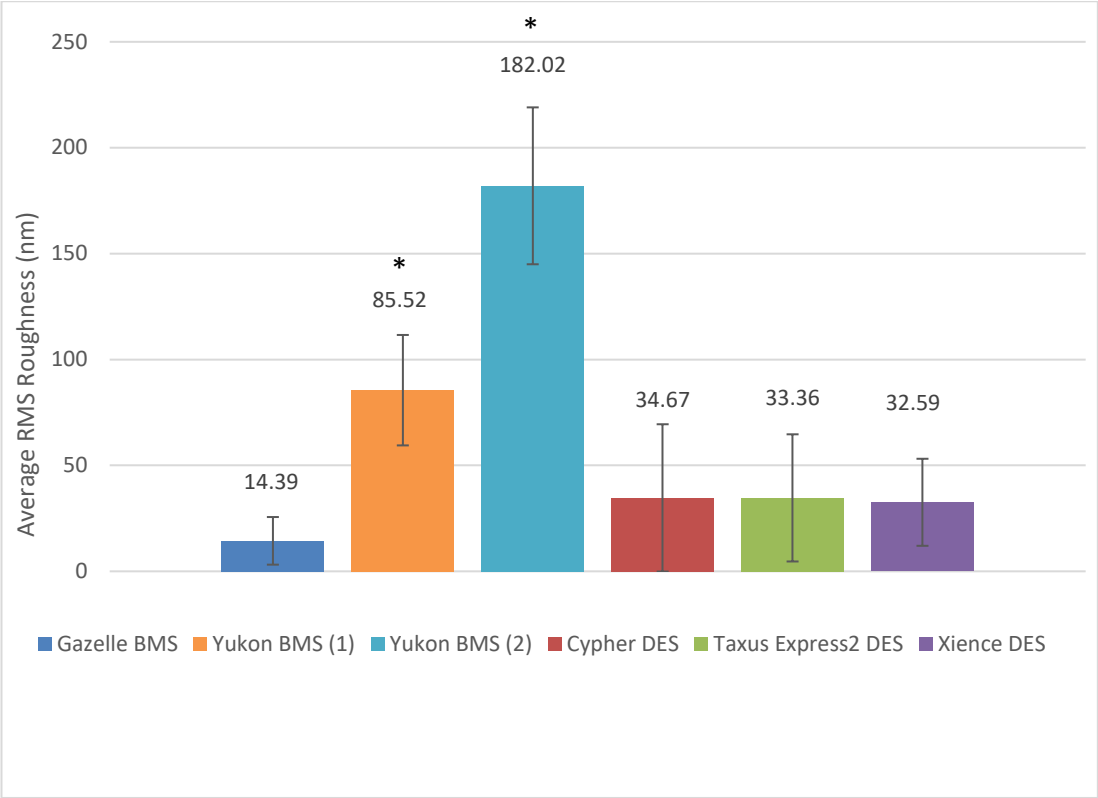

*Figure 3-35: Bar chart showing mean RMS roughness values for BMS and DES. Values labelled above bar is mean RMS roughness value for that particular stent surface. Error bars are indicative of standard deviation values calculated from four points per sample (n=3 for all stent types except n=2 for Yukon® BMS post drug release). (1) indicates Yukon® BMS pre-drug application, (2) indicates Yukon® BMS post drug release. * indicates significant difference between all other stent types.*

3.3.3. Effect of Drug Release on Surface Topography of DES

The surfaces of two Taxus® Express $^{2\ TM}$ stents were imaged by AFM and SEM analysis throughout a 28-day drug elution period by the method discussed in section 3.2.4. The findings on the change in surface topography and morphology throughout this period will be presented in the following section.

3.3.3.1. Taxus® Express^{2TM}

AFM analysis produced height retrace images of the surface of the Taxus® Express$^{2\ TM}$ stent throughout the 28-day drug elution period. The AFM height retrace images show visible pores at the 48 hour time point (see 48 hr panel, Figure 3-37) compared to a lack of pores pre-drug elution (see pre-elution panel, Figure 3-37). At the 28-day time point, AFM height retrace images show the presence of large voids (see 28-day panel, Figure 3-37). These have been shown in a different colour to previous AFM images in this study to better visualise pore formation.

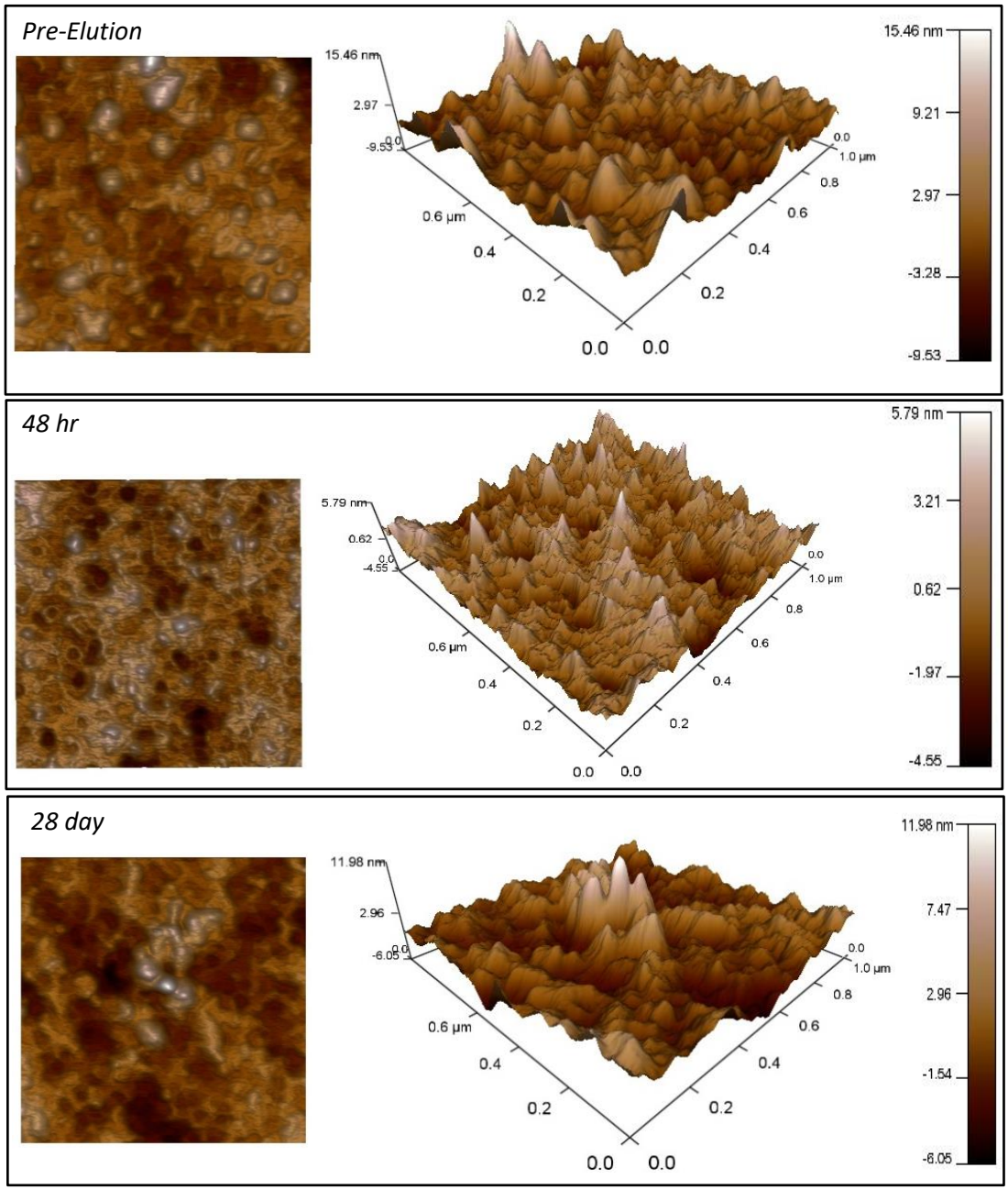

Figure 3-38: Sample: Taxus® Express 2 ™ at different stages of drug elution (pre-elution, 48 hr post-drug elution and 28 day post-drug elution, as labelled). AFM height retrace image (ortho projection LHS, standard 3D RHS), Scan size 1 µm. Images have been flattened. Peaks shown by white colour, indicating areas of large height in images pre-elution. No pores visible pre-elution. Small pores shown by dark brown colour, indicating areas of low height in images 48 hour post-elution. Large pores/voids shown by dark brown colour, indicating areas of low height in images 28 day post-elution. Areas of white colour indicate large height.

Overlying the height retrace image with the phase retrace image at a small scan size of 1 µm shows a shift in phase angle on the surface. The peaks are blue indicating decreased phase angle and there is a worm like structure shown in green indicating increased phase angle (see Figure 3-39, Figure 3-40, Figure 3-41). The blue peaks become smaller over the drug elution period, suggesting that the drug has been eluted. The green worm like structures are present

throughout the drug elution period, implying it to be a feature of the permanent polymer structure. This is discussed in section 3.4.4.

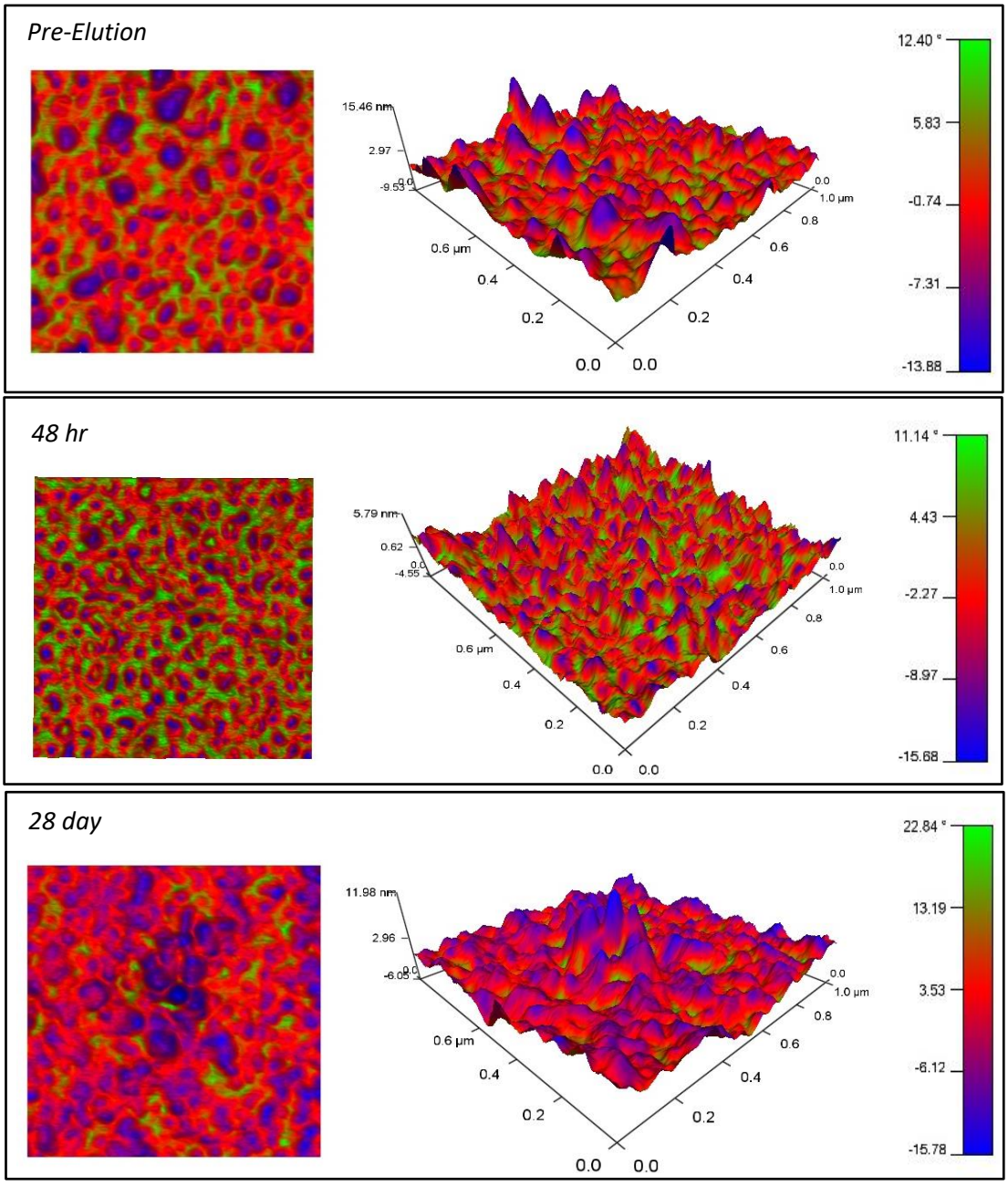

Figure 3-41: Sample: Taxus® Express [2] ™ stent at different stages of drug elution (pre-elution, 48 hr post-drug elution and 28-day post-drug elution, as labelled). AFM height retrace image with phase overlay (ortho projection LHS, standard 3D RHS) Scan size 1 µm. Image has been flattened by AFM software. Areas coloured blue indicate areas of decreased shift in phase angle and areas coloured green indicate areas of increased shift in phase angle. Worm-like structure visible at all time points.

The values of average R_{RMS} do not appear to significantly change over the drug eluting period, remaining in the range of 30 - 39 nm from 0 hour – 28 day. At the 48-hour time point, the average peak-to-valley distance increases from 273.41 nm ± 259.36 nm (pre-drug elution) to 312.89 nm ± 197.92nm (48 hour time point). An average kurtosis of >3 is also noted at the 48 hour time point, indicating sharp peaks, consistent with the AFM images and presence of pores following suspected paclitaxel release. See *Table 3-5* for full list of results.

Table 3-5: Table of mean values of RMS roughness (R_{RMS}), surface area (SA), peak-to-valley distance (Ry), kurtosis (R_{KU}) and skewness (R_{SK}) calculated by AFM software at a scan size of 5 µm. Samples are Taxus® Express $^{2\ TM}$ stent throughout the drug elution period. Mean values and standard deviation (SD) values calculated from four points per sample (n=2). One-way ANOVA ($p<0.05$), Multiple Paired T-tests with Bonferroni correction ($p<0.00625$). No statistically significant difference between data from different time points and sample pre-elution.*

Sample	**Mean R_{RMS} ± SD (nm)**	**Mean SA ± SD (µm^2)**	**Mean Ry ± SD (nm)**	**Mean (R_{SK}) ± SD**	**Mean (R_{KU}) ± SD**
Pre-elution	34.67 ± 34.77	25.27 ± 0.34	273.41 ± 259.36	2.66 ± 3.66	0.71 ± 0.88
15 min	38.65 ± 33.15	25.61 ± 0.70	286.75 ± 103.94	0.59 ± 0.54	2.04 ± 2.15
2 hours	32.75 ± 20.46	25.35 ± 0.40	251.03 ± 103.40	-0.18 ± 0.52	1.73 ± 2.15
1 day	35.86 ± 30.91	25.36 ± 0.50	246.66 ± 150.43	0.07 ± 0.83	1.63 ± 2.20
2 day	36.09 ± 25.30	25.49 ± 0.50	312.89 ± 197.92	0.33 ± 0.90	3.39 ± 6.46
7 day	33.15 ± 33.72	25.51 ± 1.08	246.91 ± 199.77	0.53 ± 0.84	2.84 ± 3.14
14 day	39.09 ± 43.30	25.66 ± 0.77	331.40 ± 320.70	0.59 ± 0.47	2.64 ± 3.29
28 day	30.12 ± 21.41	25.33 ± 0.27	224.70 ± 203.63	0.30 ± 0.79	1.93 ± 2.69

As mentioned in section 3.3.2.2.2, AFM imaging of the Taxus® Express $^{2\,TM}$ stent prior to drug elution exhibited two different 'types' of surfaces (sharp peaks and smoother surface). This was consistent throughout the drug elution period, leading to variations in surface topography between sample points, hence the large standard deviation values.

SEM imaging took place following the 28 day drug release period. On the surface of one sample, crystallisation of drug or PBS appears to have taken place on the surface (see Figure 3-42, insert A). This may be due to the fact that the sample was not rinsed prior to analysis. To counteract this problem, the second sample was rinsed with fresh PBS/Tween20 prior to being dried in a gentle stream of argon which appears to solved this issue (see Figure 3-42, insert B).

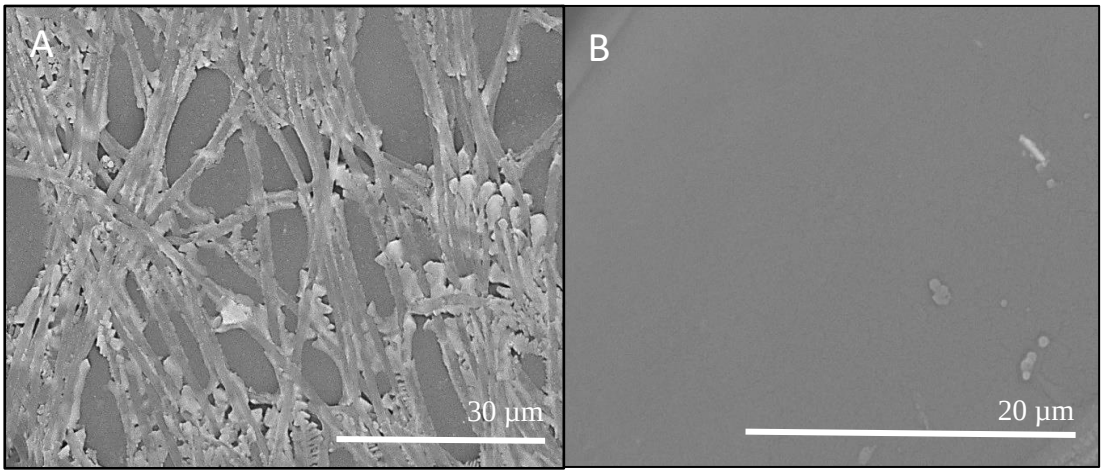

Figure 3-42: SEM images of surface of Taxus® Express $^{2\,TM}$ following drug release. A: Crystallised drug or PBS visible on surface. Image representative of one stent surface. B: Sample rinsed and dried post-drug release. Featureless surface with no crystalline drug or PBS present. Image representative of one stent surface.

No difference is observed between the SEM images before (see Figure 3-25, insert A) and after drug release (see Figure 3-42, insert B), this is likely to be due to the limitation of the SEM microscope at the micrometre scale, making it impossible to visualise pore formation.

3.3.4. Cell Culture Studies – Effect of Surface Topography on Viability of ECs

Experimental studies were performed in line with the methods outlined in section 3.2.5. Porcine ECs were seeded onto stainless steel (316L) stent struts of known surface roughness (Gazelle^{TM,} mean R_{RMS} = 14.39 ± 11.24 nm or Yukon®, mean R_{RMS} = 85.52 ±26.07 nm). Cell viability was analysed by means of live/dead staining and LDH assay. The method, seeding density and incubation time were all altered in the present study to obtain optimum experimental conditions. The results obtained will be outlined in the following sections.

3.3.4.1. Preliminary Studies

In the initial studies, live/dead staining was performed in line with the standard method used in the department, which included several washing steps. It was found that very few cells were present on the surface at the point of imaging, with some samples showing zero cells on the surface. This was despite light microscopy showing cells surrounding the samples. It was concluded that cells were removed from the surface in the washing steps and so these steps were eliminated from the subsequent experiments.

3.3.4.2. Increased Seeding Density

Initial studies were performed at a seeding density of 1 x 10^5 cells/cm^2 for an incubation period of 6 days. There were minimal cells present on the surfaces of the two sample types, so cells were not formally quantified at this seeding density. The seeding density was increased in further experiments and the results outlined in the following section.

The seeding density was increased from 1 x 10^5 to 2 x 10^5 cells/cm^2, maintaining the incubation time at 6 days. Live/dead staining images show cells around the edges of both sample types. In some images (see Figure 3-43), the cells appear to begin to grow over the surfaces. By visual inspection, there appeared to be more cells present on the live/dead staining images of these sample surfaces than those in the previous study performed at the lower seeding density (seeding density 1 x 10^5 cells/cm^2). However, cells did not fully form over the surfaces of either sample type and so the numbers of adherent cells were not formally quantified at this preliminary stage of the study.

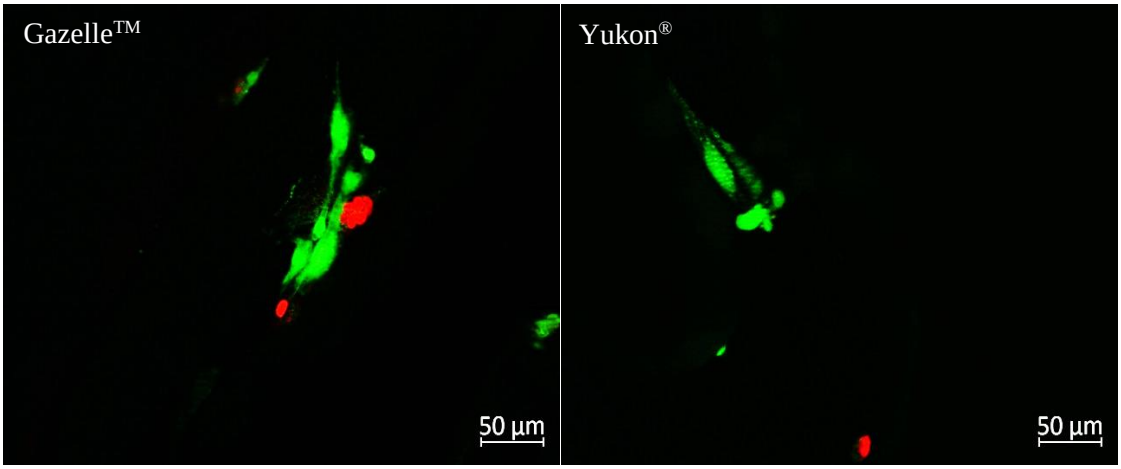

Figure 3-43: live/dead staining images of porcine ECs grown on surface of stents struts of thickness 112 µm (Gazelle™) LHS, 87 µm (Yukon®) RHS) Seeding density 2 x 10^5 cells/cm^2, incubation period 6 days. Green indicates live cell, red indicates dead cell. Images are representative of 3 samples Small number of cells adhered to surface of stents struts.

3.3.4.3. Increased Incubation Time

In the next phase of experiments, the cell seeding density was maintained at 2 x 10^5 cells/cm^2 but the incubation time was increased from 6 days to 13 days. This increased incubation period was implemented to allow greater levels of cell growth over the surface of the stent samples. At the 13 day time point, five random areas per sample were imaged using live/dead staining; cells were counted using imaging software (ImageJ). The mean number of cells was calculated from 15 figures (5 values per 3 samples) to formally quantify the number of cells on the surfaces. The standard deviation values were also taken from 5 values per 3 samples. LDH assays were performed at the following time points (3 day, 6 day, 9 day, and 13 day).

At the 13 day time point, the number of cells observed on the surfaces of both stent types had appeared to increase in comparison to the 6 day time point (see section 3.3.4.2). From the live/dead staining images, it is evident that there was a visual difference between the coverage of the cells on the two different stent surfaces, with more coverage observed on the surface of the Yukon® stent (see Figure 3-44). This was confirmed by the observed difference in mean number of cells on each surface type (55 ± 41 (Gazelle™), 91 ± 62 (Yukon®)) (see Table 3-6 for full list of values). Values of mean percentage live/dead cells were found to be similar between the two sample types, with a larger proportion of live cells in each case (see Table 3-6 for percentage live/dead values). Despite the large difference in cell number on each

surface and the difference in cell coverage observed qualitatively, statistical analysis showed no significant difference between the values on the surfaces of the two stent types.

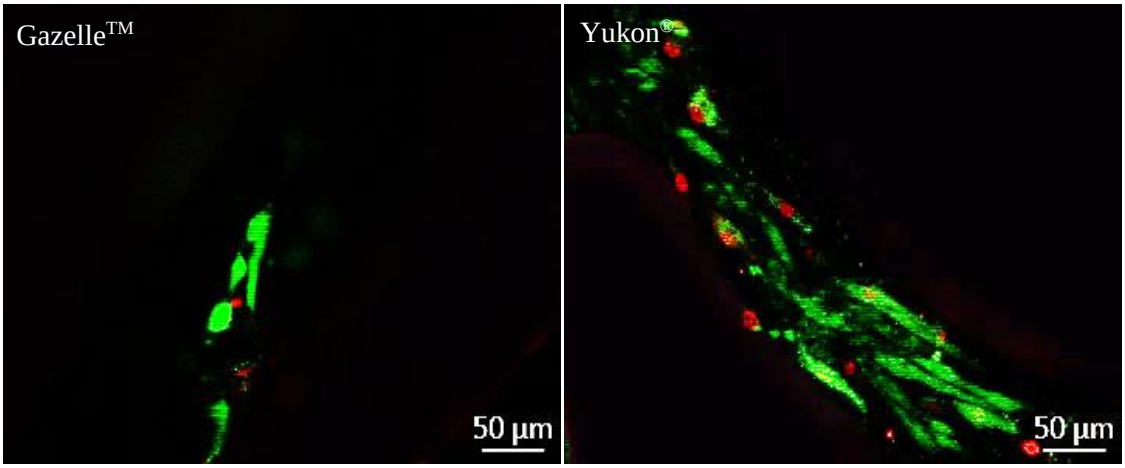

Figure 3-44: live/dead staining images of porcine ECs grown on surface of stents struts of thickness 112 µm (Gazelle™) LHS, 87 µm (Yukon®) RHS). Seeding density 2 x 10^5 cells/cm^2, incubation period 13 days. Green indicates live cell, red indicates dead cell. Images representative of 5 sample points per sample from 3 samples.

Table 3-6:Table of mean values of percentage live, percentage dead and total number of cells for porcine ECs grown on surface of stents struts of thickness 112 µm (Gazelle™), 87 µm (Yukon®)). Seeding density 2 x 10^5 cells/cm^2, incubation period 13 days. Mean values calculated from 5 sample points per sample from 3 samples. Table includes standard deviation (SD). Two-tailed T test ($p<0.05$) proved no significant difference between data presented in this table.

Gazelle™		**Yukon®**	
Mean Percentage Live Cells ± SD (%)	56.44 ± 0.05	Mean Percentage Live Cells ± SD (%)	58.87 ± 0.07
Mean Percentage Dead Cells ± SD (%)	43.56 ± 0.05	Mean Percentage Dead Cells ± SD (%)	41.13 ± 0.07
Mean Total Cell Number ± SD	55 ± 41	Mean Total Cell Number ± SD	91 ± 62

3.3.4.3.1. Pre-treatment with FBS

Maintaining the seeding density (2 x 10^5 cells/cm^2) and total incubation period (13 day), the next phase of experiments introduced a pre-incubation of the stent samples with FBS (1 hr, 37 °C) prior to use. This was in an attempt to improve cell attachment to the stent surfaces.

It was found that the use of FBS led to a slight increased total number of adherent cells on the Gazelle™ stent samples after 13 days, compared to the non FBS treated samples (see section 3.3.4.3). However, a decrease in total number of adherent cells was observed for the Yukon® samples under the same conditions. It was further found that there was a difference in the adherence of the cells to the two different stent types, with a larger number of cells found on the Gazelle™ surfaces (68 ± 44) than the Yukon® surfaces (29 ± 23) after 13 days (see Table 3-7 for list of data). This difference is shown qualitatively by live/dead images in Figure 3-45 where the growth of cells across the Gazelle™ surface is visible compared to the presence of the cells only around the edges of the Yukon® stent strut. This is in contrast to what was found in the study in the absence of the pre-treatment with FBS.

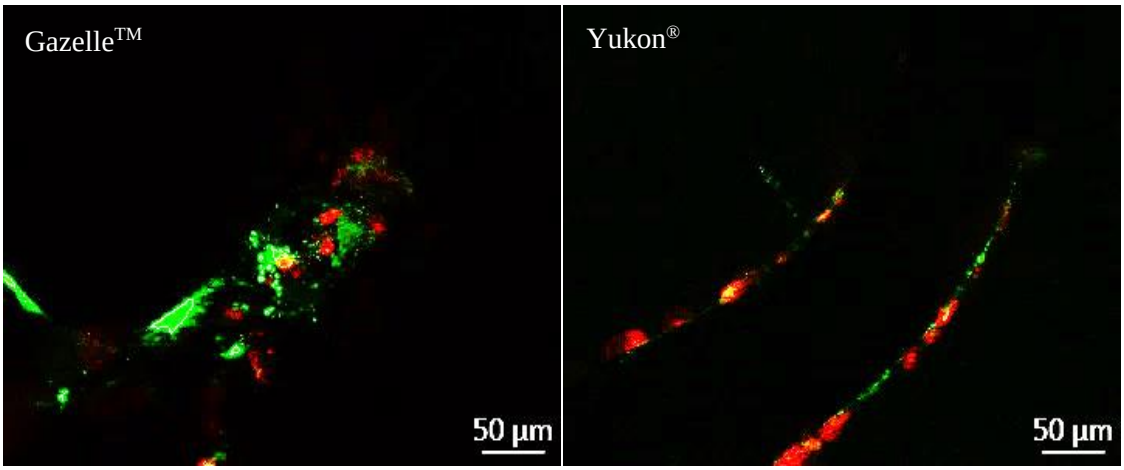

Figure 3-45: live/dead staining images of porcine ECs grown on surface of stent struts of thickness 112 µm (Gazelle™) LHS, 87 µm (Yukon®) RHS). Seeding density 2 x 10^5 cells/cm^2, incubation period 13 days, pre-treatment with FBS for 1 hour. Green indicates live cell, red indicates dead cell. Images representative of 5 sample points per sample from 3 samples. Samples pre-treated with FBS.

Table 3-7: Table of mean values of percentage live, percentage dead and total number of cells for porcine ECs grown on surface of stents struts of thickness 112 µm (Gazelle™) LHS, 87 µm (Yukon®) RHS). Seeding density 2 x 10^5 cells/cm^2, incubation period 13 days. Samples pre-treated with FBS. Mean values calculated from 5 sample points per sample from 3 samples. Table includes standard deviation (SD). Two-tailed T test ($p<0.05$) proved no significant difference between data presented in this table.

Gazelle™		**Yukon®**	
Mean Percentage Live Cells ± SD (%)	52.35 ± 0.05	Mean Percentage Live Cells ± SD (%)	44.20 ± 0.16
Mean Percentage Dead Cells ± SD (%)	47.65 ± 0.05	Mean Percentage Dead Cells ± SD (%)	55.80 ± 0.16
Mean Total Cell Number ± SD	68 ± 44	Mean Total Cell Number ± SD	29 ± 24

3.3.4.4. Removal of Sample to Fresh Well Post Cell Seeding

To allow the viability of cells directly in contact with the surface to be monitored, eliminating the influence of the cells that additionally form over the base of the well, the sample must be removed following initial cell attachment. Initially, stent samples were removed following 1 hour incubation with the cell suspension and placed in a fresh well (no pre-treatment with FBS). Analysis was performed in line with previous experimental methods in section 3.2.5 (seeding density (2 x 10^5 cells/cm^2) and incubation period (13 day)). It was found that very few cells were present on the surfaces following the 13-day time point.

Subsequently, the experiment was repeated with the addition of pre-treatment with FBS (1 hour) and a prolonged initial incubation period with the cell suspension of 24 hours. The findings from this set of experiments will be outlined in this section.

From the live/dead staining images, it was apparent that the greatest number of cells were found to be adherent to the stent surfaces using these updated experimental conditions, when compared to any of the experimental conditions previously used (see sections 3.3.4.2, 3.3.4.3,

3.3.4.3.). There was a slightly larger total number of cells found on the Gazelle™ samples (114 ± 47) when compared to the Yukon® samples (101 ± 57), however, this difference is not statistically significant. In terms of percentage live/dead cells, there was a slightly larger percentage of live cells (52.31 ± 0.09 %) compared to dead cells (47.69 ± 0.09 %) on the Gazelle™ stent samples. The opposite was observed on the Yukon® samples with a slightly higher percentage of dead cells (50.49 ± 0.52 %) than live cells (49.51 ± 0.52 %) present on the surface (see Table 3-8 for full list of values).

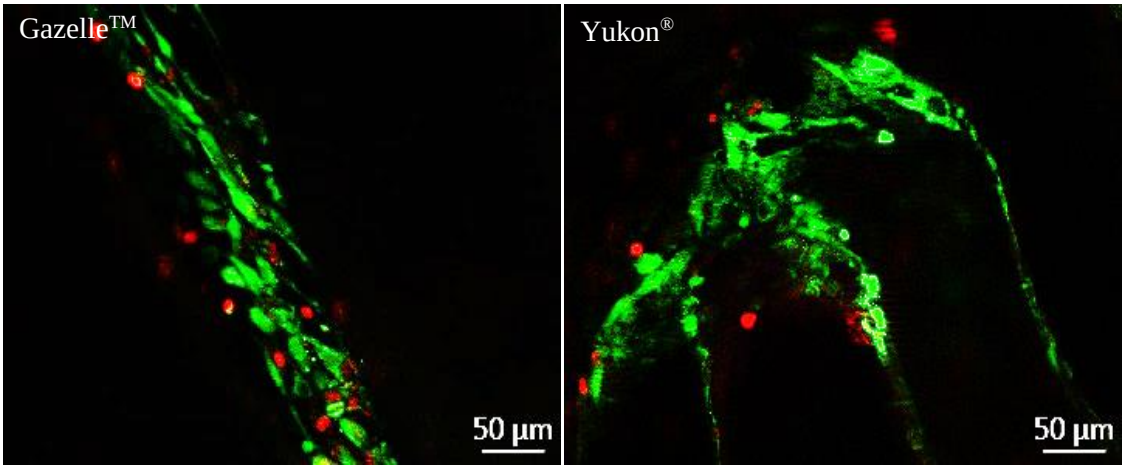

Figure 3-46: live/dead staining images of porcine ECs grown on surface of stents struts of thickness 112 µm (Gazelle™) LHS, 87 µm (Yukon®) RHS). Seeding density 2 x 10^5 cells/cm^2, incubation period 13 days, pre-treatment with FBS for 1 hour. Samples removed to fresh wells following incubation with cells for 24 hours. Green indicates live cell, red indicates dead cell. Images representative of 5 sample points per sample from 3 samples.

Table 3-8: Table of mean values of percentage live, percentage dead and total number of cells for porcine ECs grown on surface of stent struts of thickness 112 µm (Gazelle™), 87 µm (Yukon®)). Seeding density 2 x 10^5 cells/cm^2, incubation period 13 days, pre-treatment with FBS for 1 hour. Samples removed to fresh wells following incubation with cells for 24 hours. Mean values calculated from 5 sample points per sample from 3 samples. Table includes standard deviation (SD). Two-tailed T test ($p<0.05$) proved no significant difference between data presented in this table.

Gazelle™		**Yukon®**	
Mean Percentage Live Cells ± SD (%)	52.31 ± 0.09	Mean Percentage Live Cells ± SD (%)	49.51 ± 0.052
Mean Percentage Dead Cells ± SD (%)	47.69 ± 0.09	Mean Percentage Dead Cells ± SD (%)	50.49 ± 0.52
Mean Total Cell Number ± SD	114 ± 47	Mean Total Cell Number ± SD	101 ± 57

In terms of cell number, there was a marginally larger number of dead cells present on the Gazelle™ surface compared to the Yukon® surface at the 13 day time point. This observation is supported by the findings from the LDH assay, which demonstrate a larger mean LDH enzyme activity on the Gazelle™ samples at the 13 day time point (see Figure 3-47).

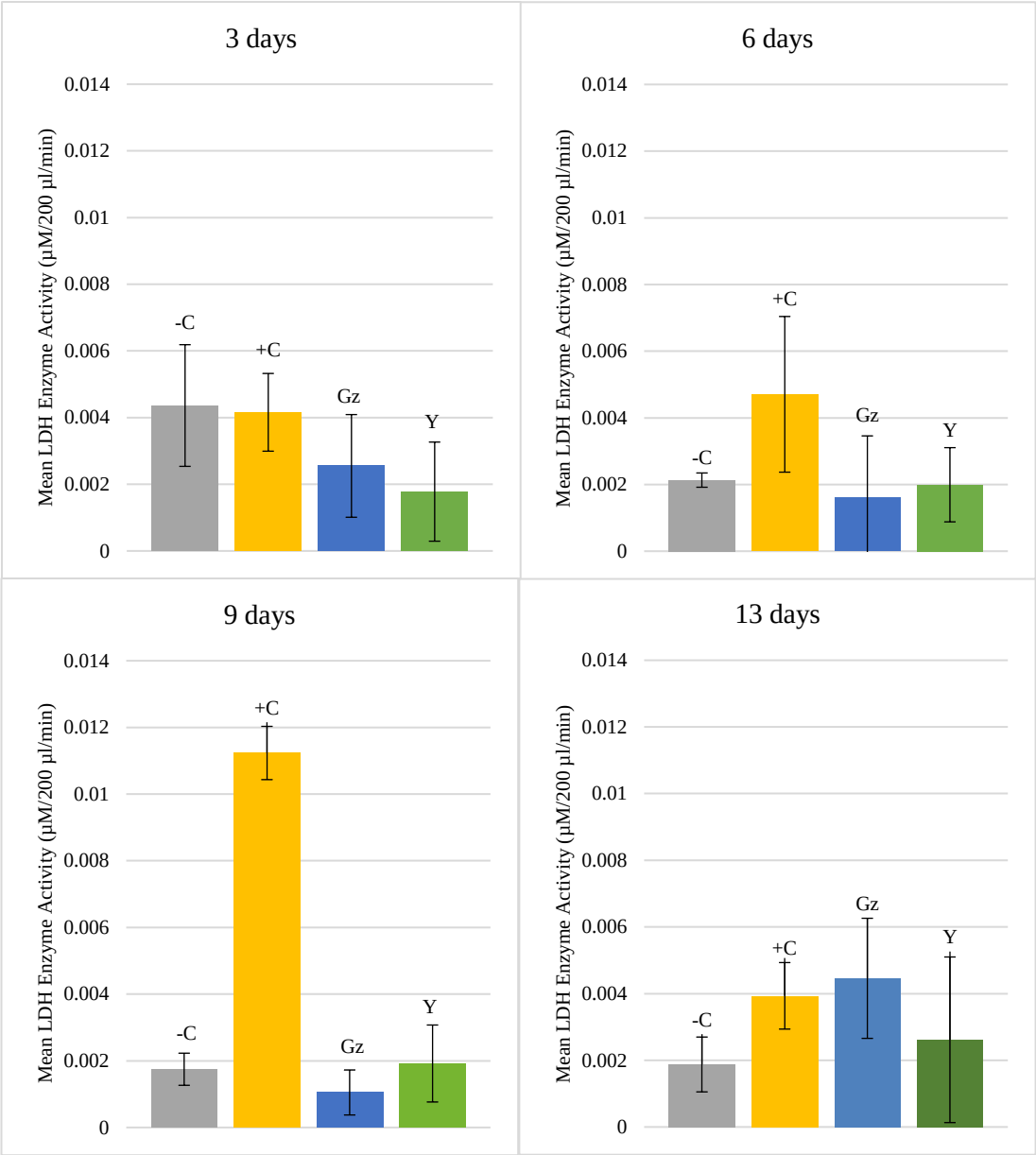

Figure 3-47: Bar chart showing levels of LDH enzyme excreted by porcine ECs on surface of stents struts (Gazelle™), (Yukon®) and positive and negative controls at 3day, 6 day, 9 day and 13 day time points. Seeding density 2 x 10^5 cells/cm^2, incubation period 13 days, pre-treatment with FBS for 1 hour. Samples removed to fresh wells following incubation with cells for 24 hours. All values are mean values calculated from n=3. Error bars are indicative of standard deviation (SD). -C indicates negative control (cells only), +C indicates positive control (cells treated with Triton-X 100), Gz indicates Gazelle™ stent and Y indicates Yukon® stent.

3.4. Discussion

Studies have revealed interest in incorporating surface topography into stent design (ter Meer et al., 2017, Palmaz et al., 2002) and this concept has been integrated into stent design for widespread clinical application (Dibra et al., 2005). Recent studies have revealed a potential link between surface topography and endothelial cell behaviour (Liliensiek et al., 2010, Samaroo et al., 2008). As the surface topography of clinically relevant stents is not widely reported, the aim of this study was to characterise the surface topography and morphology of a range of clinically relevant stents, investigate how this changes during the drug elution period and how it could affect the behaviour of endothelial cells. The surfaces were characterised by AFM and SEM analysis and the cell behaviour analysed by live/dead staining and LDH assays. The outcomes from this study are discussed in the following section.

3.4.1. Method Development and Validation

The preliminary work in this study involved the characterisation of medical grade (316L) stainless steel (SS) surfaces to assess whether the characterisation techniques (AFM and SEM) are appropriate for the analysis of stent surfaces. The surfaces of four different SS (316L) materials (polished SS plate, unpolished SS plate, untreated SS wire, pre-treated SS wire) were analysed.

SEM analyses successfully showed a difference in the surface features of polished and unpolished SS (316L) plates at the micrometre scale. Grain boundaries are visible on the unpolished SS (316L) plate whereas their absence is noted from the surface of the polished SS (316L) plate (see section 3.3.1). These surfaces were imaged at the same magnification, allowing a fair comparison to be made between the surface features. SEM analysis was performed on treated (SiC in ultrasonic bath) and untreated SS (316L) wires, again showing the ability of the SEM technique to characterise surface features, in this case pits, created by the surface treatment. This was of importance in this study as the surfaces of stents can be bare metal (containing grain boundaries), microporous (containing pits) or a polymer surface (fairly featureless).

AFM analyses was used in a similar way to SEM analyses to identify the surface features of the SS (316L) materials, but at the nanometre scale. The grain boundaries observed in the SEM images were successfully captured in the AFM height retrace images with additional detail, including their dimensions. The lack of these features was noted in the height retrace images

of the polished SS (316L) plate, showing the ability of this technique to capture surface features of varied dimensions. Height retrace images of the untreated/pre-treated SS (316L) wire allowed the dimensions of the pits to be analysed, successfully showing the surface features before the treatment and then after the treatment.

Average R_{RMS} roughness values have been obtained for all of these surfaces, showing the smallest average R_{RMS} value for the polished SS (316L) plate (4.07 ± 2.71 nm) and the largest average R_{RMS} value for the unpolished SS (316L) plate (44.64 ± 8.07 nm). A large difference in average R_{RMS} roughness is also observed between the untreated SS (316L) wire (23.53 ± 8.13 nm) and pre-treated SS (316L) wire (43.57 ± 14.10 nm), showing that the AFM can image surface roughness at the nanometre scale.

Average values of peak-to-valley distance (R_y) have been successfully obtained for all samples, showing the average distance between the peaks and valleys (see section 3.3.1). The largest difference was observed between the polished (average R_y = 34.50 ± 14.12 nm) and unpolished (average R_y = 428.56 ± 46.81 nm) SS (316L) plate. This was expected as the AFM analyses shows a very smooth surface for the polished plate compared to the presence of many peaks and valleys due to the grain boundaries on the unpolished surface. Although the untreated SS (316L) wire samples exhibited many surface defects, contributing towards a large average R_y value (171.60 ± 37.47 nm), an average R_y value of more than double that is observed for the surface of the pre-treated SS (316L) wire (379.58 ± 97.18 nm). This emphasises the ability of the AFM to identify even the smallest pit present on the surface. This is of importance when analysing the surface of DES throughout the drug elution period as the elution of a drug from the stent surface will often leave a pore of nanometre dimensions.

Values of kurtosis and skew are also included in this preliminary work with the view of using these values for surface analysis during the drug elution period. The kurtosis (Ku) gives a measure of the peaks on a surface with large values indicating a small number of high peaks or very low valleys. This is useful for further understanding the development of pores on a surface throughout the drug elution period.

The skewness (Sk) is a measure of the asymmetry of the distribution of heights within the surface with a negative value indicating the presence of pits and depressions and a positive value indicating a flat surface. Negative average skew values were noted for the untreated SS (316L) wire and SS (316L) plate. This is as expected due to the presence of grain boundaries and surface defects in these two sample types. It would therefore be expected that the pre-treated SS (316L) wire which has pits throughout the surface would exhibit a negative skew

value. However, this was not the case and a positive value was obtained. Although this was not expected, the skew value is less than half the value obtained for the polished SS (316L) plate which had a very flat surface.

3.4.2. Surface Topography of Bare Metal Stents

The main surface feature identified on the Gazelle™ BMS surface is the presence of grain boundaries. The surface within these boundaries appear featureless with only 'brush marks' present, shown by SEM images. This is characteristic of the surface features of the SS (316L) materials previously reported in the literature (Mohd Daud et al., 2016) and in the preliminary work performed in this study.

The Gazelle™ BMS exhibited the lowest average R_{RMS} value of all of the stent types examined. The average R_{RMS} value (14.39 ± 11.24 nm) is similar to that of the untreated SS (316L) wire surface (23.53 ± 8.13 nm). The similarity between the average R_{RMS} values of these two surfaces helps justify the use of the untreated SS (316L) wire to mimic a stent material as is studied in chapter 4. The Gazelle™ BMS and untreated wire surfaces are greatly different to that of the Yukon® stent surface post drug release (182.02 ± 37.04 nm). The average R_{RMS} value of the Yukon® stent is more than 10x larger than the Gazelle™ BMS due to the microporous surface morphology.

The average R_{RMS} values of the two Yukon® stents (both post drug release) exhibit quite large standard deviation values, relative to those obtained when analysing the SS (316L) plates and wires. This suggests significant variations exist between the different locations examined on the Yukon® stent surface and may be due to the sandblasting manufacturing technique. Although an alternative method (Nano focus white light interferometer) was used to determine the R_{RMS} value in the study by Dibra et al, a similar value range of 0.09 – 0.21 nm was obtained. This not only shows similarities to the average R_{RMS} roughness value obtained in the present study but also suggests variability. Such variability in the stent coating may have important implications on not only the uniformity of drug load across the stent surface, but also on the biocompatibility of the stent. Whilst SEM is a very useful method of obtaining information on the uniformity of the stent surface and gross topographical features, AFM analysis provides enhanced resolution and quantifies important surface parameters.

AFM data shows that the average R_y value of the Yukon® surface (1784.31 ± 208.78 nm, scan size 20 µm, post drug release) is similar to the pore size reported by the manufacturer (2000 nm) (Translumina, 2009). Despite a pore size of approximately 2 µm being stated by the manufacturer, it is unclear how this value was obtained and there is no standard deviation value available. The average R_y standard deviation value obtained in the present study suggests inconsistent size of pores, again likely to be due to the random nature of the manufacturing technique. This could have an impact on the mass of drug stored in the pores and subsequently released into the artery wall.

To our knowledge this is the most comprehensive investigation of the Yukon® stent surface carried out to date. The average R_{RMS} value reported in the present study is in the range of that reported by Dibra et al (using white light interferometer), whilst to our knowledge this is the first time that a value of surface area has been reported in the literature. Although pore size was also reported by Dibra et al, we have provided an average peak-to-valley distance value including a value of standard deviation which provides greater understanding into the variation in surface topography. Quantifying the properties of the stent surface in this way could help provide new insights into stent performance that are not possible through the use of the more standard techniques such as SEM.

In this study, SEM images also revealed flat areas of the Yukon® stent (post drug release) which appear to correspond to flat areas of larger height on the 3D height retrace graphs. As previously discussed, this may be due to the random nature of the sandblasting manufacturing technique not impacting areas of the stent surface. However, a shift in phase angle is recognised at certain sample points which could indicate the presence of residual rapamycin following drug release.

To further investigate this issue, analysis was performed on three Yukon® CHOICE 4 DES, freshly opened and prior to the application of a drug layer. SEM images again successfully show the microporous surface of the Yukon® stent (pre-drug application), although they appear less well defined than the surfaces of the Yukon® stents post drug release. Flat areas were also visible on these stents, indicating this feature to be typical of the manufacturing process rather than the presence of drug remaining on the surface. SEM analyses confirms the microporous structure throughout the surface of the Yukon® stent which is in agreement with the literature (Dibra et al., 2005).

The differences between these two surfaces (pre-drug application/ post drug elution) is further highlighted using AFM analysis, with an average R_y value of the Yukon® stent (pre-drug application) much smaller (1167 ± 271.13 nm) than those post drug release (1782.9 ± 214.92). The average R_y value of the Yukon® stent pre-drug application (1167 ± 271.13 nm) no longer shows much similarity to the pore size reported by the manufacturer (2 μm). However, the R_{RMS} value pre-drug application is in the range of that reported by Dibra et al.

The three stents, analysed in the present study were all fresh from the packet, the same dimensions (diameter and length) and all obtained from the same batch. This could suggest that the surface of the Yukon® stents may have some variability between batches. As previously mentioned in this section, variability in this microporous structure could influence biocompatibility and performance issues.

Although the Yukon® stents were not analysed pre drug elution (with the drug layer intact) in the present study, SEM analysis of the pre-elution surface has been found in the literature (Abizaid and J. Ribamar Costa, 2010). At the micrometre scale, the pre-drug elution surface appears as a uniform layer because the drug has completely filled the underlying microporous structure (Abizaid and J. Ribamar Costa, 2010). It is important to note that when used clinically, the stent is initially implanted into the artery with a uniform surface. The drug release period of the Yukon® stent is up to 4 weeks (Translumina, 2009) which suggests that the underlying microporous layer is not fully exposed until 4 weeks post stent implantation. According to the in-stent restenosis time line (see section 1.3.2), this is after the early stages of thrombosis, inflammation and proliferation have already begun. It is imperative that re-endothelialisation is rapid post stent implantation and should be targeted immediately. It is likely that any beneficial effect of the microporous surface will be in the period post drug elution, therefore, it is questionable how much of an effect the microporous surface would have in the crucial early stages post stent implantation.

3.4.3. Surface Topography of Drug Eluting Stents

Surface analysis of three drug eluting stents (Cypher™/ Taxus® Express^{2} ™ /Xience Pro) indicate similarities in their surface topography and morphology. The similarities in these surfaces were initially outlined by SEM analyses, with the outermost polymer layer showing a fairly featureless surface in all cases. Unlike the BMS (Gazelle™/Yukon®), there is a distinct

lack of large surface features visible at the micrometre scale for all DESs. However, coating irregularities are noted in almost all of the DES and these will be discussed in section 3.4.3.1.

All numerical AFM data from the three different types of DESs are found to be significantly different to that of the Yukon® stent. Significantly larger average R_y values are noted for all DES compared to the Gazelle™ stent. The R_y value can be indicative of a defect present which in this case further demonstrates surface irregularities present on the polymer coatings.

The average R_{RMS} value of the Gazelle™ stent is found to be significantly less than that of the Xience Pro stent but not the Cypher™ or Taxus® Express^{2} ™ stents. This is likely to be due to the large standard deviation values of the roughness data of the Cypher™ and Taxus® Express^{2} ™ stents, indicating variation between sample points. This surface variation is discussed later in this section. There is no statistically significant difference between the average R_{RMS}, SA or R_y values obtained for the three DES types.

Values of $R_{RMS,}$ SA and R_y have not previously been reported in the literature for the Xience Pro stent, with partial data sets reported for the Cypher™ and Taxus® Express^{2} ™ stents (Biggs et al., 2012, Ranade et al., 2004). The results from this study allow a new insight into the surface of a widely used DES (Xience Pro) and also allows its surface to be directly compared to other clinically relevant DES and BMS.

Although no information regarding the numerical values of the Xience Pro stent is available in the literature for comparison, the study by Ding et al does include height retrace analysis of the Xience Pro surface (Ding et al., 2009). It reports a 'granular' texture at a scan size of 2 μm and no difference in phase is reported. A similar outcome is noted in the present study at a scan size of 1 μm and 5 μm.

Analysis of the phase/height retrace images of the Xience Pro surface shows no difference in the phase of the surface in this study. This suggests that the surface topography is a result of the polymer and not related to the presence of the drug which agrees with the study by (Ding et al., 2009). This is an interesting finding as there is no topcoat present on the Xience Pro stent, so the outermost layer is a mixture of polymer and drug which would be expected to exhibit a difference in phase. Although this has previously been observed (Ding et al., 2009), it is still interesting to note that the presence of the drug does not lead to a change in phase that may have been expected. A drug elution study would have to take place on this surface to analyse what effect drug release would have on the surface topography and phase.

Phase/height retrace images of the Cypher™ stent display some interesting results (see Figure 3-24). Although most sample points exhibit minimal shift in phase angle, some points show a larger phase shift. The outermost layer of the Cypher™ stent is a mixture of two polymers (PEVA and PBMA) but no drug is present. The final drug free layer allows for the sirolimus to slowly migrate towards the stent surface, providing only a small initial burst. It is possible that the phase difference observed in some sample points is representative of the difference in the two polymers (PEVA and PBMA). It is also possible that the drug may have migrated to the outermost layer during storage causing a phase shift. The migration of drug during storage would also explain the drug crystallisation thought to be identified by SEM analysis (see Figure 3-21).

The lack of phase difference observed in the outermost layer of the Xience and Cypher ™ stents is in contrast to the Taxus®Express² ™ stent where a phase difference is much more apparent. The phase/height images of the Taxus® Express² ™ stent surface show the decreased phase angle to correspond with the larger height values. When compared to the literature, it can be suggested that the areas of decreased phase angle and large height (blue spots on image) correspond to the paclitaxel particles which exist as discrete particles within the polymer matrix (Kamath, Barry et al. 2006). The Taxus® Express²™ stent, with the drug visible on the stent surface has an initial 48 hour burst where the drug is rapidly released (Ranade, Miller et al. 2004). On the other hand, the Cypher™ stent, with no drug particles visible on its' surface has only a small initial burst of drug release (see Figure 3-24 and Figure 3-29).

Areas of decreased phase angle may correspond to areas of low surface stiffness; therefore, it is suggested that paclitaxel particles within the Taxus® Express² ™ coating have a lower stiffness than the polymer. It is not only the difference between the polymer and drug that exhibits a shift in phase angle. The SIBS co-polymer on the Taxus® Express² ™ stent consists of two domains (PS and PIB) which is represented in the phase/ height retrace images (see Figure 3-29) as a 'worm-like' structure (green/red sections). These findings are backed up by the literature (Ranade, Miller et al. 2004). The shift in phase angle does not give numerical values of the surface stiffness, but it does give an indication of the difference in stiffness that could be present within the surface of a stent, not only by the presence of a drug but also polymer.

Surfaces of varied stiffness are reported to have an impact on the behaviour of cells, including endothelial cells. A study by (Murikipudi et al., 2013) compared the growth rate of human aortic endothelial cells (HAECs) on 3D scaffolds of different stiffness. It was found that the

HAEC growth rate and cell number were highest on the scaffolds of intermediate stiffness (508 Pa) and poorest on the stiffest (1100, 1300 Pa) and softest (~ 200, 400 Pa) scaffolds.

Areas of varied surface stiffness were identified on the surfaces of DESs in this study although these were not expressed quantitatively; this may be beneficial to look at in future studies. With so many different materials used in stents it is likely that a difference in surface stiffness will be observed and consequently an effect on cell behaviour would be observed. Given the emerging importance of substrate stiffness on cell response, this novel information may therefore be useful in both interpreting the performance of existing stents and in the optimisation of future devices.

3.4.3.1. Coating Irregularities

A number of coating irregularities were observed on the surface of all three of the DES (Cypher™, Xience Pro and Taxus® Express^{2} ™) that were analysed.

At the micrometre scale, stress cracks are noted on the edge of the stent struts for both the Cypher™ and Xience Pro stents (see Figure 3-21, Figure 3-30). Although the presence of stress cracks has been reported in the SSED of the Cypher™ stent (SSEDCypher, 2003), it has not been reported in the safety documents of the Xience Pro stent (SSEDXience, 2008) or other studies that have analysed the integrity of these coatings by SEM analysis (Basalus et al., 2009, Basalus and Clemens, 2010). However, it is important to recognise that despite the stents being expanded according to manufacturer's guidelines, findings reported in the present study were obtained by imaging drug eluting stents that were beyond their use-by date and hence interpretation of these findings should be carried out in this context.

AFM images of the Cypher™ stent appears to capture a crack of ~3 μm in length (see Figure 3-21), which may be the corner of a stress crack located along the edge of a strut. When a stress crack is formed, the under layers of the coating become exposed. In the case of the Cypher™ stent, where the concentration of rapamycin is expected to be higher in the under layer (polymer/drug) than the outer drug-free layer drug (polymer only), there is a possibility of accelerated drug elution which could have important implications on stent performance.

Similar capture of a stress crack is evident on the height retrace image of the Xience Pro stent. The crack was initially imaged at scan size of 10 μm, and then a smaller section of the surface was scanned at 1 μm. The difference in phase observed at the smaller scan size may be a

combination of the polymer in the disturbed under layer, the polymer/ drug matrix in the outermost layer or even the polymer/bare metal stent platform.

Other irregularities of the surface of the Xience Pro stent included webbing, wrinkles and exposed areas of the bare metal platform which have also been reported elsewhere (Basalus et al., 2009). The concerns associated with the exposure of the bare metal platform is that the local drug delivery is reduced making the performance of the drug in this area of the stent less effective. It also exposes an alternative surface which has not necessarily been designed to be in direct contact with the vessel wall as the coating is not biodegradable. Additionally, if fragments of the coating are released into the vessel wall, there could be implications on the inflammatory response (Ding et al., 2009, Virmani et al., 2004).

Although stress cracks are not visible on the surface of the Taxus® Express$^{2\ TM}$ stent, ripple marks highlight an uneven coating that is likely to have formed during the coating process. SEM analyses also gave an indication of two different 'types' of surfaces on the Taxus® Express$^{2\ TM}$ stent. SEM images show some sections of the stent to be smooth and featureless, similar to that reported in the literature (Kamath et al., 2006) and the other to have particles present on the surface. The presence of particles is visible at random points throughout the stent surface and may be the presence of paclitaxel particles that have migrated to the surface during storage, similar to the Cypher^{TM} stent.

3.4.4. Impact of Drug Elution on Surface Topography

This section of the study looks at the change in surface topography of the Taxus® Express$^{2\ TM}$ stent surface throughout the drug elution period. This study is largely based on the method found in the literature by (Ranade et al., 2004) which analysed a surface similar to the Taxus® Express$^{2\ TM}$ stent produced on an Express$^{2\ TM}$ BMS over a 48 drug release period Although similar to the Taxus® Express$^{2\ TM}$, an actual Taxus® Express$^{2\ TM}$ stent was not analysed in the study by Ranade et al.

In the present study, the average R_{RMS} and SA values do not significantly change over the drug elution period (28 days), however smaller changes in the AFM numerical data are noted. The largest difference is observed in the average R_y values, changing from 273.41 nm ± 259.36

(pre-drug elution) to 312.89 nm ± 197.92 (48-hour time point). This change is likely to be due to the release of paclitaxel from the surface, forming pores and subsequently increasing the average peak-to-valley distance values. The formation of pores is qualitatively identified by the height retrace images. An average kurtosis of >3 is also noted at the 48-hour time point, indicating few sharp peaks and the presence of pores which is consistent with the AFM height retrace images and suspected release of paclitaxel.

The release of paclitaxel at these time points is further supported by the findings in the literature (Kamath et al., 2006, Ranade et al., 2004) which reports paclitaxel release after several hours *in vitro*. The data in the present study continues over a period of 28 days, extending beyond the 48 hour release period examined in the studies by (Ranade et al., 2004) and (Kamath et al., 2006). This provides a representation of the changes in the surface topography over a prolonged period of time. This time period is of great importance with regards to the in-stent restenosis timeline as further changes to the surface topography of the implanted material may have an impact on the vessel which is in the initial stages of healing following stent implantation. From the data obtained in this study it appears that the pores from the apparent paclitaxel release begin to join together making them less noticeable as individual pores and more as wider voids. This is the first time this data has been reported, and is a result of the extended drug release period used in the present study.

From the AFM data obtained over the drug eluting period (see Table 3-5), a large standard deviation value is recorded throughout. This is likely to be due to the different 'types' of surfaces that were discussed in the previous section. One of the limitations of the present study is that the same sample point was not imaged throughout the drug elution period, instead random points were analysed each time. This means that the change in these two 'types' of surfaces over the drug elution period is not specifically observed, hence, more definite conclusions cannot be made about the nature of these surfaces.

SEM imaging took place following the 28 day drug release period. In one sample, crystallisation of drug or PBS appears to have taken place on the surface. This may be due to the fact that the sample was not rinsed prior to analysis. To counteract this problem, the second sample was rinsed with fresh PBS/Tween20 prior to being dried in a gentle stream of argon which appeared to solve the issue. No difference was observed between the SEM images before and after drug release in this second sample which is likely to be due to the limitation of the SEM microscope at the micrometre scale, making it impossible to visualise the pores.

In order to identify if the release of paclitaxel agrees with the increase in pore formation over the drug elution period, the release medium from each time point must be analysed by UV spectroscopy/HPLC and could be attempted in future studies.

3.4.5. Preliminary Cell Studies

The initial seeding density used in this study (1 x 10^5 cells/cm^2) was based on the literature (Prasad et al., 2005) and other studies within the department that used the same cell type (porcine ECs) on similar surfaces (Holland, 2016). It was found that following 6 days of incubation, very few cells were present on the PPy/ Sa coated SS surfaces. The wells were examined by light microscopy, showing cells to be visible but not confluent on the base of the wells. One reason for the lack of cells on the samples surface may be that the cells did not have adequate time to adhere and then proliferate on the samples surfaces at this 6-day incubation period. However, given that it is known that this cell type grows rapidly on standard tissue culture plastics, doubling in number approximately daily, it would have been expected that a substantial number of cells would have been visible at the 6-day time point. In one study by (Prasad et al., 2005), the growth of HUVECs over stents was measured using a starting cell density ranging from 2 x 10^4 - 2 x 10^6 cells/cm^2. Based on these findings, the cell density for the present study was increased from 1 x 10^5 cells/cm^2 to 2 x 10^5 cells/cm^2. It is important to note that many studies referred to in the present study have used HUVECs instead of porcine ECs. It is likely that the growth rate of the two cell types would differ, another factor to take into consideration.

3.4.6. Analysis of Cell Growth on Yukon® and Gazelle™ Stents

It has previously been shown that surface topography affects cell behaviour in a number of studies (Eugene A. Sprague et al., 2012, Chung et al., 2003, Xu et al., 2004). The findings from these studies show differing results for various cell types, in particular, what surfaces are described as ‘rough’ or ‘smooth’. Translumina introduced the first coronary stent using surface topography to target improved endothelial healing (Yukon®). The surface of this stainless steel stent is treated to provide a rough, microporous structure that is thought to help control drug release (Translumina, 2009).

The impact of this surface on re-endothelialisation has been investigated *in viv*o, with results indicating that the rough surface stents enhanced endothelialisation (Translumina, 2009, Dibra et al., 2005). However, this effect was not found to be statistically significant and the impact of such surface roughness on endothelial cells remains unclear. There are no *in vitro* studies that have analysed the growth of endothelial cells on the Yukon® microporous surface. Given the significant differences in surface roughness between the Gazelle™ and Yukon® stents examined in the present study, it was therefore decided to investigate if this difference would lead to differences in endothelial cell adhesion, growth and viability. This type of analysis allows the healing potential of these medical products to be investigated at the cellular level.

The cell seeding density and incubation duration were altered until cells were completely confluent on the surrounding base of the well when analysed by light microscopy (2×10^5 cells/cm^2, 13 days). Under these conditions, cells were shown to be much more confluent on the surface of the Yukon® stent than at the lower seeding density (1×10^5 cells/cm^2), but there was only a slight increase in cell growth on the Gazelle™ samples. Qualitatively (live/dead staining), it is evident that the cells covered the Yukon® surface, whereas only few cells formed over the Gazelle™ surface.

Both stent types are composed of stainless steel, only differing in their surface topography. Previous surface analysis from the present study (see section 3.3.2.1), showed the surfaces to have different topographical features and subsequently different surface roughness values. Values of mean R_{RMS} were found to be significantly different between the two stent surfaces (14.39 ± 11.24 nm Gazelle™, 85.52 ± 26.07 nm Yukon®) with a larger R_{RMS} roughness for the Yukon® samples, showing this surface to have a larger surface roughness. The difference in surface roughness between the two stent samples may be a reason for the difference in growth of the ECs on the two surface types a this stage.

The improved growth of cells onto the surface of larger roughness is in line with the claim from the manufacturer, Translumina, that states the microporous surface promotes rapid re-endothelialisation (Translumina, 2009). As was discussed in chapter 1, there are a number of studies whose findings are in agreement with the claim by Translumina, that increased surface roughness promotes endothelialisation. The study by (Chung et al., 2003) suggests that an increase in surface roughness (Ra) of ~20 nm (scan size 2µm) improves the growth and proliferation of HUVECs. Another study looked into the effect of increased nano roughness on the densities of RASMCs (Rat aortic smooth muscle cells) and RAECs (Rat aortic endothelial cells) (Miller et al., 2004) which were both found to increase with increased nano roughness. In contrast to these studies, (Xu et al., 2004) reported improved

proliferation/adhesion of HCAECs onto 'smooth' PLLA surfaces (R_{RMS} 137 ± 17 nm, scan size 50 µm x 50 µm) compared to the 'rough' surfaces (R_{RMS} 1557 ± 211 nm, scan size 50 µm x 50 µm). In terms of cell type, the study by Xu et al, is most relevant to the present study as it used HCAECs which are present at the site of stent implantation. It is possible that the roughness of the 'rough' surfaces produced by Xu et al are too rough to encourage rapid re-endothelialisation. The present study and the study by Chung et al appear to have smaller sample surface roughness values, more similar to the 'smooth' surface roughness values in the study by Xu et al. It is difficult to compare roughness values obtained in separate studies with variation in scan sizes, method and machines used, however, some comparison can be made between these studies.

3.4.7. Effect of Surface Features on Behaviour of ECs

It is not only surface roughness values that have an impact on cell behaviour, as specific surface features such as particle size and pore depth are also greatly important in understanding the behaviour of cells. AFM analysis was used in the present study to analyse the difference in peak-to-valley distance of the stent surfaces, giving numerical values for pore depth (Yukon®, Ry ~1.2 µm) and grain boundary depth (Gazelle™, Ry ~ 0.1 µm) (see section 3.3.2.2.3, Table 3-4 for full table of values).

Similar to the microporous surface of the Yukon® stent, previous studies have investigated different patterned surfaces to reduce incidences of in-stent restenosis. (Eugene A. Sprague et al., 2012) investigated the growth of HAECs on 'micro grooved' and 'smooth' metal surfaces. They found that the parallel micro patterned surface, with grooves (depth 2 x 0.5 µm) increased cell proliferation, nitric oxide production and reduced rates of apoptosis following 7 days *in vitro* incubation. They also used a porcine coronary injury model to assess neointimal thickness following the implantation of three stainless stent types with different luminal surface features ('smooth', 'micro grooved' and commercially available BMS (control, Multi-Link Vision)). An additional aspect of the micro grooved surface is that the grooves are parallel in the direction of coronary flow. Following 28 days of stent implantation, porcine arteries with the implanted micro grooved stents had significantly lower neointimal thickness when compared to the arteries with the other stent types. This study supports the initial findings from the present study that the microporous surface (Ry ~ 1.2 µm) of the Yukon® stent promotes

improved EC growth when compared to the commercially available BMS control (Gazelle™, Ry ~ 0.1 µm).

3.4.8. Effect of Pre-treatment with FBS on EC Growth

As has been the subject of the present study, the surface of a coronary stent can have major impact on the process of re-endothelialisation. One contributing factor is how easily the initial adsorption of plasma proteins (including fibrinogen, fibronectin, IgG and von Willebrand factor) takes place on the surface of biomaterials, as this can influence the subsequent attachment of cells (Thevenot et al., 2008). Protein adsorption onto a surface can be determined by wettability, hydrophobicity and surface charges of the surface. For example, surfaces of increased hydrophilicity have been proven to improve the biocompatibility of surfaces *in vitro* (Delivopoulos et al., 2015).

In the last phase of the present study, stent samples underwent pre-treatment with Foetal Bovine Serum (FBS) for a period of 1 hour in an attempt to further encourage the proliferation of ECs onto the stent surfaces. An increase in cell number was observed for the Gazelle™ stent when compared to the experiment with no pre-treatment, although statistical analysis showed no significant difference. The effect of pre-treatment with FBS had the opposite effect on cell growth on the Yukon® stent surfaces, with a decrease in mean total cell number (91 ± 62 (no pre-treatment), 29 ± 24 (pre-treatment with FBS)). This is an interesting finding as the FBS contains fibronectin which becomes adsorbed to the surface and usually encourages cell growth (Thevenot et al., 2008). One explanation for this difference is that the FBS changed the chemistry of the surface causing the cells to initially grow rapidly on the surface of the Yukon® stent, causing a dense layer to form. Over time, these cells became too dense within the confined environment of the 96-well plate, becoming saturated with waste products. This may have caused cell death and their detachment from the stent surface.

It is also possible that the purposefully manufactured microporous surface which has been designed to enhance re-endothelialisation has become masked by the FBS treatment. Treatment of this surface with FBS may have allowed the components of the serum to become encased in the pores, blocking them and therefore changing the dimensions of the pits within the surface. The potential effect of surface dimensions on cell behaviour has been discussed throughout this study and more recently in section 3.4.7. To understand the true impact

treatment with FBS had on the dimensions of the pores within the stent surface, further analysis would be required.

3.4.9. Cell Behaviour in Direct Contact with Sample Surface

To determine the viability of cells directly on the stent sample surface, eliminating the influence of the cells in the surrounding well, stent samples were removed from the well 24 hours after the initial cell seeding and placed into fresh wells (samples were pre-treated with FBS). The mean total number of cells present on both stent surface types was the highest obtained from any of the experiments in the present study. The values are very similar between the two surface types, with a slightly larger cell number present on the Gazelle™ samples (114 ± 47 (Gazelle™), 101 ± 57 (Yukon®)).

These findings suggest that removal of the samples into a fresh well following cell suspension is the optimum method. Not only do the cells have the availability of more nutrients and space for gas exchange but the LDH values are only concerned with the cells that have become attached to and grown over the stent surfaces. This allows for a more accurate representation of the viability of cells growing over the stent surfaces, showing the true effect of surface roughness of EC cell viability.

3.4.10. Study Limitations and Future Work

Some limitations of the study thus far have been included in the discussion above. If time and sample availability permitted, it would be advantageous to repeat the cell culture study with the removal of the sample but without the initial sample pre-treatment in FBS. This would confirm the true effect of the surfaces of the two stent types, and may verify the findings from the initial experiment (no pre-treatment, 13 days) that increased surface roughness does improve EC growth. Additionally, sample size could be increased for each experiment and cells quantified at each time point (3 day, 6 day, 9 day, 13 day) to ascertain whether rapid cell growth and subsequent premature cell death is the cause of low cell number and high variation in levels of LDH at certain sample points.

One limitation of the cell culture experiments is that they were carried out in the absence of flow which is an important consideration in considering blood flow within an artery.

Therefore, future cell culture experiments could be attempted in an alternative experimental setup, for example in a perfusion chamber.

Finally, although the surface topography of a range of clinically relevant DES and BMS have been investigated in the present study, there are now newer generation stents available. It may therefore be beneficial to characterise the surfaces of these stents and indeed assess their effect on the behaviour of ECs.

3.4.11. Summary and Conclusions

In conclusion, the surface morphology and topography of clinically relevant stents has been identified using AFM and SEM in the present study. Results show the surface of bare metal and drug eluting stents to differ between products with similarities noted between the DES surfaces. This has also helped identify the suitability of SEM and AFM as methods for future characterisation of potential DES coatings as is presented in chapter 4.

The effect drug release has on surface morphology and topography has been successfully determined for the Taxus® Express$^{2\,TM}$ stent, showing pore formation but little change in R_{RMS} roughness values. It is also interesting to note that little difference was observed between the topography of the DES investigated in the present study and these appear to have quite similar performances clinically.

The identification of coating irregularities on DES coatings suggests the need for improved coating methods. An investigation into the optimisation of the method for production of a uniform novel polypyrrole/salicylate coating for potential use in DES is investigated in chapter 4.

Finally, the effect surface topography has on the growth of ECs has been studied on stent surfaces of distinct surface roughness values. Findings have shown that without pre-treatment with FBS, cell growth is improved on the surface type with larger R_{RMS} roughness value (Yukon®) compared to the smaller R_{RMS} roughness value (Gazelle™). These findings suggest the potential importance of stent surface topography on healing post stent implantation and further cell culture studies may reinforce this importance. On the whole, the findings presented in this chapter have been brought together to produce one of the most wide-ranging analysis of stent surface topography yet reported for a wide range of stent types.

Chapter 4

4. Development and Characterisation of Polypyrrole Coatings for Use Within Drug Eluting Stents

Chapter 4 will outline the chemistry of polypyrrole, following on from the information regarding electropolymerisation, surface topography and drug release that was outlined in Chapters 1 and 2. The specific aims surrounding the subjects of surface topography and drug release from Polypyrrole/Salicylate coated surfaces will be presented in section 4.2. Results will be presented in section 4.4 and an in-depth discussion surrounding the issues mentioned will conclude this chapter in section 4.5.

4.1. Background

The topic of conducting polymers has been introduced in chapter 1, in terms of their potential application in medical devices. The conducting polymer, polypyrrole (PPy), has been recognised for its potential as a DES coating for a number of reasons including its good biocompatibility and ability to entrap biological molecules which can be subsequently released into the body (Guimard et al., 2007). Studies which have investigated the potential of PPy as a DES coating report short drug release periods (Okner et al., 2008, Arbizzani et al., 2007, Okner et al., 2007). Additionally, there is a lack of information on the biocompatibility of such coatings for cardiovascular applications.

4.1.1. Conducting Polymers

For polymers to be electrically conductive, their structure must have a conjugated backbone consisting of alternate single and double carbon bonds. The strength of the polymer chain is maintained by the sigma-bond present in both single and double bonds. The additional pi bond in the double bond allows the delocalisation of electrons by the overlapping of p-orbitals (see Figure 4-1 for visual example of structure of electrically conducting polymer). The polymer must also be doped by oxidation or reduction, resulting in the availability of extra electrons and holes, creating an electrically conductive material.

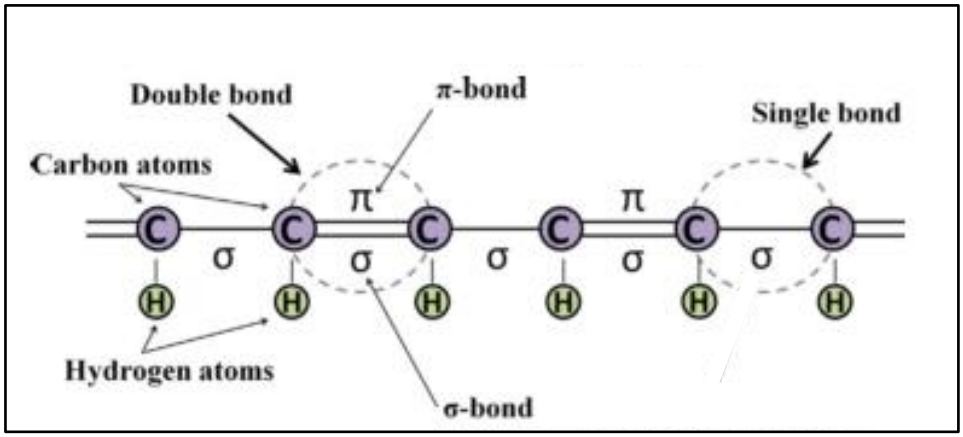

Figure 4-1: Example of electrically conductive polymer. Image shows conjugated backbone consisting of alternate single and double carbon bonds. The strength of the polymer chain is maintained by the sigma-bond present in both single and double bonds. The additional pi bond in the double bond allows the delocalisation of electrons by the overlapping of p-orbitals Image adapted from (Balint et al., 2014).

4.1.2. Chemistry of Polypyrrole

Polypyrrole is a conducting polymer that can be synthesised on stainless steel with relative ease through the electrochemical oxidation of its monomer, pyrrole (Py), allowing the transfer of electrons and the loss of hydrogen ions. This has been achieved in the studies by (Okner et al., 2009, Shi and Zhitomirsky, 2010) through the use of SS plates and stents.

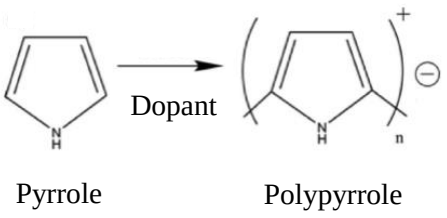

Figure 4-2: Molecular equation of oxidation of Pyrrole to Polypyrrole, in presence of a dopant.

Pyrrole is soluble in water, which enables the controllable film formation in aqueous medium (Su and Iroh, 1997). The chemical equation describing the electropolymerisation of pyrrole is shown in Figure 4-3. The first step (see Figure 4-3, Step 1) of the reaction occurs at the working electrode where pyrrole (monomer) undergoes oxidation to produce a radical cation. This radical cation then reacts with other monomers or radical cations at Stage 2 of the reaction (see

Figure 4-3, Stage 2) to form a coating of insoluble polymer chains on the surface of the working electrode (Guimard et al., 2007).

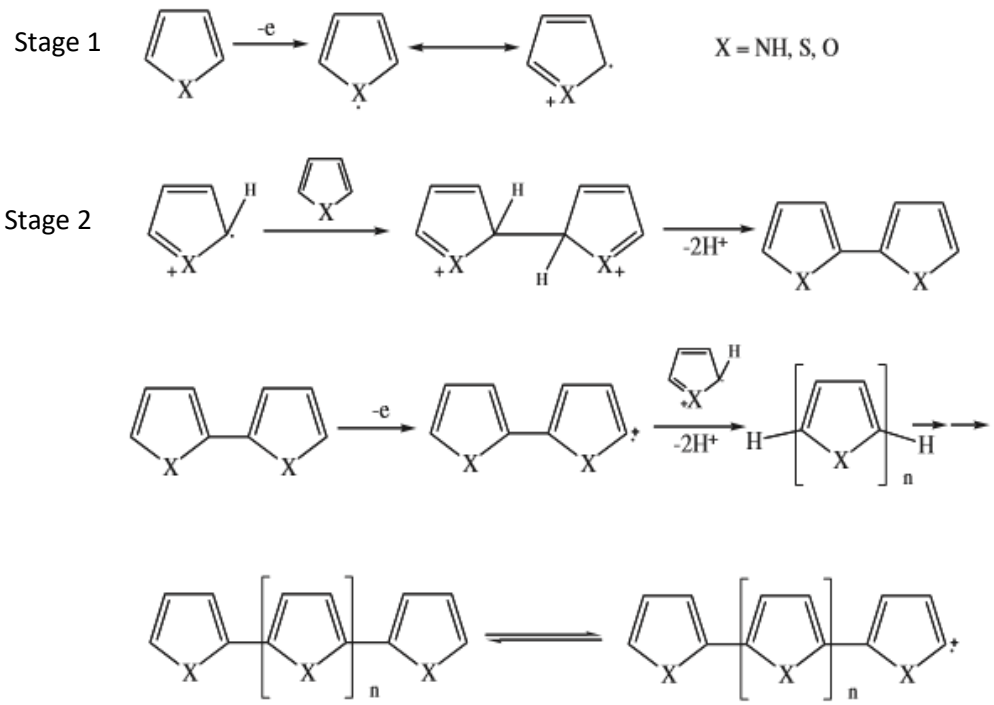

Figure 4-3: Chemical equation representing electropolymerisation of Pyrrole. Step 1 - monomer undergoes oxidation to produce a radical cation. Stage 2 - this radical cation reacts with other monomers or radical cations to form polymer. Image adapted from (Guimard et al., 2007, Xu et al., 2004).

4.1.3. Dopant Ions

There are two types of doping (p-doping, n-doping) that can be used to incorporate ions into a polymer structure. With p-doping, the polymer is oxidised and the overall charge on the polymer is positive whereas for n-doping, the polymer is reduced and the overall charge is negative (Balint et al., 2014). In the present study, an anionic drug is incorporated into p-doped polypyrrole.

4.1.3.1. Uptake and Release of Drug

When considering the incorporation of drug into a polymer coating produced by means of electropolymerisation, there are two main approaches to consider; during

electropolymerisation or after electropolymerisation. The chosen method is dependent on both the type of drug and polymer. This is to say; some drugs are more easily incorporated into the coating during the electropolymerisation process whereas others are best incorporated into the coating once it is established.

4.1.3.2. After Electropolymerisation

The incorporation of a drug into polypyrrole after electropolymerisation was achieved in the study by (Okner et al., 2007) which reported the incorporation of paclitaxel into a PPy coating post electropolymerisation. Bare metal stents (stainless steel) were coated with PPy by cyclic voltammetry and then immersed in paclitaxel ethanolic solution (20 mg/ml) for 30 min to incorporate the drug into the coating. Results showed the release of the absorbed paclitaxel over a 30-day period *in vitro* (PBS (pH7.4) + 3% SDS). Release media was analysed by HPLC, showing 60 % of the paclitaxel to be released in the first 24 hours, with the remaining drug released slowly over the remaining period.

The study by (Okner et al., 2007) was the basis of previous work in the department (Allahverdi, 2013) which involved the immersion of the PPy coated sample into a sirolimus solution of known concentration. Findings from the study by (Allahverdi, 2013) suggest that the mass of sirolimus incorporated into the coating is dependent on the sirolimus concentration in which it is immersed, with higher concentrations of sirolimus corresponding to a larger sirolimus uptake and subsequent release. The main finding of this study (Allahverdi, 2013) was that all of the sirolimus that had been incorporated into the coating was released within a 24 hour period. This would be a rapid release period for sirolimus in terms of use for DES as it is targeting the proliferation of SMCs which is most prominent in the initial 30 days post stent implantation. In relation to clinically relevant stents that release drugs with a similar mode of function to sirolimus, the release period is between 14 (Endeavour™ ZES) and 30 days (Xience EES, Cypher™ SES).

4.1.3.3. During Electropolymerisation

Incorporation of a drug into a conducting polymer coating during electropolymerisation is an alternative method. This allows for less processing steps; an advantage when considering future manufacturing aspects of the coating technique and its potential scale up. This method has been reported by (Arbizzani et al., 2007) with dopant ions including naproxene and salicylate.

4.1.3.4. Salicylates

Salicylates fall under the category of non-steroidal anti-inflammatory drugs (NSAID). They are, in the form of aspirin (acetylsalicylic acid), used as a component of dual anti-platelet therapy (DAPT) and are therefore recognised for their anticoagulant and anti-inflammatory properties (DeVile and Foëx, 2010). Salicylate is known to inhibit the proliferation of SMCs (Marra et al., 2000) and would therefore be beneficial as a component of a DES coating. Sodium salicylate (NaSa) has previously been incorporated into PPy coatings intended for use in DES by means of electropolymerisation (Arbizzani et al., 2007). NaSa has also been successfully incorporated into PPy coatings on planar stainless steel surfaces previously in the department (Reay, 2012). The fact that salicylates are already recognised for use in cardiovascular disease, known to inhibit the proliferation of SMCs and can be easily incorporated into PPy coatings makes them an ideal choice for use in the present study.

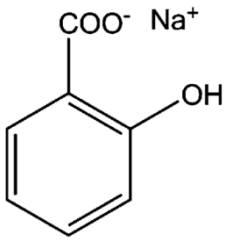

Figure 4-4: Chemical structure of Sodium Salicylate (NaSa)

4.2. Aims and Objectives

Chapters 1, 2 and the introduction to the present chapter provided background information regarding the electropolymerisation of PPy onto metal surfaces, highlighting the potential benefits of its use in DES coatings. Surface topography has been reported to influence the behaviour of cells (Chung et al., 2003, Miller et al., 2004) and this has also been investigated in chapter 3. The surface morphology and topography of PPy/Sa coatings is not widely reported in the literature. The release of Sa from PPy/Sa coatings has also been reported to be suboptimal for use in DES coatings, with 90 % release reported by (Arbizzani et al., 2007) over a period of 2 days. It is therefore our aim to investigate the optimum experimental conditions to achieve a PPy/Sa coating on SS wire that is uniform and provides optimum release of Sa from the coated surface. As was also identified in chapter 3, the surfaces of commercially available DES vary, with coating irregularities including cracking and webbing commonly observed. This is a potential problem for future DES coatings. This aim can be broken down to the four main objectives below.

1) Investigate the effect electropolymerisation duration has on the morphology/topography of PPy/Sa coatings.
2) Investigate the effect electropolymerisation duration has on the release of Sa from PPy/Sa coatings.
3) Investigate the effect electropolymerisation method (potentiostatic vs galvanostatic) has on the morphology/topography of PPy/Sa coatings.
4) Investigate the effect electropolymerisation method (potentiostatic vs galvanostatic) has on the release of Sa from PPy/Sa coatings.

4.3. Materials and Method

4.3.1. Electropolymerisation

4.3.1.1. Materials and Equipment

Sodium Salicylate (NaSa), Silicon Carbide (SiC), Ethanol (absolute) and Pyrrole (reagent grade 98 %) were all purchased from Sigma Aldrich, UK. Both the stainless steel wire (AISI 316L grade, annealed, Diameter 0.2 mm) and the platinum wire counter electrode (Diameter 1 mm) were purchased from Goodfellow Cambridge Limited, UK. The KR5 reference electrode was purchased from Thermo Fisher Scientific UK Ltd, UK.

An Electrochemical Interface Potentiostat (SI 1287, Solartron Analytical, Hampshire, England) was used to perform the electropolymerisation.

4.3.1.2. Experimental Procedure

Sodium Salicylate (8.006 g), distilled water (490 ml) and pyrrole (distilled, 3496 µl) were combined to make a solution of 0.1 M Pyrrole (Py) 0.1 M Sodium Salicylate (NaSa) that was freshly prepared for each set of experiments. For potentiostatic electropolymerisation, the apparatus was set up in a three-electrode configuration; working electrode (stainless steel wire (30 mm x 0.2 mm diameter)), counter electrode (Pt wire, (30 mm x 1 mm diameter)) and reference electrode (KR5). This setup was based on the literature and previous studies within the department (Arbizzani et al., 2007, Reay, 2012). For galvanostatic electropolymerisation, the reference electrode was eliminated to achieve a two-electrode configuration, a setup based on previous studies (Holland, 2016).

Prior to the commencement of the electropolymerisation procedure, the working and counter electrode were washed with Ethanol and left to dry at room temperature. The reference electrode was rinsed in distilled water. All three electrodes were treated in the same way for each electropolymerisation experiment performed.

The three electrodes were immersed in a glass beaker (100 ml) containing 0.1 M Pyrrole 0.1 M NaSa solution (60 ml). It was ensured that the electrodes were the same distance apart each time (10 mm between WE and CE) and not in contact with each other or the beaker. An ice bath surrounded the beaker containing the electrolyte solution, maintaining the temperature of

the electrolyte solution in the range of 0-4 °C. Potentiostatic electropolymerisation was performed at 0.9 V for a variety of durations up to a maximum of 20 minutes using the PGSTAT (based on previous studies (Arbizzani et al., 2007, Reay, 2012)). Galvanostatic electropolymerisation was performed in the absence of the reference electrode (maintaining 10 mm between WE and CE) at a current of 7.885×10^{-5} A – 1.577×10^{-4} A for various durations between 10 and 15 minutes (based on previous studies (Velhal et al., 2014, Kim et al., 1997)). For each time period, 8 samples were obtained (3 samples for surface analysis, 5 samples for drug release measurements). All coated samples were left to dry at room temperature overnight. Data was collected using Core Ware and analysed using Core View software to achieve current density vs time graphs for potentiostatic analysis and potential vs time graphs for galvanostatic analysis.

Pre-treatment of Electrode

Pre-treatment of the working electrode was performed on a small number of samples for a section of this study in line with the method outlined in section 2.3.1.3.

4.3.2. Drug Release Measurements

4.3.2.1. Materials and Equipment

Phosphate Buffered Saline (PBS) was purchased from Sigma Aldrich, UK. Eppendorf tubes (1.5 ml) were used to contain the PPy/Sa coated wires during drug release. An incubator with agitation was used to hold the samples for the duration of the drug elution. A UV spectrophotometer (UV 2401 PC, Shimadzu Coorporation) was used to analyse the absorbance of NaSa in this study.

4.3.2.2. Experimental Procedure

PPy/Sa Coated Wires

PPy/Sa coated samples produced using the procedures detailed in section 4.3.1.2 were immersed in PBS (0.01 M, 500 µl) in an Eppendorf tube and agitated at 10 rpm at a temperature of 37 ˚C (physiological conditions) for 28 days. The release media was removed and replaced with fresh PBS at regular time points (10 min, 1 h, 6 h, 1d, 3 d, 7 d, 14 d, 28 d) over a period

of 28 days and the release media for each time point stored in the freezer (-20 °C) for further analysis.

Sodium Salicylate Analysis

The typical UV spectroscopy trace of absorbance vs wavelength for sodium salicylate (NaSa) exhibits three peaks at approximately 297 nm, 238 nm and 203 nm (Nussbaum and Paz, 2012). In preliminary work within the current study, it was found that the highest and most distinct peak was found at 296 nm and this was chosen for the remainder of the study to identify the concentration of NaSa.

Quartz cuvettes containing reference solution (PBS 0.01 M, 500 µl) and sample solution (500 µl) were analysed. A baseline value of PBS (0.01 M) was used prior to sample analysis in order to provide a blank control to account for any signal due to the PBS alone.

Statistical Analysis

In order to compare the data between two independent sample groups and assess its significance, Two-tailed T test ($p<0.05$) was used.

4.3.3. Surface analysis

The principles of operation of the Scanning Electron Microscope is available in chapter 2, section 2.2 and the workings of the Atomic Force Microscope is available in chapter 2, section 2.1.

4.3.3.1. Materials and Equipment

A Scanning Electron Microscope (Hitachi, TM-1000 Tabletop Microscope, 20 x – 10,000 x magnification) was used to perform surface analysis at the micrometre scale. Adhesive carbon tape was used to mount samples onto the SEM sample holder. An Atomic Force Microscope (MFP 3D, Asylum Research, USA) was used to perform surface analysis at the nanometre scale. A rectangular silicon probe with an aluminium coating was used to analyse all samples in this study (160 TS, Olympus). The spring constant of this cantilever type was 26 Nm^{-1}. Standard microscope slides and nail polish were used to mount samples.

4.3.3.2. Experimental Procedure

Each sample was cut in half with scissors and one half was secured to a SEM stub with adhesive carbon tape. All analysis was performed at a magnification varying from x 100 to x 5000.

The other half of the sample was used for AFM analysis and secured to a glass microscope slide with nail polish. The AFM analysis was performed in intermittent contact mode in air (unless otherwise specified), imaging four random points per sample. AFM scans were performed at a frequency of 1 Hz with scan size ranging from 1 µm – 20 µm to obtain images of important surface features, such as nodules and coating irregularities. Quantitative measures of surface topography ($R_{RMS,}$ $R_{y,}$ SA, Sk and Ku) were obtained at a scan size of 5 µm to allow comparison between samples. Unless otherwise stated, data are presented as the mean ± standard deviation (SD) from three independent samples and four points per sample.

Statistical Analysis

In order to compare the AFM data between two individual sample groups and assess its significance, Two-tailed T test ($p<0.05$) was used. To identify the significance between more than two independent groups, one-way ANOVA ($p<0.05$) and Tukey Post Hoc test was used.

4.4. Results

The following set of experiments were performed in line with the experimental methods described in section 4.3. Experimental parameters including electropolymerisation duration, method (potentiostatic or galvanostatic) and applied current were altered to investigate the effect each change had on coating topography and in an attempt to extend drug release.

4.4.1. Effect of Varying Electropolymerisation Duration on Surface Topography and Morphology

Samples in this section were produced by potentiostatic electropolymerisation under the following conditions (0.1 M Py 0.1M NaSa, 0.9 V) for a duration of 15 or 25 minutes.

4.4.1.1. Current-Time Profiles

As illustrated in Figure 4-13 for both sample types (15 min/25 min), the potentiostatic current density decreased rapidly in the initial 30 seconds, after which it began to gradually increase until the end of the procedure (see Figure 4-14).

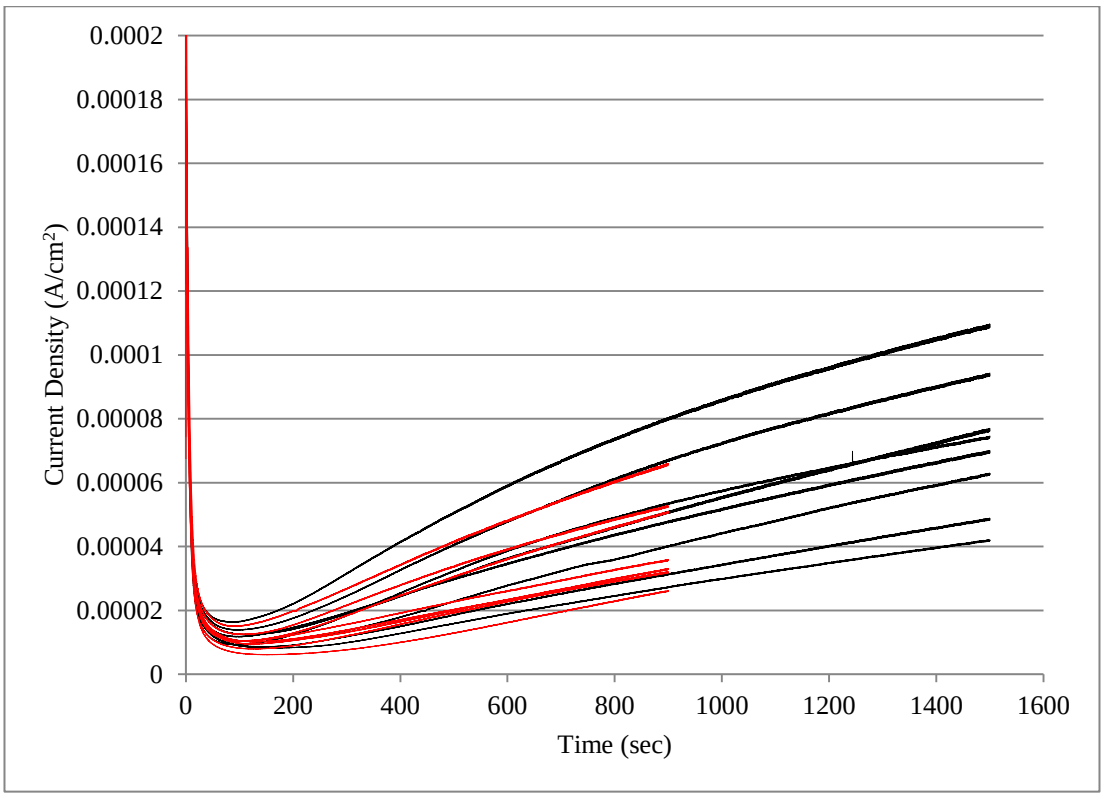

Figure 4-14: Graph of potentiostatic current density Vs time for SS wire coated by electropolymerisation method: potentiostatic 0.9V, 0.1M Py 0.1M NaSa, 15/25 min. Red – 15min, black – 25min. Each line represents an individual sample.

Although the experimental parameters were kept constant, a slight difference in the current-time profile was observed between samples. An example of this can be seen when comparing the maximum current density reached in the production of the following two samples: 25min (2) (maximum current density 0.00011 A/cm^2) and 25 min (6) (maximum current density 0.000065 A/cm^2) (see Figure 4-15), amounting to a difference of 0.000045 A/cm^2. Although the distance between the electrodes were measured before each experiment, slight changes in their position may have influenced the coating process, causing variation between samples. The effect this has on polymer formation is detailed in section 4.4.1.3 and further discussed in section 4.5.

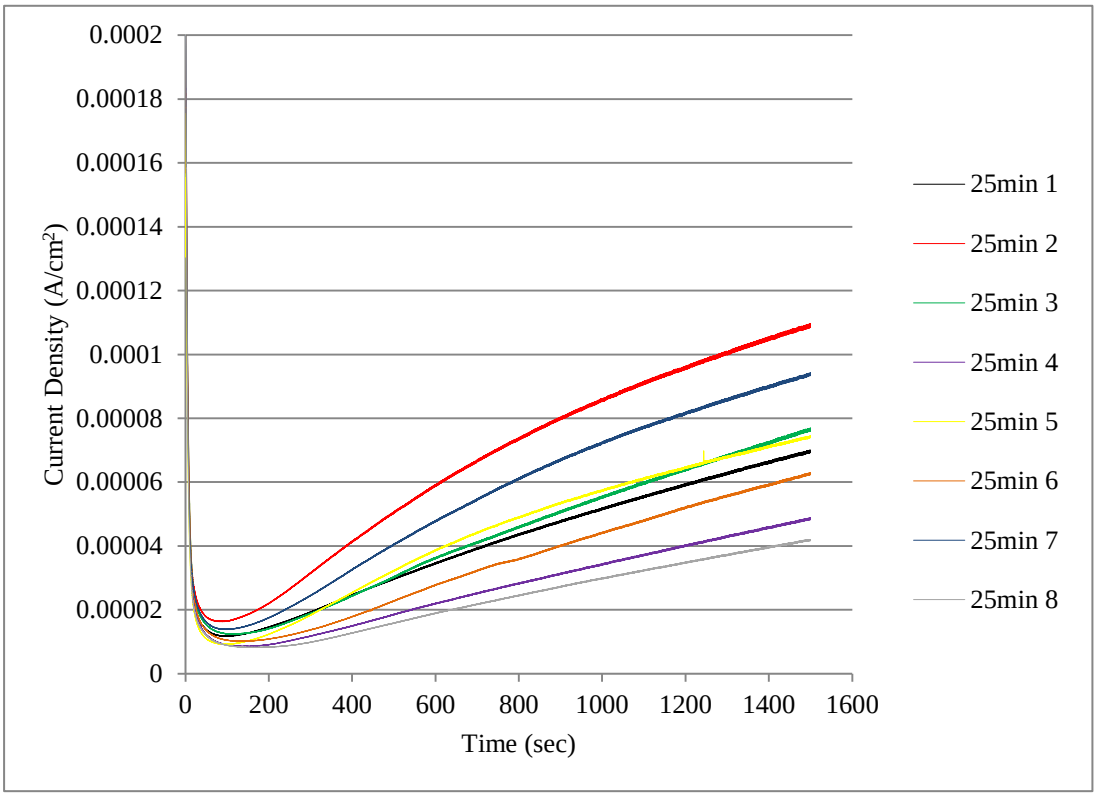

Figure 4-15: Graph of potentiostatic current density Vs time for SS wire coated by electropolymerisation method: potentiostatic 0.9V, 0.1M Py 0.1M NaSa, 25 min. Each line represents an individual sample.

4.4.1.2. Release of Salicylate from Polypyrrole/Salicylate Coatings

Cumulative Mass

When comparing the total cumulative mass of salicylate released from the coatings (15 min/25 min), a difference in the values was noted. The mass of salicylate released from the 15 min samples was less than half that released from the 25 min samples (see Table 4-1 for values). Statistical analysis showed a significant difference between the cumulative mass of salicylate released from the two sample groups.

*Table 4-1: Table of mean total cumulative mass of salicylate released from 15/25 min samples, including standard deviation values (n=5). Two-tailed T test (*p<0.05).*

Sample	Mean Total Cumulative Mass of Salicylate Release (µg) ± SD
15 min	*5.20 ± 2.35
25 min	13.84 ± 5.05

These findings suggest that coatings formed over a longer electropolymerisation duration, uptake and subsequently release a larger mass of salicylate compared to coatings produced following a shorter period of electropolymerisation. This is graphically represented in Figure 4-25 showing the relationship between average total cumulative mass of salicylate release vs time and will be discussed further in Section 4.5.

Rate of Release

The total mass of salicylate was released from all 25 min samples by the 24 hr time point. In light of these findings, drug release media from the 15 min samples was analysed for the early time points and stopped when no more salicylate was detectable by UV spectroscopy. This was at a time point of 6 hours and for some samples it only took a period of 1 hour for the total salicylate to be released. (See Figure 4-25 for relationship between average cumulative salicylate release percentage and time). Although time points after 6 hours were not analysed for the 15 minute samples by UV-Spectroscopy, both sample types (15 min/ 25 min) were left in physiological conditions for 28 days.

For the 15 min samples, an average of 84 % of the total salicylate was released by the 10 min time point compared to only 33 % from the 25 min sample. At this initial time point, the average mass of Sa released from each coating is very similar (~4 µg). The average percentage cumulative mass of Sa release rose to 94 % for the 15 min sample at the 1 hr time point and 64 % for the 25 min sample. For one of the 15 min samples, 100 % of the salicylate was released within the first hour with the remaining four samples releasing within 6 hours. Most of the 25 min samples experienced 100 % salicylate release within 24 hours with one sample releasing it within 6 hours. Therefore by increasing the electropolymerisation duration, the cumulative mass of salicylate from the coating was increased and the rate of release extended.

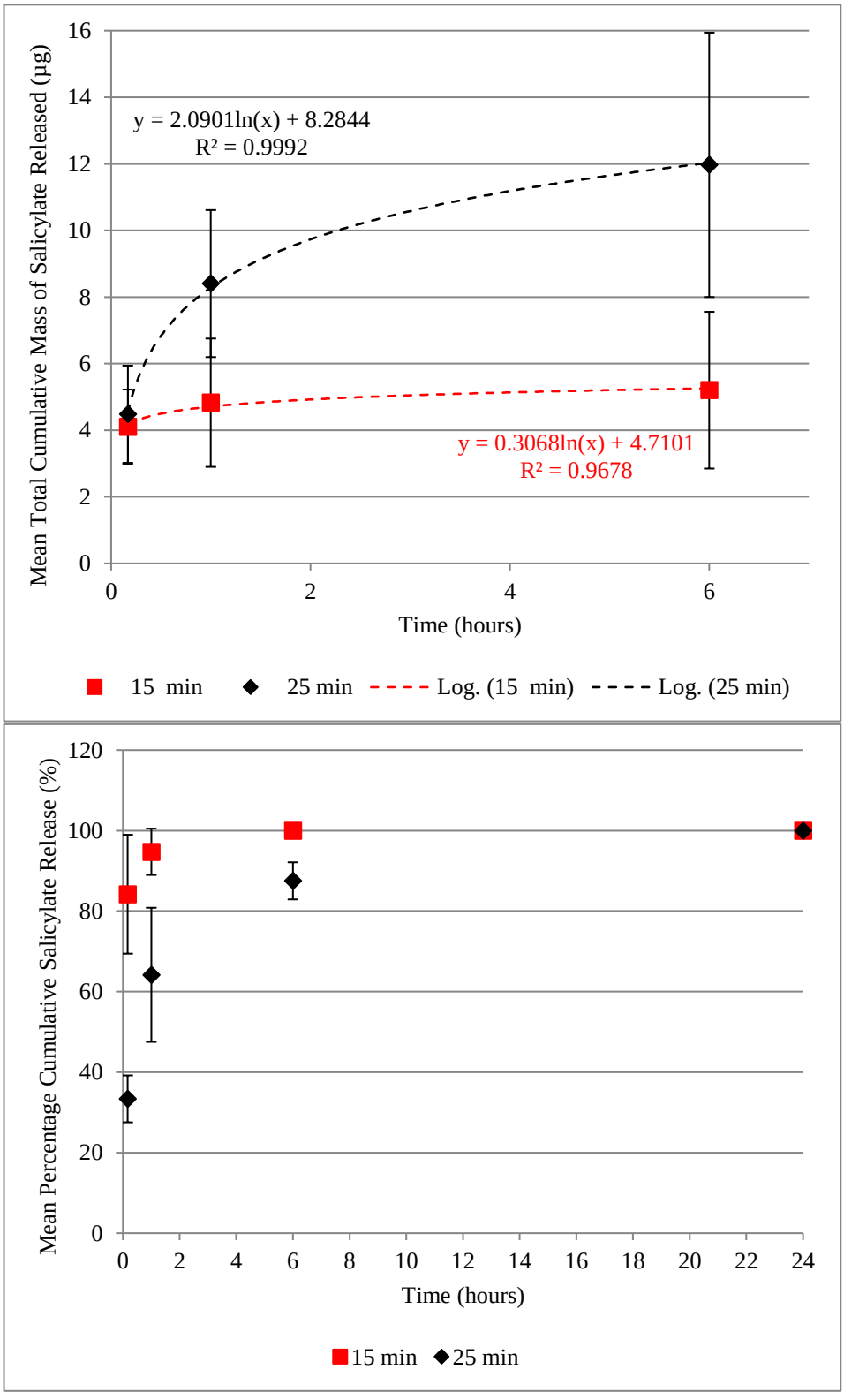

Figure 4-16: Graphical relationship of salicylate release from PPy/Sa coatings produced by potentiostatic electropolymerisation for various durations (15 min – red, 25 min – black). Top: Mean total cumulative mass of salicylate release vs time (initial 6 hours). Bottom: Mean percentage cumulative salicylate release vs time over 24 hours. Error bars are indicative of SD. N=5. Equations on graphs are logarithmic trendlines.

4.4.1.3. SEM Analysis of Polypyrrole/Salicylate Coatings Pre/Post Salicylate Release

SEM analysis was undertaken on PPy/Sa coated SS wires pre-and post-salicylate release. SEM images of the 25 min samples pre-salicylate release showed uniform coatings with typical cauliflower morphology throughout the surface (see Figure 4-17). Following the total salicylate release from the coatings, it may be expected that the surface topography, morphology or phase angle would change as the chemistry of the surface changes. By comparing the SEM images pre-salicylate release to the SEM images post-salicylate release (see Figure 4-17), it is apparent that there is not a noticeable change between the samples pre- and post-salicylate release. There was also no change in the size of PPy nodules on the surface. The coatings on the 25 min samples remained uniform with no cracks or delamination present.

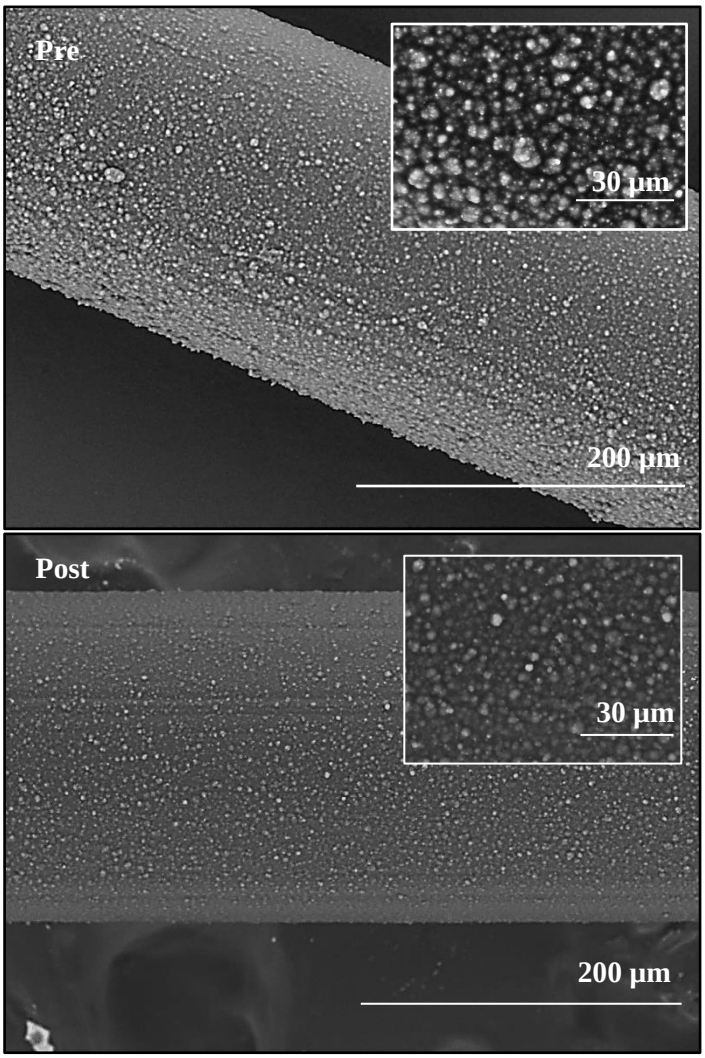

Figure 4-17: SEM images of PPy/Sa coated SS wire coated at the following conditions: potentiostatic, 0.9V, 25min, 0.1M Py 0.1M NaSa. Pre-and post-salicylate release. Sample: 25min (2). Pre (top)/Post (bottom) salicylate release as indicated on images.

As detailed in section 4.4.1.1, the current-time profiles showed variations between samples and this was also observed in the SEM images, showing a difference in coating morphology between the samples (see Figure 4-17 (pre, top) and Figure 4-18). The coating that reached a lower current density (25 min (6)) had a patchier appearance than the coating that reached a higher current density (25 min (2)), suggesting less polymer formation on the surface.

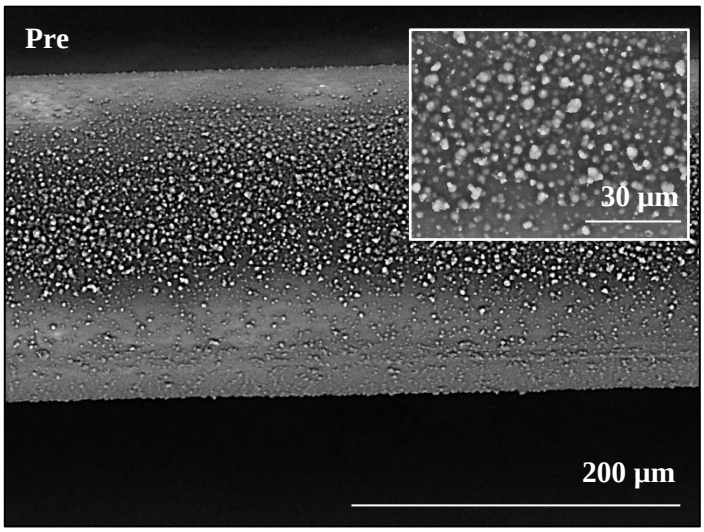

Figure 4-18: SEM image of PPy/Sa coated SS wire produced at the following conditions: potentiostatic, 0.9V, 25min, 0.1M Py 0.1M NaSa. Sample: 25min (6), pre-salicylate release.

In comparison to the 25 min samples, the coatings on the 15 min samples were very patchy pre-salicylate release with the underlying stainless steel platform still visible (see Figure 4-19 (top, pre)). Despite the uneven coating, the initial stages of the formation of cauliflower morphology were still visible. SEM analysis post salicylate release showed that the 15 min coated samples remained patchy with the underlying stainless steel still visible (see Figure 4-19 (bottom, post).

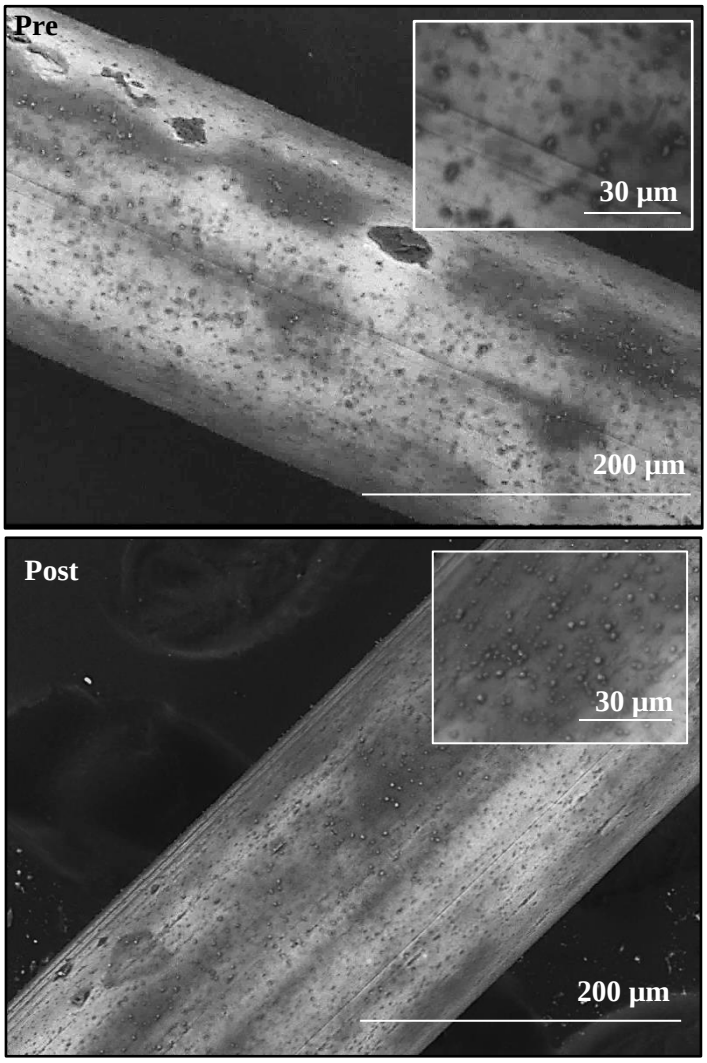

Figure 4-19: SEM image of PPy/Sa coated SS wire coated at the following conditions: potentiostatic, 0.9V, 15min, 0.1M Py 0.1M NaSa. Pre (top)/Post (bottom) salicylate release as indicated on images.

Following these initial results, it can be suggested that the following electropolymerisation conditions produce PPy/S coatings of good uniformity: potentiostatic, voltage: 0.9V, electrolyte solution: 0.1M Pyrrole 0.1M Salicylate, duration 25 min.

4.4.1.4. AFM Analysis of Polypyrrole/Salicylate Coatings Pre/Post Salicylate Release

4.4.1.4.1. Numerical Data

Pre

AFM analysis was performed on the PPy/Sa coated SS wires pre-salicylate release. Values of average R_{RMS}, SA and R_y calculated by the AFM software for the 15 min/25 min samples are displayed in Table 4-2. The average R_{RMS} value of the 15 min samples (82.44 ± 39.50 nm) was found to be smaller than the average R_{RMS} value of the 25 min samples (129.49 ± 77.49 nm). The value of average peak-to-valley distance was also found to be smaller for the 15 min samples than the 25 min samples. It was confirmed that increasing the electropolymerisation duration increases the average R_{RMS} roughness of the coatings.

Despite this difference, statistical analysis confirmed that there was no significant difference between the average R_{RMS} value or indeed any of the numerical AFM data between the two sample groups pre-salicylate release.

Post

AFM analysis of the PPy/Sa surfaces post salicylate release showed a slight increase in the average R_{RMS} values following salicylate release from both sample types (see Table 4-2 for full quantitative results). There were also slightly different values obtained for the average R_y and SA values, however, statistical analysis showed no significant difference between the two sample groups or within the same sample group pre/post salicylate release.

*Table 4-2: Table of mean values of RMS roughness (R_{RMS}), surface area (SA) and peak-to-valley distance (Ry) of coatings Pre/Post salicylate release. Coatings produced by electropolymerisation method: potentiostatic, 0.1M Py 0.1M NaSa, 0.9V, 15 or 25 min (as indicated). Table of AFM data obtained at 5µm, 1Hz. Mean taken from 4 points per sample and three samples (pre-salicylate release)/ five samples (post salicylate release. One-way ANOVA was significant ($p<0.05$). *$p<0.05$ significant difference between 15 min (post) vs 25 min (post) (Tukey post hoc test).*

Sample	Mean R_{RMS}± SD (nm)	Mean SA ± SD (µm^2)	Mean Ry ± SD (nm)
15 min (pre) n=3	82.44 ± 39.50	27.75 ± 1.46	604.52 ± 205.83
15 min (post) n=5	88.93 ± 39.37	27.47 ± 1.47	601.34 ± 202.66
25 min (pre) n=3	129.49 ± 77.49	29.17 ± 2.46	832.22 ± 475.22
25 min (post) n=5	*144.50 ± 48.00	29.09 ± 1.95	931.04 ± 295.93

4.4.1.4.2. Height Retrace Analysis

Pre

Despite a lack of statistical difference in the quantitative data between the two sample groups, it is apparent from the AFM height retrace images and the SEM images that the morphology of the coatings do vary between sample groups.

The lack of cauliflower morphology on the 15 min samples is visible on the SEM images, showing few nodules (see Figure 4-19). This finding is backed up by the AFM height retrace images at a scan size of 5 µm (see Figure 4-20), showing few small orange/yellow mounds and mostly blue flat areas. In contrast, the AFM height retrace images of the 25 min samples (see Figure 4-21) show large rounded nodules, with smaller nodules also present.

Post

In line with the AFM numerical data and the SEM images, which suggest that there is no significant change in surface topography pre/post salicylate release, there is also no difference

in AFM height/phase retrace images of the 15 min/25 min sample surfaces pre/post salicylate release.

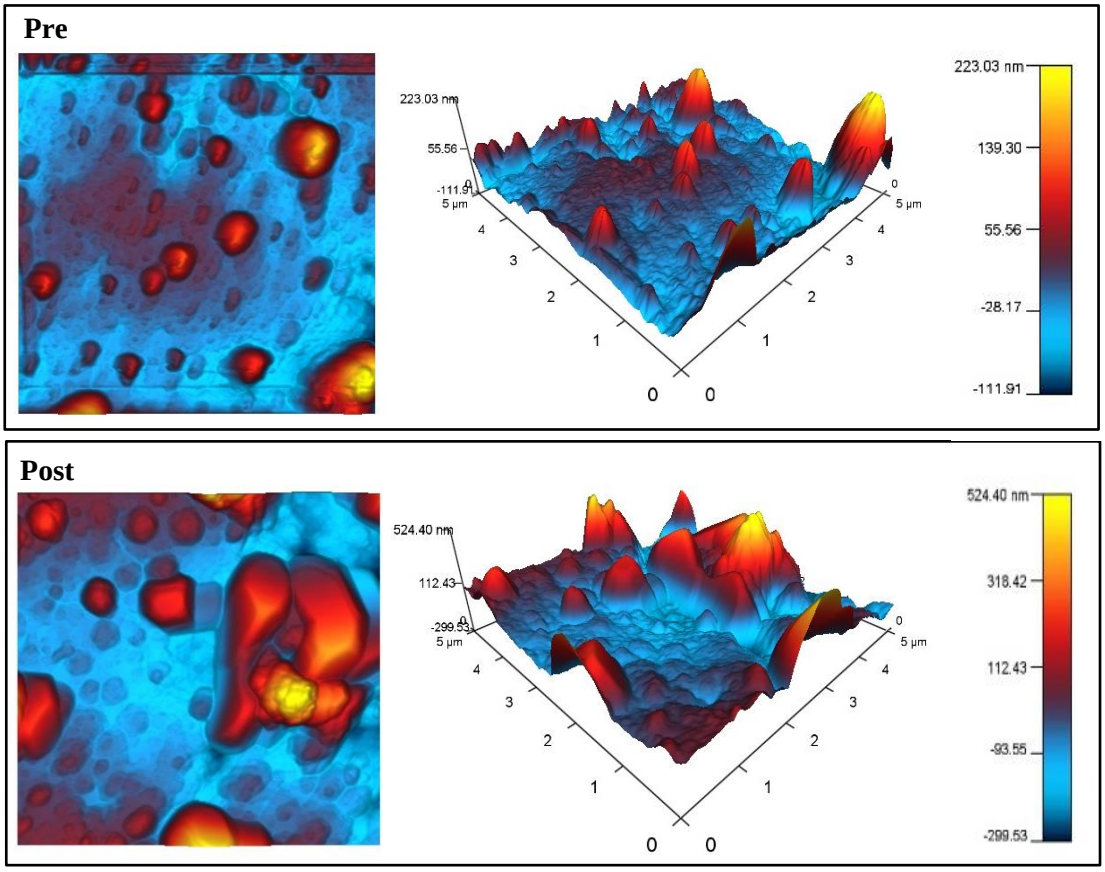

Figure 4-20: Sample: 15min coating (potentiostatic, 0.1M Py 0.1M NaSa, 0.9V) pre (top) and post (bottom) Sa release as labelled. AFM height retrace image (ortho projection LHS, standard 3D RHS), Scan size 5 µm, Scan rate 1Hz. Few PPy nodules clearly identified by yellow/orange peaks indicating areas of larger height. Image shown is representative of 3 separate samples pre- salicylate release and 5 separate samples post salicylate release.

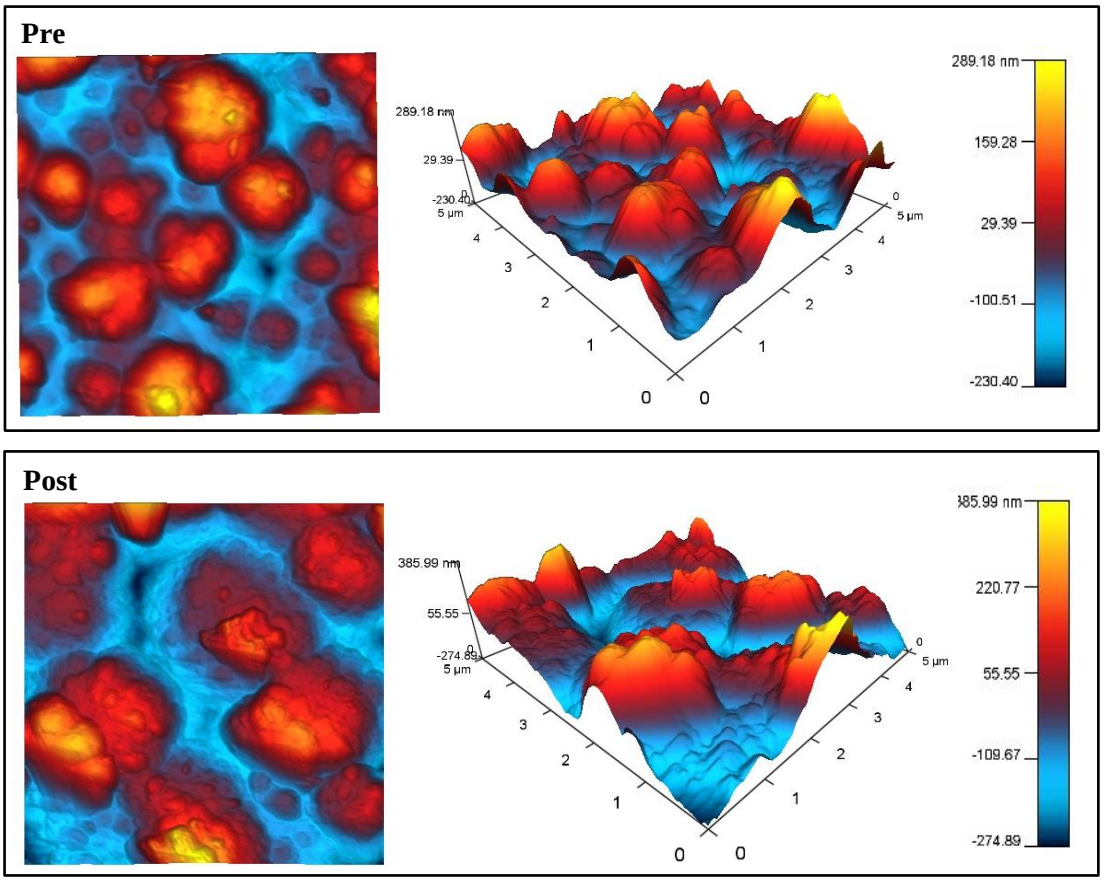

Figure 4-21: Sample: 25min coating (potentiostatic, 0.1M Py 0.1M NaSa, 0.9V) Pre (top)/ Post (bottom) Sa release. AFM height retrace image (ortho projection LHS, standard 3D RHS), Scan size 5 µm, Scan rate 1Hz. Cauliflower morphology is clearly identified by yellow/orange mounds indicating areas of larger height. Image shown is representative of 3 separate sample pre-Sa release and 5 separate samples post Sa release.

4.4.1.4.3. Phase Analysis

When imaged at a scan size of 1 µm, it is possible to identify a shift in phase angle of the tip amplitude relative to the drive frequency of the surface. In this case, the green colour, indicates a larger shift in phase and the blue colour, indicates a smaller shift in phase angle. The phase/height retrace image of the 15 min sample showed areas of decreased phase angle (blue colour) corresponding to areas of large height. There are also green wormlike structures of increased phase angle (green colour) surrounding the blue areas.

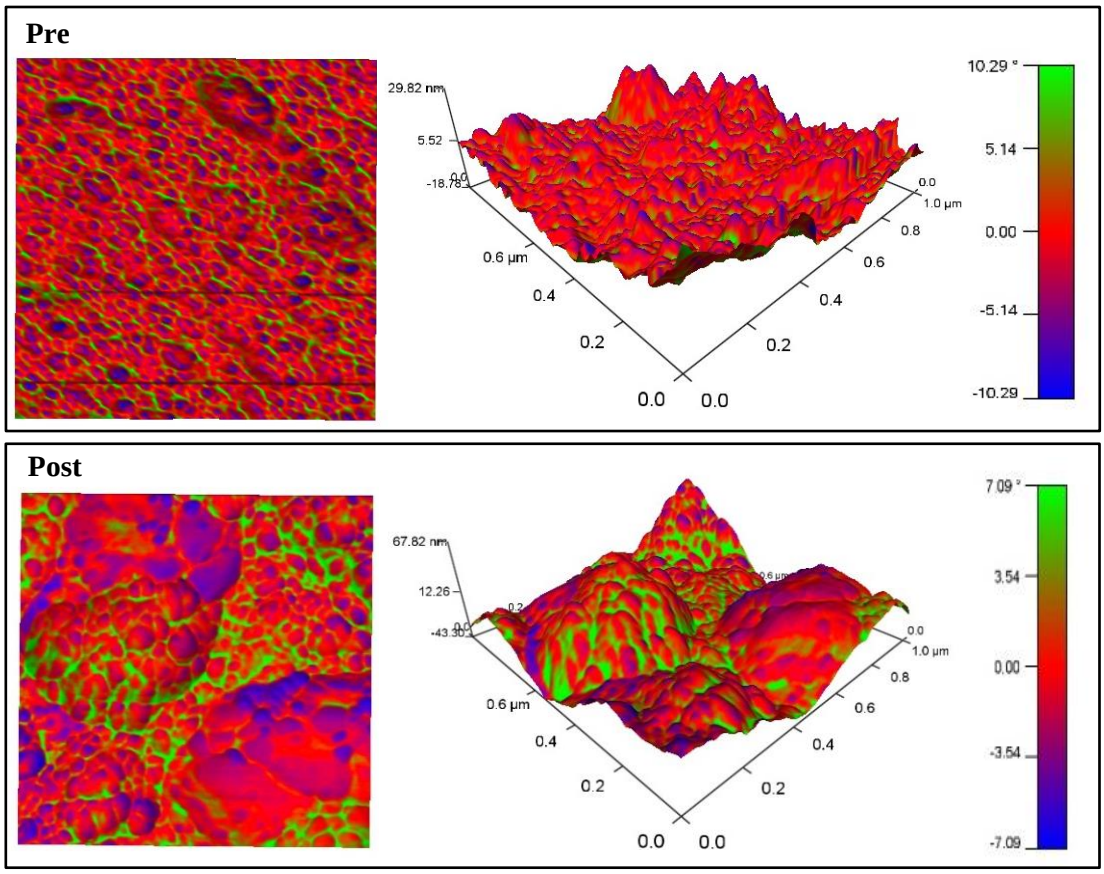

Figure 4-23: Sample: 15min coating (potentiostatic, 0.1M Py 0.1M NaSa, 0.9), pre(top) and post(bottom) Sa release. AFM height retrace image with phase overlay (ortho projection LHS, standard 3D RHS), Scan size 5 µm, Scan rate 1Hz. Blue spots indicate areas of a decreased shift in phase angle, these correspond to areas of larger height in this image. Green areas indicate areas of an increased shift in phase angle, showing worm-like structure. Image shown is representative of 3 separate samples pre-Sa release and 5 separate samples post Sa release.

Analysis of the phase/height retrace images of the 25 min samples showed the surface features to be bigger, with larger spots of decreased shift in phase angle. The areas of increased shift in phase angle are also less well defined.

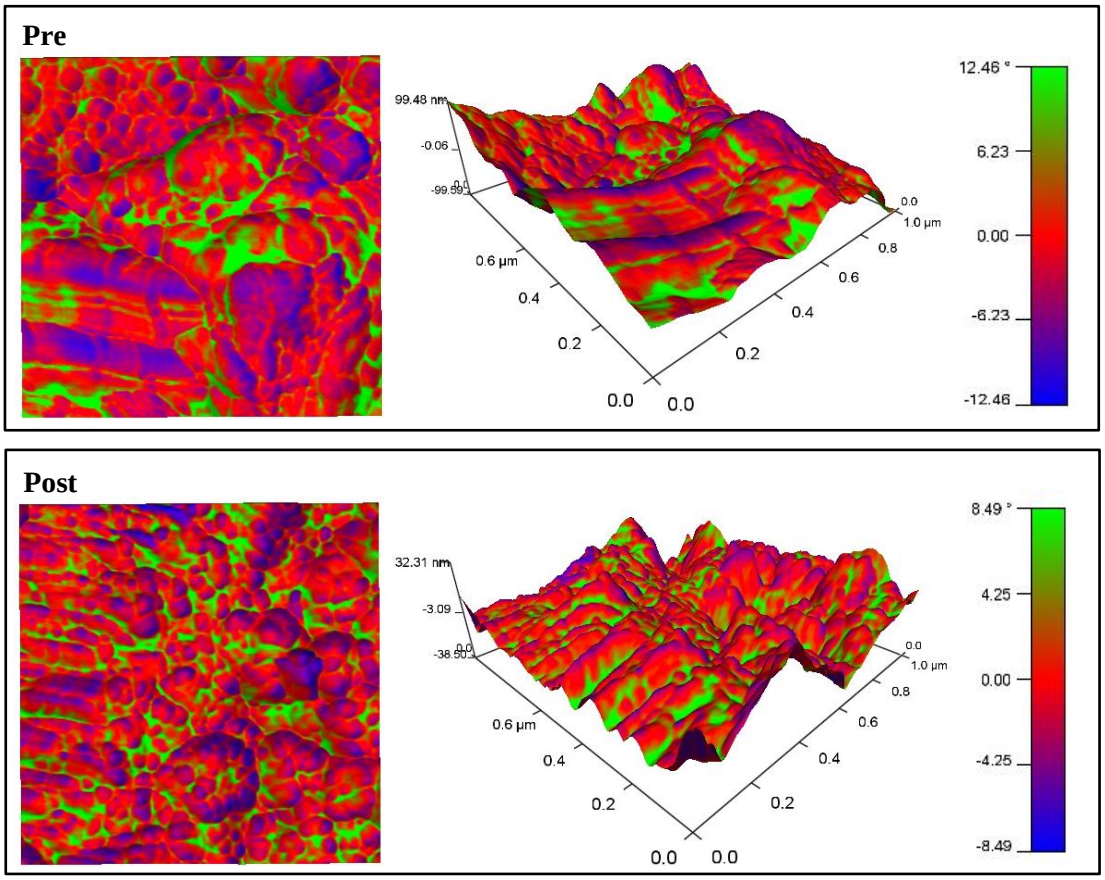

Figure 4-24: Sample: 25min coating (potentiostatic, 0.1M Py 0.1M NaSa, 0.9V) pre (top) and post (bottom) Sa release. AFM height retrace image with phase overlay (ortho projection LHS, standard 3D RHS), Scan size 5 µm, Scan rate 1Hz. Blue spots indicate areas of decreased shift in phase angle, green areas indicate areas of increased shift phase angle. Image shown is representative of 3 separate samples pre-Sa release and 5 samples post Sa release.

4.4.2. Effect of Varying Electropolymerisation Method on Surface Topography and Morphology

Given the relatively rapid release profile achieved with potentiostatic polymerisation, which is in contrast to the process of restenosis that occurs over days and months, it was decided to investigate different methods of electropolymerisation in an attempt to extend the Sa release period. With manufacturing processes in mind, the bulky reference electrode used in potentiostatic electropolymerisation was also identified as a drawback of the process. The results in the following sections were achieved through galvanostatic electropolymerisation performed in line with the two-electrode setup outlined in section 4.3.1.

4.4.2.1. Potential-Time Profiles

In this case, the applied current and electropolymerisation duration were altered in an initial attempt to achieve a uniform coating that covered the wire with no bare stainless steel areas visible by SEM imaging. The coating was initially produced at a current density of 1 mA/cm^2 for electropolymerisation durations of 10 and 15 minutes. This was based on a previous studies (Velhal et al., 2014, Kim et al., 1997, Holland, 2016).

The potential/time curves for the 15 min samples are shown in Figure 4-26, showing values to rapidly increase in the initial 30 seconds after which it slightly decreases and then remains steady. The potential/time curves for the 10 min samples show the same trend, stopping at the 600 second time point.

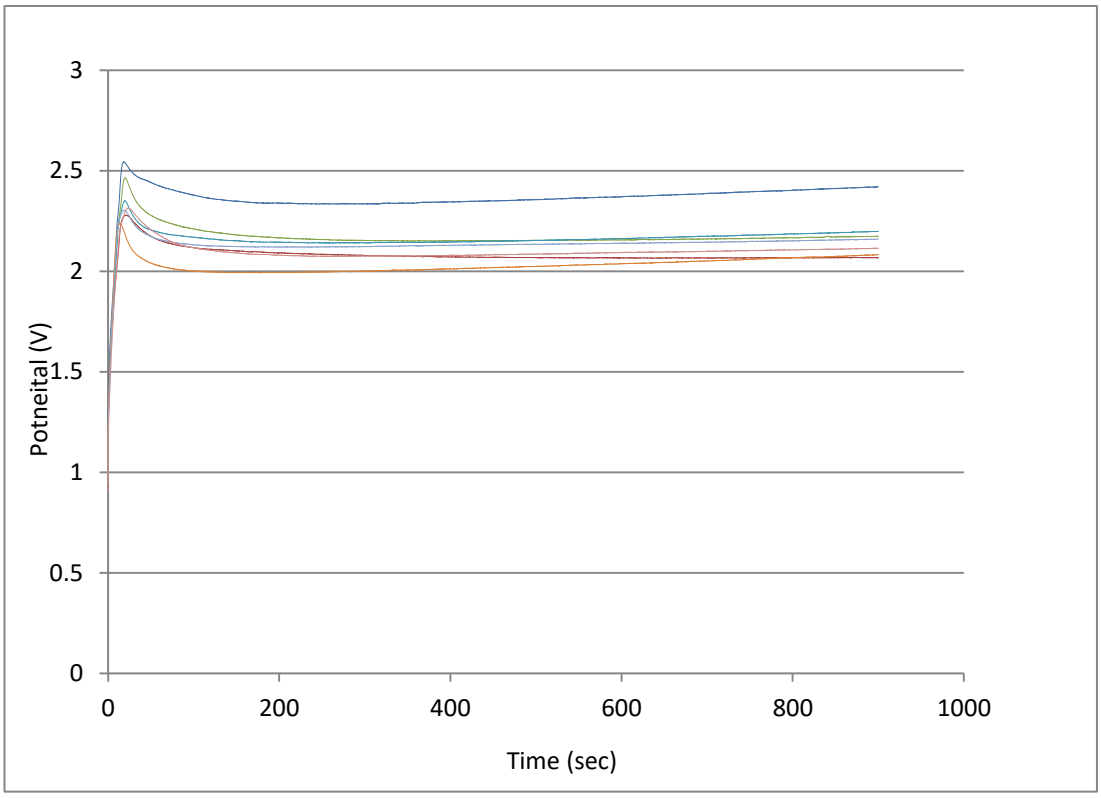

Figure 4-26: Graph of potential (V) vs time (seconds) for SS wire coated by electropolymerisation method: galvanostatic, 1 mA/cm^2*, 0.1M Py 0.1M NaSa,15 minutes.*

4.4.2.2. SEM Analysis of Polypyrrole/Salicylate Coatings Pre/Post Salicylate Release

Pre

SEM analysis of the 10 min/15 min samples (1 mA/cm^2) prior to drug release measurements showed coatings with good coverage of the stainless steel surface and visible cauliflower morphology (see Figure 4-27 and Figure 4-28). Present in both images of the samples (10min/15min, 1mA/cm^2) are the formation of outgrowths, observed on the surfaces of all samples (see Figure 4-27 and Figure 4-28, as labelled). As can be seen from the SEM images, there was little difference in the SEM analysis of the two coating types, despite the difference in electropolymerisation duration.

Post

SEM analysis from both sample types (10 min/ 15 min, 1 mA/cm^2) post salicylate release showed large cracks on the surface of the coatings, exposing the underlying stainless steel (see Figure 4-27 and Figure 4-28, as labelled). These cracks were 'U' shaped and present throughout the whole surface of the wire. In some areas of the coating, it was possible to see the coating become detached from the stainless steel (see Figure 4-27, indicated by red arrow).

When compared to the SEM images of the surfaces pre-salicylate release, it is apparent that the outgrowths are no longer present on the SEM images of the surfaces post salicylate release. Instead, there are bare patches of stainless steel (see Figure 4-27, Figure 4-28, labelled by red circle).

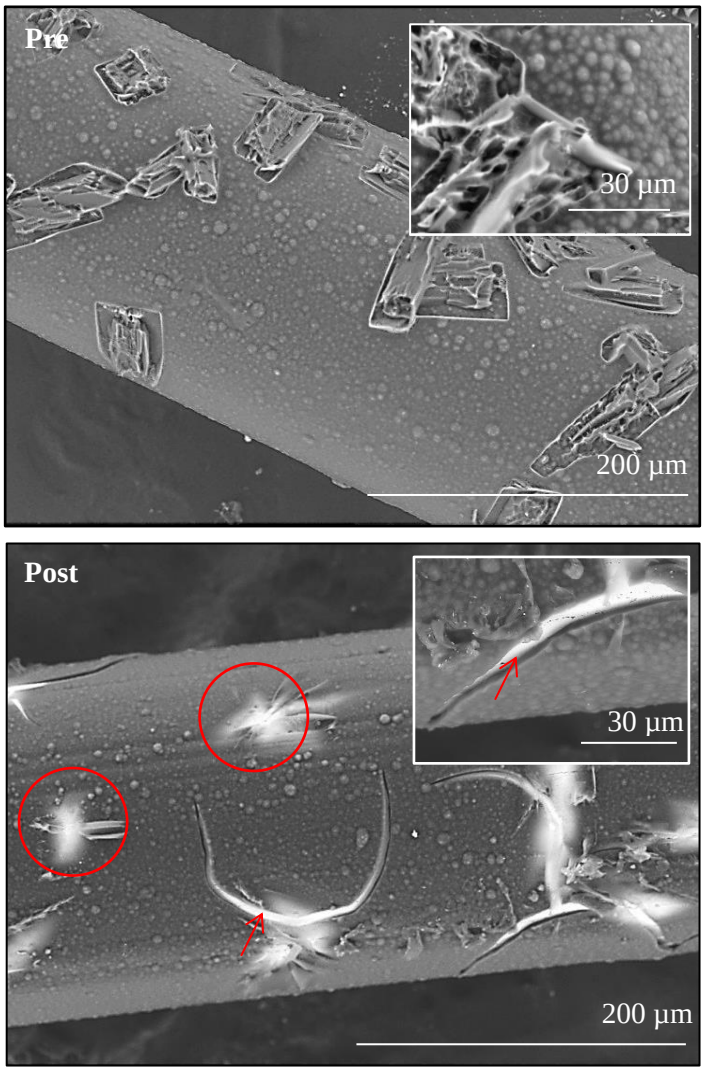

Figure 4-27: SEM image of polypyrrole/salicylate coated SS wire pre- and post- salicylate release. Sample: galvanostatic, 10min, 1mA/cm^2. Top: Pre-salicylate release. Bottom: Post salicylate release. U shaped cracks in coating, exposing underlying stainless steel indicated by red arrows. Red circles indicate bare stainless steel.

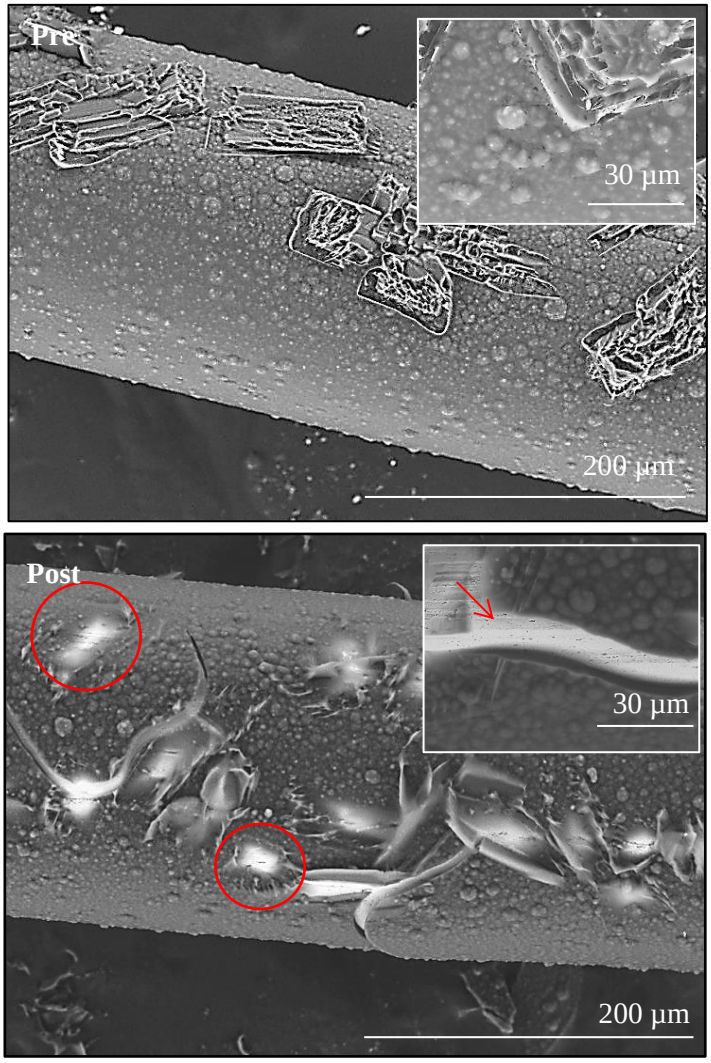

Figure 4-28: SEM images of polypyrrole/salicylate coated SS wire pre- and post-salicylate release. Sample: 15min, 1mA/cm^2. Top: Pre-salicylate release. Bottom: Post salicylate release. U shaped cracks in coating, exposing underlying stainless steel. Red arrow indicates area of delamination. Red circles indicate bare stainless steel.

4.4.2.3. AFM Analysis of Polypyrrole/Salicylate Coatings Pre/Post Salicylate Release

4.4.2.3.1. Numerical Data

Pre

Values of average R_{RMS}, SA and Ry were calculated by the AFM software and are displayed in Table 4-3. The average RMS roughness value of the 10 min samples (107.15 ± 32.55 nm) was found to be smaller than the average RMS roughness value of the 15 min samples (112.73 ± 43.15 nm). The value of average peak-to-valley distance was also found to be smaller for the 10 min samples than the 15 min samples. Despite this slight difference, further statistical analysis confirmed that there is no significant difference between the RMS roughness data or indeed any of the numerical AFM data between the two coatings that differ only in electropolymerisation duration.

Post

AFM analysis was performed post salicylate release on the two coating types (10 min/ 15 min, 1 mA/cm^2). The average R_{RMS} value of the 10 min samples decreased from 107.15 ± 32.55 nm (pre-salicylate release) to 88.93 ± 39.37 nm (post-salicylate release). The average value of peak-to-valley distance also decreased from 778.54 ± 320.17 nm (pre-salicylate release) to 601.34 ± 202.66 nm (post-salicylate release).

AFM analysis showed the opposite effect on the 15 min samples. The average value of R_{RMS} increased from 112.73 ± 43.15 nm (pre-salicylate release) to 144.50 ± 48.00 nm (post-salicylate release). The average Ry value also increased from 822.90 ± 358.74 nm (pre-salicylate release) to 931.04 ± 295.93 nm (post-salicylate release). With such a difference noted between the appearance of the coatings by SEM analysis (pre/post salicylate release), this change in AFM data is not unexpected, however, no significant difference was observed by statistical analysis (see Table 4-3 for full list of values).

*Table 4-3: Table of mean values of RMS roughness (R_{RMS}), surface area (SA) and peak to valley distance (Ry) of coatings pre-salicylate release. Coatings produced by electropolymerisation method: galvanostatic, 0.1M Py 0.1M NaSa, 1 mA/cm^2, 10-15 min (as indicated). Table of AFM data obtained at 5µm, 1Hz. Mean taken from 4 points per sample and three samples (pre-Sa release)/five samples (post Sa release. One-way ANOVA was significant ($p<0.05$). *$p<0.05$ significant difference between 10 min galvanostatic (post) vs 15 min potentiostatic (post) (Tukey post hoc test).*

Sample	**Mean R_{RMS} ± SD (nm)**	**Mean SA ± SD (µm^2)**	**Mean Ry ± SD (nm)**
10 min galvanostatic (pre) n=3	107.15 ± 32.55	27.08 ± 1.24	778.54 ± 320.17
10 min galvanostatic (post) n=5	88.93 ± 39.37	27.47 ± 1.47	601.34 ± 202.66
15 min galvanostatic (pre) n=3	112.73 ± 43.15	27.71 ± 2.43	822.90 ± 358.74
15 min galvanostatic (post) n=5	*144.50 ± 48.00	29 ± 1.95	931.04 ± 295.93

4.4.3. Effect of Varying Electropolymerisation Method on Salicylate Uptake and Release

The applied current was reduced from 1 mA/cm^2 to 0.05 mA/cm^2 in an attempt to reduce the cracking of the coatings following the release of salicylate.

Cumulative Mass

The average mass of salicylate released from the galvanostatic (10 min, 0.05 mA/cm^2) and potentiostatic (25 min) samples is shown in Table 4-4. The total cumulative mass of salicylate released from the 10 min galvanostatic samples is 11.90 ± 0.74 µg compared to the 13.84 ± 5.05 µg released from the 25 min potentiostatic samples. This difference is not statistically significant. The standard deviation values suggest less variation between the galvanostatic samples than the potentiostatic samples, an important factor to consider in the future commercialisation of the coating technique.

Table 4-4: Table of mean total cumulative mass of salicylate released from galvanostatic (10 min, 0.05 mA/cm^2) and potentiostatic (25 min) coatings, including standard deviation values (n=5). Two-tailed T test ($p<0.05$).

Sample	Mean Total Cumulative Mass of Salicylate Released (µg) ± SD
Galvanostatic (10 min, 0.05 mA/cm^2)	11.90 ± 0.74
Potentiostatic (25 min)	13.84 ± 5.05

The mass of salicylate released over the 3-day period is graphically represented in Figure 4-29.

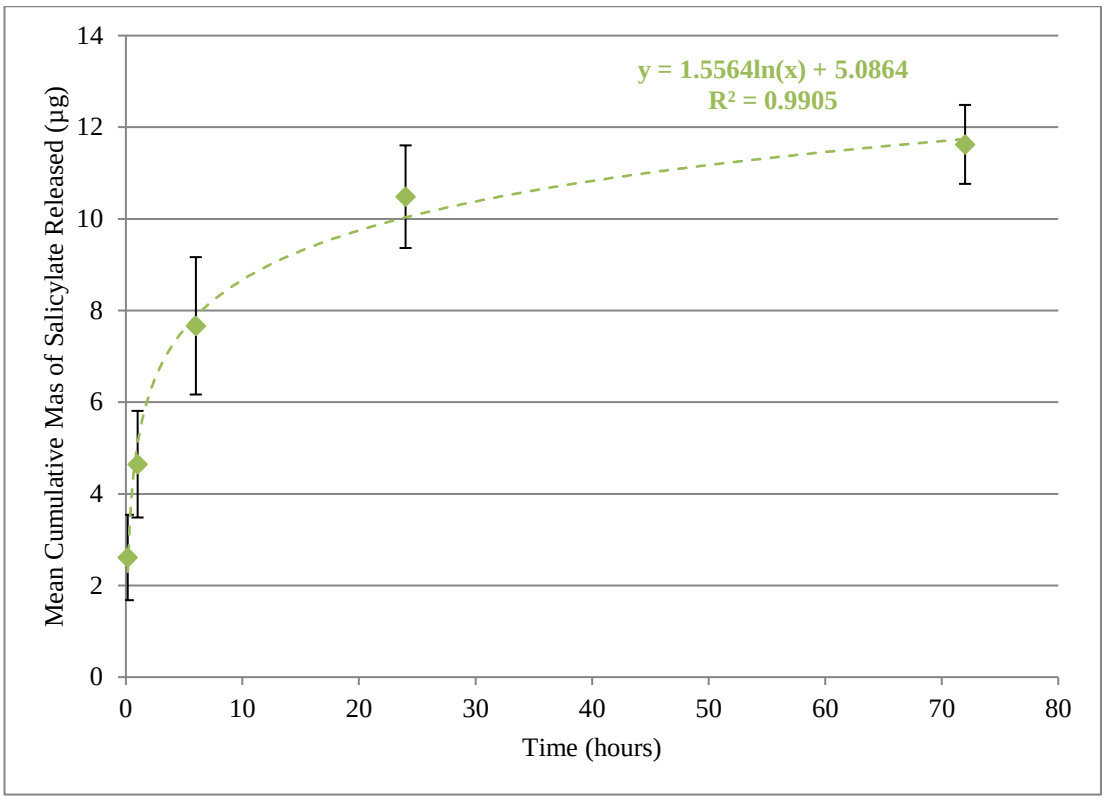

Figure 4-29: Graph representing mean cumulative salicylate release (µg) vs time (hours) of PPy/Sa coated wires. Wires coated by electropolymerisation method: galvanostatic, 0.1 M Pyrrole, 0.1M NaSa, 0.05 mA/cm^2, 10 min. Error bars indicative of standard deviation values taken from 5 samples (n=5). Equation on graph is of logarithmic trendline.

Rate of Release

More than 97 % of the total mass of salicylate was released from all of the 10 min (0.05 mA/cm^2) galvanostatic samples by the 3-day time point with 100% salicylate release occurring within 7 days. This is in comparison to the coatings produced by means of potentiostatic electropolymerisation which had a maximum release period of 24 hours for the 25 min samples.

The 10 min galvanostatic samples released on average 38.70 ± 7.4 9 % of the total salicylate by the 1 hr time point. This is comparison to the 64.18 ± 16.65 % released by the potentiostatic samples (25 min) in the same period. By the 6-hr time point, 64.01 ± 8.95 % of the salicylate was released from the 10 min galvanostatic samples and 87.52 ± 4.61 % from the 25 min potentiostatic samples. A comparison between the salicylate release from the two sample types is shown in Figure 4-30 . The rapid release of salicylate from both sample types in the first hours and a steadier release over the following 48 hours is observed.

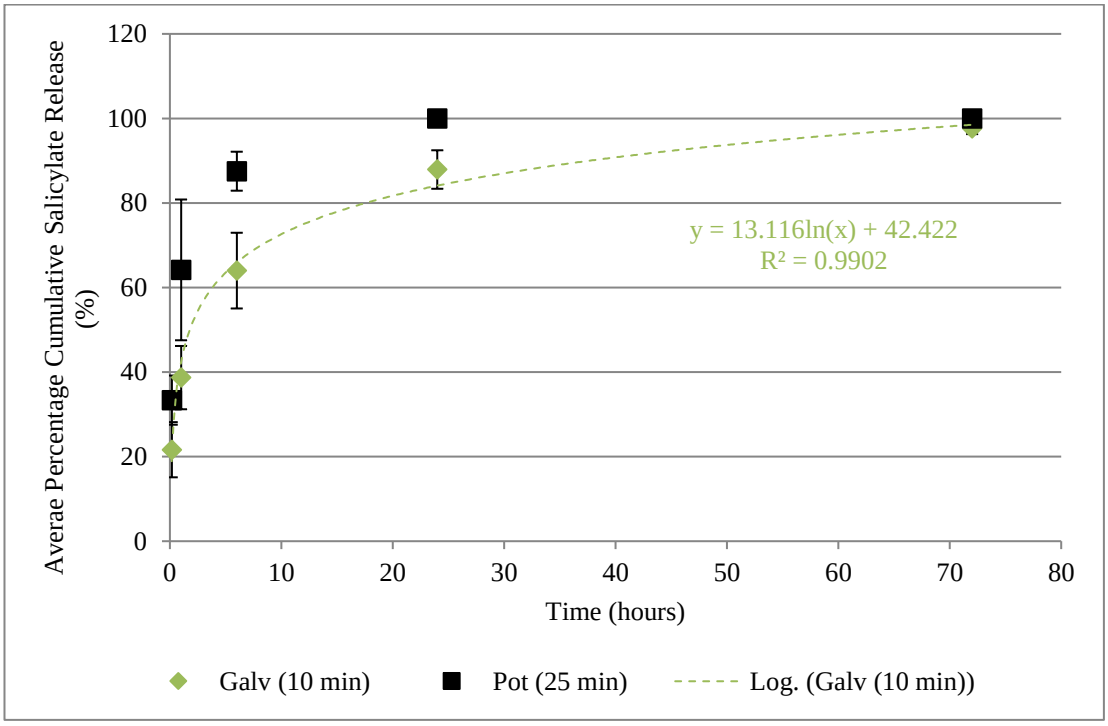

Figure 4-30: Graph representing cumulative salicylate release percentage (%) vs time (hours) of PPy/Sa coated wires. Wires coated by electropolymerisation method: galvanostatic, 0.1 M Pyrrole, 0.1M NaSa, 0.05 mA/cm^2, 10 min and potentiostatic, 0.1 M Pyrrole 0.1M NaSa, 0.9 V, 25 min. Error bars indicative of standard deviation values taken from 5 samples (n=5). Equation on graph is logarithmic trendline through galvanostatic points.

4.4.4. Effect of Varying Electropolymerisation Current on Coating Morphology/Topography

4.4.4.1. SEM Analysis of Polypyrrole/Salicylate Coatings Pre/Post Salicylate Release

SEM images show the coatings produced at the smaller current (0.05 mA/cm^2) (see Figure 4-31) to be more uniform than those produced at the larger current (1 mA/cm^2) (see Figure 4-27). The outgrowths are absent from these new coatings produced at the smaller current (0.05 mA/cm^2).

SEM analysis was performed post-salicylate release, showing no cracks or delamination. When compared to the coatings produced at the larger current, there was a lack of outgrowths and is it fair to also say that the coating appears thinner, with potentially exposed parts of the bare metal underneath.

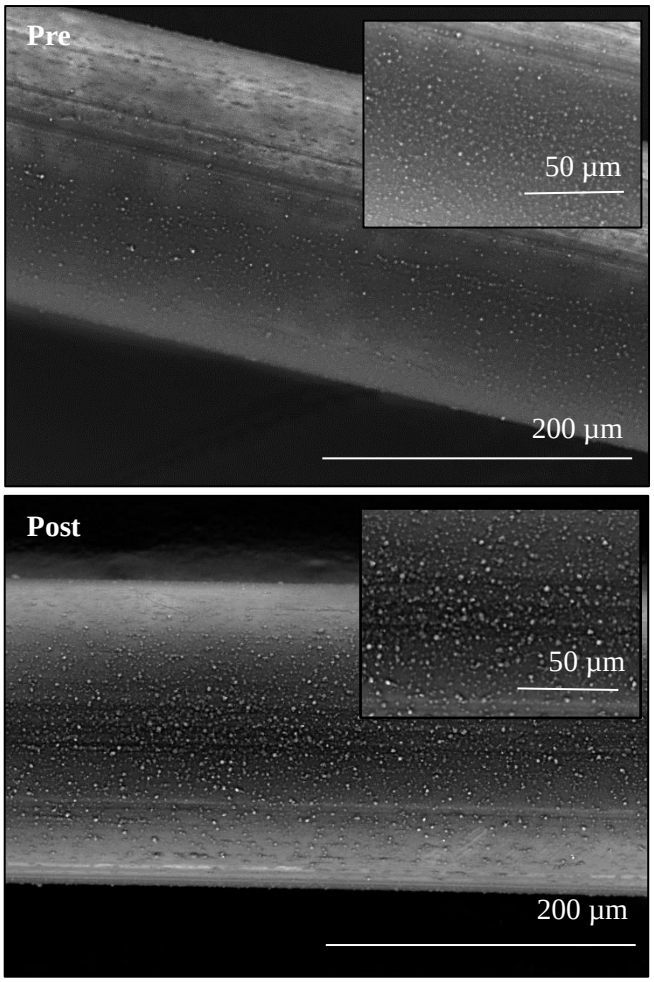

Figure 4-31: SEM images of PPy/Sa coated SS wire pre(top) and post (bottom) salicylate release. Sample: galvanostatic, 0.1M Py 0.1M NaSa, 0.05 mA/cm^2,10 min. No outgrowths or cracks visible.

4.4.4.2. AFM Analysis Pre/Post Salicylate Release

Pre

AFM analysis was performed pre-salicylate release on galvanostatic samples produced at the lower current. The results are presented in Table 4-5. It can be seen that the average R_{RMS} value of 50.69 ± 19.92 nm is significantly lower than the average R_{RMS} values produced for the same duration at a larger current (88.93 ± 39.37 nm). The average Ry value is also significantly lower (425.54 ± 146.33 nm) than that produced at the larger current density (601.34 ± 202.66 nm).

Post

AFM analysis of the samples post salicylate release showed an increase in the average R_{RMS} value (± SD) from 50.69 ± 19.92 nm to 77.29 ± 31.73 nm. The average Ry value also increased from 425.54 ± 146.33 to 538.15 ± 226.70 nm.

*Table 4-5: Table of mean values of RMS roughness (R_{RMS}), surface area (SA) and peak to valley distance (Ry) of coatings post-salicylate release. Coatings produced by electropolymerisation method: galvanostatic, 0.1M Py 0.1M NaSa, 0.05 mA/cm^2, 10 min. Table of AFM data obtained at 5µm, 1Hz. Mean taken from 4 points per sample and three samples (pre)/five samples (post) Sa release. Two-tailed T test (*p<0.05) showed significant difference between 10 min galvanostatic (pre) vs 10 min galvanostatic (post).*

Sample	**Mean R_{RMS}± SD (nm)**	**Mean SA ± SD (µm^2)**	**Mean Ry ± SD (nm)**
10 min, 0.05 mA/cm^2, galvanostatic (pre) n=3	50.69 ± 19.92	26.25 ± 0.50	425.54 ± 146.33
10 min, 0.05 mA/cm^2, galvanostatic (post) n=5	*77.29 ± 31.73	27.03 ± 0.69	538.15 ± 226.70

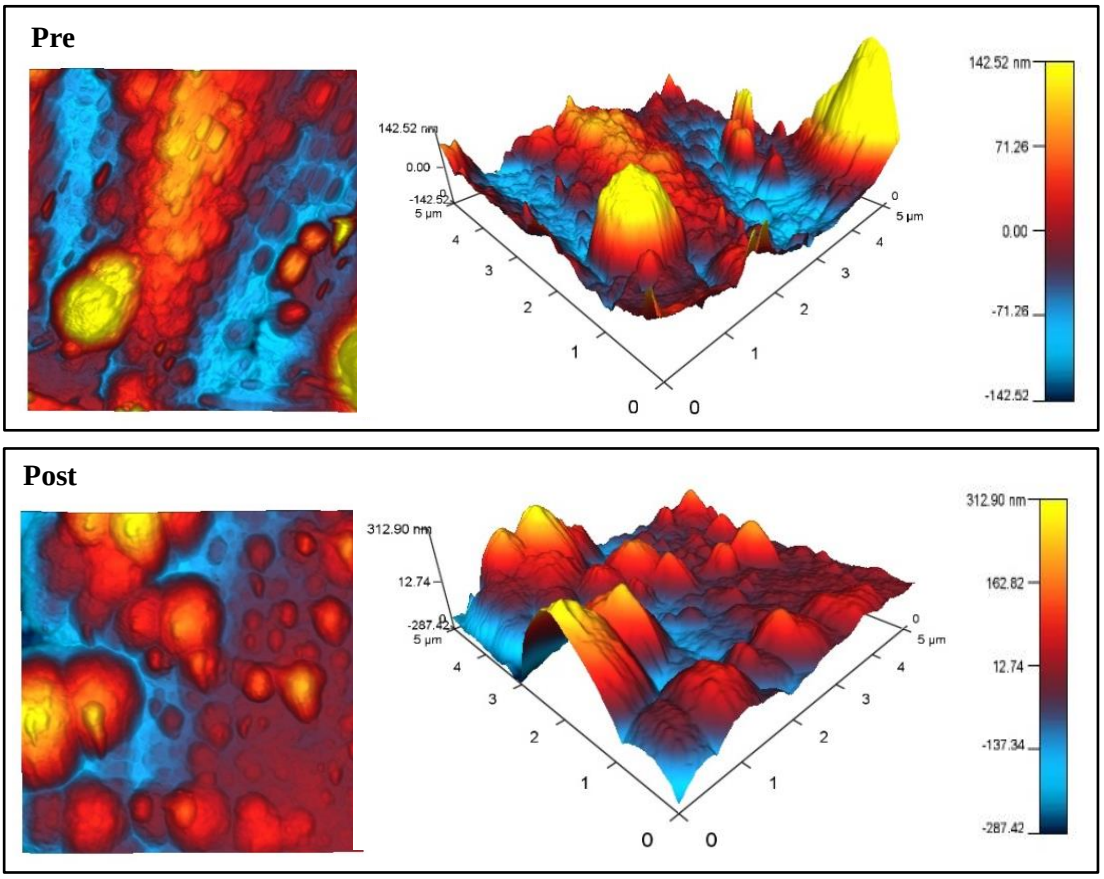

Figure 4-32: Sample: 10 min coating (galvanostatic, 0.1M Py 0.1M NaSa, 0.05 mA/cm^2) pre (top) and post (bottom) Sa release. AFM height retrace image with phase overlay (ortho projection LHS, standard 3D RHS), Scan size 5 µm, Scan rate 1Hz. Image shown is representative of 3 separate samples pre-Sa release and 5 samples post Sa release.

4.4.5. Effect of Pre-treatment of Electrode on Coating Morphology/Topography

SS wire was treated as in 2.3.1.3 and samples coated by means of potentiostatic electropolymerisation. This was in an attempt to assess whether Sa release could be extended.

4.4.5.1. Current-Time Profiles

As illustrated in Figure 4-13 for both sample types (treated/untreated), the potentiostatic current density decreased rapidly in the initial 30 seconds, after which it began to gradually

increase until the end of the procedure. There current-time curves are overlapping in some places, showing little difference between the two sample types.

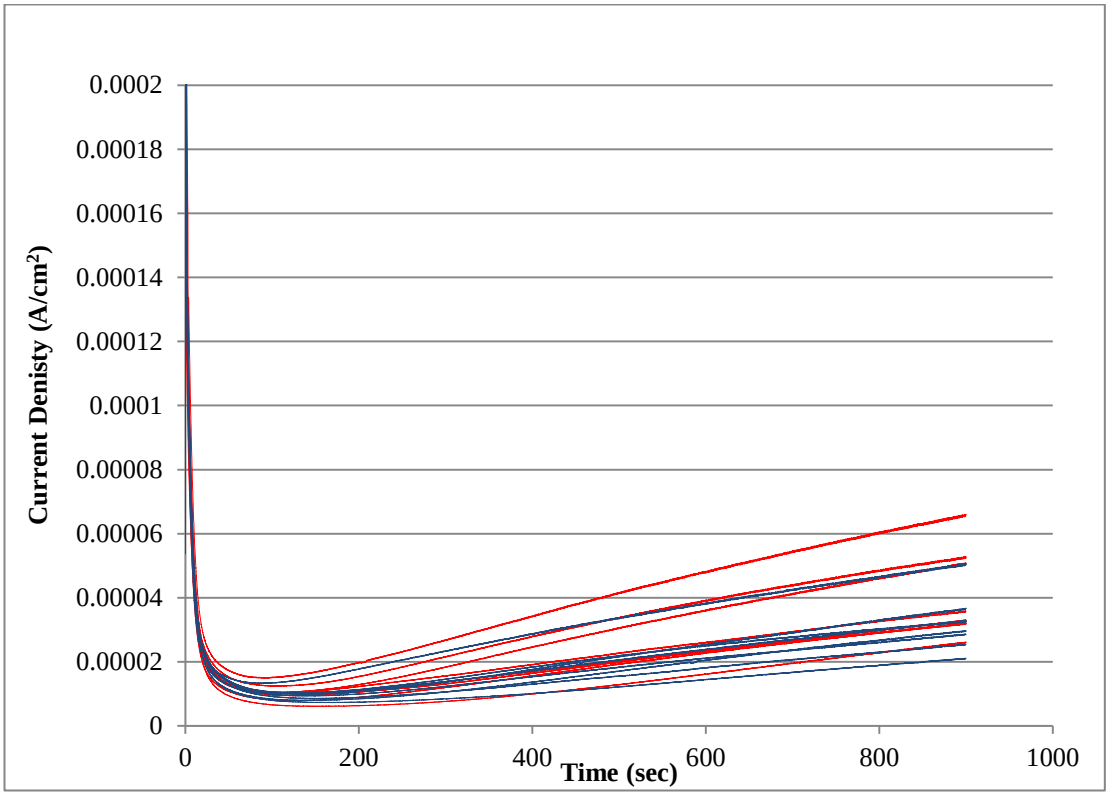

Figure 4-33: Graph of potentiostatic current density Vs time for SS wire coated by electropolymerisation method: potentiostatic 0.9V, 0.1M Py 0.1M NaSa, 15min, red – untreated, blue – pre-treated.

4.4.5.2. SEM Analysis Pre-Salicylate Release

SEM analysis of the two sample types of PPy/Sa coatings (pre-treated and untreated) show patchy coatings in both cases (see Figure 4-34). The coatings varied over the length of the wire with random patches of PPy/Sa coating covering the surfaces.

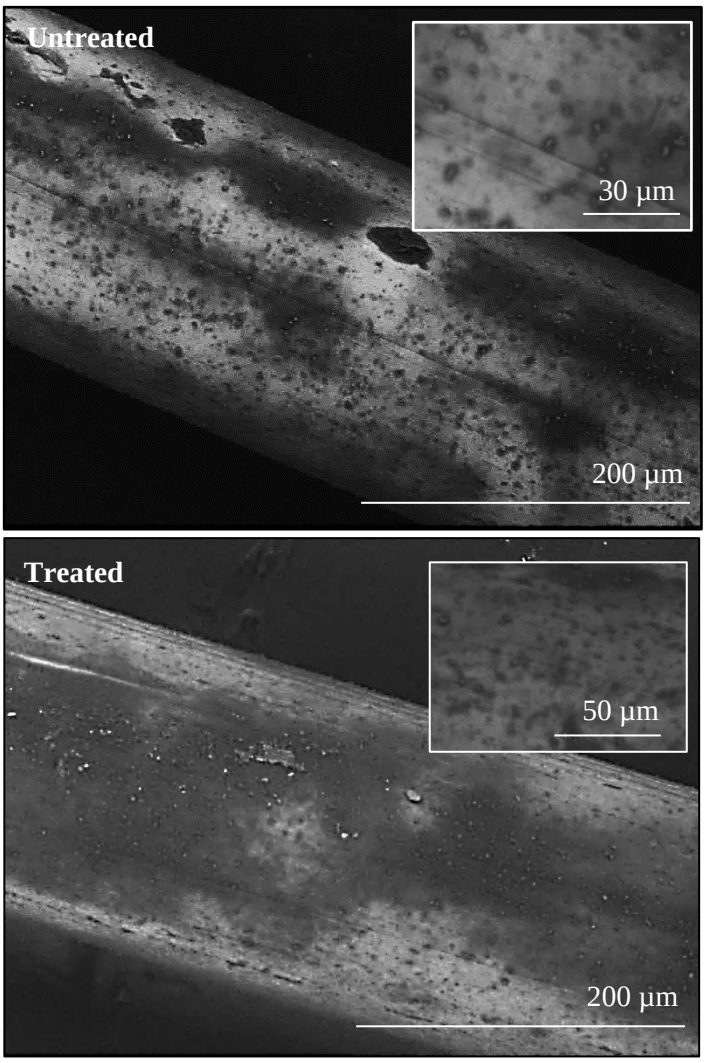

Figure 4-34: SEM images of PPy/Sa coated SS wire. Top: untreated SS wire. Bottom: treated SS wire. Both wires coated by potentiostatic electropolymerisation, 0.9V,15 min..

4.4.6. Effect of Pre-treatment of Electrode on Salicylate Uptake and Release

Cumulative Mass

The average mass of salicylate released from the PPy/Sa coated wires (pre-treated and untreated) samples is shown in Table 4-6. The total cumulative mass of salicylate released from the pre-treated samples is 3.94 ± 2.36 µg compared to the 5.20 ± 2.36 µg released from the untreated samples. This difference is not statistically significant. There was also no

difference in the rate of release of the two sample types as all Sa was released within the first 6 hours, as in section 4.4.1.2.

*Table 4-6: Table of mean total cumulative mass of salicylate released from potentiostatic (15 min, treated and pre-treated) coatings, including standard deviation values (n=5). Two-tailed independent T test (*p<0.05),*

Sample	**Mean Cumulative Mass of Salicylate Released (µg) ± SD**
15 min (untreated)	5.20 ± 2.36
15 min (treated)	3.94 ± 2.36

4.5. Discussion

Polypyrrole has been investigated as a DES coating in a limited number of studies to date (Okner et al., 2007, Arbizzani et al., 2007). Surface topography has been reported to influence the behaviour of cells. However, those studies that have examined the use of PPy as a potential stent coating have not reported on the surface topography of the surfaces generated and there are no surface topographical information of the novel PPy/Sa coatings produced in this study. The release of Sa from PPy/Sa coatings has also been reported to be suboptimal for use in DES coatings, with a 90 % release reported by (Arbizzani et al., 2007) over a period of 2 days. It was therefore our aim to investigate the optimum experimental conditions to achieve a PPy/Sa coating on SS wire that is uniform and provides optimum release of Sa from the coated surface. Coatings were produced by means of electropolymerisation, surfaces were characterised by AFM and SEM analysis and drug release measurements were analysed by UV-spectroscopy. The outcomes from this study are discussed in the following section.

4.5.1. Effect of Varying Electropolymerisation Duration on Surface Topography of PPy/Sa Coatings

Surface Morphology

In the present study, the PPy/Sa coatings were assessed by SEM analysis for uniformity and coverage to determine optimum conditions for coating production. Coating uniformity is an important factor for DES as it allows for even drug distribution on the surface and subsequent release into the surrounding vessel. Electropolymerisation duration was increased until the underlying SS wire platform was no longer visible and the coating appeared uniform when analysed by SEM imaging.

It was found that at an electropolymerisation duration of 15 minutes (potentiostatic, 0.9 V, 0.1 M Py 0.1 M NaSa, 0-4 °C), the underlying SS was still visible. When the electropolymerisation duration was increased to 25 minutes, coatings were uniform throughout the entire surface of the wire. It was concluded that for optimum uniformity and coverage, the following electropolymerisation conditions should be used: potentiostatic, 0.1M NaSa 0.1M Py, 0.9 V, 25 min, 0-4 °C.

From the SEM analysis, it is evident that electropolymerisation duration affects the morphology of the PPy/Sa coating deposited on SS wires. The SEM images of the PPy/Sa coated wire samples following the two different electropolymerisation durations (15 min/ 25 min) are indicative of how the coating may have formed on the surface. SEM images of the 15 minute electropolymerisation samples (see Figure 4-19) demonstrate how the coating appeared to form in patches. The SEM images of the 25 minute electropolymerisation samples (see Figure 4-17) show these patches to be less obvious and a uniform coating to have formed. It is suggested that the coating initially forms in patches and with increased electropolymerisation time more patches form, eventually covering the majority of the surface. This produced the typical 'cauliflower morphology' surface which has been referred to in the literature (Wanekaya et al., 2006).

The morphology of PPy/Sa coatings produced under the conditions used in the present study has not previously been reported in the literature. Additionally, characterisation of PPy/Sa surfaces is not widely reported in the literature; therefore, no direct comparison can be made to the PPy/Sa coatings produced in the present study. However, there are a number of studies that have analysed Polypyrrole surfaces produced by different experimental methods and electrolyte solutions and these will be referred to in the following sections.

The study by (Wanekaya et al., 2006) investigated the surface characteristics of Cl doped Polypyrrole with results showing similar morphology to the coatings produced in the present study. These coatings were produced on 'glassy carbon' as the working electrode and Cl as the dopant ion. The findings by Wanekaya et al report coatings with cauliflower morphology and a smooth under layer, confirming the 'cauliflower morphology' is typical of the PPy component of the coating. The coatings do differ in the quantity and distribution of nodules throughout the surface but the overall appearance of these surfaces is similar to those obtained in the present study. The coatings produced in the study by Wanekaya et al were not specifically designed for use in DES and therefore the experimental conditions such as electrode type and dopant ion are more appropriate in the present study.

Mass of Coating

In the present study, the mass of the PPy/Sa coating on the SS wire was initially measured, but the difference could not be accurately measured by the balance available in the laboratory (0.1 mg) and was therefore estimated to be less than 0.1 mg.

Although the mass of the coatings could not be analysed in the present study, SEM analysis was used to assess the coverage of the underlying SS surface. It does appear that increasing electropolymerisation duration under these conditions does increase the amount of coating on the sample surface which suggests an increase in coating mass.

The study by (Shi and Zhitomirsky, 2010) demonstrates coatings of similar morphology to the coatings in the present study. There is visible cauliflower morphology throughout the coatings and a smooth under layer is also evident. This similarity is as expected as the components of the electrolyte solution are the same in each case, although in varied concentration. The coatings produced by Shi et al used higher concentrations of Pyrrole (0.25 M) and Sodium Salicylate (0.5 M) than were used in the present study (0.1 M Pyrrole 0.1 M NaSa). It appears that the increased concentration enables a coating of thicker appearance to be produced than the coatings in the present study.

Surface Topography

It was observed from SEM analysis that the surface morphology of the PPy/Sa coatings produced at different electropolymerisation durations were different. It was therefore expected that the numerical surface topography data would also vary. From the AFM images of the 15 min sample surfaces, few nodules were visible, randomly spaced over the surface (see section 4.4.1.4). In comparison to the 25 min samples, these nodules have a smaller diameter and range in height from high to low. The nodules on the 25 min samples had a larger diameter and were noted to overlap in certain areas of the surface. It is evident that the initial small nodules on the 15 min samples have continued to grow over the additional electropolymerisation duration (additional 10 mins), eventually covering the majority of the surface. From the SEM and AFM images, it also appears that the coating continues to be deposited on the initial patches in addition to creating new nodules; therefore, the coating may be thicker in some places than in others. The large standard deviation values of the Ry values are indicative of the difference in nodule size and distribution throughout the surfaces of all sample types. This finding is consistent with the literature and the apparent random formation of the polypyrrole coating (Perez et al., 2001).

In the present study, the larger nodules on the 25 min samples resulted in a larger average RMS roughness value (129.49 ± 77.49 nm) than the smaller nodules on the 15 min sample surfaces (82.44 ± 39.50). This suggests increasing electropolymerisation duration leads to a surface of larger R_{RMS} roughness. This is in contrast to the study by Perez et al which reports that an increase in electropolymerisation duration leads to surfaces of decreased roughness

(Perez et al., 2001). The results obtained by Perez et al, were from samples electropolymerized for a much shorter time frame than in the present study and the electrode material and electrolyte solution also differed (Pt on glass working electrode, potentiostatic and voltammetric electropolymerisation, acetonitrile/Py solution). Such methodical differences may help explain the apparent discrepancy between the present study and that of Perez et al.

The studies by (Gelmi et al., 2010, Gelmi et al., 2012) performed similar surface characterisation to that in the present study, on hyaluronic acid and chrondroitin sulphate doped polypyrrole surfaces. The height-retrace images of these surfaces by Gelmi et al are similar to those obtained in the present study. The scan size used in the present study ranged from 1 µm – 20 µm whereas Gelmi et al used a smaller scan size of 0.5 µm (500 nm). The 1µm height retrace images from the present study are very similar to those from the studies by Gelmi et al, showing the detail of the cauliflower morphology and the individual nodules. In the present study, additional height-retrace images were obtained at scan sizes 5µm, 10 µm and 20 µm. This additional data provides a greater understanding of the growth of the PPy/Sa coatings and the size of the nodules. The size of a human artery endothelial cell is 10 - 20 µm in diameter (McGeachie et al, 1998). It is therefore important to gain a topographical map of larger surface features (10 – 20 µm) that would be in contact with endothelial cells, should it be used as a DES coating.

Findings from the present study display an apparent relationship between the electropolymerisation duration and the surface morphology and topography of the resultant coatings, showing the average R_{RMS}, Ry and SA values to increase with increasing electropolymerisation duration. However, the standard deviation values suggest that variance between repeated samples is large, making the identification of trends within the data difficult to confirm with certainty. The reason for these large standard deviation values are likely to be due to the nature of the coating formation, making achieving more statistically significant data difficult. The cauliflower morphology of the coating shows a distribution of nodules of different sizes. By imaging more points per sample and eliminating the definite outliers, it may be possible to achieve average values with a smaller standard deviation. Additionally, if surface roughness values were obtained as a measure of Average Roughness (Ra) as opposed to Root-Mean-Squared Roughness (R_{RMS}), larger peaks would be eliminated from the calculated value. This may be achievable in future work.

Surface Phase

In the present study, there was a phase shift difference observed on the PPy/Sa coatings. This appeared visually as a worm-like structure, with phase shift differences noted between the nodules and the surrounding areas. There was no noticeable difference in the phase shift of the surface pre/post salicylate release which suggests that the phase shift difference of the surface was due to the nature of the polymer and not the release of salicylate.

The studies by (Gelmi et al., 2010, Gelmi et al., 2012) also visually reported the phase shift of polypyrrole surfaces with different dopants (hyaluronic acid/ chondroitin sulphate doped). Performed at a scan size of 0.5 µm, the images are very similar to those in the present study which were performed at a scan size of 1 µm. The phase shift difference that was observed in the present study between the nodules and the perimeter of the nodules was also reported by Gelmi et el. As different dopant ions were used in the present study and the study by Gelmi et al, it can be suggested that the difference in phase angle shift is due to the polypyrrole and not the nature of the dopant.

Similar AFM analysis of another conducting polymer surface, polybiothiophene, has also been reported in a study by (Wallace et al., 2012). The surface phase image shows similar areas of large and small shifts in phase angle thought to be due to the nanostructure of the polymer and different areas of crystallinity within the polymer structure. This further suggests the theory that the phase shift difference of the PPy/Sa surfaces are due to the polymer.

4.5.2. Effect of Varying Electropolymerisation Duration on Release of Sa from PPy/Sa Coatings

Rate of Release

Salicylate release experiments were performed on PPy/Sa coated wire samples (potentiostatic, 0.9 V, 15 min or 25 min, 0.1 M Py 0.1 M NaSa, 0-4 ˚C). It was found that increasing the electropolymerisation duration and maintaining all other experimental conditions, extended

the Sa release from the PPy/Sa coated wire samples. Increasing the electropolymerisation duration from 15 min to 25 min extended the release from 6 hr to 24 hr. The extended release of salicylate from PPy/Sa coated wires under the conditions performed in this study has not previously been reported.

In the present study, the conditions were in a physiological environment ((pH 7.4), temperature (T = 37 °C)) and agitation was incorporated to mimic blood flow. A similar study by (Arbizzani et al., 2007) reported the release of Salicylate from PPy/Sa coated Platinum (Pt) foil in a physiological solution but at room temperature and with no agitation. Arbizanni et al reports a Sa release profile over a period of 7 days for the PPy/Sa coated Pt foils. However, from the Sa release profile presented by Arbizanni et al, it is evident that the majority of the Sa is released within the first 24 hours, as was also found in the present study. The experimental study by Arbizanni et al was also performed at room temperature which is not a typical environment for drug release from a DES. The difference in temperature may influence the rate at which the Sa is released from the coating. The higher temperature in the present study (37 °C) compared to the lower temperature in the study by Arbizanni et al (room temperature) may induce the release of Sa from the coating, causing a faster release rate in the present study.

Additional improvements of the present study from the study by Arbizanni et al is that the PPy/Sa coating was formed on medical grade stainless steel wires as opposed to Pt foils. Medical grade stainless steel is commonly used in DESs and is a cheaper alternative to Pt. The advantage of the wire over the foil is that the wire is a similar thickness to a stent strut, again showing the potential of the coating to form over a surface of similar dimensions.

The release of salicylate from the coatings in the present study (potentiostatic, 0.9 V, 25 min, 0.1MPy 0.1M NaSa, 0-4 ˚C) occurs over a maximum of 24 hours. Salicylate is an anti-inflammatory agent and in terms of the stent inflammation timeline (Inoue et al., 2011), it would be beneficial if it was released throughout the inflammation stage. As mentioned in Chapter 1, it is reported that inflammation occurs 0-7 days post stent implantation whereby leukocytes are recruited at the site of injury. The presence of an anti-inflammatory agent in this time period (0-7 days) may have a positive effect on this inflammation process. In this context, it may be desirable to increase the duration of release and therefore alternative electropolymerisation methodologies were investigated (see sections 4.4.2).

Mass of Salicylate Release

Increasing the electropolymerisation duration not only extended the rate of release but also increased the total cumulative mass of salicylate released from the coatings. The total cumulative mass of salicylate was increased from 5.20 ± 2.35 µg for the 15 min samples to 13.84 ± 5.05 µg for the 25 min samples.

The average total cumulative mass of salicylate released from the 25 min coatings (82.60 µg/cm^2) is in line with the mass of drug released from commercially available stents (100 µg/cm^2) (Iqbal et al., 2013). This is an encouraging finding to show similarities to commercially available products. Nevertheless, the drug release from the PPy/Sa coatings has not previously been incorporated into a DES coating and therefore its performance at this concentration is not fully understood. Further work involving cell growth onto these coatings is shown in chapter 5 will give a better insight into this factor.

4.5.3. Effect of Electropolymerisation Method on Morphology/Topography of PPy/Sa Coating

One drawback of the coatings produced by means of potentiostatic electropolymerisation (0.9 V, 25 min, 0.1M Py 0.1M NaSa, 0-4˚C) in the present study is the relatively long synthesis time (25 min). When considering production in a manufacturing environment, synthesis time should be as short as possible. For example, the dose-adjustable stent coating system developed by Translumina (Translumina, 2009) takes place within a cath lab to provide on-site patient specific coatings that can be almost immediately implanted into the patient after production.

Another reason to prolong the release of Sa is that *in vitro* studies from the literature have shown Sa to inhibit SMC proliferation (Marra et al., 2000). The proliferation of SMCs occurs in the initial weeks post-stent implantation and therefore the release of a SMC inhibitor (Sa) may be beneficial over this time.

The potentiostatic method used in the present study relies upon a three-electrode setup, with a bulky reference electrode, therefore it would be beneficial to eliminate this from the experimental setup. This would potentially allow a smaller volume of electrolyte solution to be used, subsequently reducing the size of the experimental setup and material cost. In an attempt to reduce synthesis time, material cost and extend the rate of salicylate release, the

electropolymerisation method was changed from potentiostatic to galvanostatic. The applied current was initially attempted at 1 mA/cm^2 based on previous experimental studies in the department (Holland, 2016, Kim et al., 1997, Velhal et al., 2014), for a duration of 10 and 15 minutes. The coatings were examined pre-salicylate release with both coatings (10 min/ 15 min) shown to have additional structures on the surface. When analysed post salicylate release, the SEM imaging showed these structures to no longer be visible and the coatings to have undergone cracks and delamination.

The current was subsequently decreased (from 0.1 to 0.05 mA/cm^2) and the duration altered (from 15 minutes to 10 minutes) until the appearance of the additional structures were no longer visible (pre-salicylate release). Following SEM imaging (Figure 4-31) it was concluded that a uniform coating could be obtained with an applied current of 0.05 mA/cm^2 and electropolymerisation duration of 10 minutes.

Surface Features

The following sections will provide a discussion in relation to the comparison between the optimum coatings produced by galvanostatic (0.05 mA/cm^2, 10 min) and potentiostatic (0.9 V, 25 min) electropolymerisation.

SEM images of the two coating types (galvanostatic 10 min and potentiostatic 25 min) pre-salicylate release did appear to differ slightly. Both surfaces had uniform coatings with cauliflower morphology present on the surfaces, but the size of the nodules were different. The polypyrrole nodules appeared more pronounced on the potentiostatic (25 min) sample surfaces. This difference is further observed in the AFM images and numerical surface data.

The average Ry value of the galvanostatic (10 min) samples (425.54 ± 146.33 nm) is smaller than that of the potentiostatic (25 min) surfaces (832.33 ± 475.22 nm). This Ry value gives a measure of the peak-to-valley distance and can therefore provide information on the height of the nodules. The Ry values obtained in this part of the study suggests the size of the polypyrrole nodules to be larger for the potentiostatic (25 min) coatings which is consistent with the SEM images. A reason for this may be the extended electropolymerisation duration of the potentiostatic (25 min) samples, resulting in increased time for the nodules to form and grow on the surface. This has been mentioned and discussed previously in relation to the comparison between the 15 min/ 25 min potentiostatic samples.

It is an aim of the present study to identify the effect surface roughness has on the behaviour of endothelial cells. An additional factor when considering the surface roughness is the size of

the surface features. In the present study, the difference in nodule size, specifically height, between the galvanostatic and potentiostatic samples could lead to varied behaviour of the endothelial cells. The size of a human artery endothelial cell is 10-20 μm in diameter (McGeachie et al, 1998). With nodules of height 0.4 – 0.8 μm (taken from peak-to-valley distance of 25 min potentiostatic coatings) it would be important to determine whether the cells would proliferate and migrate over such a feature. Previous results from Chapter 2 show that endothelial cells successfully grew over the Yukon® stent with pores of around 1-2 μm in depth. It would therefore be expected that the size of the nodules on the PPy/Sa coatings in the present study would not have a negative effect on endothelial cell growth and this will be investigated in chapter 5.

The difference in R_{RMS} and SA values also demonstrate the difference between the two surfaces. The average R_{RMS} value of the galvanostatic (10 min) surfaces is significantly smaller (50.69 ± 19.92) than that of the potentiostatic (25 min) surfaces (129.49 ± 77.49 nm). The large standard deviation values for R_{RMS} and Ry are consistent with the varied nodule size across both sample surfaces, especially for the potentiostatic (25 min) samples (previously discussed). The effect of the different surface topography of these two sample types on the growth of porcine ECs was studied and the results are presented in Chapter 5.

When comparing the surfaces of the polypyrrole coatings to the surfaces of commercially available coronary stents it was found that the R_{RMS} values (~50 – 130 μm) are in the range of the commercially available stents (~30 – 180 μm, identified in chapter 3), which is an encouraging finding. However, the influence surface roughness has on artery healing following stent implantation is an ongoing study and so the importance of this similarity is yet to be fully understood.

Surfaces Post Sa Release

SEM images of the surface of both coating types (galvanostatic 10min, potentiostatic 25 min) post salicylate release demonstrate that there are no stress cracks or delamination following 28 days in physiological conditions. This is a promising result as it suggests the potential of both coating types (galvanostatic 10 min, potentiostatic 25 min) to perform as a DES coating and withstand a physiological environment. The surface of a PPy/Sa coated wire pre/post salicylate release has not previously been reported in the literature.

The findings from the present study show how the morphology of PPy/Sa coatings can change with varying electropolymerisation duration. Combining this finding with those from the

literature (Gelmi et al., 2010, Gelmi et al., 2012, Wanekaya et al., 2006, Shi and Zhitomirsky, 2010) it becomes apparent that the morphology of coatings is dependent on many factors including dopant type and concentration, polymer concentration and experimental method.

4.5.4. Effect of Electropolymerisation Method on Sa Release from PPy/Sa Coatings

Rate of Release

Changing the electropolymerisation method from potentiostatic to galvanostatic enabled a uniform coating to be achieved at a reduced electropolymerisation duration. It also enabled the prolonged Sa release in reduced synthesis duration. More than 97 % of the Sa was released within 3 days from the galvanostatic coatings which is 3 times longer than the release period of the potentiostatic (25 min) coatings. At the next time point (7 days), 100% of the Sa was released from the galvanostatic coatings (10 min). The extended release of Sa from PPy/Sa coatings that were produced in less than half the electropolymerisation duration is a promising result. As discussed above, the release of an anti-inflammatory agent (Sa) throughout the inflammation period post-stent implantation (0-7 days) may be beneficial.

Despite this extended release, it is still less than the release period of drugs from clinically relevant DES. The drug release from commercially available stents varies from product to product, ranging from 20 – 168 days as detailed in chapter 1. However, there are stents that experience an initial burst of drug in the first 48 hours, such as the Taxus Express^2 stent where a large mass of the drug is released in a short period of time (Martin and Boyle, 2011). Improving the rate of salicylate release from the polypyrrole/salicylate coatings should be a focus for future studies.

Comparable Mass of Release

We have shown that to extend the duration of Sa release from the PPy/Sa coatings, you cannot simply increase the electropolymerisation duration and form a thicker coating as this will also increase the cumulative mass of salicylate release. It is also important to optimise other conditions including experimental design and applied current. By changing the electropolymerisation method from potentiostatic to galvanostatic, we have successfully extended the Sa release profile from 24 hours to 3 days. Not only is the release period extended

from the galvanostatic coatings, but the mass of Sa released is similar from both coatings. The cumulative mass of salicylate released from the galvanostatic (10min) coatings (11.90 ± 0.74 µg) is similar to the 13.84 ± 5.05 µg released from the potentiostatic (25 min) coatings.

There was no significant difference between the average cumulative mass of salicylate released from both coating types (potentiostatic and galvanostatic). However, there is a significant difference between the numerical surface topographical data of the two sample types. This allows any effect the two surface types may have on the behaviour of ECs to be identified and this will be investigated in chapter 5.

4.5.5. Study Limitations and Future Work

Although the exact effect of Sa release on events following stent implantation is not fully understood, it may be of interest to further extend the Sa release period from the PPy/Sa coatings. This would enable a database of the experimental method and drug release data to be created, allowing coatings with various doses to be available.

Coating integrity has been examined by SEM/ AFM imaging pre-salicylate release and 28 days post salicylate release, however, the effect of extended time in a physiological environment has not been investigated. This is an important factor to consider as the stability on the coating over a longer period may have an impact in its performance as a stent coating.

Mechanical testing, for example three-point bending of the PPy/Sa coated wires would provide an insight into how the coating would perform if it was subjected to mechanical stress during stents expansion. Additionally, it would be of interest to coat a real BMS with the PPy/Sa coating, to investigate the effect of a more complex geometry on coating formation.

4.5.6. Summary and Conclusions

To conclude, two PPy/Sa coatings (Potentiostatic 0.9 V, 25 min, Galvanostatic 0.05 mA/cm^2, 10 min) with different surface topography and drug release capabilities have been identified in the present chapter as potential DES coatings.

The findings from this chapter demonstrate that the potential PPy/Sa DES coating was improved by changing the experimental conditions. The effect of increasing electropolymerisation duration from 15 min to 25 min on surface topography showed an increase in surface roughness and surface coverage of PPy/Sa coatings produced by

potentiostatic electropolymerisation. It was also found that increasing the electropolymerisation duration from 15 min to 25 min increases the mass of Sa subsequently released from the coating.

The electropolymerisation method was successfully changed from potentiostatic to galvanostatic and the current and electropolymerisation duration varied until a uniform coating was achieved. The optimum galvanostatic electropolymerisation duration was found to be 10 minutes, which is less than half the time it took to produce the initial potentiostatic coating, subsequently reducing synthesis time. The galvanostatic coatings produced in this study have similar morphology to the potentiostatic coating (25 min) but with smaller nodules which led to a surface of significantly smaller RMS roughness. It may be this coating morphology of smaller nodules that has led to the extended Sa release period. The effect of the different surfaces of these two sample types on the growth of porcine ECs will be investigated in chapter 5.

Changing the electropolymerisation method from potentiostatic to galvanostatic enabled the Sa release period to be extended from 24 hours to 3 days without significantly changing the cumulative mass of Sa released. The effect of this extended drug release period on the growth of porcine ECs will also be analysed in chapter 5.

Chapter 5

5. An *In Vitro* Assessment of the Biocompatibility of Polypyrrole/Salicylate Coated Wires

Chapter 5 will outline the biocompatibility of polypyrrole in various forms and will present relevant research that has been undertaken to identify the biocompatibility of polypyrrole with different cell types. The specific aims surrounding the biocompatibility of PPy/Sa coated wires will be outlined in section 5.2. Those aspects of the materials and methods not covered in chapter 2 will be presented in section 5.3. Results will be presented in section 5.4 and an in-depth discussion surrounding the issues mentioned will conclude this chapter in section 5.5.

5.1. Biocompatibility of Polypyrrole

5.1.1. Growth of Cells onto Polypyrrole Surfaces

Current research efforts are now focused on the development of stents which encourage rapid endothelial cell re-growth and so a better understanding of the interaction between the stent surface and the endothelium is therefore required (ter Meer et al., 2017, Martin and Boyle, 2011). It is thought that the migration and adhesion of cells on biomaterials are of great importance for the promotion of wound healing and in tissue regeneration (Lamers et al., 2010).

The biocompatibility of a stent is a measure of how compatible the device is with a biological system, which in this case is the surrounding vessel wall. The stent surface must also be non-thrombogenic, biologically inert and capable of avoiding neointimal proliferation. The biocompatibility of the conducting polymer, polypyrrole (PPy), has been investigated in a number of forms by both *in vitro* and *in vivo* studies. The most relevant findings to the present study will be discussed in this section.

(Wang et al., 2004) investigated the biocompatibility of PPy for its potential use in peripheral nerve tissue supports. The study was performed both *in vitro* and *in vivo,* using a number of animal and cell types. One area of the study by Wang et al compared the migration of Schwann

cells on a PPy membrane to a bare glass surface, with results showing improved migration on the PPy membrane. Another area of the study analysed PPy in powder form, and found it did not cause toxicity or subacute toxicity in the animals they analysed. They also found it to be not mutagenic, allergenic, pyrogenic and haemolytic. These are all important factors when considering a new biomaterial and all tests were performed in accordance with international standard (ISO 10993 and ASTM F1748-82). The study by Wang et al shows the biocompatibility of PPy in both powder and membrane form, and emphasises its potential as a biomaterial when used with nerve tissue.

Cell type is an important factor in analysing the effectiveness of a biomaterial for a particular purpose and has been mentioned in chapter 1. For research in the field of coronary stents, vascular cells (preferably human) are favoured as they are a good representation of the target environment (Busch et al., 2014, Li et al., 2013). Therefore, the study by Wang et al is an adequate study in displaying the general biocompatibility of PPy, in particular for use with nerve tissue, but not in the area of cardiovascular research.

The study by (Jakubiec et al., 1998) was in the field of cardiovascular research and consequently used chick embryo aorta to investigate the behaviour of endothelial cells on a potential vascular implant. *In vitro* analysis was performed on woven fabrics with a PPy coating. The study focused on the electrical conductivity of the coatings and found an optimal conductivity range for improved endothelial cell behaviour. It also reported that PPy surfaces with high conductivity values were a poor environment for the growth, migration and viability of endothelial cells. This finding provides another dimension of conducting polymers to consider for use in biomaterials.

A more relevant study, in terms of cell choice, by (Garner et al., 1999), studied the behaviour of HUVECs (Human Umbilical Vein Endothelial Cells) onto heparin-doped PPy surfaces. The main findings from this study were that cells attached well to the heparin-doped PPy surfaces and the tissue plastic control but did not attach to the nitrate-doped PPy surface type. This study suggests the cell attachment to the PPy surfaces was more dependent on the dopant than the PPy surface.

The studies by (Stewart et al., 2012, Garner et al., 1999), suggest that heparin-doped PPy surfaces are favourable for the growth of HUVECs. The presence of heparin in both of these studies is stated as a major contributing factor to the cell behaviour. Despite the focus on the dopant in these studies, it does not appear that there were any negative effects of PPy, in terms

of biocompatibility. This further emphasises the potential of PPy as a biomaterial for cardiovascular devices.

There are a number of studies available in the literature that have researched the biocompatibility of PPy in various forms, with results showing the great potential of PPy as a biomaterial. These studies have included the use of many cell types, including those of vascular and non-vascular origin. However, there are limited studies available in the literature that have investigated the biocompatibility of a PPy material for potential use in vascular implants, in particular coronary stent coatings. The present study is broadly based upon the study by (Arbizzani et al., 2007) which produced a Sa-releasing PPy coating for potential DES application. The study by Arbizzani et al did not investigate the biocompatibility of the stent, in terms of the growth of ECs on these stents. The study by (Okner et al., 2008) has also been referred to numerous times in the present study. PPy coated stents and bare metal stents were implanted subcutaneously into mice and after 7 days the stents with the surrounding tissue were removed. Samples were examined by histopathological evaluation and results showed no difference between the tissue in contact with the stents or in the absence of stents. Further biocompatibility tests were performed on the tissue in contact with the stents, showing no evidence of inflammation, which further suggests the biocompatibility of PPy.

It is clear that whilst there are numerous reports on the biocompatibility of PPy in various forms, no study has examined the compatibility of the coatings of the type produced in the present study (PPy/Sa onto SS) with vascular cells. We therefore aimed to address this gap in the literature. Preliminary work carried out in the laboratory by (Reay, 2012) had indicated that endothelial cells can adhere and proliferate on PPy surfaces. However, the optimal coating conditions were not identified and use of planar surfaces did not adequately capture the nature of the struts used in coronary stents. In the present study, we therefore set out to further improve upon the experimental design by Reay et al. PPy coated stainless steel wires with a similar diameter to a stent strut will be used, making the experimental conditions more relatable to stent implantation and samples will be incubation with cells for extended periods.

5.2. Aims and Objectives

The biocompatibility of PPy has been introduced in section 5.1.1, with a number of *in vitro* and *in vivo* studies showing the potential of PPy as a biomaterial (Garner et al., 1999, Stewart et al., 2012)(Jakubiec et al., 1998). However, studies relating the biocompatibility of PPy to cardiovascular applications are limited. The present study is broadly based upon the study by (Arbizzani et al., 2007) which produced a Sa-releasing PPy coated Pt platform, however, the biocompatibility of the PPy/Sa coatings were not investigated by Arbizzani et al. This leads on to the main aim of this chapter which is to investigate the biocompatibility of the novel PPy/Sa coatings produced in the present study. This aim can be broken down to the three main objectives below.

1) Analyse the adhesion of porcine ECs onto the PPy/Sa coated SS wires.
2) Determine whether cell viability changes on PPy/Sa coatings with different Sa release profiles.
3) Determine whether cell viability changes on PPy/Sa coatings with different surface roughness.

5.3. Materials and Methods

5.3.1. Cell Culture

Cell culture studies were performed in line with the method described in chapter 2. Each sample comprised a section of PPy/Sa coated SS wire (0.2 mm diameter, 6 mm length). Each wire was either coated by means of galvanostatic electropolymerisation (10 min, 0.05 mA/cm^2) or potentiostatic electropolymerisation (0.9 V, 25min) in electrolyte solution (0.1 M Py, 0.1 M NaSa) in line with the method outlined in section 4.3.

The samples were sterilised by brief immersion in Ethanol and then left to dry in a sterile culture cabinet. Samples were either used immediately after sterilisation or were incubated (37 °C) with Foetal Bovine Serum (FBS) for one hour prior to use. The section of wire was placed in a 96 well plate well with media (Medium 200 with 2% LSGS, 1% PenStrep, ~200 µl) and the cell suspension pipetted directly on top. The total volume of media/ cell suspension was 200 µl in each well. For the control experiments, cell suspension was pipetted directly into wells containing media. For a positive control, media was removed from the control wells (analysed by LDH assay as negative control) and replaced with Triton X-100 (1 wt %). Following incubation, the Triton X-100 solution was removed and analysed by LDH analysis as positive controls. N=3 for all sample types unless otherwise specified. The experimental setup is shown in Figure 5-1.

Media was removed every 3-4 days (3 day, 6 day, 9 day, 13 day) and cell viability analysis was performed by LDH assays (see section 3.2.6 for experimental protocol). Samples were stained (live/dead) and imaged at the experimental end point, following the procedure in section 3.2.7.

Variations on this method were also performed, including increased incubation time, pre-treatment with FBS and removal of sample into a fresh well after cell seeding. Details of these changes will be provided alongside the relevant results sections.

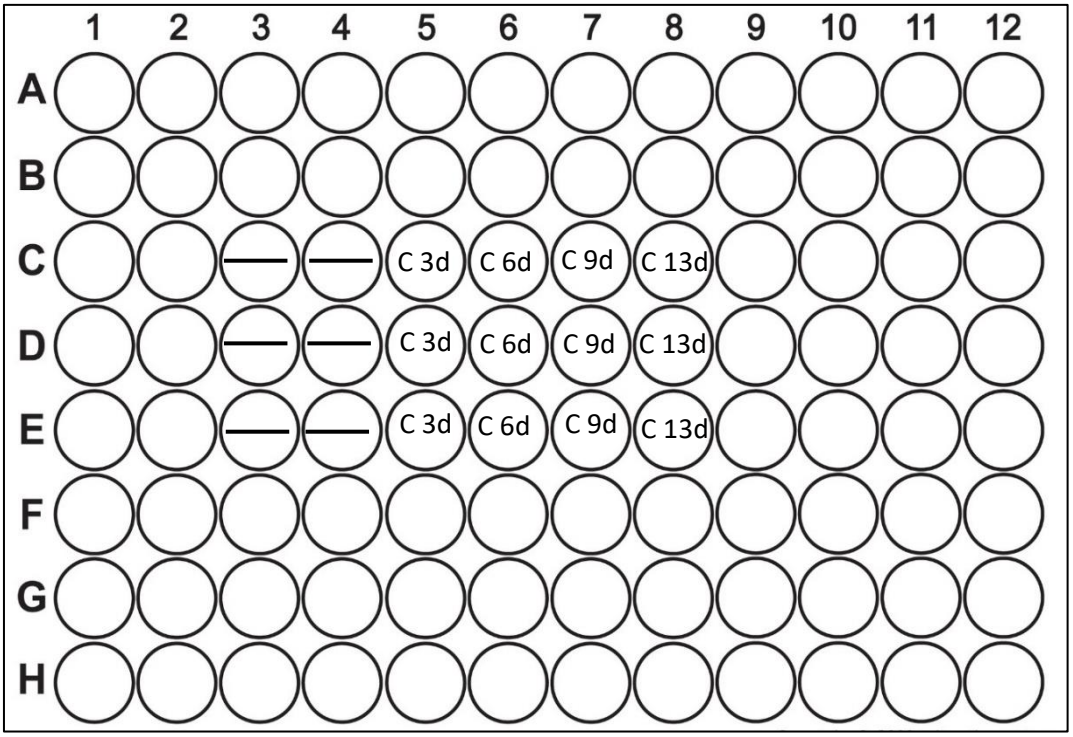

Figure 5-1: Schematic representation of experimental setup. Lines represent PPy/Sa coated wire samples (Coated by potentiostatic or galvanostatic electropolymerisation). C indicates control wells (cells only) for various time points. N=3 for all sample types.

5.4. Results

Experimental studies were performed in line with the method outlined in section 5.3. Porcine endothelial cells were seeded onto PPy/Sa coated stainless steel wires by means of potentiostatic (0.9V, 25 min) or galvanostatic (10 min, 0.05 mA/cm^2) electropolymerisation. Cell viability was analysed by means of live/dead staining and LDH assay. The method, seeding density and incubation time were all altered in this study and the results will be outlined in the following sections.

5.4.1. Increased Seeding Density

Initial studies were performed at a seeding density of 1 x 10^5 cells/cm^2. There were minimal cells present on the surfaces of the two sample types assessed by live/dead staining following 6 days incubation, so further experiments at this seeding density were not attempted.

The seeding density was increased from 1 x 10^5 – 2 x 10^5 cells/cm^2, maintaining the incubation time at 6 days. Live/dead staining images show cells around the edges of both sample types after 6 days incubation (see galvanostatic, potentiostatic Figure 5-2). In some images (see galvanostatic, Figure 5-2), the cells appear to begin to grow over the surfaces. There are more cells present on the live/dead staining images of these sample surfaces than those in the previous study performed at the lower seeding density (seeding density 1 x 10^5 cells/cm^2). However, the PPy/Sa coated wire samples are still not completely covered and were therefore not formally quantified at this preliminary stage of the study.

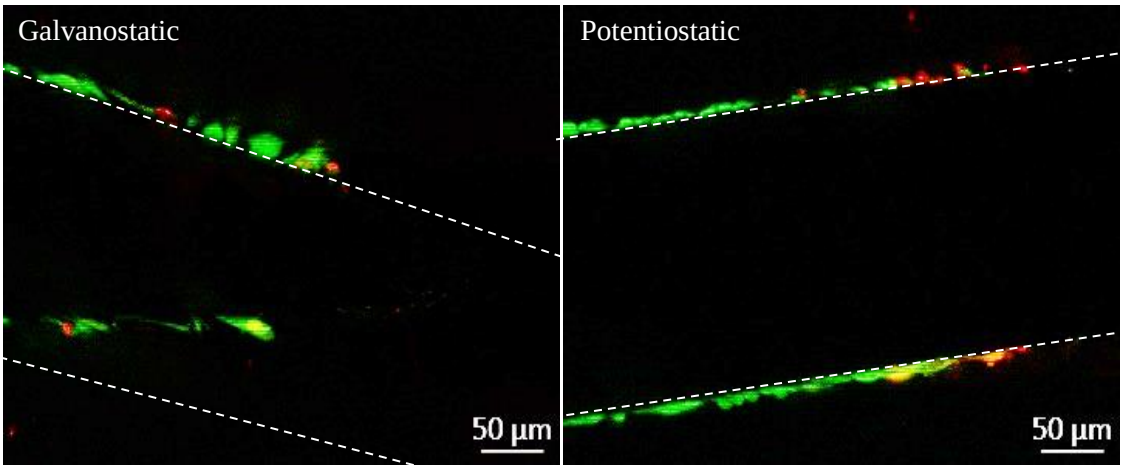

Figure 5-2: live/dead staining images of porcine ECs grown on PPy/Sa coated wire samples (galvanostatic LHS, potentiostatic RHS).Seeding density 2 x 10^5 cells/cm^2, incubation period 6 days. Green indicates live cell, red indicates dead cell. Images are representative of 3 samples. Cells are adhered to edges of coated wires. Few cells adhered to middle of wire seen on galvanostatic samples (LHS).

At the 6 day time point, LDH analysis showed that cells in contact with the galvanostatic samples excreted higher levels of LDH enzyme than the potentiostatic samples and negative controls (cells in media) (see Figure 5-3 for bar chart of LDH values). At the 3 day time point, it was the cells in contact with the potentiostatic samples that excreted marginally larger levels of LDH enzyme than the galvanostatic samples.

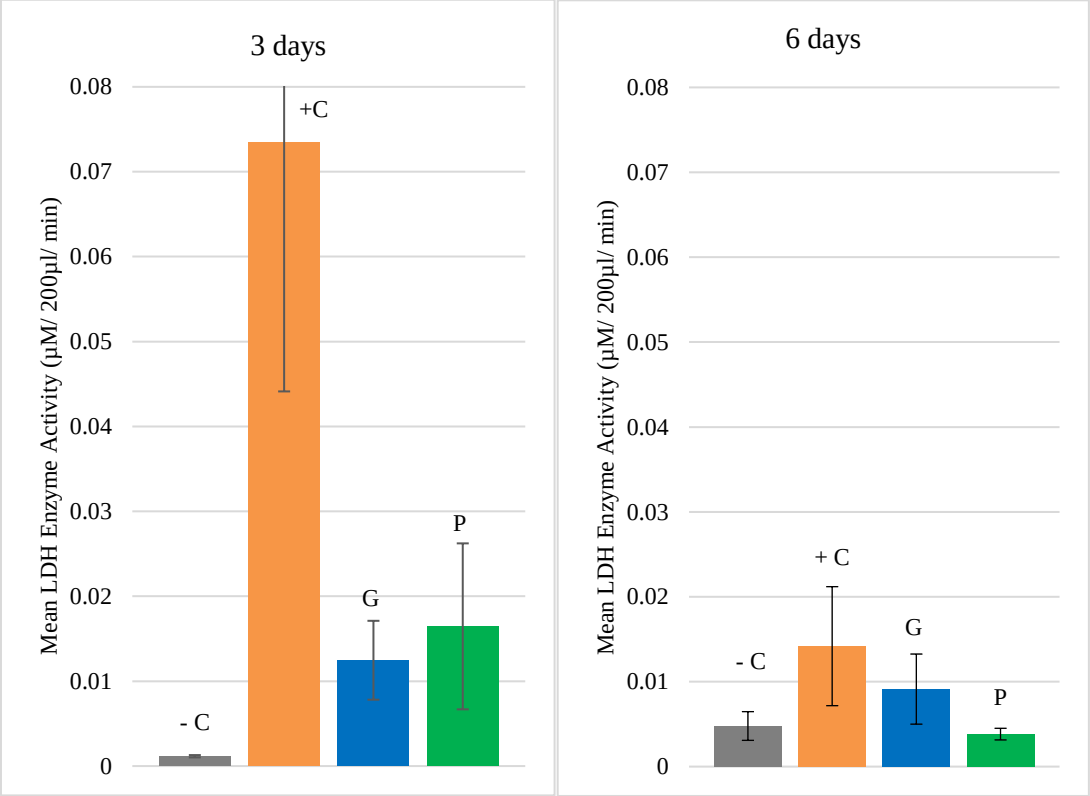

Figure 5-3: Bar chart showing levels of LDH enzyme excreted by porcine ECs grown on PPy/Sa coated wire samples and +ve/-ve controls at 3 day, 6 day time points. Seeding density 2 x 10^5 cells/cm^2. Negative control (cells only), positive control (cells + TritonX-100). All values are mean values calculated from n=3. Error bars are indicative of standard deviation (SD). - C indicates negative control, +C indicates positive control, G indicates Galvanostatic samples, P indicates Potentiostatic samples.

5.4.2. Increased Incubation Time

Maintaining the seeding density of 2 x 10^5 cells/cm^2, the incubation period was increased from 6 days to 13 days. This was in an attempt to improve cell growth on the PPy/Sa coated wire surfaces, allowing the cells additional time to form over the surfaces. At the 13 day time point, five random areas per sample were imaged using live/dead staining; cells were counted using imaging software (ImageJ). The average number of cells was calculated from 15 figures (5 values per 3 samples) to formally quantify the number of cells on the surfaces. The standard

deviation values were also taken from 5 values per 3 samples. From the live/dead staining images, it appears that the additional incubation time has enabled the cells to form over the surfaces of both sample types. This can be identified by the abundance of green areas (live cells) and red areas (dead cells) on the images (see Figure 5-4). There is also a lack of cells on the edge of the coated wires when compared to Figure 5-2, which are likely to have become detached when the sample was removed from the base of the well for staining. The extended incubation time of 13 days may have caused the dense cells that have initially formed at the edges of the stent struts to die and subsequently become detached form the stent struts.

Visually, it appears that the cells have formed in a similar way over both sample surfaces and are of a similar quantity. This was quantified, showing the galvanostatic samples to have an average of 82 ± 42 total number of cells/1.3 mm^2 present on the surface and the potentiostatic samples to have an average of 78 ± 51 total number of cells/ 1.3 mm^2 (see Table 5-1 for full list of values). This difference is not statistically significant. The standard deviation of the total number of cells on both of these surface types is quite large, suggesting variation between sample points. It was found that from the five random points that were imaged per sample, there was variation in the number of cells present. This issue will be further discussed in section 5.5.

Another observation from the live/dead staining images is that there is an almost even distribution of live (green) and dead (red) cells over the two surfaces. Further analysis shows a slightly larger percentage of dead cells on the galvanostatic surfaces (54.45 ± 0.20 %) than on the potentiostatic surfaces (45.00 ± 0.08 %). However, this difference is not statistically significant (Table 5-1 for full list of values).

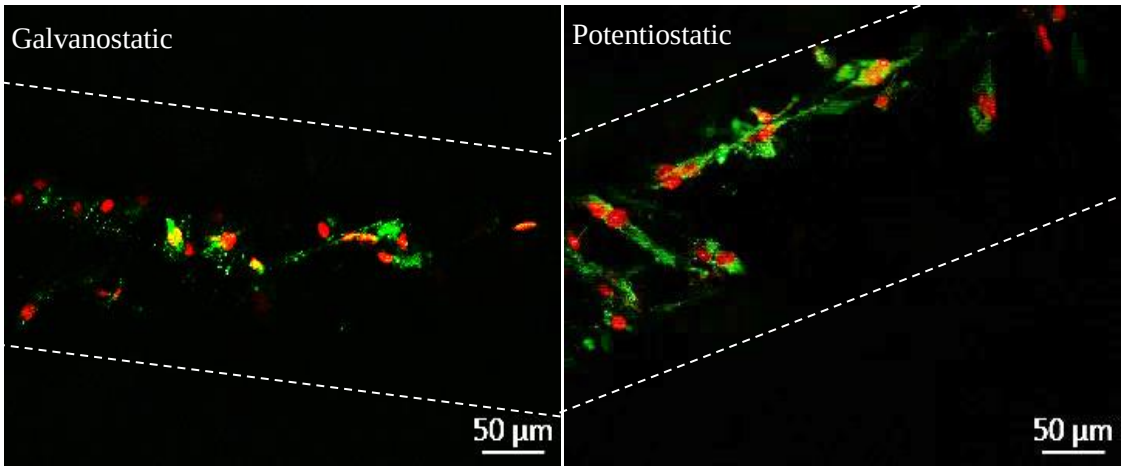

Figure 5-4: live/dead staining images of porcine ECs grown on PPy/Sa coated wire samples (galvanostatic LHS, potentiostatic RHS). Seeding density 2 x 10^5 cells/cm^2, incubation period 13 days. Green indicates live cell, red indicates dead cell. Images representative of 5 sample points per sample from 3 samples.

Table 5-1: Table of mean values of percentage live, percentage dead and total number of cells for porcine ECs grown on PPy/Sa coated wire samples (galvanostatic and potentiostatic). Seeding density 2 x 10^5 cells/cm^2, incubation period 13 days. Mean values calculated from 5 sample points per sample from 3 samples. Table includes standard deviation (SD). Two-tailed T test ($p<0.05$) proved no significant difference between data presented in this table.

Galvanostatic		**Potentiostatic**	
Mean Percentage Live Cells ± SD (%)	45.55 ± 0.20	Mean Percentage Live Cells ± SD (%)	55.00 ± 0.08
Mean Percentage Dead Cells ± SD (%)	54.45 ± 0.20	Mean Percentage Dead Cells ± SD (%)	45.00 ± 0.08
Mean Total Cell Number ± SD	82 ± 42	Mean Total Cell Number ± SD	78 ± 51

Results from the LDH assay show that cells exposed to the galvanostatic surfaces excreted less LDH enzyme than cells exposed to the potentiostatic surfaces at the 13 day time point (see Figure 5-5 for bar chart of LDH values). This was also observed at the 6 day and 9 day time points. At the 3 day time point, the cells in contact with the potentiostatic samples excreted lower levels of LDH enzyme, but this difference was very small. At the 3 day and 6 day time points, the LDH levels are higher in the negative control that the positive control. This may be due to an uneven distribution of cells between the wells. There is no statistically significant difference between the levels of LDH enzyme excreted from the two sample types at any time point in this experimental study.

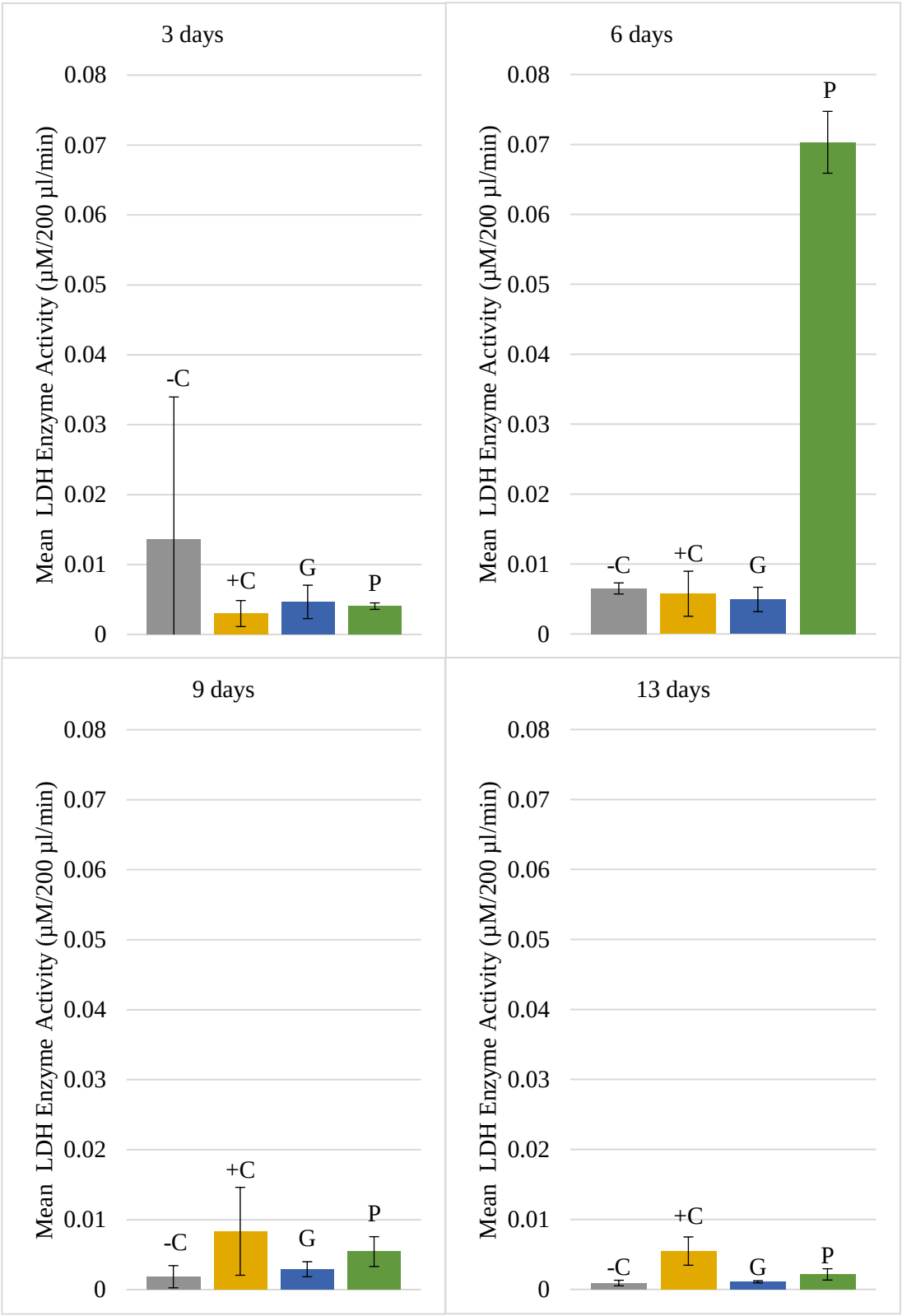

Figure 5-5: Bar chart showing levels of LDH enzyme excreted by porcine ECs grown on PPy/Sa coated wire samples and +ve/-ve controls at 3 day, 6 day, 9 day and 13 day time point. Seeding density 2 x 10^5 cells/cm^2. Negative control (cells only), positive control (cells + TritonX-100). All values are mean values calculated from n=3. Error bars are indicative of standard deviation (SD). -C indicates negative control, +C indicates positive control, G indicates Galvanostatic samples, P indicates Potentiostatic samples.

5.4.3. Pre-treatment with FBS

5.4.3.1. Initial Study

Maintaining the seeding density (2 x 10^5 cells/cm^2) and incubation period (13 day), the experiment was carried out this time including the pre-incubation of the coated wires with FBS (1 hr, 37 °C) prior to seeding of the cells. This was an attempt to improve initial cell attachment to the PPy/Sa coated wire surfaces.

Live/dead staining images show increased cell coverage over the surface of both sample types in comparison to the results obtained in sections 5.4.1 and 5.4.2 with no pre-treatment. The average total number of cells (92 ± 60 (galvanostatic), 90 ± 84 (potentiostatic)) on both surfaces is also larger than was found in the study with no pre-treatment of the surfaces (section 5.4.2) or indeed any of the previous experimental procedures. However, this difference is not statistically significant.

From the live/dead staining images, it is apparent that there was little difference between the coverage of cells on the galvanostatic and potentiostatic surfaces (see Figure 5-6). This is confirmed by very similar values for average total number of cells between the two surface types (see Table 5-2 for full list of values). The distribution of live and dead cells was also very similar between the two surface types, amounting to an average of 48.47 ± 0.13 % live cells on the potentiostatic surfaces and 50.72 ± 0.21 % live cells on the galvanostatic surfaces. There is no significant difference between any of the results obtained for the two sample types in this section.

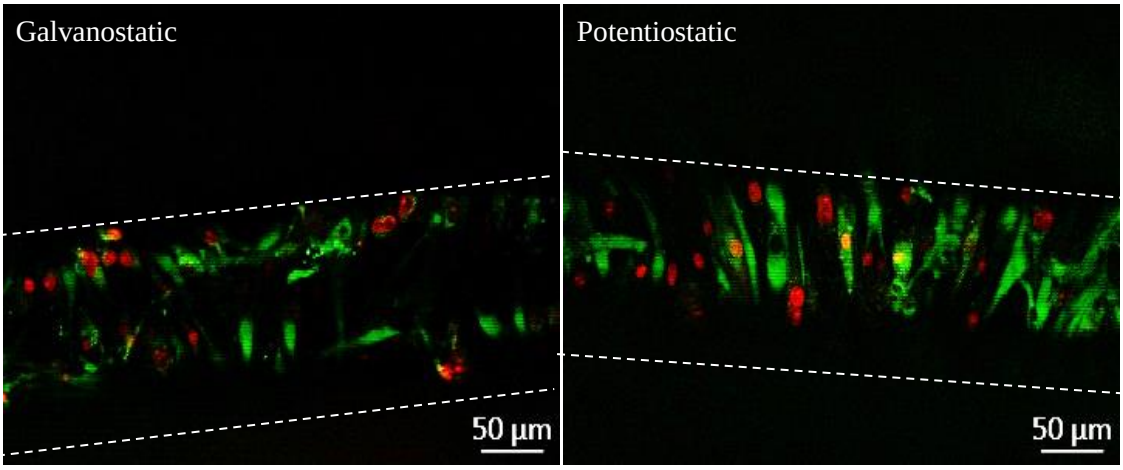

Figure 5-6: live/dead staining images of porcine ECs grown on PPy/Sa coated wire samples (galvanostatic LHS, potentiostatic RHS). Seeding density 2 x 10^5 cells/cm^2, incubation period 13 days. Wire samples pre-treated with FBS. Green indicates live cell, red indicates dead cell. Images representative of 5 sample points per sample from 3 samples.

Table 5-2: Table of mean values of percentage live, percentage dead and total number of cells for porcine ECs grown on PPy/Sa coated wire samples (galvanostatic and potentiostatic) Seeding density 2 x 10^5 cells/cm^2, incubation period 13 days. Samples pre-treated with FBS. Mean values calculated from 5 sample points per sample from 3 samples. Table includes standard deviation (SD). Two-tailed T test ($p<0.05$) proved no significant difference between data presented in this table.

Galvanostatic		**Potentiostatic**	
Mean Percentage Live Cells ± SD (%)	50.72 ± 0.21	Mean Percentage Live Cells ± SD (%)	48.47 ± 0.13
Mean Percentage Dead Cells ± SD (%)	49.28 ± 0.21	Mean Percentage Dead Cells ± SD (%)	51.53 ± 0.13
Mean Total Cell Number ± SD	92 ± 59	Mean Total Cell Number ± SD	90 ± 84

From LDH analysis, it is evident that cells in contact with the potentiostatic samples excrete larger levels of LDH enzyme at the 3 day, 6 day and 9 day time points than observed in those experiments with the galvanostatic samples. This difference is marginal at 3 days and 9 days but a larger difference is observed at the 6 day time point. LDH assay results of the 13 day time point show little difference between the LDH values present in the culture media of both samples types (potentiostatic/galvanostatic), with a slightly lower level experienced for the galvanostatic samples. These results are graphically represented in Figure-5-7 with the error bars indicative of standard deviation.

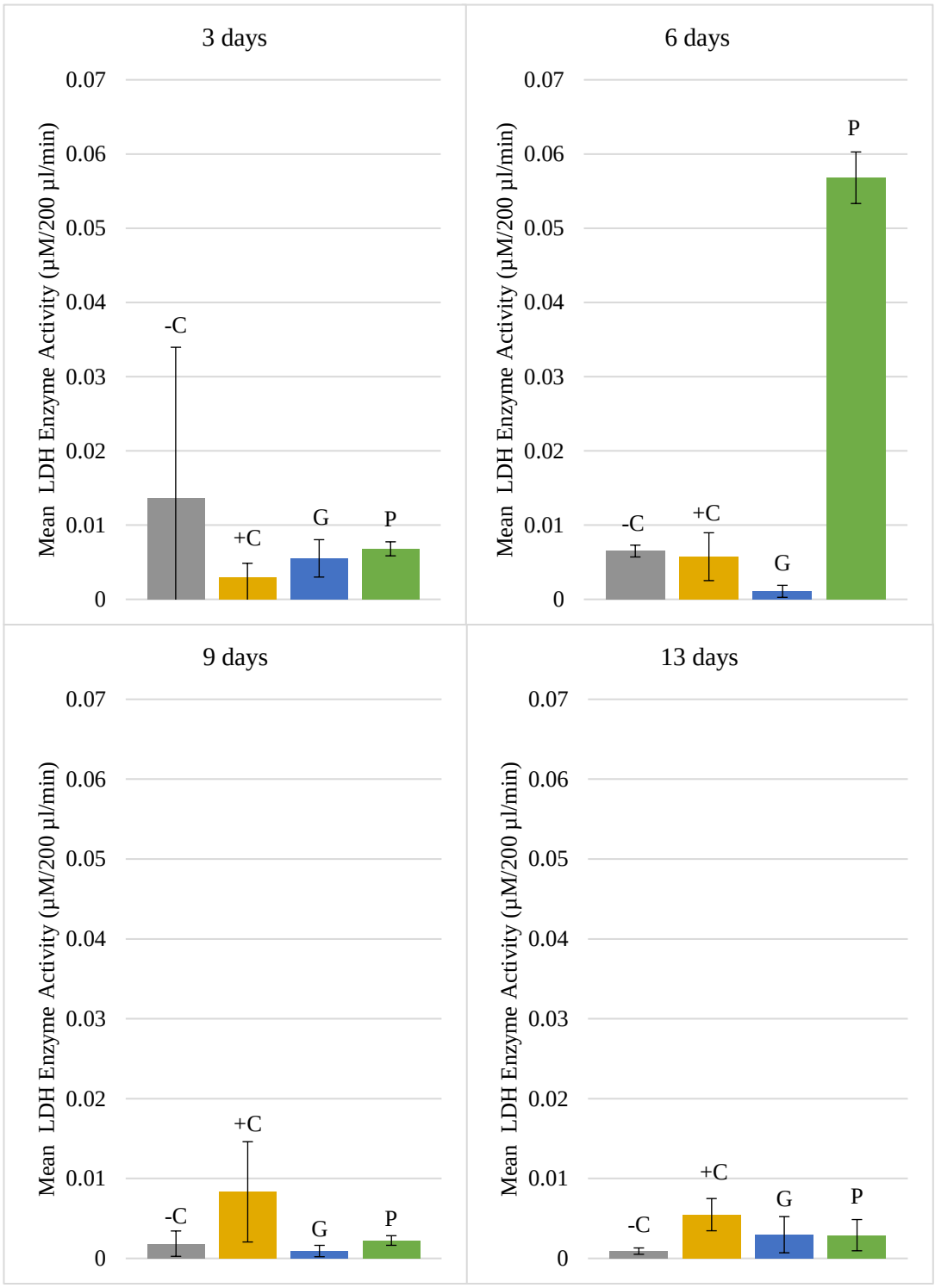

Figure-5-7 Bar chart showing levels of LDH enzyme excreted by porcine ECs grown on PPy/Sa coated wire samples and +ve/-ve controls at 3 day, 6 day, 9 day and 13 day time point. Negative control (cells only), positive control (cells + TritonX-100). Seeding density 2 x 10^5 cells/cm2, incubation period 13 days. Wire samples pre-treated with FBS, sample removed following 24hr into fresh well. Control wells not pre-treated. All values are mean values calculated from n=3. Error bars are indicative of standard deviation. -C indicates negative control, +C indicates positive control, G indicates Galvanostatic samples, P indicates Potentiostatic samples.

5.4.3.2. Second Study

As a result of the large standard deviation values reported in section 5.4.3.1, the study was repeated. The experiment was altered, increasing the number of control wells to five so any outliers could be eliminated from the final results, a technique reported in the literature (Kaja et al., 2015). The highest and lowest LDH values were eliminated from the final data set to give a final sample size of 3.

In this study, a difference between the number of live/dead cells on the surfaces of the galvanostatic and potentiostatic surfaces was observed. There was a larger average total number of cells on the potentiostatic surfaces (103 ± 31) than the galvanostatic surfaces (88 ± 58), mimicking what is shown qualitatively by the live/dead images (see Figure 5-8). The mean percentage of live/dead cells was found to be very similar between these two surface types, amounting to an average of 51.61 ± 0.06 % live cells on the galvanostatic surfaces and 51.75 ± 0.07 % live cells on the potentiostatic surfaces. Statistical analysis reveals that there is no significant difference between the cell count values obtained for both of these surfaces.

Large standard deviation values are observed for total number of cells on both sample types. This was experienced in previous experiments within this study and will be further discussed in section 5.5.

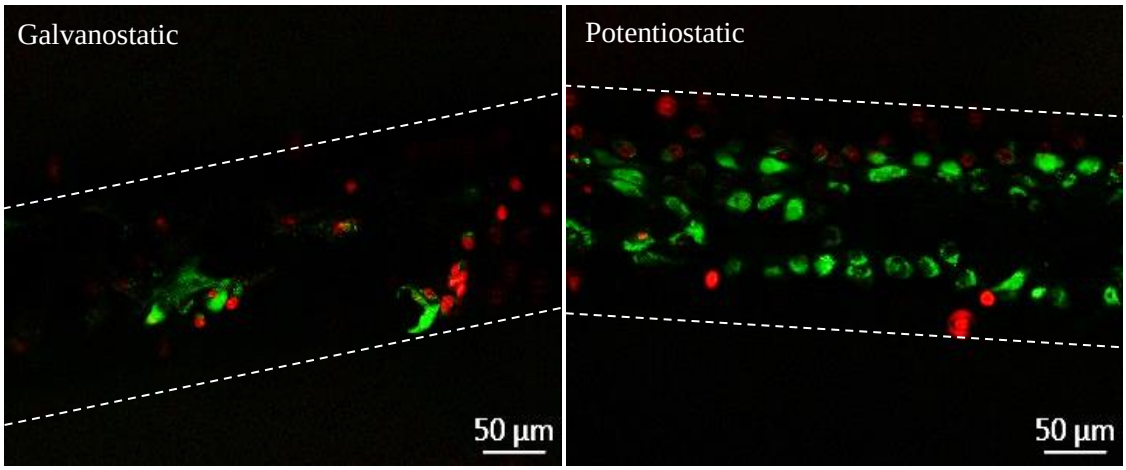

Figure 5-8: live/dead staining images of porcine ECs grown on PPy/Sa coated wire samples (galvanostatic LHS, potentiostatic RHS). Seeding density 2 x 10^5 cells/cm^2, incubation period 13 days. Samples pre-treated with FBS. Green indicates live cell, red indicates dead cell. Images representative of 5 sample points per sample from 3 samples.

Table 5-3: Table of mean values of percentage live, percentage dead and total number of cells for porcine ECs grown on PPy/Sa coated wire samples (galvanostatic and potentiostatic). Seeding density 2 x 10^5 cells/cm^2, incubation period 13 days. Samples pre-treated with FBS. Mean values calculated from 5 sample points per sample from 3 samples. Table includes standard deviation (SD). Two-tailed T test ($p<0.05$) proved no significant difference between data presented in this table.

Galvanostatic		**Potentiostatic**	
Mean Percentage Live Cells ± SD (%)	51.61 ± 0.06	Mean Percentage Live Cells ± SD (%)	51.75 ± 0.07
Mean Percentage Dead Cells ± SD (%)	48.39 ± 0.06	Mean Percentage Dead Cells ± SD (%)	48.25 ± 0.07
Mean Total Cell Number ± SD	88 ± 58	Mean Total Cell Number ± SD	103 ± 31

LDH assay results show the potentiostatic reaction media to contain higher levels of LDH than the galvanostatic reaction media at the 13 day and 3 day time point (see Figure 5-9 for graphical presentation of LDH enzyme activity at 3 day, 6 day, 9 day and 13 day). This difference is not statistically significant but suggests a higher number of damaged cells on the potentiostatic surfaces at the 13 day time point which was found to be the case (identified by live/dead staining, see Table 5-3). At the 6 day and 9 day time points, the LDH levels excreted by cells in contact with the galvanostatic samples are slightly larger than those experienced with the potentiostatic samples.

The values of standard deviation, indicated by the error bars are quite large for both sample types. This may be indicative of varied number of cells between samples, as has been previously mentioned in this study, and will be discussed in 5.5.

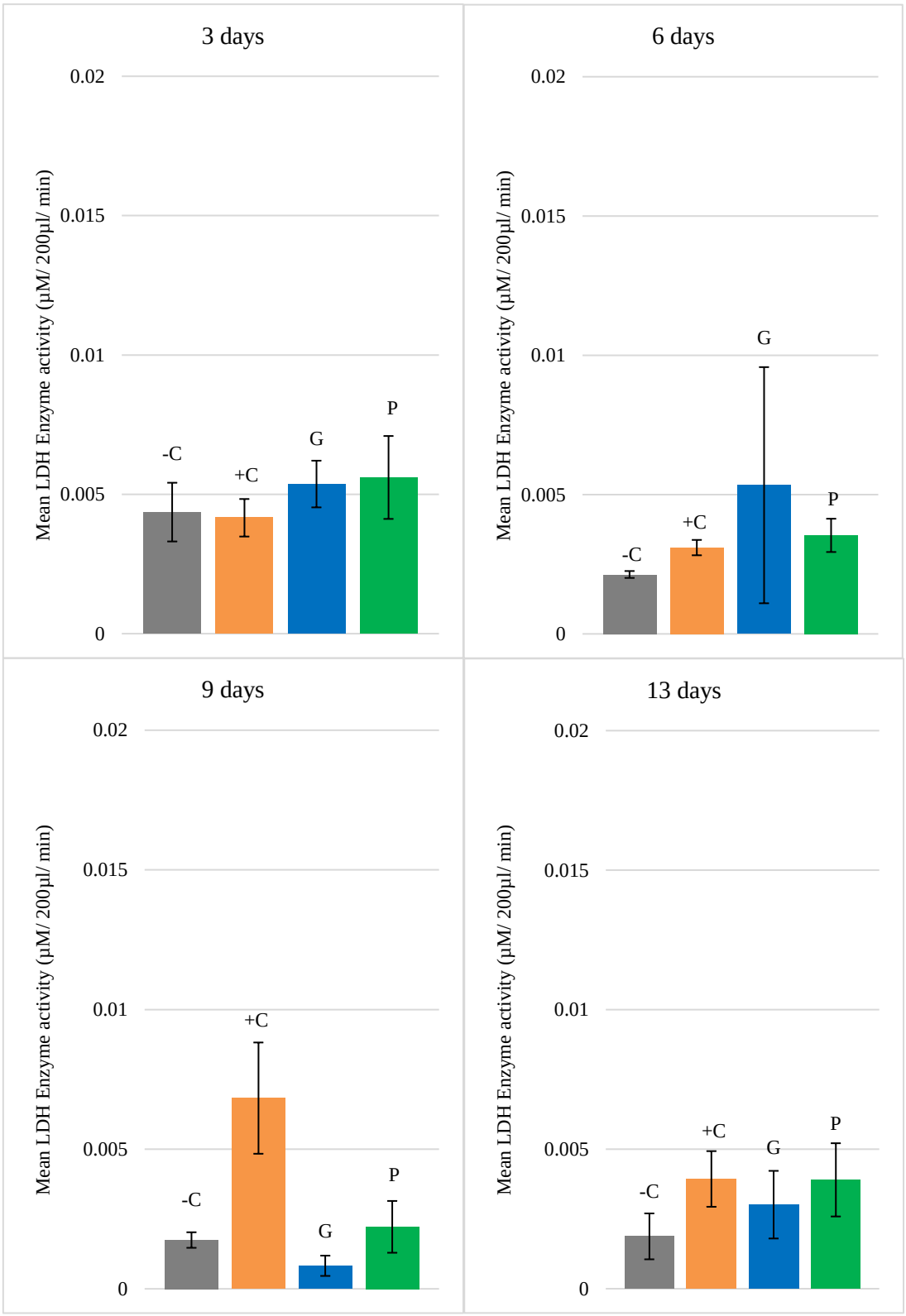

Figure 5-9: Bar chart showing levels of LDH enzyme excreted by porcine ECs grown on PPy/Sa coated wire samples and +ve/-ve controls at 3 day, 6 day, 9 day and 13 day time point (as indicated on graph). Negative control (cells only), positive control (cells + TritonX-100). Seeding density 2 x 10^5 cells/cm^2, incubation period 13 days. Wire samples pre-treated with FBS, sample removed following 24hr into fresh well. Control wells not pre-treated. All values are mean values calculated from n=3. Error bars are indicative of standard error mean. -C indicates negative control, +C indicates positive control, G indicates Galvanostatic samples, P indicates Potentiostatic samples.

5.4.3.3. Removal of Sample to Fresh Well Post Cell Seeding

Up until now, the experiments described have involved seeding cells onto a wire sample that is then left within the cell culture well for the duration of the experiment. To allow the viability of cells directly in contact with the surface to be monitored, eliminating the influence of the cells that additionally form over the base of the well, the sample must be removed following cell attachment. Therefore, in a preliminary experiment, PPy/Sa coated wire samples were removed following 1 hour incubation with the cell suspension and placed in a fresh well. Analysis was performed in line with previous experimental methods in sections 5.4.1 and 5.4.2 with no pre-treatment with FBS. From live/dead staining of the surfaces it was found that very few cells were present on the surfaces.

Subsequently, the experiment was repeated with the additional pre-treatment with FBS and a prolonged incubation period of 24 hours before withdrawal of the wire sample to fresh culture media. The findings from this set of experiments will be outlined in this section.

Live/dead staining showed that there was a larger total number of cells found on the potentiostatic surfaces (87 ± 56) when compared to the galvanostatic surfaces (56 ± 44), however this difference was not statistically significant (see Figure 5-10 to qualitatively visualise proportion of live/dead cells on each sample type). In terms of percentage live/dead cells, the values of both sample types were very similar (see Table 5-4 for full list of results). Both sample types had a slightly larger average percentage of dead cells than live cells present on the sample surface, with 55.45 ± 0.20 % dead cells on the galvanostatic samples and 54.67 ± 0.08 % dead cells on the potentiostatic samples.

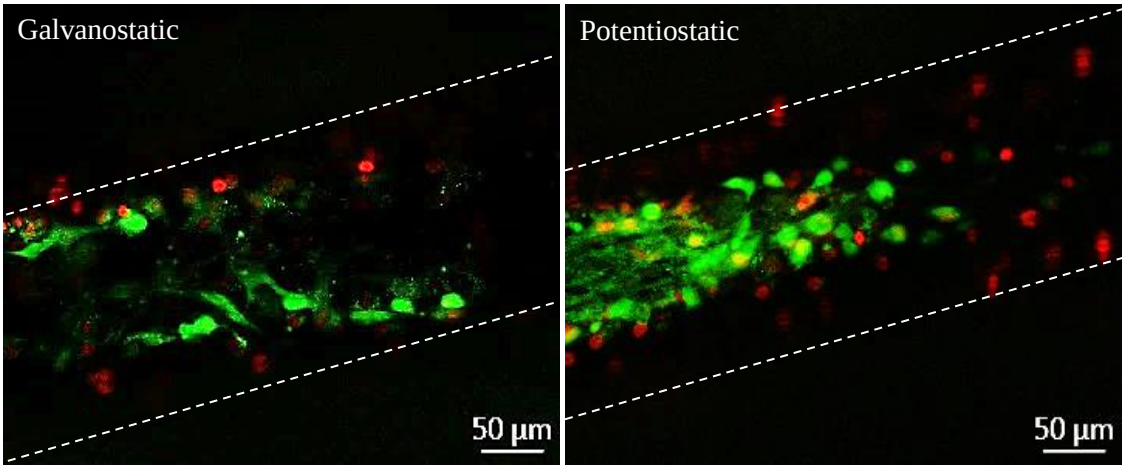

Figure 5-10: live/dead staining images of porcine ECs grown on PPy/Sa coated wire samples (galvanostatic LHS, potentiostatic RHS). Seeding density 2 x 10^5 cells/cm^2, incubation period 13 days. Samples pre-treated with FBS. Samples incubated with cell suspension for 24 hour before removing into fresh well for remainder of incubation period. Green indicates live cell, red indicates dead cell. Images representative of 5 sample points per sample from 3 samples.

Table 5-4: Table of mean values of percentage live, percentage dead and total number of cells for porcine ECs grown on PPy/Sa coated wire samples (galvanostatic and potentiostatic). Seeding density 2 x 10^5 cells/cm^2, incubation period 13 days. Samples pre-treated with FBS. Samples incubated with cell suspension for 24 hour before removing into fresh well for remainder of incubation period. Mean values calculated from 5 sample points per sample from 3 samples. Table includes standard deviation (SD). Two-tailed T test ($p<0.05$) proved no significant difference between data presented in this table.

Galvanostatic		**Potentiostatic**	
Mean Percentage Live Cells ± SD (%)	44.55 ± 0.20	Mean Percentage Live Cells ± SD (%)	45.33 ± 0.08
Mean Percentage Dead Cells ± SD (%)	55.45 ± 0.20	Mean Percentage Dead Cells ± SD (%)	54.67 ± 0.08
Mean Total Cell Number ± SD	56 ± 44	Mean Total Cell Number ± SD	87 ± 56

At time points 3 day, 6 day and 13 day, the LDH levels of the cells in contact with the galvanostatic samples were found to be higher than those associated with the potentiostatic samples (Figure 5-11, for graphical presentation of LDH enzyme activity at 3 day, 6 day, 9 day and 13 day). There was minimal difference found between the LDH values at the 13-day time point which is shown graphically in Figure 5-11.

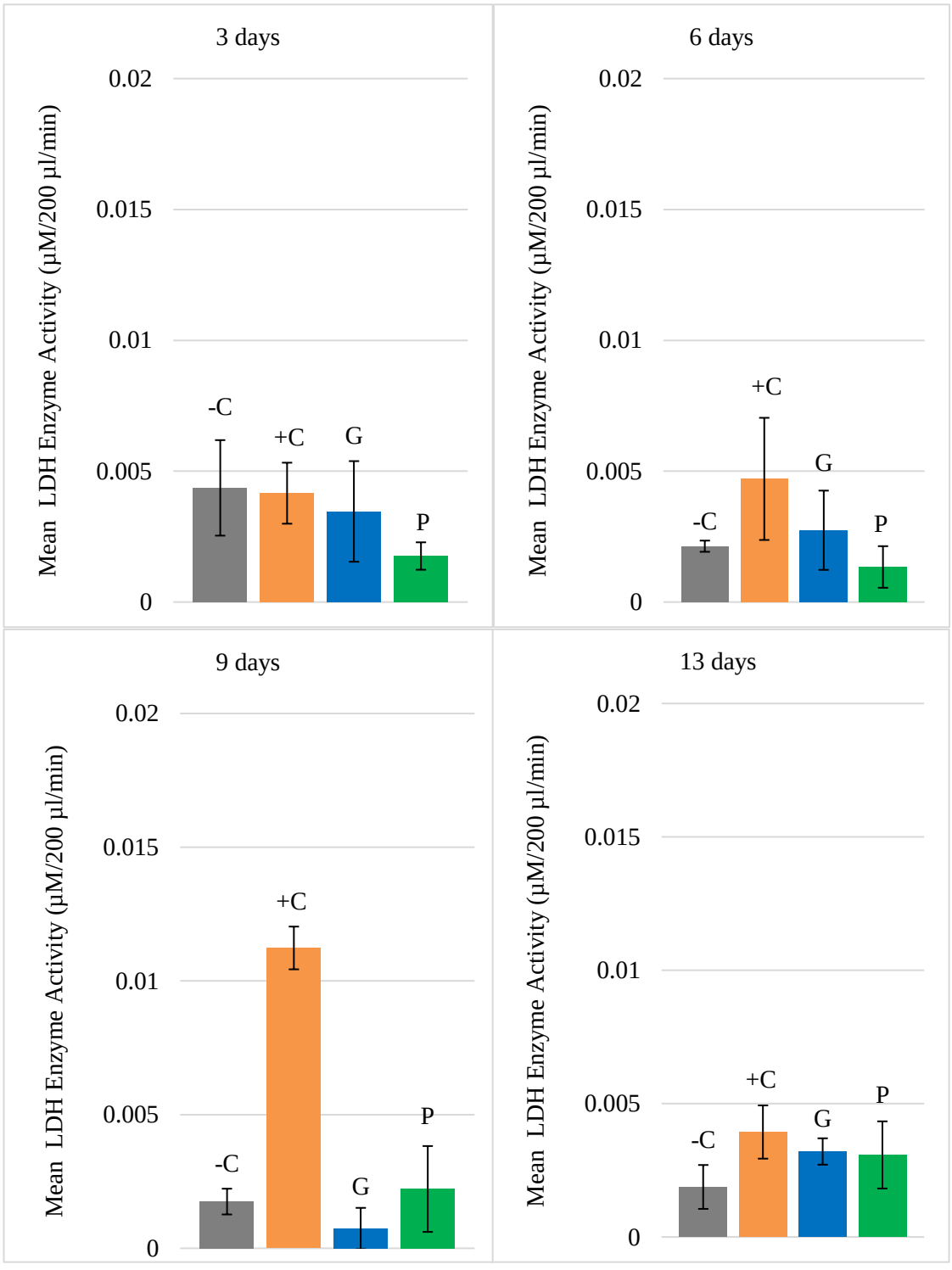

Figure 5-11: Bar chart showing levels of LDH enzyme excreted by porcine ECs grown on PPy/Sa coated wire samples and +ve/-ve controls at 3 day, 6 day, 9 day and 13 day time point. Negative control (cells only), positive control (cells + TritonX-100). Seeding density 2 x 10^5 cells/cm^2, incubation period 13 days. Samples pre-treated with FBS. Samples incubated with cell suspension for 24 hour before removing into fresh well for remainder of incubation period. Control wells not pre-treated. All values are mean values calculated from n=3. Error bars are indicative of standard deviation (SD). -C indicates negative control, +C indicates positive control, G indicates Galvanostatic samples, P indicates Potentiostatic samples.

5.5. Discussion

The biocompatibility of PPy in various forms has been studied in the literature, with outcomes proving promising (Wang et al., 2004, Stewart et al., 2012, Garner et al., 1999). Despite the availability of these studies, there is no existing study that has investigated the biocompatibility of PPy/Sa coatings on SS wires, for the potential use in DES coatings. Polypyrrole has been investigated as a DES coating in a limited number of studies to date (Okner et al., 2007, Arbizzani et al., 2007). The aim of this study was to assess biocompatibility of PPy/Sa coated SS (316L) wires. The viability of porcine ECs on the samples surface were analysed by LDH assay and live/dead staining.

5.5.1. Investigation of EC Growth on PPy/Sa Coated Wires

The initial seeding density used in this study (1×10^5 cells/cm^2) was based on other studies within the department that used the same cell type (porcine ECs) on similar surfaces (Holland, 2016) and the literature (Prasad et al., 2005). Little growth was observed on the coated wire samples, similar to the findings in Chapter 3 regarding EC growth on BMS. The slow growth on the PPy surfaces observed in the present study may be due to the seeding density being too low, as discussed in chapter 3.

5.5.1.1. Increased Seeding Density

As this was still the preliminary stages of the experimental study, samples were only visually inspected by live/dead staining and not formally quantified. It was found that increasing the cell density from $1 \times 10^5 – 2 \times 10^5$ cells/cm^2 and maintaining all other experimental conditions, resulted in increased cell growth within the well. Light microscopy revealed cells reaching confluency on the base of the well and live/dead staining confirmed cells (both live and dead) were present around the edges of the samples following staining. The presence of the cells only around the edges of the samples indicate that the cells preferentially form on the base of the well as opposed to the samples surface. It appears that once formed on the base of the well, they then begin to form over the samples surface. This may be expected as the surface of these wells are composed of tissue culture plastic that has been designed to encourage cell adhesion.

This finding also indicates that the release of Sa from the PPy/Sa coatings does not inhibit endothelial cell growth within the well. This is interesting as Sa has been shown to inhibit the growth of smooth muscle cells (Marra et al., 2000).

LDH assay results at the 6-day time point (cell density 2 x 10^5 cells/cm^2, 6 days incubation period) show cells present in the wells containing galvanostatic samples to excrete larger levels of LDH than cells present in the wells containing the potentiostatic samples. This would suggest that cells in contact with the galvanostatic samples are under more stress and subsequently undergo necrosis, excreting LDH. However, this difference is not significant and therefore definite conclusions cannot be made. LDH levels excreted from both sample types are below the levels from the positive control, indicating that not all cells have undergone cell death following the 6-day incubation period.

5.5.1.2. Increased Incubation Period

Increasing the cell density from 1 x 10^5 – 2 x 10^5 cells/cm^2 did increase the growth of cells onto the sample edges but they did not fully cover the sample surfaces. One of the factors contributing towards the lack of cells on the samples surface is that the incubation time may have been too short, not allowing the cells adequate time to fully proliferate and thus cover the surface. In terms of the stent restenosis timeline (Inoue et al., 2011), proliferation occurs in the first 30 days following stent implantation with cellular events ongoing for subsequent months. This is a much longer period that the initial experiment of 6 days.

The experiment in the present study was performed in a 96 well plate which is a very confined environment for cells to grow over a long period. Cells require adequate space to be able to undergo gas exchange, adequate nutrients to proliferate and media that is not saturated with waste product. It is for these reasons that it is difficult to perform an experiment under these conditions for a prolonged period of time.

With this in mind, the incubation time was increased until cells were completely confluent on the surrounding base of the well when analysed by light microscopy. At the increased incubation time of 13 days (see Figure 5-8), the live/dead images show cells present on both sample types. These cells were formally quantified, showing similar mean total number of cells on both sample types.

5.5.2. Effect of Salicylate Release on the Behaviour of ECs

In the study discussed in section 5.5.1.2, the LDH analyses shows the cells in contact with the potentiostatic samples to excrete larger levels of LDH enzyme at the 13-day time point. At the 6 day and 9-day time points, it is also the cells in contact with the potentiostatic samples that excreted increased levels of LDH. This is in contrast to the experiment performed over 6 days which found samples in contact with the galvanostatic samples to excrete increased levels of LDH.

At the 3-day time point, the LDH levels associated with both sample types are very similar. The behaviour of cells in contact with the two surface types may have been influenced by the mass of Sa released from the samples. According to previous analysis presented in chapter 4, the mass of Sa eluted from the galvanostatic samples by 3 days is 11.9 ± 0.74 µg and the mass of Sa eluted from the potentiostatic samples is 13.84 ± 5.05 µg. There is no significant difference between these two values, suggesting minimal effect on cell behaviour.

Nevertheless, the rate of release of Sa over the 3-day period is different for the two sample types. More than 97 % of the Sa is eluted from the galvanostatic samples within the 3-day period whereas 100 % of the Sa is eluted from the potentiostatic samples within a shorter time frame of 24 hours. This suggests that that there is very little release of Sa from the galvanostatic samples and no Sa release from the potentiostatic samples following the 3-day time point. When the release media is changed at day 3, nearly all of the Sa that has been released from the samples will be removed from the reaction. Therefore, differences noted between the two samples following the 3-day time point is unlikely to be a result of the presence of Sa.

Sa is reported to have an effect on the behaviour of SMCs. A study by Marra et al analysed the effect Sa had on human saphenous vein smooth muscle cells *in vitro* (Marra et al., 2000). The study found that at a salicylate concentration of 138.121 µg/ml added to the incubation media, reduced the proliferation of SMCs. In the present study, a salicylate concentration of ~2.8µg/200µl a value much smaller than that reported in the literature. This is in comparison to the control in the absence of Sa that the cells grew as normal. The study by (Marra et al., 2000) suggests that salicylate does have an antiproliferative effect on SMCs. Growth of porcine SMCs has been previously reported in the department with similar coatings (Reay,

2012) . It may therefore be beneficial to attempt the growth of porcine SMCs on the PPy/Sa coated wires to identify if the Sa release would inhibit the growth of SMCs in future work.

5.5.2.1. Effect of Pre-treatment of Samples with FBS on EC Growth

By pre-treating the sample surfaces with Foetal Bovine Serum (FBS) prior to incubation with cells, the chemistry of the surface becomes altered. Foetal bovine serum contains fibronectin which becomes adsorbed onto the sample surface. This strategy has been reported in the literature to improve adhesion of cells (Fan and Karino, 2008) and has previously been used in the department to improve EC and SMC adhesion to PPy planar surfaces (Reay, 2012).

In the present study, samples underwent pre-treatment with FBS for a period of 1 hour in an attempt to further encourage the proliferation of ECs onto the sample surfaces. An increased total mean number of cells was observed on both sample surfaces; however, this increase was not found to be significant. Protein adsorption happens almost immediately (minutes – hours) following implantation of a biomaterial *in vivo* (Thevenot et al., 2008*)*, therefore it is expected that incubation of the sample with FBS for 1 hour is sufficient time for adsorption of the proteins onto the sample surface. As previously stated, the adsorption of proteins is dependent on many factors. In this case, the polymer: protein interaction influences the rate at which proteins are adsorbed onto the sample surface and subsequently, increased treatment with FBS may be advantageous.

LDH assay analysis at the 13-day time point showed little difference between the two sample types (galvanostatic/ potentiostatic), with similar LDH levels excreted in both cases. These results also demonstrate little difference between these samples and the samples without the pre-treatment with FBS. Despite this, the live/dead staining did qualitatively show a difference between the cell coverage on the samples (pre-treatment/ no pre-treatment) with increased cell coverage observed on the pre-treated samples. The lack of statistical significance may have been contributed to by the low n number, making it difficult to quantify this difference.

5.5.2.2. Removal of Sample to Fresh Well Post Cell Seeding

To ascertain the viability of cells directly on the sample surface as opposed to the inclusion of the cells on the base of the well, samples were removed from their wells following cell suspension. Initially, based on the study by (Prasad et al., 2005), cells were seeded and the samples removed following 1 hour of incubation. It was found that this was not adequate time for the cells to attach to the sample surface with very few cells found on the surface when identified by live/dead staining at the 13-day timepoint.

By increasing the incubation period with the cells to 24 hours and with the additional pre-treatment of FBS, cells were found to have fully covered the surface (see Figure 5-6). There is a difference between the mean total number of cells present on both sample surfaces, with a larger mean total number of cells on the potentiostatic samples. This is the largest difference observed between the two sample types from all of the experimental outcomes in this study but it is still not found to be statistically significant. As previously mentioned, the lack of statistical significance maybe owed to the low n number which is ultimately a function of the high variability in the data.

The standard deviation of the mean total number of cells is very high for all experiments performed in this study. This demonstrates the difference in cell growth throughout the surface of each individual sample. This was visually evident from the live/dead staining images which showed random areas of the surface to have minimal cell coverage. The reason for this may have been the technique of pipetting cell suspension into each well, with cells not being distributed evenly throughout the sample surface. Another reason may be that cells with minimal coverage were actually previously dense with cells. These cells may have undergone cell death and become detached from the surface. Another possible explanation is that the cells required further time to fully proliferate the surface.

It is important to note that the surface variation of the PPy/Sa coatings may have influenced the cell growth. Surface analysis was performed on PPy/Sa coatings and the results discussed in chapter 4. SEM analysis showed that the PPy/Sa surfaces were patchy in some samples which could result in different rates of Sa release throughout the whole coating. Variation was also noted in R_{RMS} roughness values and this will be further discussed in the following section.

5.5.2.3. Effect of Surface Roughness on Behaviour of ECs

According to the literature, a difference in surface roughness of $10^1 – 10^2$ nm does have an effect on the growth and proliferation of HUVECs (Chung et al., 2003). HUVECS had a more pronounced adhesion/proliferation on surfaces with larger roughness (39.79 ± 10.48 nm/34.58 ± 9.89 nm) compared to surfaces of a lower roughness (20.10 ± 7.87 nm/ 18.63 ± 5.30 nm). The difference in surface roughness is at the nanometre scale which is relevant to the present study. This study by Chung et al suggests that endothelial cells will have improved adhesion and proliferation on surfaces of larger surface roughness. This would suggest that we would have observed improved cell adhesion/proliferation on PPy/Sa coatings produced by the potentiostatic method (R_{RMS} = 129.49 ± 77.49 nm) compared to the coatings produced by the galvanostatic method (R_{RMS} = 50.69 ± 19.92 nm). Although no significant differences have been found between the behaviour of cells on the two different surface types in the present study, there have been general trends in data. When measured qualitatively by live/dead staining there has been a larger mean total number of cells on the potentiostatic samples in some studies and where the galvanostatic samples have a larger mean number of cells, the difference has been very small (<5 cells). This would agree with the hypothesis that surfaces with larger surface roughness improves EC growth.

The study by Chung et al used HUVECs in their experimental procedure, a different cell type to the porcine ECs used in the present study. As was discussed in chapter 1, different cell types respond differently to different surfaces (Miller et al., 2004, Chung et al., 2003, Xu et al., 2004). This is to say the porcine ECs may not grow at the same rate or respond in the same way to varied surface roughness. Additionally, the study by Chung et al had an incubation period of just 36 hours, compared to the 3 day – 13 day used in the present study.

The surface type is an important factor to consider when comparing the study by Chung et al to the present study. Different polymer surfaces were used in the two studies with the additional drug release in the present study. Different polymers not only possess different surface roughness but they also differ in surface chemistry. This is another aspect to consider which is beyond the scope of the present study.

A final aspect to take into consideration regarding the lack of observed difference between the growth of cells on the surfaces of different roughness is the low n number that was used in the

present study. By increasing the n number, a better impression of the cell growth on the different surfaces could be identified and the statistical analysis could be greatly improved.

5.5.3. Study Limitations and Future Work

With additional time, it may have been possible to alter experimental design to achieve results over a prolonged period. The limitations within this chapter, somewhat mimic the limitations experienced in Chapter 3 whereby the cell culture studies were performed by EC growth on BMS. This includes the opportunity to repeat the cell culture study with the removal of the sample but without the initial sample pre-treatment in FBS. This would confirm the true effect of the surfaces of the two PPy/Sa coatings. As has been mentioned throughout this chapter, sample number could be increased for each experiment and cells quantified at each time point. Additionally, the experimental setup used in the present study could include a perfusion chamber to take into account the effect of flow with regards to blood flow, to make the experiment more relevant for use in DES.

Finally, the effect of Sa directly onto ECs could be further examined to ascertain the true effect it has on EC growth. This would also further investigate the effect of the surface topography of the PPy/Sa coatings, as any influence of Sa release would be better understood.

5.5.4. Summary and Conclusions

In this chapter, the adhesion of porcine ECs onto PPy/Sa coated wires was successfully analysed. There was no significant difference in cell viability on PPy/Sa surfaces with different Sa release profiles. There was also no significant difference in cell viability on PPy/Sa surfaces of different surface roughness, although general trends in data including improved growth of ECs on surfaces of larger roughness were observed.

Taking into consideration the lack of significant difference in the behaviour of ECs on these two surface types, and looking at the coating method and drug release profiles of the resultant coatings, it is fair to suggest that the galvanostatic coating would be more suitable as a stent coating. The galvanostatic coatings are produced in less than half the duration of the potentiostatic coating, in a process that does not require an additional reference electrode. This reduces the material cost and process duration, making the process more efficient for use in a manufacturing environment. By eliminating the bulky reference electrode, the size of the

beaker may be reduced, allowing for a smaller volume of electrolyte solution and further reducing the cost of production.

Chapter 6

6. An Investigation into the Antioxidative Properties of Polypyrrole/Salicylate Coated Wires

In the previous chapters it has been shown that electropolymerisation can be used to produce PPy coatings with similar surface roughness to a range of clinically approved coronary stents. We have also demonstrated that the release profile of salicylate, a drug with potentially therapeutic effects of relevance to the stent treatment, may be modified by selection of different coating durations and electropolymerisation methods. The biocompatibility of the PPy/Sa surface coatings generated in this work has been investigated, with promising results demonstrating that endothelial cells adhere to these surfaces. In the final part of this study, we will now go on to investigate a further aspect of these surface coatings that may provide a novel means of enhancing their performance for use as coronary stent coatings. This novel aspect relates to the potential of PPy coatings to act as anti-oxidant surfaces. The present chapter will therefore outline what is currently known about the association between oxidative stress and complications following coronary stenting. It will then discuss relevant research that has been undertaken to prevent the occurrence of oxidative stress in this instance. The specific aims surrounding the subjects of antioxidative agents will be outlined in section 6.2. Results will be presented in section 6.4 and an in-depth discussion surrounding the issues mentioned will conclude this chapter in section 6.5.

6.1. Background

6.1.1. Oxidative Stress

Oxidative stress can be defined as an imbalance between reactive oxygen species (ROS) and antioxidant defences, with the potential to cause cell damage (Schulze and Richard T. Lee, 2005). Some studies have reported a link between oxidative stress and altered endothelial and smooth muscle cell function following stent implantation. These changes have the potential to cause restenosis, thrombosis and impaired endothelial function in the stented artery (Juni et al., 2013).

It is thought that the implantation of a coronary stent leads to an increase in pathophysiological levels of vascular reactive oxygen species (ROS) such as superoxide anions ($O_2^{\cdot -}$)

(Kochiadakis et al., 2010). One of the implications of the presence of ROS within the vessel is that they scavenge nitric oxide (NO). Nitric oxide is an important compound that regulates vascular homeostasis and cellular signalling within the body (Schulze and Richard T. Lee, 2005). When the nitric oxide has been scavenged, there is reduced nitric oxide bioavailability, leading to the impairment of endothelium-mediated vasorelaxation and a procoagulant state.

The presence of ROS within a vessel can also modify proteins, nucleotides and lead to pro-inflammatory signalling which can further produce ROS. This can lead to altered endothelial cell function and the development of stent thrombosis (Juni et al., 2013). This has resulted in research surrounding the area of re-balancing NO levels, including the investigation of nitric-oxide donor coated stents, and anti-oxidative agents administered both locally and orally (Nunes et al., 2006, Watt et al., 2013).

6.1.1.1. Occurrence of Oxidative Stress Associated with BMS and DES

Many DES contain antiproliferative agents that have the ability to inhibit SMC proliferation and migration post stent implantation. However, the presence of these drugs can, in fact, be the cause of ROS production in the stented vessel. There are a number of studies in the literature, which have examined differences in the occurrence of oxidative stress associated with the implantation of a BMS or a DES (Kochiadakis et al., 2010, Pendyala et al., 2009). These studies could establish whether a change in material or drug component could have an effect, or indeed reduce the occurrence of oxidative stress following stent implantation and these findings will be discussed in this section.

A comparative study with human subjects was undertaken by (Kochiadakis et al., 2010), whereby half of the patients were implanted with a BMS and half with a Sirolimus Eluting Stent (SES). A sample of each patient's blood was taken at various time points 24 hours pre-stent implantation and post-stent implantation (24 hr, 48 hr and 1 month). The total peroxides (TP) concentration was measured from each blood sample as a measure of oxidative stress. The results showed that the levels of TP present in the patients' blood who were implanted with the BMS were significantly higher at the 24 hr and 48 hr time points post-stent implantation than pre-stent implantation. These concentrations decreased following the 48 hr time point to a value slightly higher than before stent implantation. In comparison, those with a SES had no significant change in TP concentration in the first 48 hr and in fact, a decrease

to below the original value was observed following 1 month. Late lumen loss was also analysed at the 6 month follow up, and was shown to positively correlate with levels of oxidative stress.

This finding not only suggests a decreased occurrence of oxidative stress through the use of a sirolimus eluting stent compared to a BMS, but also displays how oxidative stress can change over the course of the first month following stent implantation. This reinforces the importance immediately post stent implantation and the events that lead to intimal hyperplasia and restenosis (Kochiadakis et al., 2010). It also supports the use of sirolimus, an immunosuppressive drug as a component for DES and may help reveal a further potentially beneficial action of this compound beyond its well established anti-proliferative effects.

Another commonly used anti-proliferative drug that has been widely used in DES is paclitaxel. As previously discussed in chapter 1, this drug has a different mode of function to immunosuppressive drugs like Sirolimus. A study by (Pendyala et al., 2009) deployed either a Paclitaxel-Eluting Stent (PES) or control BMS into the coronary artery of pigs and measured levels of superoxide anions ($O_2^{\cdot-}$) in the stented arterial tissue, neointimal thickness and endothelial vasomotor function over a period of 1 month. It found that the paclitaxel-eluting stent produced lower neointimal formation, but increased levels of superoxide anions ($O_2^{\cdot-}$). The group with the implanted PES also experienced impaired endothelial vasomotor function which is thought to have been caused by high levels of superoxide anions. It is therefore suggested that the presence of paclitaxel in the DES increases the occurrence of oxidative stress.

It is important to note that these two studies cannot be directly compared, as the study by Kochiadakis et al used human subjects whereas the study by Pendyala et al was performed on pig subjects. Occurrence of oxidative stress was also characterised by different methods; total peroxide concentration was measured in the study by Kochiadakis et al and superoxide anions, vasomotor function and neointimal thickness was measured in the study by Pendyala et al. Despite these limitations, it is clear that the implantation of a stent leads to the occurrence of oxidative stress. From the studies by Kochiadakis and Pendyala, it has been highlighted that the drug component of DES is likely to influence the occurrence of oxidative stress post stent implantation. With further *in vitro* and *in vivo* studies, it may be possible to confirm the most suitable drug to reduce oxidative stress without negatively impacting on endothelial function.

6.1.2. Antioxidative Agents in Coronary Stents

Given the potentially damaging effects of oxidative stress following coronary stenting, it has been suggested that an 'anti-oxidant stent' may be advantageous (Watt et al., 2008). Such a stent would have the potential to scavenge free radicals generated following stent implantation, thereby reducing the negative effects following stent implantation. One way to incorporate antioxidative activity would be the presence of an antioxidative agent on a coronary stent. This has been investigated in a number of studies, which will be discussed below. Although some of these investigations have produced very promising results, others have not and the clinical impact of such strategies has ultimately been limited to date.

6.1.2.1. Oral Administration of Antioxidative Agents

Probucol and Succinobucol

The simplest way to provide protection against oxidative stress following stenting was thought to be through oral administration of anti-oxidant agents. A number of clinical trials have been undertaken in this area, in patients who have undergone stent implantation. One study by (Nunes et al., 2006), administered probucol to patients alongside the implantation of a BMS. Probucol is an antioxidant drug that is capable of limiting the production of oxygen free radicals and also scavenge superoxide anions. It has previously been shown to reduce restenosis by inhibiting SMC proliferation following balloon angioplasty, making it a potential agent to reduce in-stent restenosis. The main conclusion from this study was that the presence of probucol in the body did not have a significant effect on neointimal formation post stent implantation. The study by (Sekiya et al., 1998) reported similar findings, deeming probucol ineffective in reducing restenosis when administered on its own. This studied the combined therapy of probucol with cilostazol, with more promising results, but more recently probucol has been removed from clinical use due to negative side effects including reduced HDL levels and prolonged QT intervals (Yamamoto, 2008).

A derivative of probucol, succinobucol, has also been administered orally following stent implantation, (Jean-Claude Tardif et al., 2003). This clinical trial (CART-1) found that patients that had been administered either probucol or succinobucol whilst undergoing PCI, experienced reduced restenosis rates. Furthermore, succinobucol did not cause the same

negative side effects experienced through the use of probucol. Despite this promising finding, succinobucol has not yet found use as a drug therapy following coronary stenting.

6.1.2.2. Antioxidative Coating on Coronary Stents

One issue with the oral delivery of antioxidant molecules is that many antioxidants possess poor biopharmaceutical properties and have variable pharmacokinetics. These include low aqueous solubility and instability in the gastrointestinal tract and are expanded upon in the study by (Jain et al., 2015). An alternative strategy to systemic administration of anti-oxidant drugs is local delivery from the stent surface. With site specific delivery, it may be possible to increase the bioavailability of the antioxidant, improving the therapeutic effect. Additionally, oral administration of the drug can take place 2 weeks prior to the PCI procedure and 4 weeks following the procedure, but systemic delivery occurs once the stent is implanted (Kim et al., 2005). Therefore, systemic delivery of the antioxidant would eliminate the need for additional treatment for the patient. It is important to note that despite certain drugs having a positive effect when administered orally, that does not imply that they will have the same effect when administered locally into the target site.

An example of this is the study by (Watt et al., 2013), which compared the effects of a succinobucol-eluting stent to a combination stent (succinobucol-sirolimus) and a bare metal control in the pig coronary artery model. It was found that the succinobucol eluting stent had an increased effect on neointimal formation and produced an increased inflammatory response. This is in contrast to the findings in the study by (Jean-Claude Tardif et al., 2003) whereby the oral administration of succinobucol whilst undergoing PCI was reported to reduce restenosis rates.

A study by (Kim et al., 2005) analysed the difference in effect of a probucol eluting coronary stent vs a carvedilol eluting stent and a bare metal control. It found the probucol eluting stent to have no effect on the rate of restenosis, a different result to when it was delivered orally in the study by (Jean-Claude Tardif et al., 2003). There are many reasons for this which have been suggested by the author, including dosage, rate of release, and the variability of how restenosis was measured between studies.

β-adrenergic Receptor Blockers

Carvedilol is a third generation β-adrenergic receptor blocker with antioxidative properties thought to be superior to probucol and vitamin E. The study by (Kim et al., 2005) analysed the

difference in effect of a probucol eluting coronary stent vs a carvedilol eluting stent. The study was performed by the implantation of the stents into pig coronary arteries. Findings from this study confirmed that the stents loaded with carvedilol reduced neointimal hyperplasia but the stents loaded with probucol did not have the same effect. This finding was reiterated in a small study on human subjects that were implanted with either a BMS or a carvedilol eluting stent (Kim et al., 2011). At the 2 year follow up it was concluded that the carvedilol eluting stent reduced the occurrence of neointimal hyperplasia. The anti-oxidant drugs discussed in the previous sections are a selection of the wider range of approaches to anti-oxidative activity which are summarised in the article by (Watt et al., 2008).

Thus far various approaches to the local delivery of antioxidants to inhibit oxidative stress have been discussed but ultimately no clinical impact has been achieved. Research is on-going in this subject and the research presented in this study will contribute towards this.

6.1.2.3. Antioxidative Properties of Conducting Polymer Coatings

One of the main developments in the present study is the use of a conducting polymer, specifically PPy, in a novel DES coating. In addition to the advantages of conducting polymers already mentioned in previous chapters, it has also been reported that some of these polymers including PANI and PPy possess antioxidative properties (Gizdavic-Nikolaidis et al., 2004b, Hsu et al., 2010). Given the potentially beneficial effect of anti-oxidants highlighted above, this may be a particularly attractive aspect of PPy as a stent coating.

The ability of PPy to act as a free radical scavenger and provide subsequent antioxidative activity has been proven by several studies in the literature (Ebrahimiasl et al., 2014, Hsu et al., 2008). The study by Ebrahimiasl et al analysed the antioxidative activity of PPy films deposited onto indium tin oxide glass substrate and a separate study by Hsu et al investigated the antioxidative potential of PPy powders. Both forms of the materials, film and powder, were found to display antioxidative properties. Both studies were performed by the reaction with the stable free radical di (phenyl)-(2, 4, 6-trinitrophenyl) iminoazanium (DPPH). These studies were focused on the potential of PPy for use in food packaging and both forms of PPy were formed by chemical and electrochemical synthesis. There are no studies in the literature which have specifically investigated the antioxidative properties of PPy coated onto metal

substrates through the use of electropolymerisation. As a result, the beneficial effect of such a potentially anti-oxidant within the context of stent coatings has therefore not been explored.

6.2. Aims and Objectives

Sections 6.1.1-6.1.2.2 provided background information regarding the occurrence of oxidative stress following stent implantation and how this could be minimised through new pharmacological approaches and technologies. The antioxidative properties of PPy were introduced in section 6.1.2.3, showing it to possess antioxidative properties in many forms (Ebrahimiasl et al., 2014, Hsu et al., 2008). It was found that this has not been investigated for use in coronary stents to specifically target the negative implications associated with the occurrence of oxidative stress following stent implantation. It is therefore our first aim of this study to investigate the antioxidative activity of a novel polypyrrole/salicylate (PPy/Sa) coating for potential use as a coronary stent coating. This aim has been broken down to the main objectives below.

1) Investigate if the PPy/Sa coating possesses anti-oxidant activity
2) Analyse the duration of the antioxidative activity of the PPy/Sa coating.
3) Analyse the effect of Sa release on the antioxidative activity of the PPy/Sa coating.
4) Determine which component of the PPy/Sa coating possesses antioxidative properties.

6.3. Materials and Methods

6.3.1. Antioxidative Activity Measurements

Antioxidative activity is commonly quantified by using a DPPH assay (Gizdavic-Nikolaidis et al., 2004b, Garcia et al., 2012). In the present study, the DPPH assay method was utilised to analyse the antioxidative activity of PPy/Sa coated wire samples and the principles of operation of this method will be discussed below.

6.3.1.1. DPPH Assay

The main principle of the DPPH assay is that the stable 2,2-diphenyl-1-picrylhydrazyl (DPPH) radical reacts with an antioxidant molecule and undergoes reduction. The initial DPPH molecule, containing an odd electron on the nitrogen atom gives a strong absorption maximum at 517 nm, corresponding to a purple colour. Once the reaction with an antioxidant takes place, this odd electron becomes paired with a hydrogen atom from the antioxidative agent to form DPPH in its reduced form (DPPH-H), corresponding to a yellow colour. The change in colour is stoichiometric, corresponding to the number of electrons that have been captured (Prakash et al.) (see Figure 6-1 for chemical equation). Therefore, a larger decrease in absorbance is indicative of larger antioxidative activity exhibited by the sample. Percentage antioxidative activity is a common way of expressing the antioxidative effect of a material and is generally calculated by equation 6-1.

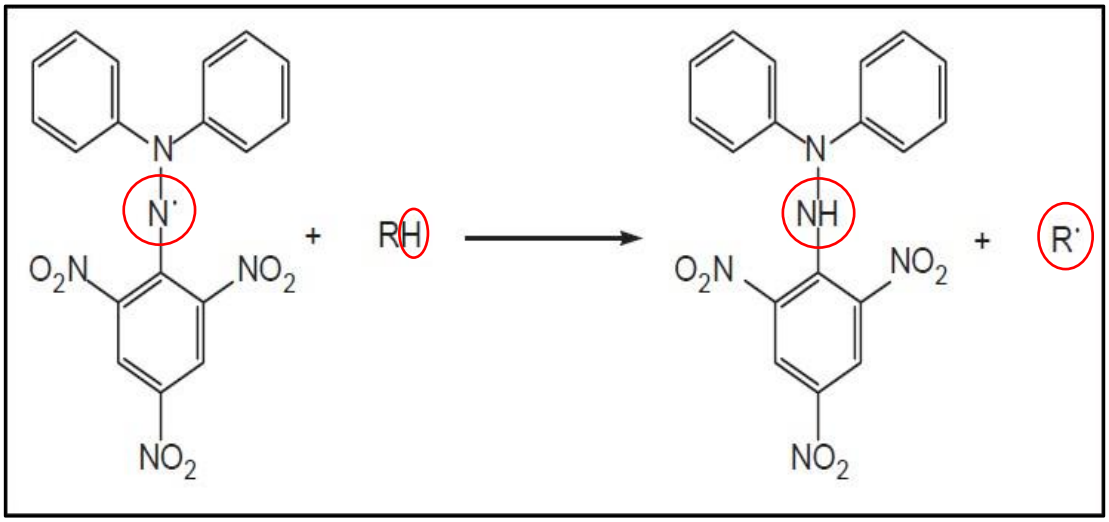

Figure 6-1: Chemical equation showing reaction of DPPH radical with antioxidant molecule. Atoms involved in reaction labelled with red circle. Image annotated (Gizdavic-Nikolaidis et al., 2004a).

$$\boldsymbol{AA\% = 100 - \left[\frac{(Abs_{sample} - Abs_{blank})x\ 100}{Abs_{control}}\right]}$$

Equation 6-1: Equation of percentage antioxidant activity (AA%) from the literature (>>) where Abs_{sample} = Peak absorbance of sample, Absblank = peak absorbance blank (EtOH), Abscontrol = Peak absorbance of control (DPPH/EtOH 158.5 µM.

6.3.1.2. Materials and Equipment

DPPH (2,2-diphenyl-1-picrylhydrazyl), Probucol and Ethanol (absolute) were purchased from Sigma Aldrich, UK. Eppendorf tubes (1.5 ml) were used for reaction solutions.

A UV spectrophotometer (UV 2401 PC, Shimadzu Coorporation) was used to analyse the absorbance of DPPH radicals in all samples.

6.3.1.3. Experimental Procedure

The experimental method used in this study is based on the study by (Ebrahimiasl et al., 2014). A stock solution of DPPH/EtOH with a DPPH concentration of 634 µM was prepared by dissolving DPPH (25 mg) in EtOH (100 ml) which was wrapped in aluminium foil between

uses to minimise exposure to light. Eppendorf tubes (1.5 ml) were also individually wrapped in aluminium foil. The sample to be tested (750 µl) or the EtOH control (750 µl) was pipetted into an Eppendorf tube with the DPPH/EtOH stock solution (250 µl, 634 µM), providing a 1 ml reaction solution with a DPPH concentration of 158.5 µM. The tube containing the reaction media was vortexed for 30 seconds and left in a dark drawer at room temperature and analysed at various time points (90 min, 5 hr, 24 hr). Each tube containing the sample/DPPH solution was prepared individually every 3 minutes to ensure each sample had the same incubation period prior to UV analysis. Each sample was analysed by UV-spectroscopy at a wavelength of 517 nm. The UV absorbance measurements were repeated three consecutive times for each sample.

The samples analysed in this experiment were as follows: SS wire, PPy/Sa coated SS wire (produced under potentiostatic conditions, 0.9 V, 25 min, 0.1 M Py 0.1M NaSa, 0-4˚C, as detailed in chapter 4), PPy/Sa coated SS wire release medium (various time points), NaSa/EtOH solution (0.0235 – 0.01 mM), Probucol/EtOH (positive control), DPPH/EtOH (negative control).

Probucol has previously demonstrated anti-oxidant activity (Santosa et al., 2016), and was therefore used as a positive control. A calibration curve (0.01 mM - 1 mM) from 1 mM stock solution (Probucol (25.8 mg)/EtOH (50 ml)) was prepared and analysed by the same method described above. Percentage antioxidative activity was calculated using equation 6-1 for each sample.

6.3.2. High Performance Liquid Chromatography (HPLC)

High Performance Liquid Chromatography (HPLC) was used in this study to separate compounds with similar peak wavelengths that could not be reliably measured using standard UV-Spectrophotometry.

6.3.2.1. Principles of Operation

High Performance Liquid Chromatography (HPLC) is an enhanced form of column chromatography whereby the solvent (mobile phase) is forced through the column at high pressure. The mixture of interest is passed through a column (stationary phase) containing

particles, which are of a smaller particle size than traditional chromatography, thereby increasing the surface area and allowing improved interaction between the stationary phase and the compounds within the mixture. The mixture is passed through the column where the components within the mixture are separated. These compounds then reach the detector where they are identified and quantified. The detector is often fluorescence, acting as in spectrofluorometry, or UV light, acting as in spectrophotometry. In the present study spectrophotometry was used as the mode of detection

There are two types of HPLC; normal phase and reverse phase. In normal phase HPLC, the column is composed of silica and the solvent is non-polar, for example hexane. This allows for non-polar compounds to pass through the column quicker than the polar compounds as the polar compounds will 'stick' to the polar silica molecules within the column. In reverse phase HPLC, the stationary phase is silica with attached hydrocarbons (e.g/. C_8, C_{18}), changing the silica to be non-polar and the mobile phase is polar (e.g/.MeOH,H_2O). This setup allows the polar compounds to pass through the column quicker than the non-polar compounds, with less attraction between the stationary phase and the polar compounds. Reverse phase HPLC was used in the present study.

The retention time (t_R) is a measure of the time taken for an individual compound to travel through the column and reach the detector. It is dependent on pressure, stationary phase, mobile phase and temperature. Therefore, it is essential to keep these conditions consistent between measurements when using retention time to identify individual compounds.

The area under the peak or the height of the peak can be used as a measure of the amount of the compound that passes through the column and subsequently reaches the detector. Calibration is performed using a standard solution of known concentrations, providing a curve of Area (or Height) vs Concentration. From this curve, the mass of the compound present in subsequent samples can be calculated.

6.3.2.2. Materials and Equipment

Sodium Salicylate (NaSa), Ethanol (absolute), DPPH (2,2-diphenyl-1-picrylhydrazyl), Phosphoric acid (85 wt %) and Acetonitrile were all purchased from Sigma Aldrich, UK. The HPLC machine used in this study was a Dionex RX200 with UV analyser.

6.3.2.3. Experimental Procedure

The method used in this study was based on the study by (Toiu et al., 2011). The conditions used in this study are summarised in Table 6-1.

Table 6-1: Table of HPLC experimental conditions used in the present study, based on study by Toiu et al.

HPLC	Reverse phase
Detector	Spectrophotometry
Mobile Phase	25 % Acetonitrile (ACN), 75 % phosphoric acid (85 wt %)/ distilled water (0.1% v/v)
Stationary Phase	C18
Column	150 mm x 4.60 mm
Particle Size	5 µm
Flow Rate	1 ml/ min
Injection Volume	20 µl
Temperature	RT
Wavelength	296 nm

The mass of salicylate present in the sample solution was calculated from the peak present at wavelength 296 nm and retention time ~ 8 min. A curve of Height vs Concentration was prepared from the standard NaSa/EtOH solutions at various known concentrations. Using this curve, the mass of salicylate present in each solution was calculated.

6.4. Results

The results in this section were obtained by the method discussed in section 6.3.1.3 by means of a DPPH assay. UV-spectroscopy and HPLC analysis was performed in line with the method discussed in sections 4.3.2 and 6.3.2.3 and used to analyse salicylate release. The results will be shown in the following sections.

6.4.1. Antioxidative Properties of PPy/Sa Coated Wire Samples

6.4.1.1. Preliminary Study

Percentage antioxidant activity (AA%) is the measure of antioxidant activity within the test sample. When probucol/EtOH solutions were analysed, the average AA % values increased with increasing concentration of probucol in solution, ranging from 4.37 ± 1.56 to 39.30 ± 3.89 % at the 90 min time point (see Figure 6-2 graphical representation of percentage antioxidative activity vs concentration of probucol). This proved the ability of the DPPH assay to determine the AA % of probucol/EtOH solution in the range of 0.01 mM – 1 mM, and provided confidence in the suitability of the assay for determining antioxidative activity.

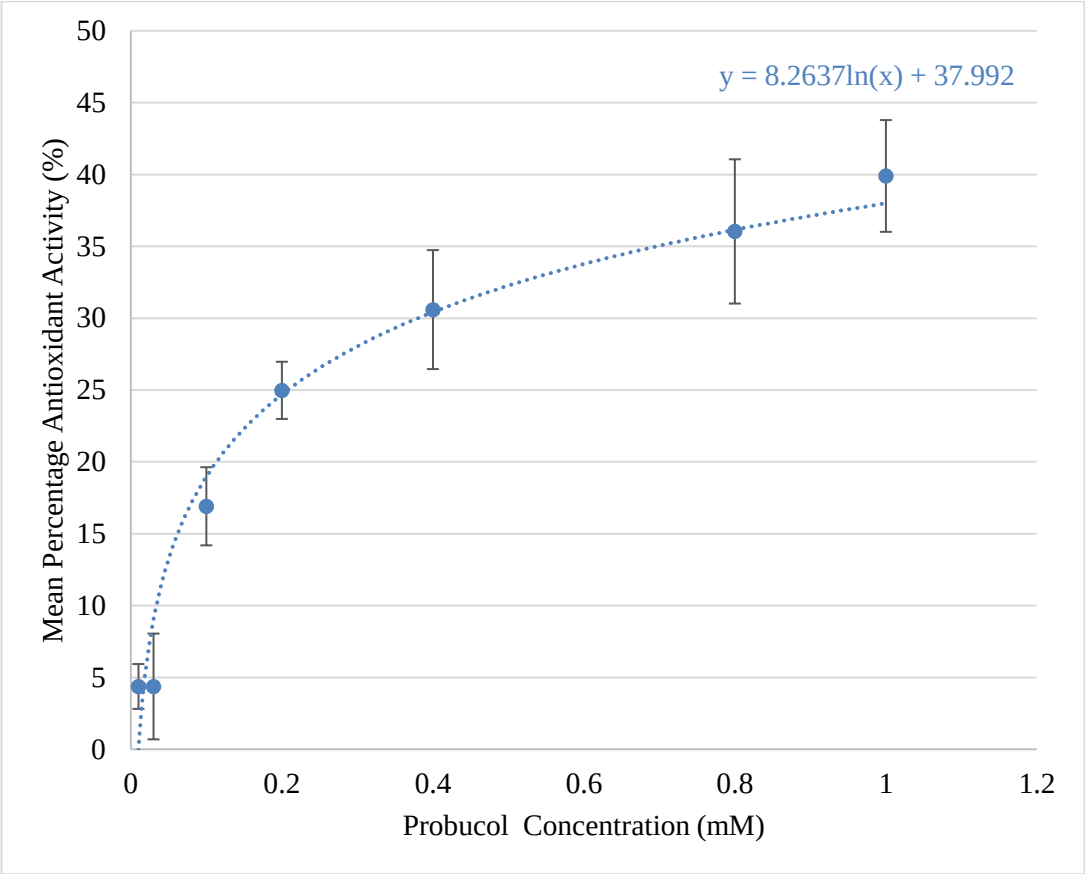

Figure 6-2: Graph of Percentage Antioxidant Activity Vs Concentration for Probucol/EtOH solutions of varied probucol concentrations (0.01 mM - 1 mM) at the 90 min time point. Error bars are indicative of standard deviation values, n=2. Trend line is logarithmic and the related equation is presented on graph.

Further results from this initial study suggest that the PPy/Sa coated wires possess antioxidative properties with an average AA% value of 11.98 ± 4.61 % at the 90 min time point. It was confirmed that the bare metal wire control exerted minimal antioxidant activity, with an average AA % value (90 min time point) of 0.00 ± 3.39 % being obtained.

It should be noted that in these preliminary studies, the results were gathered over a period of days using various solutions (DPPH/EtOH and probucol/EtOH) that were stored in the fridge before being brought to room temperature prior to each experiment. This may have had an impact on the results obtained. For this reason, and to ensure consistency in results from experiment to experiment, it was decided to repeat the experiment using fresh solutions for each set of experiments. Furthermore, as antioxidative activity was recognised at this initial timepoint, it was decided to include further timepoints to address whether antioxidative activity could be observed at extended timepoints.

6.4.1.2. Antioxidant Activity of PPy/Sa coatings

The study was repeated with freshly prepared PPy/Sa coated wires and at additional time points (90 min, 5 hr, 24 hr). Results were all obtained on the same day with freshly prepared solutions, thereby addressing a potential weakness within the preliminary study.

The findings from this study support the conclusion from the preliminary study that the PPy/Sa coated wire samples do possess antioxidative properties. The percentage antioxidant activity of the various samples is displayed in Figure 6-3. An average AA% value of 23.11 ± 5.71 % was observed for the PPy/Sa samples at the 90 min time point, a value greater than the preliminary study. This larger average AA % value of the PPy/Sa coated wires in this second study may be due to the varied current density reached when the sample coatings were produced between the two studies and will be further referred to in the following section. It was further found that the average AA % increased to 38.57 ± 5.91 % at the 5 hr time point and 71.13 ± 8.36 % following 24 hours incubation (see Figure 6-3 for graphical representation). These results suggest that the PPy/Sa samples continue to have an antioxidative effect up to the 24 hour time point.

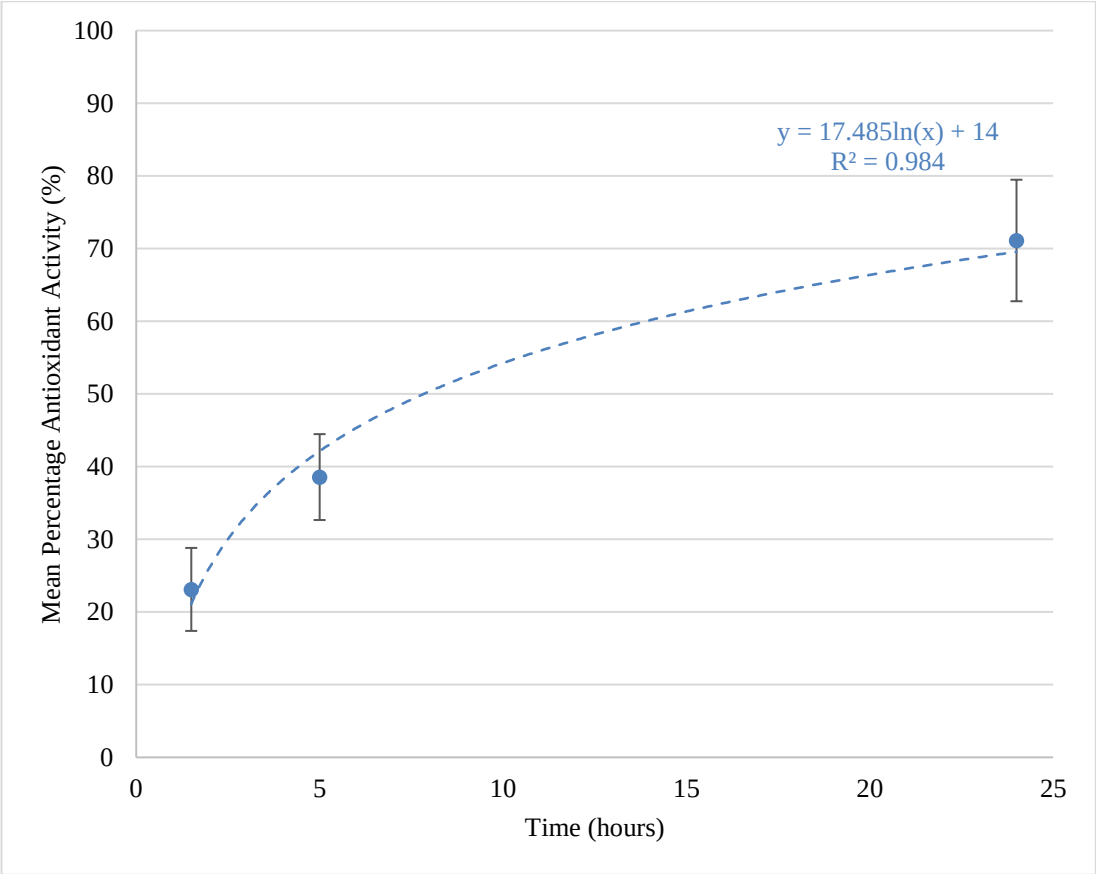

Figure 6-3: Graph of Mean Percentage Antioxidant Activity Vs Time for PPy/Sa coated wire samples (potentiostatic conditions, 0.9 V, 0.1 M Py 0.1 M NaSa, 25 min) at various timepoints (90 min, 5 hours, 24 hours). Error bars are indicative of standard deviation values, n=5. Equation on graph is from logarithmic trendline.

6.4.1.3. Increased Reaction Time

As antioxidative activity was still being exhibited at the 24 hour time, it was decided to further increase the reaction time to 48 hours. This would address whether the PPy/Sa coated wire samples were capable of producing an antioxidative effect at the extended time point. Additionally, to ensure accurate readings from the UV-spectrophotometer, each sample was scanned three consecutive times by the UV-spectrophotometer and an average taken.

The results from this second study support the findings from the initial studies that the PPy/Sa coated wire samples do possess antioxidative properties. The average AA% values of the various samples are displayed in Figure 6-4. An average AA% value of 9.73 ± 8.65 % was observed for the PPy/Sa samples at the 90 min time point. This increased to 28.22 ± 17.47 % at the 5 hour point and 55.82 ± 30.09 % following 24 hours.

Samples for 48 hour analysis could not be analysed due to sample loss at previous time points and possible evaporation. The remaining volume was not sufficient to be accurately measured by the UV-Spectrophotometer. For this reason, the results from the 48 hour time point were disregarded from this study.

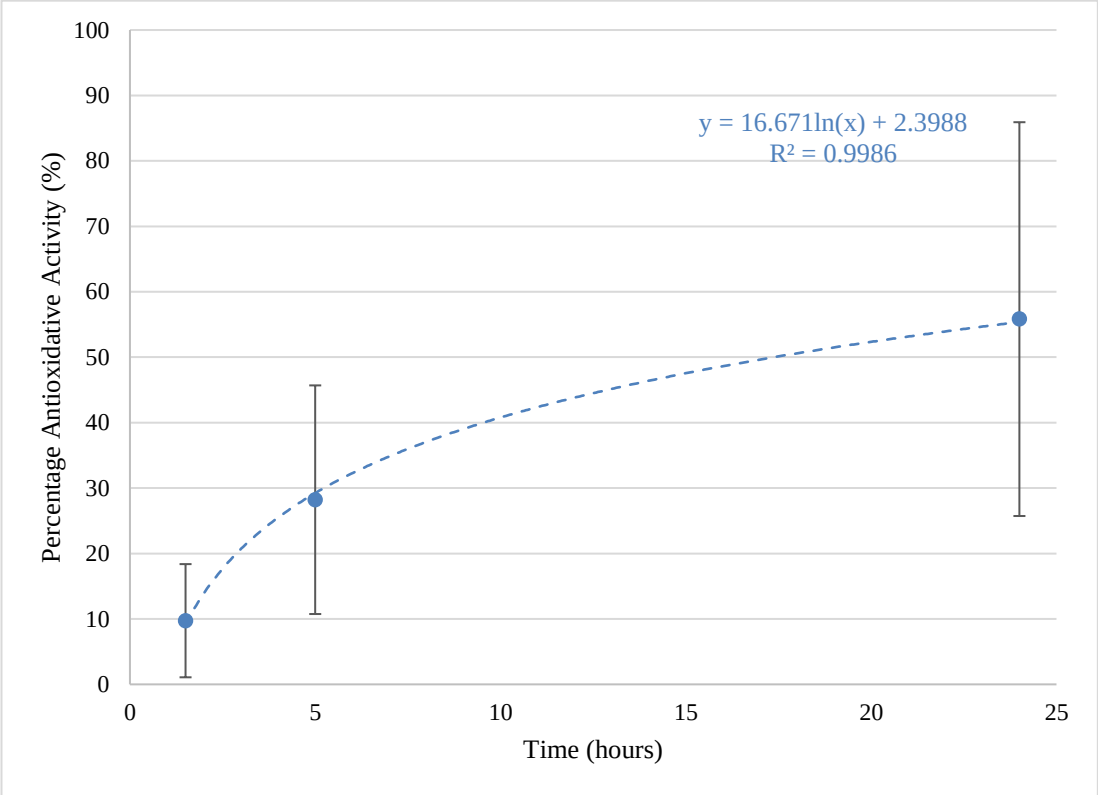

Figure 6-4: Graph of Mean Percentage Antioxidant Activity Vs Time for PPy/Sa coated wire samples (potentiostatic conditions, 0.9 V, 0.1 M Py 0.1 M NaSa, 25 min) at various timepoints (90 min, 5 hours, 24 hours). Error bars are indicative of standard deviation values, n=5. Equation on graph is from logarithmic trendline.

These values are lower than those calculated in the initial studies with the standard deviation values noted to be higher. This variation in values may have been contributed to by the varied charge density values reached during the production of the coatings. It was observed that the PPy/Sa coated wire samples that reached a smaller charge density on production, exhibited a smaller AA % overall. The relationship between charge density and AA % for samples used in sections 6.4.1.2 and 6.4.1.3 is displayed in Figure 6-5. From this graph, it is apparent that there is a rapid increase in percentage antioxidative activity from around 10 % - 70 %, when the charge density is increased from around 0.1 – 0.3 C/cm^2. For values of charge density larger than 0.3 C/cm^2 to around 1.12 C/cm^2 the increase in percentage antioxidative activity is smaller, increasing from around 70 % to 90%. This relationship will be further discussed in section 6.4.

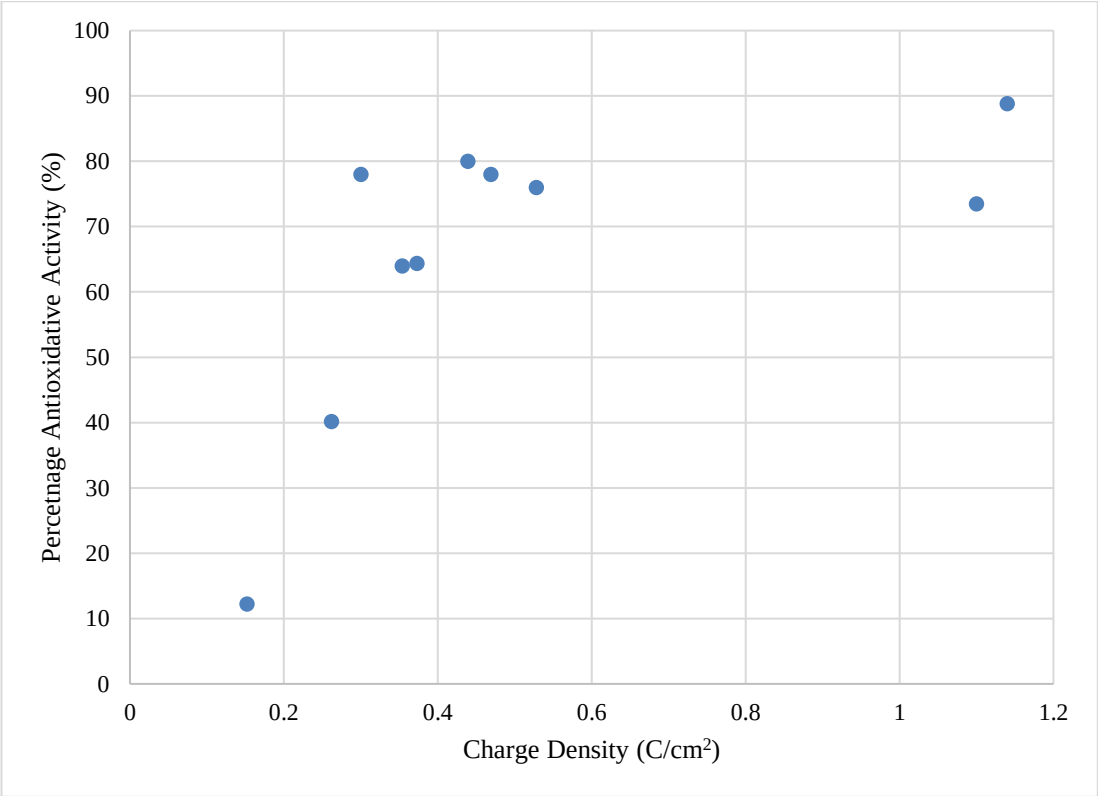

Figure 6-5: Graph of percentage antioxidant activity vs charge density of PPy/Sa coated wire samples (potentiostatic conditions, 0.9 V, 0.1 M Py 0.1 M NaSa, 25 min). AA % shown to increase with increasing charge density. AA% values taken from 24 hour time point.

6.4.1.4. Effect of Sa release on Antioxidative Activity

The next step in this study was to identify which component of the coating is responsible for the antioxidative effect. The reason for this experiment was to analyse whether it is due to the dopant ion (Sa) eluted from the sample or the permanent PPy coating and to confirm the negligible antioxidative activity of the underlying SS platform.

Bare SS wires were analysed for their antioxidative effect with an average AA% value of less than zero experienced at all time points. This confirms the bare SS to have a negligible antioxidative effect or indeed a slightly pro-oxidant effect.

The effect of Sa release on AA% was analysed. The PPy/Sa coated wire samples were immersed in EtOH for various durations (90 min, 5 hours, 24 hours). The wires were removed

and the EtOH reaction media was analysed for antioxidant activity. The average AA% values for all samples were negligible, suggesting that components eluted into the release media from the coated wires are not responsible for the antioxidative activity of the sample. These findings will be further discussed in section 6.4.1.4.

A solution of NaSa/EtOH (0.0235 M) was tested for percentage antioxidative activity and an average value of less than zero was confirmed. This supports the lack of antioxidative activity of Sa.

6.4.1.4.1. Mass of Salicylate Released from PPy/Sa Coated Wires in Presence of DPPH

UV analysis of the reaction solution from the DPPH assay samples was performed (600 – 200 nm) in an attempt to analyse the mass of Salicylate (Sa) released from the PPy/Sa coated wire samples. The absorption spectrum of the DPPH/EtOH control displayed three peaks in total, with two of the peaks very close to the 296 nm Sa peak that would be observed if Sa was present (see Figure 6-6). This made analysis of the 296 nm peak difficult and unlikely to be accurate, especially at such small concentrations.

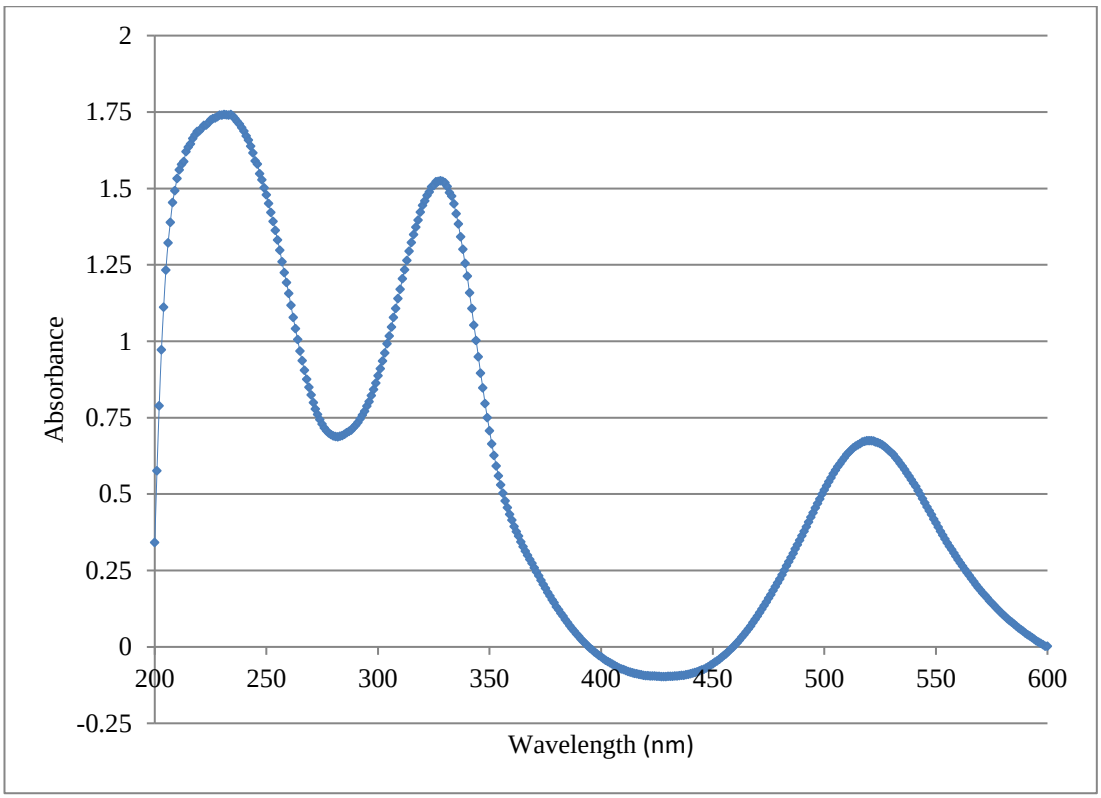

Figure 6-6: Graph of Absorbance vs Reaction Time of DPPH/EtOH negative control analysed by DPPH assay.

HPLC analysis was performed on DPPH assay samples to enable the separation and quantification of Sa in varying concentrations. Standard solutions of NaSa were analysed by HPLC at a wavelength of 296 nm and retention time ~ 8 min, providing a calibration curve. Sample release media (PPy/Sa coated wire sample in Ethanol) was analysed in the same way, confirming the presence of Sa (5.65 ± 5.22 µg) This confirms that the Sa was successfully eluted from the coated wire into the release media (Ethanol) and was therefore present for the anti-oxidant assay. Despite this, these solutions displayed no anti-oxidant activity when analysed and confirms that the release of Sa is therefore not responsible for the anti-oxidant activity exhibited from the coated wire samples.

6.4.1.4.2. Effect of the Presence of DPPH on the Release of Sa

Using the same HPLC method as in the previous section, it was investigated whether the presence of oxidative stress (in the form of DPPH radicals) could induce the release of Sa from

the coated wire samples. There was no significant difference between the mass of Sa released from the PPy/Sa coated wire samples placed directly into the DPPH/EtOH reaction solution (5.65 ± 5.22 µg) and the mass of Sa released in the absence of DPPH (5.26 ± 2.79 µg) (see Table 6-2). This suggests that the presence of DPPH (ROS) does not induce the release of Sa from the PPy/Sa coated wires and is further discussed in section 6.4.1.4.2.

Table 6-2*: Table of mean percentage antioxidant activity (AA %) values ± standard deviation (SD) values obtained from DPPH assay performed as detailed in section 6.3.1.3 Table also shows mass of Sa released ± standard deviation (SD) values. 3 times per sample at each time point. An AA% was calculated from the mean of these three values and then an average AA% was taken from the 5 samples which is listed in the table (n=4 for PPy/Sa coated wire samples due to loss of sample). Standard deviation (SD) values from n=5.*

Sample	**Mean AA % ± SD (90 min)**	**Mass of Sa released ± SD (µg)**
PPy/Sa coated SS wire (n=4)	9.73 ± 8.65	5.65 ± 5.22
PPy/Sa coated SS wire immersed in EtOH (90 min), wire removed. Release medium analysed. (n=5)	0.00 ± 2.04	6.53 ± 4.11
PPy/Sa coated SS wire immersed in EtOH (5 hr), wire removed. Release medium analysed. (n=5)	0.00 ± 3.34	5.47 ± 3.32
PPy/Sa coated SS wire immersed in EtOH (24 hr), wire removed. Release medium analysed. (n=5)	0.00 ± 2.82	5.26 ± 2.79

6.4.1.5. Effect of Physiological Conditions on Antioxidative Activity

Since the assessment of anti-oxidant activity experiments described above were carried out in Ethanol in accordance with the literature (Ebrahimiasl et al., 2014), in the following set of experiments it was decided to attempt to use a more physiologically relevant solution. This involved introducing PBS (pH 7.4) into the reaction media in place of Ethanol, at different ratios. Due to the limited solubility of DPPH in aqueous solutions, the reaction media had to be carefully altered to ensure that the DPPH did not precipitate out of the solution. The various solution ratios for the reaction media and the outcomes are listed in Table 6-3. The largest volume of PBS that could be included in the reaction media without the DPPH precipitating out was in the ratio of 1: 2: 1 (DPPH/EtOH solution: EtOH: PBS). The pH of the original reaction media (ratio of 1: 3: 0) was 7.95-8.10 and the pH of the altered reaction media (ratio 1: 2: 1) was 7.99 - 8.02. The ongoing presence of a relatively high concentration of Ethanol and the minimal change in pH failed to greatly increase the physiological relevance and so the experiment was not performed under these new conditions.

Table 6-3: Table showing composition of reaction solution, whether DPPH precipitated out of the solution and the final pH of the solution.

Ratio **DPPH/EtOH solution: EtOH: PBS**	**Did DPPH precipitate out?**	**pH of solution**
1: 3: 0	NO	7.95-8.10
1: 2: 1	NO	7.99-8.02
1: 1: 2	YES	n/a
1: 0: 3	YES	n/a

6.5. Discussion

Studies have suggested a possible link between oxidative stress and vessel healing following stent implantation (Kochiadakis et al., 2010, Juni et al., 2013). This prompted the development of drug-eluting stents containing antioxidative agents, including probucol (Kim et al., 2005) and succinobucol (Watt et al., 2013). Polypyrrole has been investigated as a DES coating in a limited number of studies to date (Okner et al., 2007, Arbizzani et al., 2007). In separate studies prepared by chemical synthesis, films and powders of PPy have been shown to possess antioxidative activity (Ebrahimiasl et al., 2014, Hsu et al., 2008). The aim of this study was to assess the antioxidative activity of PPy/Sa coated SS (316L) wires that were produced by electropolymerisation. The antioxidative activity of various samples was analysed using a DPPH assay. The outcomes are discussed in the following section.

6.5.1. Duration of Antioxidative Activity of PPy/Sa Coated Wires

The initial study examined the antioxidative activity of the PPy/Sa coated wire samples (potentiostatic, 0.9 V, 25 min, 0.1 M Py 0.1 M NaSa, more details available in chapter 4) using a DPPH assay, showing the samples to possess antioxidative properties. The mean AA % of the PPy/Sa coated wire samples was shown to increase with increasing time (90 mins – 24 hours), reaching ~70 % at the 24-hour time point in the initial study (see Figure 6-3 for graphical representation). These results suggest that the PPy/Sa samples continue to have an antioxidant effect up to the 24 hour time point. In this initial study, the variation in AA% of the five PPy/Sa coated wire samples at the 24 hour time point was minimal, ranging from 64 – 71 %.

In the subsequent study, there was a larger difference in values of AA % at the 24 hour time point, ranging from 12 – 88 % at the 24 hour time point. In an attempt to understand the difference in variation between the samples, the variation in charge density that was reached during the production of each PPy/Sa coating was analysed. Charge density gives an insight into the coating mass and availability of the antioxidative agent (PPy). It became apparent that samples from the initial study with minimal variation in AA% values had little variation in charge density values (0.3-0.528 C/cm^2). In comparison, samples from the subsequent study with larger variation in AA% values had a much larger difference in charge density values (0.152 – 1.12 C/cm^2, see Figure 6-5 for relationship between AA% and charge density from

both initial and subsequent studies). This larger variation allowed the relationship between charge density and antioxidative activity to be determined. It was found that there was a rapid increase in percentage antioxidative activity from around 10 % - 70 %, when the charge density is increased from around 0.1 – 0.3 C/cm^2. For values of charge density larger than 0.3 C/cm^2 to around 1.12 C/cm^2 the increase in percentage antioxidative activity is smaller, increasing from around 70 % to 90%. The general trend from the data collected in the present study suggests that PPy/Sa coated wire samples that reached a larger charge density during production, exhibited larger AA % values. Samples that reach a larger charge density also have a coating of larger mass. This suggests that samples that reach a larger charge density have an increased coating thickness, resulting in greater anti-oxidant capacity. Electropolymerisation may therefore be a useful and novel method of developing surfaces with tuneable antioxidant activity.

It is understood that the presence of the N-H group in the polypyrrole structure is responsible for its antioxidative effect (Upadhyay and Kumar, 2013). The H atom is transferred from the N-H bond to the DPPH free radical, neutralising it to form DPPH. Subsequently, the absorbance of the DPPH radical is reduced, leading to a larger value of AA %.

A comparison of the antioxidative effect of the PPy/Sa coated wire samples to the probucol solutions found them to be in the range of 0.1-0.2 mM probucol. As has been discussed in section 6.1.2.2, probucol has been studied for use in coronary stents and by making this comparison, an indication of the ability of PPy/Sa coated wires to act as an antioxidant can be determined.

The antioxidative effect of PPy found in the samples produced in the current study, is in line with the studies by (Hsu et al., 2008) and (Ebrahimiasl et al., 2014) which demonstrated the antioxidative activity of PPy in both powder and film form respectively. The antioxidative activity of a PPy/Sa coating onto a SS substrate has not previously been reported in the literature. Additionally, the utilisation of the antioxidative properties of PPy has not previously been incorporated into a DES coating, including the study by (Arbizzani et al., 2007) on which many aspects of this overall study has been based.

6.5.2. Effect of Salicylate Release on Antioxidative Activity

Although the antioxidative capacity of the PPy/Sa coated wire samples was demonstrated using the DPPH assay in this study, the next step was to confirm which component of the coating was responsible for the antioxidative effect. The reason for this experiment was to analyse whether it is a component eluted from the sample (e.g Sa) that is responsible or whether it is some interaction with the permanent surface of the PPy/Sa coated wire that elicits the anti-oxidant activity. There are studies available which have suggested an antioxidative effect of salicylate without confirming the mode of function.

In the present study, this was achieved by immersing the PPy/Sa coated wire samples in EtOH for various time points (90 min, 5 hr, 24 hr), removing the wire and analysing the reaction media by DPPH assay. Percentage antioxidative activity values for these samples confirm that there was no antioxidative agent released from the PPy/Sa coated wires that was detected by the DPPH assay. These initial results suggest that it is the surface of the PPy/Sa coated wire samples that exhibits the antioxidative effect.

To further eliminate the effect of Sa on the antioxidative activity exhibited by the PPy/Sa coated wire samples, Sa release from the PPy/Sa coated wire samples in the conditions of the DPPH assay (in EtOH at room temperature) was investigated. Identified by HPLC analysis, the average mass of Sa released over a 24 hour period was 5.26 ± 2.79 µg. The release of Sa from PPy/Sa coated wires in physiological conditions (pH 7.4, 37°C) has previously been presented in chapter 4, amounting to 13.84 ± 5.05 µg over a period of 24 hours. These findings show that there is a difference between the average mass of Sa released in physiological conditions (13.84 ± 5.05 µg) and the average mass of Sa released in Ethanol at room temperature (5.26 ± 2.79 µg) which will be discussed in section 6.5.3. However, it does confirm that Sa is eluted from the PPy/Sa coated wire samples and is therefore present in the EtOH reaction media that was analysed for antioxidative activity. Subsequently, the release of Sa from these samples does not appear to be responsible for the antioxidative activity of the PPy/Sa coated wire samples.

6.5.3. Effect of Physiological Conditions on Antioxidative Activity

As previously mentioned, there is a difference in the mass of Sa released from the PPy/Sa coated wires in EtOH and in PBS. One reason for this difference may be the difference in temperature between the two experimental setups. The experiment performed at physiological conditions was at a temperature of 37 °C, whereas the experiment performed in EtOH was at room temperature (~ 22 °C). The solubility of sodium salicylate in water at a temperature of 25 ° is 125 g/100g solvent and at a temperature of 78.5 °C is 145.8 g/100g solvent (Anatolievich, 2016). This suggests that the solubility of sodium salicylate at the higher temperature (37 °C) would be greater than at the lower temperature of 25 °C. This reduced solubility at the lower temperature of the anti-oxidant assay experiment may help explain, at least in part, the lower mass of salicylate released. Another potential reason for the variation in salicylate release may have been the difference in solubility of sodium salicylate in PBS and in EtOH. Sodium salicylate is more soluble in water (solubility = 108 g/100g solvent at temperature 15 °C) than in EtOH (solubility = 45 g/100g solvent at temperature 15 °C) (Anatolievich, 2016). This suggests that salicylate would be eluted more freely from the PPy/Sa coated wires in a water based solution (PBS, 0.01M) than in Ethanol. This was found to be the case in the present study.

Given this, and in an attempt to make the experimental conditions more physiologically relevant, the reaction media was altered. Phosphate Buffered Saline (PBS 0.01M, pH 7.4), which is normally used for *in vitro* procedures was introduced to the reaction media in place of EtOH, at various ratios. DPPH is relatively insoluble in water and thus the volume of PBS was gradually increased until DPPH was observed to precipitate out of the solution (see Table 6-3 for the various ratios of solution in the reaction media and the outcomes). It was found that there was no noticeable difference between the pH (7.95 – 8.10) of the original solution and the pH (7.99 – 8.02) of the solution with the introduction of PBS. For this reason, it was decided that the experiment should not be attempted with this change in conditions as it is minor. If a pH closer to 7.4 was achieved, the experiment would have been repeated under these altered conditions.

6.5.4. Component of PPy/Sa Coating Which Exhibits the Antioxidative Effect

An important part of this study was to identify whether the presence of a ROS (DPPH radical) could induce the release of the anti-inflammatory agent, salicylate. HPLC analysis identified that there was no difference between the average cumulative mass of Sa released from the PPy/Sa coated wire samples in the absence and presence of a DPPH radical (see section 6.4.1.4.2). This suggests that the presence of ROS (DPPH radical) does not induce the release of Sa from the PPy/Sa coated wire samples. In terms of use for a DES, this means that if a ROS is present in the stented vessel, this would not accelerate the release beyond the rate determined by diffusive and convective transport that is thought to drive drug release from stents and initiate the release of the salicylate (Venkatraman and Boey, 2007).

The findings from this part of the study also confirm that the antioxidative properties of the permanent PPy/Sa coating are unlikely to be due to the released Sa. There is a significant difference between the average AA % of the PPy/Sa coated wires directly in reaction with the DPPH radicals (~ 55.82 ± 30.09 %) when compared to the release media (~ 0 %). This large difference in percentage antioxidative activity is despite the fact that there is no significant difference between the mass of Sa present in each case, confirming that the Sa is not responsible for the antioxidative effect of the coating.

A solution of NaSa/EtOH (0.0235 mM) was analysed for its antioxidative properties, with AA % values of less than zero achieved for all five samples. It was concluded that the NaSa/EtOH solution does not exhibit an antioxidative effect.

To confirm the antioxidative activity of the permanent PPy/Sa coating, the antioxidative activity of the bare SS (316L) platform must also be excluded. Bare SS (316L) wires were analysed in the same way as previous samples, showing values of AA % to be less than zero in each case. This supports the theory that the antioxidative effect is due to the PPy/Sa coating and not the underlying stainless steel and confirms that the permanent PPy/Sa coating is responsible for the antioxidative effect.

6.5.5. Study Limitations and Future Work

To gain a better understanding as to the exact reaction that occurs on the surface of the PPy/Sa coated wires, the composition of the surface could be analysed pre/post reaction with DPPH. The composition of polypyrrole films has been examined in previous studies through the use of powder X-Ray diffraction (Chougule et al., 2011). By assessing the chemical composition of the surface, the reaction could be better understood.

As was mentioned in the present study, attempts to extend the reaction time beyond 24 hours were not successful. In future studies, the experimental design could be improved upon, for example using individual samples for each time point or using larger volumes of solution so to ensure there is sufficient sample volume for analysis at extended time points. This could give an indication as to the true antioxidative effect of the PPy/Sa coated wires and if this could be extended beyond the 24 hours identified by the present study.

A relationship between charge density and antioxidative effect has also been identified in the present study. By manipulating the charge density to more extreme values when producing the PPy/Sa coatings, this relationship could be better understood with the potential to tune the antioxidative effect of the coatings.

6.5.6. Summary and Conclusions

To conclude, it has been identified that the PPy/Sa coated wires produced in this study do possess an antioxidative effect which extends to 24 hours. It was confirmed that the Sa component released from the PPy/Sa coatings does not possess the antioxidative properties. Combing this finding with those from the literature, it was concluded that it is the interaction between the surface of the PPy/Sa coating itself (PPy) that exhibits the antioxidative effect. It was also confirmed that the release of Sa is not initiated by the presence of an oxidant (DPPH radicals).

The findings from the present study have shown the capability of a potential novel DES coating to possess antioxidative properties. Combining this with the research that suggests oxidative stress post stent implantation could contribute to restenosis, it is a positive outcome that the PPy/Sa coated wires produced in the present study could possess such properties that could potentially counteract oxidative stress.

Chapter 7

7. Overall Discussion

7.1. Summary of Conclusions

Coronary DES designs are constantly evolving, with current manufacturers focused on the development of devices that can inhibit restenosis more consistently and achieve this without adversely affecting recovery of the endothelium. The stent coating plays a key part in the performance of a DES, providing the mechanism by which drug delivery to the artery wall can be maintained at a therapeutic level for the duration required. It must also be capable of withstanding the stresses of expansion within an artery without experiencing delamination or polymer fragmentation. Such events could lead to inflammatory responses within the stented vessel and subsequent neointimal thickening (Virmani et al., 2004), thus, the coating material must be carefully selected and its ability to perform as a stent coating examined.

Conducting polymers, such as PPy, have particular promise as DES coatings by virtue of their ability to incorporate biological molecules and subsequently release them into the body. When incorporated through electropolymerisation, a drug can be simultaneously incorporated into the PPy coating during the coating process, potentially providing fine control over drug dose and elution kinetics. This process may also help overcome some of the other challenges associated with conventional stent coating methods, including variability in the production process, webbing during polymer deposition, as well as delamination and cracking of the coating during stent deployment.

Surface Topography

A number of studies have suggested that there is a link between surface roughness and endothelial cell behaviour (Chung et al., 2003, Liliensiek et al., 2010, Xu et al., 2004). Surface topography has previously been considered for use in coronary stent design (Palmaz et al., 2002) and is becoming of increasing interest (ter Meer et al., 2017) but it is only recently that surface topography has been integrated into stent design for widespread clinical application (Dibra et al., 2005). In this context, surface roughness has been identified as a potential promoter of rapid re-endothelialisation. Given this, it was important that the surface topography of the novel polypyrrole coatings produced in the present study were characterised and could be compared to the topography used in existing stent platforms. However, surface

topography data of DES was lacking, with studies more focused on performance *in vivo* and drug elution characteristics.

It was therefore the first aim of chapter 3 to characterise the surface topography and morphology of a range of clinically relevant stents. The surfaces of BMS and DES were successfully analysed at the micrometre and nanometre scales, showing differences in surface topography and morphology. Surface roughness (RMS) values ranged from 14 ± 11 nm (Gazelle™) to 182 ± 37 nm (Yukon®). The surface morphology of those DES examined were found to be similar between stent types and surface roughness values also showed great similarities.

For a selected DES (Taxus™ Express^{2} ™), it was also decided to investigate if drug elution from its surface led to changes in surface characteristics. Despite the qualitative difference observed throughout the 28 day drug elution period, including pore formation, numerical differences in the surface roughness was absent. The surface of the Taxus™ Express^{2} ™ stent was examined over a 28 day period, far extending the 48 hours reported by (Ranade et al., 2004) in a similar study. This has given greater insight into the change in surface topography of this stent type over an extended period, a time when healing is in its early stages and could ultimately be influenced by a change in surface topography.

The surface morphology and topography of PPy coatings is not widely reported in the literature and with the link between surface topography and cell behaviour, the aim was to investigate the surface topography and morphology of novel PPy/Sa coatings. The effect of increasing electropolymerisation (potentiostatic) duration from 15 min to 25 min on the surface topography of PPy/Sa coatings showed an increase in surface roughness (from 82 ± 40 nm to 129 ± 77 nm) and substrate coverage. It was therefore concluded that under the potentiostatic conditions used in the present study, increasing the electropolymerisation duration from 15 min to 25 min, increases the surface roughness of the coating. Subsequently when compared to the PPy/Sa coatings produced by galvanostatic electropolymerisation, surfaces of decreased roughness (51 ± 20 nm) were achieved. Two PPy/Sa coating types identified for their uniformity and good substrate coverage were successfully produced by potentiostatic (25 min) and galvanostatic (10 min) electropolymerisation, with their surfaces roughness values found to be within the range of those found for the clinically relevant stents.

Vascular Biocompatibility

The manufacturer of the Yukon® stent has identified the microporous structure as a potential promoter of rapid re-endothelialisation (Translumina, 2009) but evidence at the cellular level

is lacking, with studies more focused on *in vivo* outcomes (Dibra et al., 2005). Comparison of two BMSs (Yukon®/ Gazelle™) showed the Yukon® stent, with purposefully manufactured microporous structure to have a mean R_{RMS} value more than 10x larger than the Gazelle™ stent. The final aim of chapter 3 was therefore to investigate the adhesion and proliferation of porcine endothelial cells onto the two BMS of distinct surface roughness as identified in chapter 3. General trends in data from this study showed that without pre-treatment with FBS, cell growth is improved on the surface type with larger R_{RMS} roughness value (Yukon®, R_{RMS} = 85.52 ± 26.07 nm) compared to the smaller R_{RMS} roughness value (Gazelle™, R_{RMS} = 14.39 ± 11.24 nm). These findings further suggest the potential importance of stent surface topography on re-endothelialisation and subsequent healing post stent implantation. The findings presented in chapter 3 have been brought together to produce one of the most wide-ranging analyses of stent surface topography yet reported for a number of clinically available stents (both BMS and DES), including a limited study on the behaviour of ECs onto two stents of distinct surface roughness.

As a potential DES coating, it was an important objective to assess the biocompatibility of the novel PPy/Sa coating identified in this study. Although there are studies that show the biocompatibility of PPy in many forms (Garner et al., 1999, Stewart et al., 2012), few have been relevant to cardiovascular applications (Jakubiec et al., 1998) and the biocompatibility of the novel PPy/Sa coating from the present study has not been analysed. The growth of porcine ECs was analysed on the two PPy/Sa coating types (potentiostatic 25 min, galvanostatic 10 min) produced in chapter 4, with different surface topography and Sa release profiles identified. No significant difference in cell viability was observed on the two PPy/Sa surfaces, although general trends in data, including improved growth of ECs on surfaces of larger roughness (potentiostatic) were observed. These findings also agree with the results from the limited investigation into the growth of ECs onto two stents of distinct roughness performed in chapter 3, which also suggested increased growth of ECs on the surface of larger roughness. Cell growth was observed on both PPy/Sa surfaces, showing the potential of these coatings for use in biomedical application as DES coatings. This is the first time cell growth has been performed on PPy/Sa coatings of this kind.

Drug Release

An important factor to consider in a DES coating is drug type and its release profile. An optimal release profile and duration are dependent on the mechanism of action of the drug that is being released. Studies which have already investigated the potential of PPy as a DES coating report short drug release periods of various drugs including salicylate and paclitaxel

(Arbizzani et al., 2007, Okner et al., 2008). The aim was therefore to investigate the optimum experimental conditions to achieve a novel PPy coating that could provide extended release of the anti-inflammatory agent, Sa, from the coated surface. Changing the electropolymerisation method from potentiostatic to galvanostatic enabled the Sa release period to be extended from 24 hours to 3 days without significantly changing the cumulative mass of Sa released (~12 µg). This was an important finding, as the stent inflammation time line states the occurrence of inflammation within the first 7 days following stent implantation. Therefore, the release of an anti -inflammatory agent within the first three days, could prevent the initial stages of inflammation, an event that is linked to in-stent restenosis. Not only was the Sa release period extended, but the synthesis time was also greatly reduced, refining the potential future commercialisation of the technique.

Antioxidant Activity

Amongst many different approaches to improve healing post stent implantation, studies have suggested a possible link between oxidative stress and altered endothelial and smooth muscle cell function following stent implantation (Kochiadakis et al., 2010, Juni et al., 2013, Pendyala et al., 2009). This prompted the development of DES containing antioxidative agents, including probucol (Kim et al., 2005) and succinobucol (Watt et al., 2013). Thus far, various approaches to the local delivery of antioxidants to inhibit oxidative stress have not been successfully incorporated into clinically available stents.

Polypyrrole has been recognised for its antioxidative properties in many forms but has not been investigated for use in coronary stents (Ebrahimiasl et al., 2014, Hsu et al., 2008). The final aim of this study was to investigate the antioxidative activity of a novel PPy/Sa coating for potential use as a coronary stent coating; this could further enhance the PPy/Sa coating as a DES. It was identified that the PPy/Sa coated wires (Potentiostatic 0.9 V, 25 min) produced in the present study and extensively researched in chapters 4 and 5 also possess an antioxidative effect which extends to 24 hours. It was concluded that the antioxidative effect was owed to the permanent polypyrrole component of the PPy/Sa coating and was not influenced by the Sa release. This was an interesting finding as it suggests that the release of Sa can be altered without losing the antioxidative properties of the PPy/Sa coating. The PPy/Sa coating produced in the present study has not been investigated for use in coronary stents to specifically target the negative implications associated with the occurrence of oxidative stress following stent implantation. This adds a further dimension to the PPy/Sa coating; the presence of an antioxidative agent that has the potential to scavenge free radicals generated following stent implantation, reducing oxidative stress.

7.1.1. Overall Study Limitations and Future Work

Vascular Biocompatibility

Limitations of the study thus far have been included in the individual discussion chapters, and this section will provide a summary of the overall limitations from each chapter. Both chapter 3 and chapter 5 contained cell culture studies and so the limitations of these sections proved to be very similar. If time and sample availability permitted, it would be advantageous to repeat the cell culture studies with the removal of the sample to a fresh well following cell seeding but without the initial sample pre-treatment in FBS. This would confirm the true effect of the surfaces of the two stent types and the two PPy/Sa coatings and may verify the findings from the initial experiments in each case (no pre-treatment, 13 days), that increased surface roughness does improve EC growth. Additionally, sample size could be increased for each experiment and cells quantified at each time point to ascertain whether rapid cell growth and subsequent premature cell death is the cause of low cell number and high variation in levels of LDH at certain sample points.

An important limitation of the cell culture experiments performed in the present study is that they were carried out in the absence of flow. It is pertinent to consider the blood flow within an artery as this could influence cell adhesion and growth. Therefore, future cell culture experiments could be attempted in an alternative experimental setup, for example in a perfusion chamber to make the experiment more relevant for use in DES.

Specifically related to the findings in chapter 5, the effect of the presence of Sa directly in contact with ECs could be further examined to ascertain the true effect it has on EC growth. This may further suggest the optimum release of Sa from the coatings by analysing its influence, if any, on EC growth and proliferation.

Surface Topography

In chapter 3, the surface topography of a range of clinically relevant BMS and DES were investigated. However, there are now newer generation stents available and so it may be beneficial to characterise the surfaces of these stents and indeed assess their effect on the behaviour of ECs in future studies.

The coating integrity of the PPy/Sa coatings produced in chapter 4 has been successfully identified following 28 days in physiological conditions, however, the effect of extended time in a physiological environment has not been investigated. This is an important factor to

consider as the stability on the coating over a longer period may have an impact in its performance as a stent coating.

It has also been mentioned in the present study that a stent must be able to withstand the mechanical strain of expansion within an artery, therefore, future mechanical analysis, for example three-point bending of the PPy/Sa coated wires would provide an insight into this. Additionally, it would be of interest to coat a clinically relevant BMS with the PPy/Sa coating, to investigate the effect of a more complex geometry on coating formation.

Drug Release

In chapter 4, the release period of Sa from PPy/Sa coatings was successfully extended form 24 hours to 3 days. Although the exact effect of Sa release on events following stent implantation is not fully understood, it may be of interest to further extend the Sa release period from the PPy/Sa coatings. This would enable a database of the experimental method and drug release data to be created, allowing coatings with various doses to be available.

Antioxidant Activity

In terms of the antioxidative activity study presented in chapter 6, the experimental design could be improved upon in future studies. For example, using individual samples for each time point or using larger volumes of solution so to ensure there is sufficient sample volume for analysis at extended time points would be advantageous. This could give an indication as to the true antioxidative effect of the PPy/Sa coated wires and if this effect could be detected beyond the 24 hours identified in the present study. Furthermore, a relationship between charge density and antioxidative effect was identified in the present study. By manipulating the current density to more extreme values when producing the PPy/Sa coatings, this relationship could be better understood with the potential to tune the antioxidative effect of the coatings.

7.1.2. Final Conclusions

To conclude, the surfaces of clinically relevant BMS and DES have been successfully analysed in the present study to provide a wealth of information that was not previously available. This has given an insight into both similarities and differences between products and has also highlighted coating irregularities that have the potential to cause complications following implantation.

Cell culture studies have shown general trends in data, suggesting surfaces with larger roughness do promote EC growth, however further studies should be performed to confirm the significance of this finding.

The present study has identified two potential PPy/Sa DES coatings, with release of an anti-inflammatory agent extending to 3 days and biocompatibility studies showing cells to successfully grow on both PPy/Sa surfaces. Finally, antioxidative properties of the novel PPy/Sa coating has been identified to extend to 24 hours, not only showing the antioxidative properties of PPy in this form for the first time but also providing another function to the potential DES coating.

8. References

ABBOTT, A. P., CAPPER, G., MCKENZIE, K. J., GLIDLEB, A. & RYDER, K. S. 2006. Electropolishing of stainless steels in a choline chloride based ionic liquid: an electrochemical study with surface characterisation using SEM and atomic force microscopy. *Physical Chemisry Chemical Physics,* 8**,** 4214 - 4221.

ABIZAID, A. & J. RIBAMAR COSTA, J. 2010. New Drug-Eluting Stents: An Overview on Biodegradable and Polymer-Free Next-Generation Stent Systems. *Circulation Cardiovascular Interventions,* 3**,** 384-393.

ACHARYA, G. & PARK, K. 2006. Mechanisms of controlled drug release from drug-eluting stents. *Advanced Drug Delivery Reviews,* 58**,** 387-401.

ALLAHVERDI, N. 2013. *Developing Polypyrrole Coated Coronary Stents for Extended Release of Sirolims.* MSc Biomedical Engineering, University of Strathclyde.

AN, N., SCHEDLE, A., WIELAND, M., ANDRUKHOV, O., MATEJKA, M. & RAUSCH-FAN, X. 2010. Proliferation, behavior, and cytokine gene expression of human umbilical vascular endothelial cells in response to different titanium surfaces. *Journal of Biomedical Materials Research Part A,* 93A**,** 364-372.

ANATOLIEVICH, K. R. 2016. *Properties of substance: sodium salicylate* [Online]. Available: http://chemister.ru/Database/properties-en.php?dbid=1&id=2993 [Accessed 22nd September 2016].

ARBIZZANI, C., MASTRAGOSTINO, M., NEVI, L. & RAMBELLI, L. 2007. Polypyrrole: A drug-eluting membrane for coronary stents. *Electrochimica Acta,* 52**,** 3274-3279.

BALAKRISHNAN, B., TZAFRIRI, A. R., SEIFERT, P., GROOTHUIS, A., ROGERS, C. & EDELMAN, E. R. 2005. Strut Position, Blood Flow, and Drug Deposition implications for Single and Overlapping Drug-Eluting Stents. *Circulation***,** 2958-2965.

BALINT, R., CASSIDY, N. J. & CARTMELL, S. H. 2014. Conductive polymers: Towards a smart biomaterial for tissue engineering. *Acta Biomaterialia,* 10**,** 2341-2353.

BASALUS, M. W. Z., ANKONE, M. J. K., MAN, F. H. A. F. D., BIRGELEN, C. V. & HOUWELINGEN, K. G. V. 2009. Coating irregularities of durable polymer-based drug-eluting stents as assessed by scanning electron microscopy. *EuroIntervention,* 5**,** 157-165.

BASALUS, M. W. Z. & CLEMENS, V. B. 2010. Benchside testing of drug-eluting stent surface and geometry. *Intervention Cardiology,* 2**,** 159-175.

BIGGS, K. B., BALSS, K. M. & MARYANOFF, C. A. 2012. Pore Networks and Polymer Rearrangement on a Drug-Eluting Stent as Revealed by Correlated Confocal Raman and Atomic Force Microscopy. *Langmuir,* 28**,** 8238-8243.

BRITISHHEARTFOUNDATION 2015. Cardiovascular Disease Statistics 2015. *In:* FOUNDATION, B. H. (ed.).

BUSCH, R., STROHBACH, A., RETHFELDT, S., WALZ, S., BUSCH, M., PETERSEN, S., FELIX, S. & STERNBERG, K. 2014. New stent surface materials: The impact of polymer-dependent interactions of human endothelial cells, smooth muscle cells, and platelets. *Acta Biomaterialia,* 10**,** 688-700.

BYRNE, R. A., KASTRATI, A., KUFNER, S., MASSBERG, S., BIRKMEIER, K. A., LAUGWITZ, K.-L., SCHULZ, S., PACHE, J., FUSARO, M., SEYFARTH, M., SCHÖMIG, A. & MEHILLI, J. 2009. Randomized, non-inferiority trial of three limus agent-eluting stents with different polymer coatings: the Intracoronary Stenting and Angiographic Results: Test Efficacy of 3 Limus-Eluting Stents (ISAR-TEST-4) Trial. *European Heart Journal,* 30**,** 2441-2449.

CECH, J., PRANOV, H., KOFOD, G., MATSCHUK, M., MURTHY, S. & TABORYSKI, R. 2013. Surface roughness reduction using spray-coated hydrogen silsesquioxane reflow. *Applied Surface Science,* 280**,** 424-430.

CHOUGULE, M. A., PAWARA, S. G., GODSEA, P. R., MULIKA, R. N., SENB, S. & PATILA, V. B. 2011. Synthesis and Characterization of Polypyrrole (PPy) Thin Films. *Soft Nanoscience Letters,* 1**,** 6-10.

CHUNG, T.-W., LIU, D.-Z., WANG, S.-Y. & WANG, S.-S. 2003. Enhancement of the growth of human endothelial cells by surface roughness at nanometer scale. *Biomaterials,* 24**,** 4655-4661.

CLARKE, J. 2016. *A Double Beam UV-Visible Absorption Spectrometer* [Online]. Available: http://www.chemguide.co.uk/analysis/uvvisible/spectrometer.html [Accessed 02 June 2016].

CONTRACTOR, H., MAMAS, M. & FRASER, D. G. 2008. Angiographic time course of in-stent restenosis with zotarolimus drug-eluting stents. *The Canadian Journal of Cardiology,* 24**,** e45-e45.

CURFMAN, G. D., MORRISSEY, S., JARCHO, J. A. & DRAZEN, J. M. 2007. Drug-Eluting Coronary Stents — Promise and Uncertainty. *New England Journal of Medicine,* 356**,** 1059-1060.

CYSEWSKA, K., VIRTANEN, S. & JASINSKI, P. 2015. Electrochemical Activity and Electrical Properties of Optimized Polypyrrole Coatings on Iron. *Journal of the Electrochemical Society,* 162.

DANGAS, G. D., CLAESSEN, B. E., CAIXETA, A., SANIDAS, E. A., MINTZ, G. S. & MEHRAN, R. 2010. In-Stent Restenosis in the Drug-Eluting Stent Era. *Journal of the American College of Cardiology,* 56**,** 1897-1907.

DELIVOPOULOS, E., OUBERAI, M. M., COFFEY, P. D., SWANN, M. J., SHAKESHEFF, K. M. & WELLAND, M. E. 2015. Serum protein layers on parylene-C and silicon oxide: effect on cell adhesion. *Colloids Surf B Biointerfaces,* 126**,** 169-77.

DEVILE, M. P. J. & FOËX, P. 2010. Antiplatelet drugs, coronary stents, and non-cardiac surgery. *Continuing Education in Anaesthesia Critical Care & Pain,* 10**,** 187-191.

DIBRA, A., KASTRATI, A., MEHILLI, J., PACHE, J. R., OEPEN, R. V., DIRSCHINGER, J. & MIG, A. S. 2005. Influence of stent surface topography on the outcomes of patients undergoing coronary stenting: A randomized double-blind controlled trial. *Catheterisation and Cardiovascular Interventions,* 65**,** 374-380.

DING, N. I., PACETTI, S. D., TANG, F.-W., GADA, M. & ROORDA, W. 2009. XIENCE V™ Stent Design and Rationale. *Journal of Interventional Cardiology,* 22**,** S18-S27.

DOMB, A. J. 2008. Electropolymerizable monomers and polymeric coatings on implantable devices prepared therefrom. Google Patents.

EATON, P. & WEST, P. 2011. *Atomic Force Microscope*, Oxford University Press Inc.

EBRAHIMIASL, S., ZAKARIA, A., KASSIM, A. & BASRI, S. N. 2014. Novel conductive polypyrrole/zinc oxide/chitosan bionanocomposite: synthesis, characterization, antioxidant, and antibacterial activities. *International Journal of Nanomedicine,* 10**,** 217-227.

ENGLAND, C. G., MILLER, M. C., KUTTAN, A., TRENT, J. O. & FRIEBOES, H. B. 2015. Release kinetics of paclitaxel and cisplatin from two and three layered gold nanoparticles. *European Journal of Pharmaceutics and Biopharmaceutics,* 92**,** 120-129.

EUGENE A. SPRAGUE, P., FERMIN TIO, M., S. HINAN AHMED, M., JUAN F. GRANADA, M. & STEVEN R. BAILEY, M. 2012. Impact of Parallel Micro-Engineered Stent Grooves on Endothelial Cell Migration, Proliferation, and Function: An In Vivo Correlation Study of the Healing Response in the Coronary Swine Model *Circulation,* 5**,** 499-507.

FAN, L. J. & KARINO, T. 2008. Effect of serum concentration on adhesion of monocytic THP-1 cells onto cultured EC monolayer and EC-SMC co-culture. *J Zhejiang Univ Sci B,* 9**,** 623-9.

FANG, Y.-I., NAMIKI, H., TSUNODA, E., SHIODA, S., SHIBATA, M., NAKATANI, M., KATAGIRI, T., TAKEYAMA, Y., OHATA, H., HONDA, K. & MOMOSE, K. 2005. Marked increase in the histamine content of neointima after stent implantation of pig coronary artery and growth-promoting effects of histamine in cultured smooth muscle cells. *Life Sciences,* 77**,** 241-251.

FORNELL, D. 2017. *Bioresorbable Polymers on Metallic Stents Show No Superiority to Durable Polymer Stents* [Online]. Available: https://www.dicardiology.com/article/bioresorbable-polymers-metallic-stents-show-no-superiority-durable-polymer-stents?eid=327991756&bid=1639949 [Accessed 18 Jan 2017 2017].

FRIEDRICHS, J., LEGATE, K. R., SCHUBERT, R., BHARADWAJ, M., WERNER, C., MÜLLER, D. J. & BENOIT, M. 2013. A practical guide to quantify cell adhesion using single-cell force spectroscopy. *Methods,* 60**,** 169-178.

FUIERER, R. 2009. Procedural Operation 'Manualette' MFP3D. *In:* RESEARCH, A. (ed.). Santa Barbara.

GARCIA, E. J., OLDONI, T. L. C., ALENCAR, S. M. D., REIS, A., LOGUERCIO, A. D. & GRANDE, R. H. M. 2012. Antioxidant activity by DPPH assay of potential solutions to be applied on bleached teeth. *Brazilian Dental Journal,* 23**,** 22-27.

GARNER, B., GEORGEVICH, A., HODGSON, A. J., LIU, L. & WALLACE, G. G. 1999. Polypyrrole–heparin composites as stimulus-responsive substrates for endothelial cell growth. *Journal of Biomedical Materials Research,* 44**,** 121-129.

GAROT, P., MORICE, M.-C., TRESUKOSOL, D., POCOCK, S. J., MEREDITH, I. T., ABIZAID, A., CARRIÉ, D., NABER, C., IÑIGUEZ, A., TALWAR, S., MENOWN, I. B. A., CHRISTIANSEN, E. H., GREGSON, J., COPT, S., HOVASSE, T., LURZ, P., MAILLARD, L., KRACKHARDT, F., ONG, P., BYRNE, J., REDWOOD, S., WINDHÖVEL, U., GREENE, S., STOLL, H.-P. & URBAN, P. 2017. 2-Year Outcomes of High Bleeding Risk Patients After Polymer-Free Drug-Coated Stents. *Journal of the American College of Cardiology,* 69**,** 162-171.

GELMI, A., HIGGINS, M. J. & WALLACE, G. G. 2010. Physical surface and electromechanical properties of doped polypyrrole biomaterials. *Biomaterials,* 31**,** 1974-1983.

GELMI, A., HIGGINS, M. J. & WALLACE, G. G. 2012. Attractive and Repulsive Interactions Originating from Lateral Nanometer Variations in Surface Charge/Energy of Hyaluronic Acid and Chondroitin Sulfate Doped Polypyrrole Observed Using Atomic Force Microscopy. *The Journal of Physical Chemistry B,* 116**,** 13498-13505.

GIZDAVIC-NIKOLAIDIS, M., TRAVAS-SEJDIC, J., BOWMAKER, G. A., COONEY, R. P. & KILMARTIN, P. A. 2004a. Conducting polymers as free radical scavengers. *Synthetic Metals,* 140**,** 225-232.

GIZDAVIC-NIKOLAIDIS, M., TRAVAS-SEJDIC, J., BOWMAKER, G. A., COONEY, R. P., THOMPSON, C. & KILMARTIN, P. A. 2004b. The antioxidant activity of conducting polymers in biomedical applications. *Current Applied Physics,* 4**,** 347-350.

GOPALAKRISHNAN, K., BIRGISSON, B., TAYLOR, P. & ATTOH-OKINE, N. O. 2011. Nanotechnology in Civil Infrastructure: A Paradigm Shift. Springer.

GROBELNY, J., DELRIO, F. W., PRADEEP, N., KIM, D.-I., HACKLEY, V. A. & COOK, R. F. 2009. Size Measurement of Nanoparticles Using Atomic Force Microscopy. Available: http://ncl.cancer.gov/NCL_Method_PCC-6.pdf.

GUIMARD, N. K., GOMEZ, N. & SCHMIDT, C. E. 2007. Conducting polymers in biomedical engineering. *Progress in Polymer Science,* 32**,** 876-921.

HARIDAS, K. K., M, S. R. & BHAT, P. 2008. Drug Eluting Stents – Do They Address the Problem of Restenosis? *Medical Update* 18.

HELFT, G. 2016. Dual antiplatelet therapy duration after drug-eluting stents: how long? *Journal of Thoracic Disease,* 8**,** E844-E846.

HOLLAND, I. 2016. *EngD Medical Devices.* University of Strathclyde.
HSU, C. F., PENG, H. & KILMARTIN, P. A. 2010. ABTS•+ scavenging activity of polypyrrole, polyaniline and poly(3,4-ethylenedioxythiophene). *Polym Int,* 60**,** 69-77.
HSU, C. F., ZHANG, L., PENG, H., TRAVAS-SEJDIC, J. & KILMARTIN, P. A. 2008. Scavenging of DPPH free radicals by polypyrrole powders of varying levels of overoxidation and/or reduction. *Synthetic Metals,* 158**,** 946-952.
HWANG, C. W., LEVIN, A. D., JONAS, M. & EDELMAN, E. R. 2005. Thrombosis Modulates Arterial Drug Distribution for Drug-Elutin Stents. *Circulation***,** 1619-1626.
I.S.U.OFSCIENCE/TECHNOLOGY. 2013. *Secondary Electrons and Detection* [Online]. Available: http://www.mse.iastate.edu/research/laboratories/sem/microscopy/how-does-the-sem-work/high-school/how-the-sem-works/secondary-electrons-and-detection/ [Accessed 22nd November 2013].
INOUE, T., CROCE, K., MOROOKA, T., SAKUMA, M., NODE, K. & SIMON, D. I. 2011. Vascular Inflammation and Repair: Implications for Re-Endothelialization, Restenosis, and Stent Thrombosis. *JACC: Cardiovascular Interventions,* 4**,** 1057-1066.
IQBAL, J., GUNN, J. & SERRUYS, P. W. 2013. Coronary stents: historical development, current status and future directions. *British Medical Bulletin,* 106**,** 193-211.
JAIN, A., MEHRA, N. & SWARNAKAR, N. K. 2015. Role of Antioxidants for the Treatment of Cardiovascular Diseases: Challenges and Opportunities. *Current Pharmaceutical Design,* 21**,** 1381.
JAKUBIEC, B., MAROIS, Y., ZHANG, Z., ROY, R., SIGOT-LUIZARD, M.-F., DUGRÉ, F. J., KING, M. W., DAO, L., LAROCHE, G. & GUIDOIN, R. 1998. In vitro cellular response to polypyrrole-coated woven polyester fabrics: Potential benefits of electrical conductivity. *Journal of Biomedical Materials Research,* 41**,** 519-526.
JAMES, P. J., ANTOGNOZZI, M., TAMAYO, J., MCMASTER, T. J., NEWTON, J. M. & MILES, M. J. 2001. Interpretation of Contrast in Tapping Mode AFM and Shear Force Microscopy. A Study of Nafion. *Langmuir,* 17**,** 349-360.
JEAN-CLAUDE TARDIF, M., JEAN GRÉGOIRE, M., LEONARD SCHWARTZ, M., LAWRENCE TITLE, M., LOUISE LARAMÉE, M., FRANÇOIS REEVES, M., JACQUES LESPÉRANCE, M., MARTIAL G. BOURASSA, M., PHILIPPE L. L'ALLIER, M., MITCHELL GLASS, M. J., EAN LAMBERT, P., MARIE-CLAUDE GUERTIN & PHD; 2003. Effects of AGI-1067 and Probucol After Percutaneous Coronary Interventions. *Circulation,* 107**,** 552-558.
JORDAN, M. A., TOSO, R. J., THROWER, D. & WILSON, L. 1993. Mechanism of mitotic block and inhibition of cell proliferation by taxol at low concentrations. *Proceedings of the National Academy of Sciences of the United States of America,* 90**,** 9552-9556.
JUNI, R. P., DUCKERS, H. J., VANHOUTTE, P. M., VIRMANI, R. & MOENS, A. L. 2013. Oxidative Stress and Pathological Changes After Coronary Artery Interventions. *Journal of the American College of Cardiology,* 61**,** 1471-1481.
KAJA, S., PAYNE, A. J., SINGH, T., GHUMAN, J. K., SIECK, E. G. & KOULEN, P. 2015. An optimized lactate dehydrogenase release assay for screening of drug candidates in neuroscience. *Journal of pharmacological and toxicological methods,* 73**,** 1-6.
KAMATH, K. R., BARRY, J. J. & MILLER, K. M. 2006. The Taxus™ drug-eluting stent: A new paradigm in controlled drug delivery. *Advanced Drug Delivery Reviews,* 58**,** 412-436.
KEREIAKES, D. J., MEREDITH, I. T., WINDECKER, S., LEE JOBE, R., MEHTA, S. R., SAREMBOCK, I. J., FELDMAN, R. L., STEIN, B., DUBOIS, C., GRADY, T., SAITO, S., KIMURA, T., CHRISTEN, T., ALLOCCO, D. J. & DAWKINS, K. D. 2015. Efficacy and Safety of a Novel Bioabsorbable Polymer-Coated, Everolimus-Eluting Coronary Stent. *The EVOLVE II Randomized Trial,* 8.
KIM, H. K., SIM, D. S., HONG, Y. J., PARK, K. H., AHN, Y., CHO, J. G., JEONG, M. H., YOON, N. S., PARK, J. C., KIM, W., YOON, H. J., KIM, S. S., KIM, K. H. & KANG, J. C. 2011. Two-Year

Clinical Outcome after Carvedilol-Loaded Stent Implantation in Patients with Coronary Artery Disease. *The Korean Journal of International Medicine*.

KIM, J., HUNG, SUNG, H., KYUNG , , KIM, J., HYUN, , YOON, C., OH ,, LEE, K. & LEE, H. 1997. Electrochemical Synthesis of Metallic Polypyrrole Films. *Korean Physical Society,* 31**,** 91-94.

KIM, W., MYUNG HO JEONG, CHA, K. S., HYUN, D. W., HUR, S. H., KIM, K. B., HONG, Y. J., PARK, H. W., JU HAN KIM, M., AHN, Y. K., KIM, M. H., CHO, J. G., PARK, J. T. & PARK, J. C. 2005. Effect of Anti-Oxidant (Carvedilol and Probucol) Loaded Stents in a Porcine Coronary Restenosis Model. *Circulation,* 69**,** 101-106.

KOCHIADAKIS, G. E., ARFANAKIS, D. A., MARKETO, M. E., SKALIDIS, E. I., IGOUMENIDIS, N. E., NIKITOVIC, D., GIAOUZAKI, A., CHLOUVERAKIS, G. & VARDAS, P. E. 2010. Oxidative stress changes after stent implantation: A randomized comparative study of sirolimus-eluting and bare metal stents. *International Journal of Cardiology,* 142**,** 33-37.

KÖSTER, R., VIELUF, D., KIEHN, M., SOMMERAUER, M., KÄHLER, J., BALDUS, S., MEINERTZ, T. & HAMM, C. W. 2000. Nickel and molybdenum contact allergies in patients with coronary in-stent restenosis. *The Lancet,* 356**,** 1895-1897.

LAARMAN, G. J., SUTTORP, M. J., DIRKSEN, M. T., VAN HEEREBEEK, L., KIEMENEIJ, F., SLAGBOOM, T., VAN DER WIEKEN, L. R., TIJSSEN, J. G. P., RENSING, B. J. & PATTERSON, M. 2006. Paclitaxel-Eluting versus Uncoated Stents in Primary Percutaneous Coronary Intervention. *New England Journal of Medicine,* 355**,** 1105-1113.

LACOMA, T. 2015. *How Does Sonication Work?* [Online]. [Accessed 12.03.15 2015].

LAMERS, E., HORSSEN, R. V., RIEN, J. T., DELFT, F. C. C., LUTTGE, T. R., WALBOOMERS, X. F. & JANSEN, J. A. 2010. The Influence Of Nanoscale Topographical Cues On Initial Osteoblast Morphology And Migration. *Journal of Eurpoean Cells and Material,* 20.

LEON, M. B., KANDZARI, D. E., EISENSTEIN, E. L., ANSTROM, K. J., MAURI, L., CUTLIP, D. E., NIKOLSKY, E., O'SHAUGHNESSY, C., OVERLIE, P. A., KIRTANE, A. J., MCLAURIN, B. T., SOLOMON, S. L., DOUGLAS JR, J. S. & POPMA, J. J. 2009. Late Safety, Efficacy, and Cost-Effectiveness of a Zotarolimus-Eluting Stent Compared With a Paclitaxel-Eluting Stent in Patients With De Novo Coronary Lesions: 2-Year Follow-Up From the ENDEAVOR IV Trial (Randomized, Controlled Trial of the Medtronic Endeavor Drug [ABT-578] Eluting Coronary Stent System Versus the Taxus Paclitaxel-Eluting Coronary Stent System in De Novo Native Coronary Artery Lesions). *JACC: Cardiovascular Interventions,* 2**,** 1208-1218.

LEON, M. B., NIKOLSKY, E., CUTLIP, D. E., MAURI, L., LIBERMAN, H., WILSON, H., PATTERSON, J., MOSES, J. & KANDZARI, D. E. 2010. Improved Late Clinical Safety With Zotarolimus-Eluting Stents Compared With Paclitaxel-Eluting Stents in Patients With De Novo Coronary Lesions: 3-Year Follow-Up From the ENDEAVOR IV (Randomized Comparison of Zotarolimus- and Paclitaxel-Eluting Stents in Patients With Coronary Artery Disease) Trial. *JACC: Cardiovascular Interventions,* 3**,** 1043-1050.

LEPRINCE, L., DOGIMONT, A., MAGNIN, D. & DEMOUSTIER-CHAMPAGNE, S. 2010. Dexamethasone electrically controlled release from polypyrrole-coated nanostructured electrodes. *Journal of Materials Science: Materials in Medicine,* 21**,** 925-930.

LI, L., MIRHOSSEINI, N., MICHAEL, A., LIU, Z. & WANG, T. 2013. Enhancement of endothelialisation of coronary stents by laser surface engineering. *Lasers in Surgery and Medicine,* 45**,** 608-616.

LILIENSIEK, S. J., WOOD, J. A., YONG, J., AUERBACH, R., NEALEY, P. F. & MURPHY, C. J. 2010. Modulation of human vascular endothelial cell behaviors by nanotopographic cues. *Biomaterials,* 31**,** 5418-5426.

LYNDON, J. A., BOYD, B. J. & BIRBILIS, N. 2014. Metallic implant drug/device combinations for controlled drug release in orthopaedic applications. *Journal of Controlled Release*.

MAGONOV, S. N., ELINGS, V. & WHANGBO, M.-H. 1997. Phase imaging and stiffness in tapping-mode atomic force microscopy. *Surface Science,* 375**,** 385-391.

MARRA, D. E., SIMONCINI, T. & LIAO, J. K. 2000. Inhibition of Vascular Smooth Muscle Cell Proliferation by Sodium Salicylate Mediated by Upregulation of p21Waf1 and p27Kip1. *Circulation,* 102**,** 2124-2130.

MARTIN, D. M. & BOYLE, F. J. 2011. Drug-eluting stents for coronary artery disease: A review. *Medical Engineering & Physics,* 33**,** 148-163.

MASSBERG, S., BYRNE, R. A., KASTRATI, A., SCHULZ, S., PACHE, J., HAUSLEITER, J., IBRAHIM, T., FUSARO, M., OTT, I., SCHÖMIG, A., LAUGWITZ, K.-L. & MEHILLI, J. 2011. Polymer-Free Sirolimus- and Probucol-Eluting Versus New Generation Zotarolimus-Eluting Stents in Coronary Artery DiseaseClinical Perspective. *The Intracoronary Stenting and Angiographic Results: Test Efficacy of Sirolimus- and Probucol-Eluting Versus Zotarolimus-Eluting Stents (ISAR-TEST 5) Trial,* 124**,** 624-632.

MEHILLI, J., KASTRATI, A., WESSELY, R., DIBRA, A., HAUSLEITER, J., JASCHKE, B., DIRSCHINGER, J. & SCHÖMIG, A. 2006. Randomized Trial of a Nonpolymer-Based Rapamycin-Eluting Stent Versus a Polymer-Based Paclitaxel-Eluting Stent for the Reduction of Late Lumen Loss. *Circulation*.

METROHM 2011. Basic overview of the working principle of a potentiostat/galvanostat (PGSTAT) – Electrochemical cell setup. *Autolab Application Note EC08.*

MILLER, D. C., THAPA, A., HABERSTROH, K. M. & WEBSTER, T. J. 2004. Endothelial and vascular smooth muscle cell function on poly(lactic-co-glycolic acid) with nano-structured surface features. *Biomaterials,* 25**,** 53-61.

MÎNDROIU, M., UNGUREANU, C., ION, R. & PÎRVU, C. 2013. The effect of deposition electrolyte on polypyrrole surface interaction with biological environment. *Applied Surface Science,* 276**,** 401-410.

MOHD DAUD, N., SAEFUL BAHRI, I. F., NIK MALEK, N. A. N., HERMAWAN, H. & SAIDIN, S. 2016. Immobilization of antibacterial chlorhexidine on stainless steel using crosslinking polydopamine film: Towards infection resistant medical devices. *Colloids and Surfaces B: Biointerfaces,* 145**,** 130-139.

MORICE , M.-C., SERRUYS , P. W., SOUSA , J. E., FAJADET , J., BAN HAYASHI , E., PERIN , M., COLOMBO , A., SCHULER , G., BARRAGAN , P., GUAGLIUMI , G., MOLNÀR , F. & FALOTICO , R. 2002. A Randomized Comparison of a Sirolimus-Eluting Stent with a Standard Stent for Coronary Revascularization. *New England Journal of Medicine,* 346**,** 1773-1780.

MORTON, A. C., WALKER, R. D. & GUNN, J. 2007. Current challenges in coronary stenting: from bench to bedside. *Biochemical Society Transactions,* 35.

MOSES , J. W., LEON , M. B., POPMA , J. J., FITZGERALD , P. J., HOLMES , D. R., O'SHAUGHNESSY , C., CAPUTO , R. P., KEREIAKES , D. J., WILLIAMS , D. O., TEIRSTEIN , P. S., JAEGER , J. L. & KUNTZ , R. E. 2003. Sirolimus-Eluting Stents versus Standard Stents in Patients with Stenosis in a Native Coronary Artery. *New England Journal of Medicine,* 349**,** 1315-1323.

MURIKIPUDI, S., METHE, H. & EDELMAN, E. R. 2013. The effect of substrate modulus on the growth and function of matrix-embedded endothelial cells. *Biomaterials,* 34**,** 677-684.

NAM, D.-H., KIM, M.-J., LIM, S.-J., SONGB, I.-S. & KWON, H.-S. 2013. Single-step synthesis of polypyrrole nanowires by cathodic electropolymerization. *J. Mater. Chem. A,* 1.

NEBEKER, J. R., VIRMANI, R., BENNETT, C. L., HOFFMAN, J. M., SAMORE, M. H., ALVAREZ, J., DAVIDSON, C. J., MCKOY, J. M., RAISCH, D. W., WHISENANT, B. K., YARNOLD, P. R., BELKNAP, S. M., WEST, D. P., GAGE, J. E., MORSE, R. E., GLIGORIC, G., DAVIDSON, L. & FELDMAN, M. D. 2006. Hypersensitivity Cases Associated With Drug-Eluting Coronary Stents: A Review of Available Cases From the Research on Adverse Drug Events and Reports (RADAR) Project. *Journal of the American College of Cardiology,* 47**,** 175-181.

NHS. 2014a. *Coronary Angioplasty and Stent Inserrtion* [Online]. Available: http://www.nhs.uk/conditions/coronary-angioplasty/pages/introduction.aspx [Accessed 03/12/2014 2014].

NHS. 2014b. *Coronary Artery Bypass Graft* [Online]. Available: http://www.nhs.uk/Conditions/Coronary-artery-bypass/Pages/Introduction.aspx [Accessed 07/08/2014 2014].

NHS. 2014c. *Coronary Artery Bypass Graft - Risks* [Online]. Available: http://www.nhs.uk/Conditions/Coronary-artery-bypass/Pages/Risks.aspx [Accessed 20/11/14 2014].

NUNES, G. L., ABIZAID, A. C., THEODORO, M. P., BRITO JR, F. S., CAIXETA, A., DA SILVA, L. F. F., MAZZOTTI, N. G., BELLÓ-KLEIN, A. & CLAUSELL, N. 2006. Role of probucol in inhibiting intimal hyperplasia after coronary stent implantation: A randomized study. *American Heart Journal,* 152**,** 914.e1-914.e7.

NUSSBAUM, M. & PAZ, Y. 2012. Ultra-thin SiO2 layers on TiO2: improved photocatalysis by enhancing products' desorption. *Phys. Chem.Chem.Phys,* 14**,** 3392-3399.

OATLEY, C. W. 1972. *The Scanning Electron Microscope Part 1 The Intsrument,* Cambridge, The Cambridge University Press.

OKNER, R., ORON, M., TAL, N., MANDLER, D. & DOMB, A. J. 2007. Electrocoating of stainless steel coronary stents for extended release of Paclitaxel. *Materials Science and Engineering: C,* 27**,** 510-513.

OKNER, R., ORON, M., TAL, N., NYSKA, A., KUMAR, N., MANDLER, D. & DOMB1, A. J. 2008. Electrocoating of stainless steel coronary stents for extended release of paclitaxel.

OKNER, R., SHAULOV, Y., TAL, N., FAVARO, G., DOMB, A. J. & MANDLER, D. 2009. Electropolymerized Tricopolymer Based on N-Pyrrole Derivatives as a Primer Coating for Improving the Performance of a Drug-Eluting Stent. *ACS Applied Materials & Interfaces,* 1**,** 758-767.

PALMAZ, J. C., BENSON, A. & SPRAGUE, E. A. 2002. Influence of Surface Topography on Endothelialization of Intravascular Metallic Material. *Journal of Vascular and Interventional Radiology,* 10**,** 439-444.

PAPAFAKLIS, M. I., CHATZIZISIS, Y. S., NAKA, K. K., GIANNOGLOU, G. D. & MICHALIS, L. K. 2012. Drug-eluting stent restenosis: Effect of drug type, release kinetics, hemodynamics and coating strategy. *Pharmacology & Therapeutics,* 134**,** 43-53.

PARAMO-GARCIA, U., IBANEZ, J. G. & BATINA, N. 2013. AFM Analysis of Polypyrrole Films Synthesized in the Presence of Selected Doping Agents. *Internation Journal of the Electrochemcal Society,* 8**,** 2656-2669.

PENDYALA, L. K., LI, J., SHINKE, T., GEVA, S., YIN, X., CHEN, J. P., KING III, S. B., ROBINSON, K. A., CHRONOS, N. A. F. & HOU, D. 2009. Endothelium-Dependent Vasomotor Dysfunction in Pig Coronary Arteries With Paclitaxel-Eluting Stents Is Associated With Inflammation and Oxidative Stress. *JACC: Cardiovascular Interventions,* 2**,** 253-262.

PENG, T., GIBULA, P., YAO, K.-D. & GOOSEN, M. F. A. 1996. Role of polymers in improving the results of stenting in coronary arteries. *Biomaterials,* 17**,** 685-694.

PEREZ, T. H.-., MORALES, M., N.BATINA & SALMON, M. 2001. Effect of the Electrosynthesis Method on the Surface Morphology of the Polypyrrole Film. *Journal of the Electrochemical Society,* 138**,** 369-375.

PRAKASH, A., RIGELHOF, F. & MILLER, E. Antioxidant Activity. *In:* LABS, M. (ed.). Minnesota.

PRASAD, C. K., RESMI, K. R. & KRISHNAN, L. K. 2005. Survival of Endothelial Cells in vitro on Paclitaxel-loaded Coronary Stents. *Journal of Biomaterials Applications,* 19**,** 271-286.

PRICE, M. J. 2013. Coronary Stenting: A Companion to Topol's Textbook of Interventional Cardiology.

PURANIK, A. S., DAWSON, E. R. & PEPPAS, N. A. 2013. Recent advances in drug eluting stents. *International Journal of Pharmaceutics,* 441**,** 665-679.

RANADE, S. V., MILLER, K. M., RICHARD, R. E., CHAN, A. K., ALLEN, M. J. & HELMUS, M. N. 2004. Physical characterization of controlled release of paclitaxel from the TAXUS™ Express2™ drug-eluting stent. *Journal of Biomedical Materials Research Part A,* 71A**,** 625-634.

REAY, R. 2012. Novel polymers to encourage rapid recovery of arterial function following coronary stenting.

RUBERT&COLTD. *Roughness Parameters* [Online]. Cheshire. [Accessed 2nd February 2016].

SAMAROO, H. D., LU, J. & WEBSTER, T. J. 2008. Enhanced endothelial cell density on NiTi surfaces with sub-micron to nanometer roughness. *International Journal of Nanomedicine,* 3**,** 75-82.

SANTOSA, D. B., ROSSAA, C., COLLEA, D., GODOIB, M., SANTOSA, A. A. D., ZIMMERMANA, L. T., HORTC, M. A., BRAGAD, A. L. & FARINAA, M. 2016. Probucol and Succinobucol display similar lipid-lowering and antioxidant effects: a subacute/subchronic study in mice. *Vittalle*.

SCHAMPAERT, E., COHEN, E. A., SCHLÜTER, M., REEVES, F., TRABOULSI, M., TITLE, L. M., KUNTZ, R. E. & POPMA, J. J. 2004. The Canadian study of the sirolimus-eluting stent in the treatment of patients with long de novo lesions in small native coronary arteries (C-SIRIUS). *Journal of the American College of Cardiology,* 43**,** 1110-1115.

SCHILDWÄCHTER, M. 2013. BIOTRONIK Orsiro Hybrid Drug-Eluting Stent lives up to Abbott's XIENCE PRIM standards. *Press release*.

SCHOFER, J., SCHLÜTER, M., GERSHLICK, A. H., WIJNS, W., GARCIA, E., SCHAMPAERT, E. & BREITHARDT, G. 2003. Sirolimus-eluting stents for treatment of patients with long atherosclerotic lesions in small coronary arteries: double-blind, randomised controlled trial (E-SIRIUS). *The Lancet,* 362**,** 1093-1099.

SCHULZE, P. C. & RICHARD T. LEE, M. 2005. Oxidative Stress and Atherosclerosis. *Current Atherosclerosis Reports,* 7**,** 242–248.

SCHWARTZ, R. S., HUBER, K. C., MURPHY, J. G., EDWARDS, W. D., CAMRUD, A. R., VLIETSTRA, R. E. & HOLMES, D. R. 1992. Restenosis and the proportional neointimal response to coronary artery injury: Results in a porcine model. *Journal of the American College of Cardiology,* 19**,** 267-274.

SCOTT, W. W. & BHUSHAN, B. 2003. Use of phase imaging in atomic force microscopy for measurement of viscoelastic contrast in polymer nanocomposites and molecularly thick lubricant films. *Ultramicroscopy,* 97**,** 151-169.

SEIDLITZ, A., NAGEL, S., SEMMLING, B., STERNBERG, K., KROEMER, H. K. & WEITSCHIES, W. 2013. In Vitro Dissolution Testing of Drug-Eluting Stents. *Current Pharmaceutical Biotechnology,* 14**,** 67-75.

SEKIYA, M., FUNADA, J., WATANABE, K., MIYAGAWA, M. & AKUTSU, H. 1998. Effects of probucol and cilostazol alone and in combination on frequency of poststenting restenosis. *The American Journal of Cardiology,* 82**,** 144-147.

SERRUYS, P., RUYGROK, P., NEUZNER, J., PIEK, J., SETH, A., SCHOFER, J., RICHARDT, G., WIEMER, M., CARRIE, D., THEUSEN, L., BOONE, E., MIGUEL-HERBERT, K. & DAEMEN, J. 2006. A randomised comparison of an everolimus-eluting coronary stent with a paclitaxel-eluting coronary stent:the SPIRIT II trial. *EuroIntervention*, 284-94.

SERRUYS, P. W., CHEVALIER, B., DUDEK, D., CEQUIER, A., CARRIÉ, D., INIGUEZ, A., DOMINICI, M., VAN DER SCHAAF, R. J., HAUDE, M., WASUNGU, L., VELDHOF, S., PENG, L., STAEHR, P., GRUNDEKEN, M. J., ISHIBASHI, Y., GARCIA-GARCIA, H. M. & ONUMA, Y. 2015. A bioresorbable everolimus-eluting scaffold versus a metallic everolimus-eluting stent for ischaemic heart disease caused by de-novo native coronary artery lesions (ABSORB II): an interim 1-year analysis of clinical and procedural secondary outcomes from a randomised controlled trial. *The Lancet,* 385**,** 43-54.

SHANSHAN, C., LILI, T., YINGXUE, T., BINGCHUN, Z. & KE, Y. 2013. Study of drug-eluting coating on metal coronary stent. *Materials Science and Engineering: C,* 33**,** 1476-1480.

SHI, C. & ZHITOMIRSKY, I. 2010. Electrodeposition and Capacitive Behavior of Films for Electrodes of Electrochemical Supercapacitors. *Nanoscale Res Lett*, 518-523.

SORRENTINO, S., GIUSTINO, G., MEHRAN, R., KINI, A. S., SHARMA, S. K., FAGGIONI, M., FARHAN, S., VOGEL, B., INDOLFI, C. & DANGAS, G. D. 2017. Everolimus-Eluting Bioresorbable Scaffolds Versus Everolimus-Eluting Metallic Stents. *Journal of the American College of Cardiology,* 69**,** 3055-3066.

SRINIVASAN, A., RANJANI, P. & RAJENDRAN, N. 2013. Electrochemical polymerization of pyrrole over AZ31 Mg alloy for biomedical applications. *Electrochimica Acta,* 88**,** 310-321.

SSEDCYPHER 2003. Summary of Safety and Effectiveness Data (SSED). 33.

SSEDXIENCE 2008. Summary of Safety and Effectiveness Data (SSED).

STEFANINI, G. G., BYRNE, R. A., SERRUYS, P. W., DE WAHA, A., MEIER, B., MASSBERG, S., JÜNI, P., SCHÖMIG, A., WINDECKER, S. & KASTRATI, A. 2012. Biodegradable polymer drug-eluting stents reduce the risk of stent thrombosis at 4 years in patients undergoing percutaneous coronary intervention: a pooled analysis of individual patient data from the ISAR-TEST 3, ISAR-TEST 4, and LEADERS randomized trial. *European Heart Journal,* 33**,** 1214-1222.

STEWART, E. M., LIU, X., CLARK, G. M., KAPSA, R. M. I. & WALLACE, G. G. 2012. Inhibition of smooth muscle cell adhesion and proliferation on heparin-doped polypyrrole. *Acta Biomaterialia,* 8**,** 194-200.

STONE, G. W., ELLIS, S. G., COX, D. A., HERMILLER, J., O'SHAUGHNESSY, C., MANN, J. T., TURCO, M., CAPUTO, R., BERGIN, P., GREENBERG, J., POPMA, J. J. & RUSSELL, M. E. 2004. One-Year Clinical Results With the Slow-Release, Polymer-Based, Paclitaxel-Eluting TAXUS Stent. *The TAXUS-IV Trial,* 109**,** 1942-1947.

STONE, G. W., MIDEI, M., NEWMAN, W. & ET AL. 2008. Comparison of an everolimus-eluting stent and a paclitaxel-eluting stent in patients with coronary artery disease: A randomized trial. *JAMA,* 299**,** 1903-1913.

STONE, G. W., RIZVI, A., NEWMAN, W., MASTALI, K., WANG, J. C., CAPUTO, R., DOOSTZADEH, J., CAO, S., SIMONTON, C. A., SUDHIR, K., LANSKY, A. J., CUTLIP, D. E. & KEREIAKES, D. J. 2010. Everolimus-eluting versus paclitaxel-eluting stents in coronary artery disease. *N Engl J Med,* 362**,** 1663-74.

STONE, G. W., TEIRSTEIN, P. S., MEREDITH, I. T., FARAH, B., DUBOIS, C. L., FELDMAN, R. L., DENS, J., HAGIWARA, N., ALLOCCO, D. J. & DAWKINS, K. D. 2011. A Prospective, Randomized Evaluation of a Novel Everolimus-Eluting Coronary Stent: The PLATINUM (A Prospective, Randomized, Multicenter Trial to Assess an Everolimus-Eluting Coronary Stent System [PROMUS Element] for the Treatment of up to Two

De Novo Coronary Artery Lesions) Trial. *Journal of the American College of Cardiology,* 57**,** 1700-1708.

STROHBACH, A. & BUSCH, R. 2015. Polymers for Cardiovascular Stent Coatings. *International Journal of Polymer Science,* 2015**,** 11.

SU, W. & IROH, J. O. 1997. Formation of polypyrrole coatings on stainless steel in aqueous benzene sulfonate solution. *Electrochimica Acta,* 42**,** 2685-2694.

SVIRSKIS, D., TRAVAS-SEJDIC, J., RODGERS, A. & GARG, S. 2010. Electrochemically controlled drug delivery based on intrinsically conducting polymers. *Journal of Controlled Release,* 146**,** 6-15.

TANDJUNG, K., BASALUS, M. W. Z., SEN, H., JESSURUN, G. A. J., DANSE, P. W., STOEL, M., LINSSEN, G. C. M., DERKS, A., VAN LOENHOUT, T. T., NIENHUIS, M. B., HAUTVAST, R. W. M. & VON BIRGELEN, C. 2012. Durable polymer-based stent challenge of Promus Element versus Resolute integrity (DUTCH PEERS): Rationale and study design of a randomized multicenter trial in a Dutch all-comers population. *American Heart Journal,* 163**,** 557-562.

TER MEER, M., DAAMEN, W. F., HOOGEVEEN, Y. L., VAN SON, G. J. F., SCHAFFER, J. E., VAN DER VLIET, J. A., KOOL, L. J. S. & VAN DEN HEUVEL, L. P. 2017. Continuously Grooved Stent Struts for Enhanced Endothelial Cell Seeding. *Cardiovascular and Interventional Radiology,* 40**,** 1237-1245.

THEVENOT, P., HU, W. & TANG, L. 2008. Surface chemistry influences implant biocompatibility. *Curr Top Med Chem,* 8**,** 270-80.

THOMAS, C. 2011. *"You can lead a cardiologist to water but, apparently, you cannot make him drink"* [Online]. Available: http://ethicalnag.org/2011/06/04/unnecessary-stents/ [Accessed 30th Apr 2014].

TMASSOCIATES. *Questions and answers about Ultrasonc Cleaning* [Online]. California. [Accessed 12.03.15 2015].

TOIU, A., VLASE, L., ONIGA, I., BENEDEC, D. & TĂMAŞ, M. 2011. HPLC ANALYSIS OF SALICYLIC DERIVATIVES FROM NATURAL PRODUCTS. *FARMACIA,* 59.

TRANSLUMINA 2009. Coronary Stent System. Translumina GmbH.

TURCO, M. A., ORMISTON, J. A., POPMA, J. J., MANDINOV, L., O'SHAUGHNESSY, C. D., MANN, T., MCGARRY, T. F., WU, C.-J., CHAN, C., WEBSTER, M. W. I., JACK J. HALL, M., MISHKEL, G. J., CANNON, L. A., BAIM, D. S. & KOGLIN, J. 2007. Polymer-Based, Paclitaxel-ElutingTAXUS Liberté Stent in De Novo Lesions. *Journal of the American College of Cardiology,* 49.

UPADHYAY, J. & KUMAR, A. 2013. Engineering polypyrrole nanotubes by 100MeV Si9+ ion beam irradiation: Enhancement of antioxidant activity. *Materials Science and Engineering: C,* 33**,** 4900-4904.

URBAN, P., MEREDITH, I. T., ABIZAID, A., POCOCK, S. J., CARRIÉ, D., NABER, C., LIPIECKI, J., RICHARDT, G., IÑIGUEZ, A., BRUNEL, P., VALDES-CHAVARRI, M., GAROT, P., TALWAR, S., BERLAND, J., ABDELLAOUI, M., EBERLI, F., OLDROYD, K., ZAMBAHARI, R., GREGSON, J., GREENE, S., STOLL, H.-P. & MORICE, M.-C. 2015. Polymer-free Drug-Coated Coronary Stents in Patients at High Bleeding Risk. *The New England Journal of Medicine*.

VAN DER GIESSEN, W. J., LINCOFF, A. M., SCHWARTZ, R. S., VAN BEUSEKOM, H. M. M., SERRUYS, P. W., HOLMES, D. R., ELLIS, S. G. & TOPOL, E. J. 1996. Marked Inflammatory Sequelae to Implantation of Biodegradable and Nonbiodegradable Polymers in Porcine Coronary Arteries. *Circulation,* 94**,** 1690-1697.

VELHAL, N., PATIL, N., JAMDADE, S. & PURI, V. 2014. Studies on galvanostatically electropolymerised polypyrrole/polyaniline composite thin films on stainless steel. *Applied Surface Science,* 307**,** 129-135.

VENKATRAMAN, S. & BOEY, F. 2007. Release profiles in drug-eluting stents: Issues and uncertainties. *Journal of Controlled Release,* 120**,** 149-160.

VIRMANI, R., GUAGLIUMI, G., FARB, A., MUSUMECI, G., GRIECO, N., MOTTA, T., MIHALCSIK, L. & TESPILI, M. 2004. Localised Hypersensitivity and Late Coronary Thrombosis Secondary to a Sirolimus-Eluting Stent. *Journal of The American Heart Association,* 109**,** 701-705.

WALLACE, G. G., HIGGINS, M. J., MOULTON, S. E. & WANG, C. 2012. Nanobionics: the impact of nanotechnology on implantable medical bionic devices. *Nanoscale,* 4**,** 4327-4347.

WANEKAYA, A. K., LEI, Y. & MYUNG, N. V. 2006. Fabrication and Properties of Conducting Polypyrrole/SWNT-PABS Composite Films and Nanotubes. *Electroanalysis***,** 1047-1054.

WANG, X., GU, X., YUAN, C., CHEN, S., ZHANG, P., ZHANG, T., YAO, J., CHEN, F. & CHEN, G. 2004. Evaluation of biocompatibility of polypyrrole in vitro and in vivo. *Journal of Biomedical Materials Research Part A,* 68A**,** 411-422.

WATT, J., KENNEDY, S., MCCORMICK, C., AGBANI, E. O., MCPHADEN, A., MULLEN, A., CZUDAJ, P., BEHNISCH, B., WADSWORTH, R. M. & OLDROYD, K. G. 2013. Succinobucol-Eluting Stents Increase Neointimal Thickening and Peri-Strut Inflammation in a Porcine Coronary Model. *Catheterization and Cardiovascular Interventions,* 81**,** 698-708.

WATT, J., WADSWORTH, R., KENNEDY, S. & OLDROYD, K. G. 2008. Pro-healing drug-eluting stents: a role for antioxidants? *Clinical Science,* 114**,** 265-273.

WEINTRAUB, W. S. 2007. The Pathophysiology and Burden of Restenosis. *The American Journal of Cardiology,* 100**,** S3-S9.

WHO, W. H. O. 2015. *Cardiovascular diseases (CVDs) Fact Sheet No 317* [Online]. Available: http://www.who.int/mediacentre/factsheets/fs317/en/ [Accessed 16th May 2016 2016].

WONG, J. Y., LANGER, R. & INGBER, D. E. 1994. Electrically conducting polymers can noninvasively control the shape and growth of mammalian cells. *Proceedings of the National Academy of Sciences of the United States of America,* 91**,** 3201-3204.

XU, C., YANG, F., WANG, S. & RAMAKRISHNA, S. 2004. In vitro study of human vascular endothelial cell function on materials with various surface roughness. 154-161.

YAMAMOTO, A. 2008. A Uniqe Antilipidemic Drug — Probucol. *Journal of Atherosclerosis and Thrombosis,* 15**,** 304-305.

ZHANG, X., ZHANG, J., SONG, W. & LU, Z. 2006. *Journal of Physical Chemistry*.

ZHOU, D. D. & GREENBAUM, E. 2010. *Implantable Neural Prostheses 2,* USA, Springer.